

$^{18}\text{O}/^{16}\text{O}$  STUDIES OF SHORT-LIVED (10-25 YEAR), FUMAROLIC (>500°C)  
METEORIC-HYDROTHERMAL EVENTS IN THE OUTFLOW SHEETS OF  
ASH-FLOW TUFFS

Thesis by

Elizabeth Warner Holt

In Partial Fulfillment of the Requirements

for the Degree of

Doctor of Philosophy

California Institute of Technology

Pasadena, California

2000

(Submitted September 30, 1999)

## Acknowledgements

I wish to thank the members of the Caltech community who have contributed to my graduate education and the development of the ideas presented in this dissertation. In particular, the members of my thesis committee, Ken Farley, Joann Stock, and Don Burnett, provided welcome comments and advice. I most especially wish to thank my Ph.D. advisor, Dr. Hugh P. Taylor, Jr., both for sharing his scientific insight and for his advocacy and advice regarding my scientific career. I wish to extend my gratitude to Roy Bailey, Tom Brikowski, Bob Criss, John Eichelberger, Carey Gazis, Fraser Goff, Wes Hildreth, John Holt, Gordon Keating, Peter Kokelaar, and Peter Lipman for their helpful discussions and critical reviews. I also owe thanks to Gail Mahood, my M.S. thesis adviser at Stanford University, for educating me in the basics of volcanology and for introducing me to the fossil fumaroles in the Bishop Tuff, which turned out to be such an important part of my Ph.D. thesis. Finally, I wish to thank Bob Sharp for his encouragement and for his faith.

There are several friends I would like to thank for their assistance in the field work for this project. I collected samples on rappel in Owens River and Rock Creek Gorges, as well as in the Valley of Ten Thousand Smokes, Alaska, and for assistance with this endeavor I wish to thank John Holt. Judy Zachariassen provided me with the opportunity to collect basalt samples along the Colorado River on her "graduation river-trip" in 1998, and for that experience I will be forever grateful. John Holt and Gene Garza helped me to collect samples in the Valley of Ten Thousand Smokes, Alaska, and John Eichelberger provided an excellent scientific introduction to that area. I would also like to thank Scott Roripaugh, of the Sierra Nevada Aquatic Research Lab in Mammoth Lakes, for his concern and hospitality during my field work in that area.

There are several people with whom I interacted in the course of completing the laboratory work for this project. Xiaomei Xu was an excellent source of information and calm in the laboratory. She helped to clean the source and replace the filament on the MAT 252 mass spectrometer, and she continues to take care of all manner of details regarding the maintenance and upkeep of that machine. Greg Holk and Carey Gazis provided instruction in the lab during my first months of working as a graduate student. Vic Nenow was a generous genius with all things electrical, and I have him to thank for helping to keep my lab running smoothly and for keeping me from electrocuting myself.

I have been assisted throughout my graduate study by members of the staff of the Division of Geological and Planetary Sciences at Caltech. First, I would like to thank Kathy Lima both for her friendship and for her excellent and eminently efficient handling of everything that she was involved with. I would also like to thank Donna Sackett, whose friendly concern and calm efficiency helped to make my graduate experience both enjoyable and almost completely free of red tape. I also extend my appreciation to Priscilla Piano, Carolyn Porter, Mary Mellon, Terry Gennaro, and Mahmoud Chaudry.

There are several sources of funding for this project that I would like to acknowledge. First and foremost is the National Science Foundation. I also received grants from the White Mountain Research Station and the Governor of California "Call to Action" Opportunity Scholarship Foundation. Further, I benefited from the generosity of Mike Scott, who provided the funds for a Caltech student trip to the Valley of Ten Thousand Smokes, Alaska, and thereby provided me with the opportunity to collect samples at that location.

The gratitude I have for my friends is the most difficult for me to articulate. Suffice to say, my friends: you know who you are, and I thank you. As for my guardian troll, may the sun always shine upon your fair noggin.

**Abstract.**  $^{18}\text{O}/^{16}\text{O}$  data from the 0.76 Ma Bishop Tuff outflow sheet provide evidence for a vigorous, short-lived ( $\approx 10\text{-}25$  years), high-temperature ( $400^{\circ}\text{-}650^{\circ}\text{C}$ ), fumarolic meteoric-hydrothermal event immediately following eruption. This is proved by: (1) the juxtaposition in the upper, partially welded Bishop Tuff of low- $^{18}\text{O}$  groundmass/glass ( $\delta^{18}\text{O} = -5$  to  $+3$ ) with coexisting quartz *and feldspar* phenocrysts having magmatic  $\delta^{18}\text{O}$  values ( $+8.4 \pm 0.3$ ;  $+7.2 \pm 0.3$ ); and (2) the fact that these types of  $^{18}\text{O}/^{16}\text{O}$  signatures correlate very well with the morphological features and mapped zones of fumarolic activity. Ten detailed  $\delta^{18}\text{O}$ -depth profiles in various parts of the Bishop Tuff outflow sheet show evidence for two types of fumarolic meteoric-hydrothermal circulation systems in the upper part of the tuff; there is a broadly based, stratigraphically bound, 20- to 40-m-thick Upper Low- $^{18}\text{O}$  Zone (ULZ) that straddles the contact between the Tableland Unit and the Gorges Unit, and there is also a set of localized, 40- to 80-m-thick zones in the partially welded tuff in which extremely  $^{18}\text{O}$ -depleted rock ( $\delta^{18}\text{O}$  as low as  $-6.5$ ) characterizes a Deep Fumarolic System (DFS). This DFS is spatially associated with steep fissures, tubular conduits, and shallow-dipping columnar joints in cylindrical volumes of rock lying beneath more than 1000 fumarolic mounds scattered across the surface of the tuff. Both of these  $^{18}\text{O}$ -depleted zones are concentrated over areas where the underlying Densely Welded Zone (DWZ) is particularly thick, namely above pre-Bishop Tuff paleodrainages. The DWZ remained largely hot, ductile, and impermeable during fumarolic activity, which prevented the heated meteoric fluids from penetrating the densely welded tuff until it cooled sufficiently so that throughgoing vertical fractures provided access to the base of the ash-flow sheet (at which time the fumarolic activity appears to have rapidly terminated). Whole-rock  $\delta^{18}\text{O}$  values of samples collected from the surface of the 1912 ash-flow sheet at the Valley of Ten Thousand Smokes (VTTS), Alaska show analogous  $^{18}\text{O}/^{16}\text{O}$  systematics and a similar range in  $\delta^{18}\text{O}$  values ( $-0.1$  to  $+12.6$ ) to surface samples collected from the Bishop Tuff outflow sheet ( $+2.5$  to  $+16.7$ ).

## TABLE OF CONTENTS

<b>Acknowledgements</b> .....	ii
<b>Abstract</b> .....	iii
<b>Table of Contents</b> .....	iv
 <b>CHAPTER 1: SUMMARY OF PREVIOUS <sup>18</sup>O/<sup>16</sup>O STUDIES</b>	
OF ASH-FLOW TUFFS AND VOLCANIC HISTORIES OF	
LONGVALLEY AND KATMAI CALDERAS	
 <b>1.1. Introduction</b> .....	 I-1
<i>1.1.1. Background to the Present Study</i> .....	I-1
<i>1.1.2. Statement of the Thesis Research Problem</i> .....	I-3
<b>1.2. The 0.76 Ma Bishop Tuff Outflow Sheet, California</b> .....	I-5
<i>1.2.1. Volcanic History Associated with Long Valley Caldera</i> .....	I-5
<i>1.2.2. Formation of Long Valley Caldera and Eruption of the</i> <i>Bishop Tuff Outflow Sheet (0.76 Ma)</i> .....	I-7
<i>1.2.3. The Bishop Tuff Magma</i> .....	I-8
<i>1.2.4. The Bishop Tuff Outflow Sheet</i> .....	I-8
<i>1.2.5. Deformation and Erosion of the Southeastern Lobe of the</i> <i>Bishop Tuff</i> .....	I-9
<i>1.2.6. Fossil Fumaroles in the Bishop Tuff Outflow Sheet</i> .....	I-10
<b>1.3. The 87-year-old Tuff from the Valley of Ten</b> <b>Thousand Smokes, Katmai National Park, Alaska</b> .....	I-11
<i>1.3.1. Geologic Setting</i> .....	I-11
<i>1.3.2. The 1912 Eruption Events and Sequence of Eruptive Products</i> .....	I-12
<i>1.3.3. The 1912 Ash-Flow Sheet</i> .....	I-13
<i>1.3.4. Fumarolic Vapors: Temperatures and Compositions</i> .....	I-15
<i>1.3.5. Sources of the Fumarolic Vapors</i> .....	I-18
<i>1.3.6. Fumarole Morphology</i> .....	I-19

1.3.7. <i>Comparison with Morphological Features of Fossil Fumaroles in the Bishop Tuff</i> .....	I-20
1.3.8. <i>Mineralogy of Fumarolic Encrustations and Associated Alteration Assemblages</i> .....	I-21
1.3.9. <i>Comparison with Mineralogical Features in the Bishop Tuff</i> .....	I-23
<b>Figure Captions</b> .....	I-24
<b>Figures</b> .....	I-26
<b>CHAPTER 2: <math>^{18}\text{O}/^{16}\text{O}</math> INVESTIGATIONS OF FUMAROLIC STRUCTURES IN THE 0.76 MA BISHOP TUFF OUTFLOW SHEET</b>	
<b>2.1. Isotope Systematics on <math>\delta^{18}\text{O}</math>-<math>\delta^{18}\text{O}</math> Diagrams</b> .....	II-1
<b>2.2. Geometry of <math>^{18}\text{O}/^{16}\text{O}</math> Distribution and Fumarolic Structures in the Bishop Tuff Outflow Sheet</b> .....	II-5
2.2.1. <i>General Statement</i> .....	II-5
2.2.2. <i>Distribution of Sample Sites</i> .....	II-7
2.2.3. <i>Overall Pattern of Whole-Rock <math>^{18}\text{O}/^{16}\text{O}</math> values in the Bishop Tuff Outflow Sheet</i> .....	II-10
<b>2.3. Temperatures and Isotopic Compositions of <math>\text{H}_2\text{O}</math> Involved in Fumarolic Activity</b> .....	II-13
<b>2.4. Detailed <math>^{18}\text{O}/^{16}\text{O}</math> relationships in and around the fumarolic conduits</b> .....	II-19
2.4.1. <i>Fumarolic Mounds</i> .....	II-19
2.4.2. <i>An Isolated Tubular Conduit (Site HT)</i> .....	II-21
2.4.3. <i>Fumarolic Zones Along Steep Fissures (Site LG)</i> .....	II-24
2.4.4. <i>Fractures and Veins in the Densely Welded Tuff</i> .....	II-28

2.4.5. <i><sup>18</sup>O/<sup>16</sup>O-Depth Profiles Beneath Fumarolic Mounds (Sites CG and CC-L)</i> .....	II-35
<b>2.5. The Bishop Tuff Outflow Sheet Away from Fumarolic Conduits</b> .....	II-38
2.5.1. <i>Two <sup>18</sup>O/<sup>16</sup>O-Depth Profiles in Areas Located Between Fumarolic Mounds</i> .....	II-38
2.5.2. <i><sup>18</sup>O/<sup>16</sup>O-Depth Profiles From Regions of Weak and/or Non-Existent Fumarolic Activity (Sites RC, CC, and UG)</i> .....	II-40
2.5.3. <i>An <sup>18</sup>O/<sup>16</sup>O-Depth Profile Near Lake Crowley (Site CR)</i> .....	II-43
<b>2.6. The Deep Fumarolic System (DFS) and the Upper Low-<sup>18</sup>O Zone (ULZ)</b> .....	II-45
<b>2.7. Volatile Sources for the Bishop Tuff Outflow Sheet Fumaroles</b> .....	II-47
2.7.1. <i>Magmatic vs. Meteoric H<sub>2</sub>O Sources</i> .....	II-47
2.7.2. <i>Meteoric H<sub>2</sub>O Beneath the Hot Bishop Tuff</i> .....	II-48
<b>2.8. Summary</b> .....	II-50
<b>Tables</b> .....	II-53
<b>Figure Captions</b> .....	II-58
<b>Figures</b> .....	II-71

**CHAPTER 3: HYDROGEOLOGY OF FOSSIL FUMARoles  
IN THE SOUTHEASTERN LOBE OF THE BISHOP TUFF  
OUTFLOW SHEET**

<b>3.1. Fossil Fumarole Distribution and Morphology</b> .....	III-1
<b>3.2. Shallow Meteoric-Hydrothermal Circulation in the ULZ</b> .....	III-3
<b>3.3. Relationship of Deep Hydrothermal Circulation in the DFS to the ULZ and the DWZ</b> .....	III-7

3.3.1. <i>Extent and General Characteristics of the Deep Fumarolic System (DFS)</i> .....	III-7
3.3.2. <i>Comparison with Features in the Valley of Ten Thousand Smokes</i> .....	III-10
3.3.3. <i>Tentative Hydrothermal Models for the DFS and the ULZ</i> .....	III-12
3.3.4. <i>Distribution of the DFS in the Bishop Tuff Outflow Sheet</i> .....	III-14
3.3.5. <i>Relationship of the DFS to the Densely Welded Zone (DWZ)</i> .....	III-17
<b>3.4. Water/Rock Ratios</b> .....	III-19
<b>3.5. Heat Balance</b> .....	III-22
<b>3.6. Fluid Fluxes</b> .....	III-24
<b>3.7. Sources of Meteoric H<sub>2</sub>O for Fumaroles in the Gorges, Southeast and Chidago Areas</b> .....	III-28
<b>3.8. Sources of Meteoric H<sub>2</sub>O for Crowley Area</b> .....	III-31
<b>3.9. Hydrogeology and Drainage Capture in the Vicinity of Tom's Place</b> .....	III-37
<b>3.10. Summary</b> .....	III-39
<b>Tables</b> .....	III-41
<b>Figure Captions</b> .....	III-43
<b>Figures</b> .....	III-51

**CHAPTER 4: COMPARISON OF THE <sup>18</sup>O/<sup>16</sup>O SYSTEMATICS OF TWO FOSSIL FISSURE FUMARoles IN THE 1912 ASH-FLOW SHEET AT THE VALLEY OF TEN THOUSAND SMOKES WITH THE BISHOP TUFF OUTFLOW SHEET AND THE CHEGEM TUFF**

<b>4.1. Description of Sampling Sites at the Valley of Ten Thousand Smokes (VTTS)</b> .....	IV-1
<b>4.2. Previous <sup>18</sup>O/<sup>16</sup>O Studies of Samples from the VTTS</b> .....	IV-4

<b>4.3. <math>^{18}\text{O}/^{16}\text{O}</math> Systematics of Samples from the VTTS.....</b>	<b>IV-5</b>
4.3.1. <i>Whole-Rock <math>\delta^{18}\text{O}</math> Values.....</i>	IV-5
4.3.2. <i>Minor Effects of Mineralogical Alteration and <math>^{18}\text{O}</math>- Exchange in the Feldspar Phenocrysts.....</i>	IV-8
<b>4.4. Geometry of fumarolic meteoric-hydrothermal circulation.....</b>	<b>IV-10</b>
4.4.1. <i>General Statement.....</i>	IV-10
4.4.2. <i>Small, Isolated Fissures (Site ML).....</i>	IV-11
4.4.3. <i>A Large Fissure and a Concentration of Smaller Fumarolic Conduits (Site KC).....</i>	IV-14
<b>4.5. Discussion.....</b>	<b>IV-16</b>
4.5.1. <i>Level of Exposure of Fumarolic Plumbing in the VTTS.....</i>	IV-16
4.5.2. <i>Lifetime of Fumarolic Activity in the VTTS.....</i>	IV-19
<b>4.6. Summary.....</b>	<b>IV-21</b>
<b>Table.....</b>	<b>IV-23</b>
<b>Figure Captions.....</b>	<b>IV-24</b>
<b>Figures.....</b>	<b>IV-29</b>

**CHAPTER 5: CONCLUSIONS AND RELATIONSHIP OF  
THIS WORK TO OTHER STUDIES**

<b>5.1. General conclusions about fumarolic activity in the upper parts of ash-flow sheets.....</b>	<b>V-1</b>
5.1.1. <i>Circulation Geometries and Origin of the Fumarolic Gases.....</i>	V-1
5.1.2. <i>Contrasting Fumarolic <math>^{18}\text{O}/^{16}\text{O}</math> Signatures in Phenocrysts and Groundmass.....</i>	V-2
5.1.3. <i>Temperature Range of Fumarolic Activity.....</i>	V-3



<b>5.2. Fumarolic Plumbing and Patterns of <math>^{18}\text{O}</math> - Depletion in the Gorges Area of the Bishop Tuff Outflow Sheet: the Deep Fumarolic System (DFS) and the Upper Low-<math>^{18}\text{O}</math> Zone (ULZ)</b> .....	V-3
5.2.1. <i>Fumarolic Mounds and the DFS</i> .....	V-3
5.2.2. <i>Patterns of <math>^{18}\text{O}</math>-depletion in the ULZ and the DFS</i> .....	V-4
5.2.5. <i>Material-Balance Water/Rock Ratios</i> .....	V-5
5.2.6. <i>Water Supply to Fumaroles</i> .....	V-6
5.2.7. <i>Heat Balance</i> .....	V-7
5.2.8. <i>Fumarolic Conduits and Permeability in Ash-Flow Tuffs</i> .....	V-7
<b>5.3. Fossil Fumaroles in the Crowley Area: an Analogue for Fumarolic Morphology in Intracaldera Tuffs?</b> .....	V-8
<b>5.4. Fumarolic Conduits in the Bishop Tuff Outflow Sheet</b> .....	V-9
5.4.1. <i>Interconnected Fumarolic Plumbing System</i> .....	V-9
5.4.2. <i>Formation and Growth of Fumarolic Conduits</i> .....	V-9
<b>5.5. Relationship of the Densely Welded Zone (DWZ) to Formation of Fumarolic Conduits</b> .....	V-10
<b>5.6. Discussion Comparing the <math>^{18}\text{O}/^{16}\text{O}</math> Systematics in the Bishop Tuff Fossil Fumaroles with Long Valley and Chegem Intracaldera Tuffs</b> .....	V-12
5.6.1. <i><math>^{18}\text{O}/^{16}\text{O}</math>-Depth Profiles</i> .....	V-12
5.6.2. <i>Intracaldera Bishop Tuff</i> .....	V-14
5.6.3. <i>Material-Balance Water/Rock Ratios in Intracaldera Tuff</i> .....	V-17
5.6.4. <i>Relationship of Climate and Abundance of Surface Water to Fumarolic Activity</i> .....	V-18

<b>5.7. Is This Type of Fumarolic Activity Confined to Welded Ash-Flow Tuffs, or Can it Also be Observed in Lavas?</b> .....	V-20
<b>5.8. Discussion About the Timescales of Fumarolic Activity and the Mechanisms by which such Activity is Terminated</b> .....	V-24
<i>5.8.1. Oxygen Isotope Clock</i> .....	V-24
<i>5.8.2. Fracturing of the Densely Welded Tuff and the Lifetime of Fumarolic Activity</i> .....	V-26
<b>Figure Captions</b> .....	V-34
<b>Figures</b> .....	V-38
<b>Appendix A: Analytical Techniques</b> .....	A-1
<b>Appendix B: Standardization</b> .....	B-1
<b>Appendix C: References</b> .....	C-1

**CHAPTER 1: SUMMARY OF PREVIOUS  $^{18}\text{O}/^{16}\text{O}$  STUDIES OF  
ASH-FLOW TUFFS AND VOLCANIC HISTORIES OF LONG VALLEY  
AND KATMAI CALDERAS**

**1.1. Introduction**

*1.1.1. Background to the Present Study*

Hydrothermal activity is one of the most important processes acting on the Earth's crust, because it is ubiquitous and because it has significance for geothermal energy and ore deposition. Hot springs, geysers, and steam vents are found wherever magma approaches sufficiently near the surface of the Earth. Even though  $^{18}\text{O}/^{16}\text{O}$  and D/H studies have been carried out on more than a hundred active and fossil meteoric-hydrothermal systems during the past few decades (see review by Criss and Taylor, 1986), it was only recently that a new and conceptually different kind of meteoric-hydrothermal oxygen-isotope signature was discovered by Gazis et al. (1996) in their study of the 2.8 Ma Chegem caldera (11 x 15 km) in the Caucasus Mountains. Those authors describe a 750-m-thick stratigraphic zone in the upper part of the intracaldera tuff where hydrothermally exchanged,  $^{18}\text{O}$ -depleted, glassy to partially devitrified groundmass coexists with feldspar and quartz phenocrysts that have closely preserved their original magmatic  $\delta^{18}\text{O}$  values. This volcanic glass contains up to 4.5 wt%  $\text{H}_2\text{O}$  and has a very low (i.e., meteoric)  $\delta\text{D}$  value, clearly demonstrating that this zone in the upper part of the tuff interacted in some way with large amounts of low- $^{18}\text{O}$ , low-D meteoric waters at high temperatures ( $> 300^\circ\text{C}$ ).

It is well known that feldspars exchange rapidly with hydrothermal fluids, both in the laboratory and in nature (e.g., O'Neil and Taylor, 1967; Taylor, 1974). Thus, a question that had to be answered by Gazis et al. (1996) was: How could feldspar phenocrysts retain their magmatic  $\delta^{18}\text{O}$  values ( $> +7$ ) while the surrounding, apparently pristine, glassy groundmass was undergoing pervasive exchange that resulted in  $\delta^{18}\text{O}$  values as low as  $-8$ ? In virtually all earlier studies of volcanic rocks from either active or fossil geothermal areas

(e.g., see Criss and Taylor, 1986; Larson and Taylor, 1986a), both the feldspar phenocrysts *and* the coexisting groundmass are: (a) at least partially hydrothermally altered and replaced by OH-bearing minerals such as sericite, saussurite, chlorite, kaolinite, etc.; and/or (b) significantly depleted in  $^{18}\text{O}$  relative to their coexisting quartz phenocrysts (quartz is one of the more resistant minerals to hydrothermal  $^{18}\text{O}$  exchange, and unlike feldspar, it usually closely retains its primary magmatic  $\delta^{18}\text{O}$  value in such situations).

Gazis et al. (1996) attempted to solve the above dilemma by postulating that the unique combination of  $^{18}\text{O}$  signatures in feldspar and glass at Chegem was the result of an intense, short-lived ( $\approx 25$  years duration), very high temperature (500-650°C) meteoric-hydrothermal event. Although such an explanation for low- $^{18}\text{O}$  rocks had never before been postulated, this seemed to be the only geologically plausible mechanism that was compatible with evidence that the Chegem event had to be (1) hot enough that typical OH-bearing hydrothermal minerals did not form, (2) sufficiently vigorous that very large amounts of low- $^{18}\text{O}$  groundwaters were advected through the upper 750 m of intracaldera tuff, and (3) on a time-scale short enough that the  $\delta^{18}\text{O}$  values of feldspar phenocrysts were virtually unchanged. The postulated mechanism was theoretically feasible because, under hydrothermal conditions, silicate glass is known to exchange  $^{18}\text{O}/^{16}\text{O}$  several orders of magnitude faster even than feldspar (e.g., Zhang et al., 1991).

Gazis et al. (1996) conjectured that the surface expressions of such a shallow, caldera-wide system might be analogous to the vigorous fumarolic activity (measured steam temperatures as high as 645°C) observed in 1916-1919 across the surface of the 20-km-long, 4- to 10-km-wide, 200-m-thick, welded ash-flow sheet that filled the Valley of Ten Thousand Smokes, Alaska (e.g., Hildreth, 1983). Enormous numbers of spectacular, high-velocity steam jets (Fig. 1.1) were seen when that valley was first visited by scientific expeditions 4 to 7 years after the June 6-7, 1912, eruption of that tuff from Novarupta volcano adjacent to Mt. Katmai (Allen and Zies, 1923; Griggs, 1922; Shipley, 1920; Zies, 1929). Unfortunately, in the limited time available for field studies at Chegem, Gazis et al.

(1996) did not observe any definitive geological evidence for fumarolic activity, and therefore they could not directly relate these newly discovered  $^{18}\text{O}/^{16}\text{O}$  systematics to the locations of fossil fumaroles.

### *1.1.2. Statement of the Thesis Research Problem*

The present thesis project was initiated in order: (1) to test the ideas and concepts put forth by Gazis et al. (1996); and (2) to integrate a set of oxygen isotope studies with previously documented mineralogical and geomorphological evidence of fumarolic activity in ash-flow tuffs. Because high-temperature fumarolic activity was actually observed and scientifically documented 80 years ago in the Valley of Ten Thousand Smokes, that was an obvious locality to consider for this type of research, particularly because on the surface of that ash-flow sheet there are numerous and spectacular fresh examples of surficial fumarolic morphology and mineralogical alteration. However, in addition to the logistical problems associated with sampling such a remote locality, there are many limitations associated with this site, most notably the fact that erosion has exposed only the uppermost 20-30 m of tuff in the thickest, most densely welded parts of the deposit, and hence only the shallowest portions of the fumarolic plumbing system are exposed. If it ever becomes possible to obtain a series of deep drill cores from the ash-flow tuff in the Valley of Ten Thousand Smokes, that locality might ultimately provide the best possible test of the mechanism proposed by Gazis et al. (1996). However, given the present circumstances, it was determined that it would be better to conduct the initial investigations on fossil fumaroles in an ash-flow tuff where the deeper parts of the fumarolic systems are already exposed by erosion.

Because of a favorable combination of scientific and logistical attributes, it was determined that one of the best localities to study the  $^{18}\text{O}/^{16}\text{O}$ -effects of fumarolic activity in ash-flow tuffs might be the Bishop Tuff, which erupted at 0.76 Ma (Bogaard and Schirnick, 1995; Izett and Obradovich, 1991) from Long Valley caldera (Bailey et al.,

1976; Hildreth, 1979; Wilson and Hildreth, 1997) in the eastern Sierra Nevada, California. This tuff formed from an ignimbrite eruption that was much larger than the one at the Valley of Ten Thousand Smokes in 1912 ( $\approx 750 \text{ km}^3$  vs.  $\approx 30 \text{ km}^3$ ; Bailey et al., 1976; Hildreth, 1983; Sheridan, 1970). However, because it also spread laterally over a much broader area, the thickness of the Bishop Tuff outflow sheet is similar to the one in the Valley of Ten Thousand Smokes ( $\approx 200 \text{ m}$ ).

Fumaroles are thought to have been active on the surface of the Bishop Tuff outflow sheet immediately after its emplacement. The outflow sheet extends southeastward for about 35-40 km from Lake Crowley toward the town of Bishop (Fig. 1.2), and fumarole morphology is well-developed over wide areas, in the form of fumarolic mounds, ridges, and mineral encrustations, etc. (Sheridan, 1970). In addition, deep gorges have locally cut more than 150 meters down into the tuff to expose the joints, fissures, and conduits that represent the inner workings of these fumarolic mounds. The morphology and structure of these fossil fumaroles have been thoroughly described by Sheridan (1970).

The petrology and geochemistry of the Bishop Tuff itself have been extensively studied, and the mineralogical and isotopic relationships at the magmatic stage are well documented (Halliday et al., 1984; Hildreth, 1979; Taylor, 1968). Also, the Bishop Tuff is even younger than the Chegem Tuff, and because of the degradation, hydration, and  $^{18}\text{O}$ -enrichment observed in all occurrences of volcanic glass/groundmass that are subjected to lengthy contact with Earth's surface environment (e.g., Taylor, 1968), it is essential that these kinds of stable isotope studies be undertaken on the most recently erupted and most deeply eroded ash-flow tuffs that one can find. Finally, no hydrothermal systems associated with later igneous activity have been superimposed upon the fumarolic features since this ash flow came to rest, nor has post-emplacement deformation significantly complicated the ash-flow tuff stratigraphy (Bateman, 1965; Sheridan, 1970).

In order to further explore the second goal of this thesis project, i.e., to integrate an  $^{18}\text{O}/^{16}\text{O}$  studies with previously documented mineralogical and geomorphological evidence

for fumarolic activity in ash-flow tuffs, a limited number of samples were also analyzed from the ash-flow tuff that filled the the Valley of Ten Thousand Smokes. Samples from the upper part of this tuff in the vicinity of fumarolic mounds and ridges were collected in 1998 to evaluate the  $^{18}\text{O}/^{16}\text{O}$  systematics of the near-surface portions of fumaroles that were active during the period 1917-1919, and which were studied by scientists who recorded the temperatures and compositions of fumarolic gases (Allen and Zies, 1923; Shipley, 1920; Griggs, 1922). Notwithstanding the limitations on sampling that come about because the level of erosion is no more than 30 m deep in the upper part of the valley where the tuff is most densely welded, samples from the Valley of Ten Thousand Smokes are important because this is the only locality on Earth where this type of fumarolic activity is part of the historical record and where such activity has been scientifically observed and documented.

## **1.2. The 0.76 Ma Bishop Tuff Outflow Sheet, California**

### *1.2.1. Volcanic History Associated with Long Valley Caldera*

Long Valley caldera is a large, elliptical (17 X 32 km), east-west oriented subsidence structure located on the west edge of the Basin and Range province on the north end of Owens Valley, and nestled against the base of the eastern edge of the Sierra Nevada frontal fault escarpment (Bailey et al., 1976). A 500-m-high resurgent dome, surrounded by an annular depression or caldera moat, is located to the west of the center of the caldera (Fig. 1.2). The younger Mono-Inyo Craters volcanic chain forms a  $\approx 27$ -km-long, locally discontinuous line of volcanic domes and craters that intersect the western margin of Long Valley caldera.

The volcanic history of the region is summarized by Bailey et al. (1989). Precaldera rocks are composed of the Mesozoic granitic rocks of the Sierra Nevada batholith and Paleozoic-Mesozoic metavolcanic roof pendants (Bailey et al., 1989). The earliest late Tertiary to Quaternary igneous activity in the area began at 3.6 Ma and consisted of

widespread eruption of trachybasaltic-trachyandesitic lavas. Between 3.0 and 2.5 Ma, quartz latite lavas and tuffs erupted on San Joaquin Ridge and Bald Mountain (Bailey et al., 1989). Activity continued with the eruption of high-silica rhyolite on Glass Mountain between 2.1 and 0.8 Ma (Metz and Mahood, 1985).

Eruption of the Bishop Tuff and consequent formation of Long Valley caldera occurred at 0.76 Ma (Bogaard and Schirnick, 1995; Izett and Obradovich, 1991). A volume of 750 km<sup>3</sup> of rhyolite magma was erupted, of which ≈600 km<sup>3</sup> was deposited within the caldera. The remainder (150 km<sup>3</sup>) was deposited outside the caldera either as (1) ash-flow tuff over ≈1200 km<sup>2</sup> of low-lying area around the caldera or (2) as ash-fall over an area extending from the Pacific Ocean (Sarna-Wodjicki et al., 1987) to Kansas (Izett et al., 1970; Izett, 1982).

Volcanic activity within the caldera continued with simultaneous eruption of aphyric rhyolite (early rhyolites, 0.7-0.6 Ma) and formation of a resurgent dome (Smith and Bailey, 1968). Subsurface injections of dikes and sills of early rhyolite in the caldera fill beneath the resurgent dome also occurred (McConnell et al., 1995). Crystal-rich rhyolite (moat-rhyolites) erupted in clockwise succession around the resurgent dome at 0.5, 0.3, and 0.1 Ma. Trachybasalt and trachyandesite magma petrologically associated with the Mono-Inyo Craters volcanic chain erupted in the western moat beginning at about 300-200 ka (Bailey et al., 1989). Later eruption of quartz latite and low-silica sodic rhyolite (200-50 ka) formed Mammoth Mountain on the western rim of the caldera.

Volcanic activity in the form of hot springs, CO<sub>2</sub> emissions, active deformation, and high levels of seismic activity occur in this region today. Most of these effects are localized in the western part of the caldera and beneath Mammoth Mountain. Heightened CO<sub>2</sub> emissions around fissures on the southeast flank of Mammoth Mountain near Horseshoe Lake, as well as localized seismic activity, has led to speculation that active shallow dike injection is occurring at the present time beneath Mammoth Mountain (Farrar et al., 1998).



### *1.2.2. Formation of Long Valley Caldera and Eruption of the Bishop Tuff (0.76 Ma)*

A model of caldera development and eruption dynamics for Long Valley caldera has been constructed using detailed volcanic stratigraphy and lithic abundances of the Bishop ash and ash-flow tuff (Hildreth and Mahood, 1986; Wilson and Hildreth, 1997). Early work suggested that eruption began in the south-central part of the caldera with Plinian activity, which then gave way to ash-flow eruption as the vent migrated counter-clockwise around the caldera ring-fracture (Hildreth and Mahood, 1986). While later work has confirmed the initial vent position, expanded data on lithic fragments and a more detailed stratigraphic evaluation of the Bishop Tuff outflow sheet indicates that Plinian and ignimbrite activity occurred simultaneously from vents along the north and south margins of the caldera, both of which propagated eastward towards Glass Mountain during eruption (Wilson and Hildreth, 1997). Caldera formation and consequent eruption and emplacement of Plinian ash-fall deposits and the Bishop Ignimbrite is estimated to have occurred over a time period of about 100 hours (Wilson and Hildreth, 1997). During this 4-day period, ash-flow tuff was deposited in three general areas; (1) to the north of the caldera in Mono Basin and Adobe Valley, (2) to the west of the caldera along the San Joaquin River drainage, and (3) to the south and southeast of the caldera at the north end of Owens Valley.

Ash-fall deposits intercalated in the southeastern lobe of the Bishop Tuff divide it into two "ignimbrite subpackages"; Ig1E and Ig2E (Wilson and Hildreth, 1997). Ig1E and Ig2E can be further subdivided based on intercalated pumice and variabilities in welding zonation into Ig1Ea and Ig1Eb and Ig2Ea, Ig2Eb, and Ig2Ec, respectively. Time breaks separating these stratigraphic units are minutes to hours at most (Wilson and Hildreth, 1997).

### *1.2.3. The Bishop Tuff Magma*

The Bishop Tuff is a compositionally zoned high-silica rhyolite, and studies of this ash-flow sheet have been the foundation of our present understanding of compositional zonation in silicic magma chambers (e.g., Hildreth, 1979; Michael, 1983; Cameron, 1984; Halliday et al., 1984; Anderson et al., 1989; Wolff et al., 1990; Anderson, 1991; Dunbar and Hervig, 1992; Hervig and Dunbar, 1992; Lu et al., 1992; Christensen and DePaolo, 1993; Bogaard and Schirnick, 1995; Duffield et al., 1995). From compositions of Fe-Ti oxide phenocrysts in the Bishop Tuff, Hildreth (1979) calculated magmatic temperatures for the rhyolite to be in the range 720°C to 790°C, and he showed that these temperatures were correlated with variations in phenocryst assemblage and composition, as well as with whole-rock major and trace element abundances. While recent reevaluation of the timing of the eruptive sequence call for some refinements of these conclusions regarding compositional zonation within the Bishop magma chamber (Wilson and Hildreth, 1997), there is no question that hotter magmatic temperatures are correlated with more mafic magma compositions.

### *1.2.4. The Bishop Tuff Outflow Sheet*

The Bishop Tuff outflow sheet crops out over a 900 km<sup>2</sup> area in roughly 3 geographical areas around Long Valley caldera: (a) a northern area, which includes Hildreth's (1979) Adobe Valley and Mono Basin Lobes; (b) a western area along the San Joaquin River encompassing Hildreth's (1979) San Joaquin Lobe; and (c) a southeastern area, which includes Hildreth's (1979) Chidago Lobe, as well as the Gorges and Tableland eruptive units. It is in the last of these areas that abundant fossil fumaroles are present in the outflow sheet (Sheridan, 1970). Although the southern limit of the southeastern lobe of the Bishop Tuff is defined by erosion along the Owens River in Pleasant Valley, the ash-flow sheet itself continues to the south buried beneath younger sediments in Owens Valley (Bateman, 1965).

The Bishop Tuff shows the characteristic zones of welding, devitrification, and vapor-phase alteration that are typical of thick ash-flow tuffs (e.g., Smith, 1960; Christiansen, 1979). The southeastern exposure of the Bishop Tuff outflow sheet, in which fossil fumaroles are abundant, is up to 200 m thick, and in middle Owens Gorge, the tuff exhibits a very densely welded, devitrified zone (up to 120 m thick) lying beneath an upper, partially welded zone affected by vapor phase alteration (up to 80 m thick). However, the Bishop Tuff is a composite sheet (Sheridan, 1968; Sheridan and Ragan, 1972; Hildreth, 1979), and the geometry of welding zonation in the southeastern exposures of the Bishop Tuff varies dramatically. The down-river portion of Owens Gorge is composed of two cooling units (Sheridan, 1968), which formed by depositional shingling of the Gorges and Tableland Units. Also, in the vicinity of the basement high in the up-river portion of Owens Gorge, the densely welded Gorges Unit is separated into two sub-units by a non-welded stratigraphic interval (Wilson and Hildreth, 1997).

#### *1.2.5. Deformation and Erosion of the Southeastern Lobe of the Bishop Tuff*

The surface of the southeastern lobe of the Bishop Tuff, which is referred to as the Volcanic Tableland, is marked by hundreds of generally north-striking fault scarps (Bateman, 1965; Sheridan, 1975). While large offsets of the Bishop Tuff occur at the margins of the fault block ranges of the Sierra Nevada, Casa Diablo Mountain, and the White Mountains (Sheridan, 1975), faults on the Volcanic Tableland are relatively small (<15 m high and < 2 km long; Bateman, 1965) and extensional in nature (Pinter, 1995; Bateman, 1965). Some of these fault scarps record active slip and tectonic deformation in northern Owens Valley (Pinter, 1995). Bateman (1965) pointed out that the Volcanic Tableland has been warped around a broad north-trending arch located just east of Owens Gorge, and he identified three pre-warp consequent drainages cutting the surface of the Volcanic Tableland in a roughly east-west direction. Two of these drainages are no longer

active, and the third hosts Rock Creek and the Owens River in Birchim Canyon and the lower part of Owens Gorge.

The southeastern lobe of the Bishop Tuff outflow sheet is dissected by three deep (up to 200 m) gorges: Rock Creek Gorge, Owens Gorge, and Chidago Canyon (Fig. 1.2). Putnam (1960) hypothesized that Owens River and Rock Creek dissected the tuff by headward erosion. His theory was that Rock Creek originally flowed into Pleistocene Long Valley Lake, which formed when the Bishop Tuff eruption impounded the stream emptying Long Valley to the south. Long Valley Lake was subsequently drained by stream capture along the Owens River drainage, and it is thought that Lower Rock Creek then captured the upper part of Rock Creek drainage (see Putnam, 1960; Fig. 3). Bailey et al. (1976) suggest that Long Valley Lake overflowed over the surface of the tuff rather than being drained by stream capture. Currently, abundant groundwater is known to flow underground between the two drainages from a sharp bend in Rock Creek near Tom's Place to springs in the west wall of Owens Gorge (Putnam, 1960).

#### *1.2.6. Fossil Fumaroles in the Bishop Tuff Outflow Sheet*

Fossil fumaroles are present in abundance only in the southeastern part of the Bishop Tuff outflow sheet (Sheridan, 1970). These fumaroles are thought to have been active immediately after emplacement of the Bishop Tuff. On the surface of the outflow sheet, fumarole morphology is well developed at numerous sites within the three broad areas (described in detail below in Chapter 3) in the form of fumarolic mounds, ridges, and mineral encrustations (Sheridan, 1970). Exposed within the three deep gorges that cut the surface of the tuff are joints, fissures, and conduits that represent the inner workings of these fumarolic mounds. On the cliff faces in the deep canyons, one can observe areas where the well-developed, typically near-vertical columnar joints locally bend around and become shallow-dipping; Sheridan (1970) has shown that such zones are invariably associated with the conduits of fossil fumaroles.

### **1.3 The 87-year-old tuff from the Valley of Ten Thousand Smokes, Katmai National Park, Alaska**

#### *1.3.1. Geologic Setting*

An extensive and fairly detailed description of the 1912 eruption at the Valley of Ten Thousand Smokes, Alaska, is given below. Such a discussion is necessary for two reasons: (1) a few samples were analyzed from this area for comparison with  $^{18}\text{O}/^{16}\text{O}$  data from fossil fumaroles in the Bishop Tuff, and (2) the hydrothermal phenomena associated with the Valley of Ten Thousand Smokes represent the only available directly observed examples of the kind of short-lived, high temperature, fumarolic activity in ash-flow tuffs that forms the main part of this thesis study. The 1912 eruption was the largest of this century and one of the three largest in recorded history. It is one of the few historic eruptions to have produced welded tuff, and it is unusual among historic eruptions in that it deposited a large volume of ignimbrite on land. It is also unusual in that persistent fumaroles were active on the surface of the ash-flow sheet up to 25 years after eruption. In addition, the eruption at the Valley of Ten Thousand Smokes was only one of two in the entire geologic history of the 2500-km-long Aleutian chain to produce high-silica (up to 77%  $\text{SiO}_2$ ) rhyolite (the other location is Unmak Island; Byers, 1961). Appreciable volumes of pyroclastic flow deposits of Holocene and late Pleistocene age are fairly common along the Aleutian arc (Miller and Smith, 1977). Although this volcanic arc is predominantly andesitic-dacitic, lavas and ejecta with  $>66\%$   $\text{SiO}_2$  occur at at least six volcanic centers.

Another thing that makes the Valley of Ten Thousand Smokes area geologically unusual with respect to the rest of the Aleutian arc is the large concentration of active volcanoes in such a small geographic area. It is also unusual in that this geographic area is located about 10 km behind (i.e., to the north of; Fig. 1.3) the main part of the volcanic arc (Hildreth, 1987). The Valley of Ten Thousand Smokes is set in the midst of five large

composite volcanoes (Mt. Mageik, Mt. Martin, Trident, Mt. Katmai, Novarupta, and Mt. Griggs) and two dacite domes (Cerberus and Falling Mountain), all within 25 km of one another and all of which have exhibited Holocene eruptive activity (Fig. 1.4). Intermittent steam vents are presently observed at all five of the large eruptive centers, as well as at the actual vent of the 1912 eruption at Novarupta dome, and 0.5 km<sup>3</sup> of andesite and dacite lava were erupted from Mt. Trident in the 1950's.

### *1.3.2. The 1912 Eruption Events and Sequence of Eruptive Products*

Hildreth (1983) gives an excellent summary of the chronology of the 1912 eruption of Novarupta and Mt. Katmai. Hildreth's (1983) summary comes mainly from the reports of Martin (1913; and unpublished USGS field notes) who visited Kodiak, Uyak, Katmai village, and Cold Bay in August of 1912 to interview people from the district about the eruption. As reported by Hildreth (1983) the most reliable information about the eruption comes from the geologic record and from visual observations recorded aboard the steamer Dora, which was plying the Shelikof Strait northeastward on its way from Uyak at the time of eruption.

Earthquake activity in the area began as early as May 31, and severe shocks were felt on June 4 and 5. On the morning of June 6, explosions were heard as far as 240 km away. That afternoon, at 1300 hours, the steamer Dora reported a tephra column, which engulfed the vessel by 1500 hours and began dropping ash on Kodiak Island at 1700 hours (see Fig. 1.3). A major earthquake shock and an explosion heard throughout the region accompanied the first sighting of the tephra column. Eruptions continued for another 60 hours, punctuated by major earthquake shocks and renewed vigorous ash falls at  $\approx$ 2300 on June 6 and  $\approx$ 2240 on June 7.

Later work in the Valley of Ten Thousand Smokes and on Kodiak Island has elucidated the sequence of eruptive products from the 1912 eruption (Curtis, 1968; Hildreth, 1983 and 1991). Curtis (1968) studied the stratigraphy of the ash fall and ignimbrite deposits in

the Valley of Ten Thousand Smokes, and he showed that most of the 1912 ejecta vented from a subsidence structure beneath Novarupta dome. Further work in the area showed that the ash-flow was erupted during the same 20-hour period that ash-fall layers A and B were being deposited from the Plinian column (Hildreth, 1983). Plinian eruptions continued after deposition of the ash-flow tuff and deposited ash-fall layers C-D and F-G (Curtis, 1968; Hildreth, 1983). Collapse of the summit of Mt. Katmai occurred synchronously with the deposition of both ash-fall layer B and the ash-flow tuff and was probably accompanied by the strong earthquake felt at  $\approx 2300$  on June 6 (Hildreth, 1991). However, no juvenile material appears to have vented from Mt. Katmai itself during the 1912 eruption (Hildreth, 1991).

### *1.3.3. The 1912 Ash-Flow Sheet*

The 1912 ash-flow extends more than 20 km from the source (Fig. 1.4) and was deposited over an area of  $\approx 120$  km<sup>2</sup> largely confined to the Valley of Ten Thousand Smokes; one flow lobe passed southward over Katmai Pass into Mageik Creek (Hildreth, 1987). The main ash-flow sheet is a composite deposit of at least one major and several minor flow units, all emplaced in quick succession (Hildreth, 1987). Pumice clasts early in the ash-flow sequence were predominantly rhyolitic (77%SiO<sub>2</sub>), and dacitic (66-64.5%SiO<sub>2</sub>), with andesitic (61.5-58.5%SiO<sub>2</sub>) pumice joining the rhyolite in proportions that generally increase upward throughout the flow sequence (Hildreth, 1983; 1987). Although the presence of banded pumice with different mixtures of all three of these compositions in the ash-flow sheet illustrates co-mingling of all three of these magmas during eruption, it is unlikely that these magmas were mixed before eruption (Hildreth, 1983). Phenocrysts of plagioclase, orthopyroxene, titanomagnetite, ilmenite, apatite, and pyrrhotite are present in all compositions of pumice; in addition, clinopyroxene is common in dacite and andesite, rhyolite contains quartz, and andesite contains rare olivine (Hildreth, 1983). The rhyolite contains only 1-2% phenocrysts, whereas the andesite and dacite

typically contain 30-45% phenocrysts. Pre-eruptive temperature estimates made using Fe-Ti oxides are 805<sup>o</sup>-850<sup>o</sup>C for the rhyolite, 855<sup>o</sup>-955<sup>o</sup>C for the dacite, and 955<sup>o</sup>-990<sup>o</sup>C for the andesite (Hildreth, 1983).

The  $\approx 11 \text{ km}^3$  of ash-flow tuff in the Valley of Ten Thousand Smokes is distributed in a sourceward-thickening pattern, the distal portions of which are unwelded. Estimates of the thickness of the tuff based on geophysical evidence (Kienle, 1991) and reconstruction of stream channels (Curtis, 1968) suggests that there is a zone of welded tuff  $\approx 200 \text{ m}$  thick in the midvalley and in the upper parts of the River Lethe and Knife Creek drainages (Fig. 1.4). A "high-sand mark" observed by Griggs (1922) along the edge of the deposit in the upper part of the Valley of Ten Thousand Smokes marks the original level of the surface of the ash-flow sheet; this surface was then lowered during differential compaction of the tuff as a result of welding in the upper part of the valley (Hildreth, 1983). Thus, although the size ( $\approx 15 \text{ km}^3$ ) of the eruption at the Valley of Ten Thousand Smokes was much less than that of the  $760 \text{ km}^3$  eruption of the Bishop Tuff, the maximum thickness of the ash-flow sheet deposited by these two events is approximately the same. This is because the Bishop Tuff outflow sheet spread out over a much wider area (see Fig. 1.2) than the tuff in the Valley of Ten Thousand Smokes, which was for the most part confined within the drainages defined by the River Lethe and Knife Creek.

Because welding depends to a great degree on thickness of the ash-flow deposit, we might *a priori* expect that the welding zonation in the Valley of Ten Thousand Smokes would be similar to that in the Bishop Tuff outflow sheet. A reinterpretation of existing geophysical data by Kienle (1991) identified a possible boundary between unwelded and partially welded tuff in both the Knife Creek and the River Lethe drainages to be at a depth between 20 and 35 m. Kienle (1991) noted that the River Lethe has cut to an erosion-resistant base about 30 m depth, which he interpreted as the depth of the boundary between unwelded and partially welded tuff in that location. This is also the approximate depth of the transition from unwelded to partially welded tuff in  $\approx 200\text{-m}$ -thick sections of the



Bishop Tuff outflow sheet exposed in Owens River Gorge (see Chapter 2). Also, Fig. 2 of Kienle (1991) shows that the boundary between partially welded and densely welded tuff is located at a depth of  $\approx 60$  m in the River Lethe drainage in a location where the tuff is  $\approx 150$  m thick. This same transition occurs at a depth of  $\approx 80$  m in the Bishop Tuff outflow sheet where the total thickness is  $\approx 200$  m. This slight difference may in part reflect the more mafic average composition of the tuff in the Valley of Ten Thousand Smokes, which would likely decrease the overburden pressure necessary to induce dense welding in the tuff. However, the major factor is undoubtedly the local variation in thickness of these ash-flow sheets.

An analogous transition in welding zonation has not been observed on seismic refraction profiles in the Knife Creek drainage, perhaps because the diffuse nature of this type of density transition makes it difficult to observe if it is not at a relatively uniform depth. The depth of this transition is probably continuous over a fairly wide area in the River Lethe drainage, which is a relatively U-shaped drainage where the thickness of the deposit is a relatively constant  $\approx 150$  m (see Fig. 3 of Kienle, 1991). In contrast, the Knife Creek drainage is more V-shaped, and the thickness of the deposit probably varies widely over short distances.

#### *1.3.4. Fumarolic Vapors: Temperatures and Compositions*

It is unfortunate that no observations were made of the Valley of Ten Thousand Smokes until 1916, 4 years after the eruption of the ash-flow tuff. However, following Robert Griggs' initial discovery of the enormous numbers of fumaroles in this area on the last day of a National Geographic Society expedition in 1916, during the next three summers there were numerous attempts to study the fumarolic gases emanating from the surface of this ash-flow tuff. During the 1917 expedition, Shipley (1920) made the first scientific observations of the fumaroles, commenting on the chemical compositions and temperatures of the fumarolic gases, as well as discussing the nature of the fumarolic

encrustations. Because of constraints associated with United States involvement in World War I, Sayre and Hagemberger were the only two researchers who returned to the valley in 1918 to measure the temperatures of the fumaroles. Their results are reported by Allen and Zies (1923), who took part in a 1919 expedition to the valley, carrying more sophisticated instruments for measuring fumarole temperatures and conducting chemical studies of the fumarolic gases and their encrustations. Documentation of the waning stages of fumarolic activity in the valley comes mainly from photographs by B. Hubbard taken in 1929, 1931, and 1935 (see Keith, 1991).

The earliest observations of fumarolic vapors conducted by Shipley (1920) in 1917 are crucial, despite the fact that the expedition that year carried just a mercury thermometer, meaning that they could only measure temperatures up to 357°C (the boiling point of mercury). At this point in time, the fumaroles had already been active for a period of 5 years, and comparative studies of fumarole temperatures later showed that there was considerable waning in fumarolic activity in the 1-year period between 1918 and 1919 (Allen and Zies, 1923). Many high-temperature fumaroles measured by Sayre and Hagemberger in 1918 could no longer be found in the following year, and the ones that could be identified had drastically reduced temperatures (Allen and Zies, 1923). It thus seems certain that the fumarolic activity in the valley had already begun to undergo a serious decline by the time that accurate temperature measurements of the fumaroles were finally being carried out.

The 1917 observations by Shipley (1920) indicate that the greatest amounts of escaping gases poured out of large, well-defined fumarolic vents. The gases from these larger vents exited under considerable pressure, and at temperatures much higher than a mercury thermometer would measure (>357°C). Volcanic emanations were also observed to be exuded from the surface of the tuff over large areas not possessing any visible orifice. The latter areas exhibited temperatures from 10°C-100°C, with the higher temperatures found only in open vents or cracks in the surface of the tuff. Shipley (1920) also reports that the

gases emitted consisted almost entirely of water vapor. However, in contrast to all of the gas samples collected in 1919 by Allen and Zies (1923), a few fumaroles studied in 1917 were observed to be emitting gases that were nearly anhydrous, and hydrochloric and hydrofluoric acids were observed to be ubiquitous constituents of the fumarolic vapors. The main component of fumarolic vapors analyzed in 1919 by Allen and Zies (1923) was H<sub>2</sub>O vapor (in all cases >98.8%), which contained an average of 0.4% of soluble gases including hydrochloric acid, hydrofluoric acid, hydrogen sulfide, and boric acid (Zies, 1929). The remaining gases collected from fumaroles in 1919 consisted mostly of CO<sub>2</sub>, H<sub>2</sub>S+H<sub>2</sub>, and N<sub>2</sub>, as well as varying smaller amounts of CO and CH<sub>4</sub>; O<sub>2</sub> and argon were probably contaminants (Allen and Zies, 1923).

In 1919, Allen and Zies (1923) used a thermocouple to measure numerous fumarolic temperatures greater than 450°C, including the highest fumarole temperature (645°C) yet recorded at the Valley of Ten Thousand Smokes. Nevertheless, they were convinced from several lines of evidence that the fumarolic activity in the valley had already begun to decline. First, in nearly every instance, the fumarole temperatures measured by Allen and Zies in 1919 were lower than those measured by Sayre and Hagelberger from exactly the same fumaroles one year earlier (Fig. 1.5). Additionally, Allen and Zies observed many extinct fumaroles in 1919, especially at the distal ends and around the margins of the ash-flow sheet. They also observed hot springs (97°C) near Three Forks (Fig. 1.4) in a location that had been observed to be vigorously steaming only two years earlier in 1917 (Griggs, 1922). Finally, Fenner reported to Zies (1929) that fumarole 148 (Fig. 1.5), which was measured at 239°C in 1919, had cooled to 97°C in 1923. Accompanying the decrease in temperature at fumarole 148 was a change in incrustation mineralogy around the fumarole from magnetite to sphalerite, galena, and copper sulfides.

These early expeditions found that it was not uncommon for temperatures from nearby fumaroles to be vastly different from one another. For example, Allen and Zies (1923) reported that in 1919, fumaroles with temperatures of ≈100°C could often be found

directly adjacent to fumaroles having much higher temperatures ( $>200^{\circ}\text{C}$ ). Also, just as Shipley (1920) discovered in 1917, Allen and Zies (1923) noted that the ground was typically at a temperature of about  $100^{\circ}\text{C}$  just below the surface in the general vicinity of fumarole vents.

#### *1.3.5. Sources of the Fumarolic Vapors*

Although the minor constituents of the fumarolic vapors ( $\text{HCl}$ ,  $\text{HF}$ ,  $\text{H}_2\text{S}$ , etc.) are undoubtedly magmatic in origin, Allen and Zies (1923) discussed several lines of evidence suggesting that the major source of  $\text{H}_2\text{O}$  supply to the fumaroles was from streams that flowed out onto the surface of the ash-flow sheet. They performed a simple mass balance calculation comparing the discharge of the two largest rivers (Knife Creek and the River Lethe), as they entered the head of the valley, with the discharge of the only watercourse that drained the valley, which at that time was a small, hot ( $72^{\circ}$ - $78^{\circ}\text{C}$ ) stream that flowed into Windy Creek near Three Forks (Fig. 1.4). Their calculation did not take into account myriad smaller watercourses that flowed into the valley or precipitation on the surface of the ash-flow sheet itself, and therefore there may be considerable errors in their estimate that 11% of the water flowing into and onto the ash-flow tuff left it downstream in Windy Creek. Nevertheless, their conclusion that at least 89% of the inflowing water was incorporated into fumarolic vapors is undoubtedly quite robust. Allen and Zies (1923) noted that many small rivers that flowed out over the surface of the tuff disappeared completely within a kilometer or so of where they entered the valley. They also showed that the percentage of  $\text{H}_2\text{O}$  in the fumarolic vapors was higher in areas that would be expected from the topography to have a higher influx of these surface-derived waters. Keith (1991) cites a lot of this evidence of Allen and Zies (1923), pointing out that fumaroles in the non-welded parts of the ash-flow sheet were concentrated along pre-eruptive river channels and along the Buttress range where surface water drains directly onto the surface of the tuff. Thus there is ample evidence from direct observations by

scientists in these early expeditions that fumaroles in the Valley of Ten Thousand Smokes were supplied primarily by meteoric H<sub>2</sub>O draining into, or falling upon, the surface of the tuff.

#### *1.3.6. Fumarole Morphology*

While early visitors to the Valley of Ten Thousand Smokes proposed a classification scheme for fumarolic vents based on morphology and temperature of fumarolic vapors (Allen and Zies, 1923), it was apparent even without the knowledge of significant depth exposures of these vents that most were essentially of the fissure type. Allen and Zies (1923) observed the rectilinear arrangement of fumarolic vents and suggested that these alignments of the majority of fumaroles in the valley indicated that they were emanating from elongate fissures that extended deep into the ash-flow sheet. Keith (1991), with the advantage of exposures of these structures afforded by erosion along stream courses in the valley, suggested that the fumarole morphologies could be subdivided into fissure and funnel types. She observed that fossil fissure fumaroles were structurally controlled by well-developed vertical to subvertical fractures trending nearly perpendicular to the original direction of flow of the sintered and welded ash-flow sheet. She also asserted that the distribution of fumaroles in the valley was controlled by the amount of induration and the degree of welding of the ash-flow sheet, which were in turn controlled by the permeability and the degree of fracturing in the tuff.

Early workers to the Valley of Ten Thousand Smokes reported the presence of large fumarolic tunnels with diameters of up to 11 m at various depths in the ash-flow tuff (Shiple, 1920; Allen and Zies, 1923). Many of these tunnels were very shallow, and fumarolic gases emanated from their partially collapsed roofs. Indeed, tunnels of this sort were a real danger to explorers of the valley, at least in 1917, because a hiker might break through the shallow crust and fall into the hot gases below. Allen and Zies (1923) studied a few of these tunnels with a plumb bob and discovered that temperatures inside were high

(165°C and 222°C for fumaroles 30 and 112, respectively, see Fig. 1.5) and quite variable due to rather strong lateral currents of gas along the length of the tunnel. At the present time, only 87 years after eruption, there are few, if any, of these shallow tunnels still preserved at the Valley of Ten Thousand Smokes, probably because they have either collapsed or been filled by run-off debris from the surface (Keith, 1991).

### *1.3.7. Comparison with Morphological Features of Fossil Fumaroles in the Bishop Tuff*

Although Sheridan (1970) concluded that the fumarolic vapors in the Bishop Tuff outflow sheet were dominantly composed of magmatic H<sub>2</sub>O derived from the underlying tuff itself, he noted that the fossil fumarole morphology in the Bishop Tuff, including the rectilinear arrangement of vents, was very similar to the kinds of observations described above for the fumaroles in the Valley of Ten Thousand Smokes. However, in comparison with tunnels observed in the Valley of Ten Thousand Smokes, the sub-horizontal tubular conduits that are commonly preserved beneath the fumarolic mounds on the surface of the Bishop Tuff occur at much greater depths in the ash-flow sheet (i.e., they are typically located directly above the top of the very densely welded tuff). It may be that shallow tunnels directly analogous to those described in the Valley of Ten Thousand Smokes also once existed in the Bishop Tuff outflow sheet, but that they have since collapsed. There are many small (10-20 m diameter) circular to elongate closed basins on the surface of the Bishop Tuff outflow sheet that could be interpreted to have resulted from this type of collapse.

Fumarolic conduits exposed in the Bishop Tuff outflow sheet are composed of a continuum of morphologies between endmembers such as steep fissures and tubular conduits (see Chapter 2). The distribution and orientation of these features appear to be controlled by the fracture characteristics and also the primary permeability of the partially welded Bishop Tuff. Diminutive versions of steep fissures analogous to those observed in the Bishop Tuff outflow sheet have been observed beneath fumarolic mounds at Site ML

and Site KC in the tuff from the Valley of Ten Thousand Smokes (see Chapter 4). Thus, we may readily infer that larger versions of these steep fissures, analogous to the ones seen in the Bishop Tuff, probably also occur in the as yet unexposed, deep parts of the fumarolic plumbing systems of the Valley of Ten Thousand Smokes.

### *1.3.8. Mineralogy of Fumarolic Encrustations and Associated Alteration Assemblages*

Early workers in the Valley of Ten Thousand Smokes reported the presence of large volumes of primary fluorides, chlorides, and sulfates around active fumaroles; these have long since been removed by weathering processes and waning fumarolic and hot spring activity (Shiple, 1920; Allen and Zies, 1923; Zies, 1924 and 1929; Keith, 1991). As the temperatures declined, mineral assemblages stable in the early, high-temperature stages of fumarolic activity commonly became unstable, particularly in the presence of liquid H<sub>2</sub>O and during development of acidic conditions around the mouths of the fumaroles (Zies, 1929). Geochemical studies of the encrustations in the upper part of the tuff indicate that early-formed, high-temperature fumarolic encrustations were subsequently attacked and leached by acid gases formed in the later, cooler stages of fumarolic activity (Zies, 1929; Keith, 1991; Kodosky and Keith, 1993 and 1995; Papike et al., 1991).

Magnetite was locally preserved as a relict of high-temperature fumarolic activity in which the earlier deposits had generally been replaced by assemblages of sulfides and sulfates formed during late-stage acidic alteration. Keith (1991) observed that relict fumarolic encrustations preserved at the Valley of Ten Thousand Smokes, which are all rich in either magnetite or hematite, were concentrated in the ash-flow sheet along the upper parts of fumarolic conduits and in the near-surface ash-fall deposits. Both "magnetite-rich" and "hematite-rich" fossil fumaroles were observed to contain cristobalite, hydrated aluminum hydroxyfluoride (AHF), kaolinite, fluorite, alunite, opal, pyrite, sulfur, illite, and various Fe-hydroxides such as limonite and goethite (Keith, 1991). The hematite-rich vents typically contain larger amounts of the low-temperature minerals.

Studies of the conduits that fed the fissure fumaroles, which appear to be aligned along cooling joints in the underlying, sintered ash-flow tuff (Keith, 1991), show that the tuff adjacent to these conduits exhibits alteration assemblages analogous to the early, high-temperature, vapor-phase encrustations in the ash-fall deposits, indicative of leaching by acid gases during the waning stages of fumarolic activity (Keith, 1991; Papike et al., 1991; Kodosky and Keith, 1993 and 1995; Spilde et al., 1993). Fumarole 212 of Keith (1991) is a 1-3 cm wide vertical joint in the dacite-rich tuff (Fig. 1.5) along which the tuff has been leached and sintered as a result of the passage of fumarolic vapors (Papike et al., 1991). Ash and pumice-fall deposits on the surface of the ash-flow sheet above this conduit have encrustations of Fe-oxides and other minerals deposited by fumarolic vapors (Keith, 1991; Papike et al., 1991). Mineralogical and geochemical studies of fossil fumarole 212 (Spilde et al., 1993; Papike et al., 1991; Kodosky and Keith, 1993 and 1995) show that, relative to the unaltered protolith, the early, high-temperature, vapor-phase transport of halide or oxyhalide species of trace metals enriched the tuff beneath the fumarolic mound and adjacent to the conduit in F, Zn, As, Cr, Pb, Br, Ni, Sn, Sb, and Au out to a distance of at least 35 cm from the conduit. Because this suite of elemental enrichments is correlative with those measured around active, high-temperature (500<sup>o</sup>-800<sup>o</sup>C) fumaroles at Merapi volcano (Symonds et al., 1987), Papike et al. (1991) concluded that the entire sampling area at fumarole 212 was from the shallow part of a larger and deeper fumarole system. Late-stage, low-temperature Fe- and Cl-rich acidic condensates (Kodosky and Keith, 1993 and 1995) leached Fe, Mg, Ca, Cl, F, Sr, V, Sc, and Cs from the tuff adjacent to the conduit, consequently bleaching the tuff, and deposited these metals in the surface ash-fall interval. This process also resulted in preferential replacement of Ca-rich feldspar phenocrysts by amorphous silica out to a distance of ≈10 cm from the conduit (Spilde et al., 1993). Because of the presence of smectite and halloysite, which are unstable above 100<sup>o</sup>-150<sup>o</sup>C (Hurst and Kunkle, 1985; Velde and Meunier, 1987), Spilde et al. (1993)



estimate that the temperatures of late-stage mineralogical alteration were considerably lower than 200°C.

#### *1.3.9. Comparison with Mineralogical Features in the Bishop Tuff*

Sheridan (1970) observed that the tuff on either side of fissures in fossil fumarole mounds in the Bishop Tuff is typically bleached white, and that the central portions of these altered zones are hematite-stained and commonly coated with opal. Sheridan (1970) also asserted that because secondary mineral coatings are not found lining random orthogonal joints (cooling joints) in the Bishop Tuff, these cooling joints must have postdated vapor phase activity. However, Keith (1991) points out that there are also no mineral deposits along cooling joints in the tuff of the Valley of Ten Thousand Smokes, because this is where leaching of the tuff occurred, thereby implying that this might also have been the case in the Bishop Tuff.

While opal is a common component of fumarole mounds in the Bishop Tuff, it is typically not found below a depth of about 20 m. The only places that opal was observed in the Bishop Tuff below a depth of 20 m was locally along the walls of steep fissures or tubular conduits. In these instances, opal coats the surfaces of the tuff and extends no more than a few millimeters into the matrix of the adjacent tuff. Less commonly, epidote also coats the surfaces of fumarolic fissures deep in the tuff. Fissures and tubular conduits in the Bishop Tuff are also coated with tridymite (Sheridan, 1970). Locally, tridymite coatings show textures suggesting that it was partially dissolved by acidic fluids during fumarolic activity.

## Figure Captions

Fig. 1.1. Photograph of the Valley of Ten Thousand Smokes taken by R.F. Griggs in 1919, when fumaroles on the floor of the valley were still active. Lines of fumaroles across the valley spring from fissures in the ash-flow tuff. View is looking northwest from the northern foot of Baked Mountain towards the Buttress Range.

Fig. 1.2. Map of Long Valley caldera and vicinity showing the distribution of the Bishop Tuff outflow sheet (dark grey shading; Hildreth and Mahood, 1986). The outcrop area of the Early Rhyolites in the resurgent dome of the caldera is shown by the hatched pattern (Bailey et al., 1976). The areas of extensive fumarolic mounds and ridges (dark stippled regions), surrounded by zones of weaker fumarolic alteration (light stippled regions), are based on mapping by Sheridan (1970).

Fig. 1.3. Map of a portion of upper Alaska Peninsula, Kodiak Island, and the Cook Inlet region showing the ash-fall distribution associated with the formation of the VTTS (modified from Hildreth, 1983). Filled black triangle is the vent for the 1912 eruption at Novarupta, and tephra isopachs are adapted from Griggs (1922). Stars on the inset are active or potentially active volcanic centers along the Aleutian chain. Letters on the inset refer to settlements that, in addition to the named towns, figured in reports on the 1912 activity: A = Ugashik; B = Kanatak; C = site of Cold Bay; D = site of Katmai village; E = Kafliia Bay; F = site of Savonoski; G = Naknek; and H = Iliamna.

Fig. 1.4. Map of the distribution of ash-flow tuff in the Valley of Ten Thousand Smokes (dark grey shading; Hildreth and Fierstein, 1987). Novarupta is a rhyolite lava dome centered on the vent of the 1912 eruption. In addition, caldera subsidence occurred atop Mt. Katmai in 1912, forming Crater Lake. Mt. Katmai, Mt. Griggs, Trident, and Mts.

Martin and Mageik (located 6 and 13 km southwest of Katmai Pass, respectively, and not shown on this map) are all andesite-dacite stratovolcanoes. Mt. Cerberus (C) and Falling Mountain (F) are Holocene dacite domes adjacent to the 1912 vent. Baked Mountain (B), Broken Mountain (Br), the Buttress Range, and Mts. Katolinat and Juhle consist of Jurassic sedimentary rocks. The light stipple pattern around the higher peaks indicates glaciers.

Fig. 1.5. Topographic map of the Valley of Ten Thousand Smokes and adjacent region showing the locations of the major fumaroles studied in 1918 and 1919 (modified from Zies, 1924). The dotted line marks the edge of the ash-flow tuff deposit "edge of Sand Flow." Four numbered fumaroles referred to in the text are shown as filled circles. Three of these were studied while they were still active: No. 30 was observed by Sayre and Hagelberger in 1918 and Allen and Zies in 1919, No. 112 was observed by Allen and Zies in 1919, No. 148 was observed by Allen and Zies in 1919 and by Fenner in 1923. Geochemical observations from fumarole No. 212 were reported by Keith in 1991.

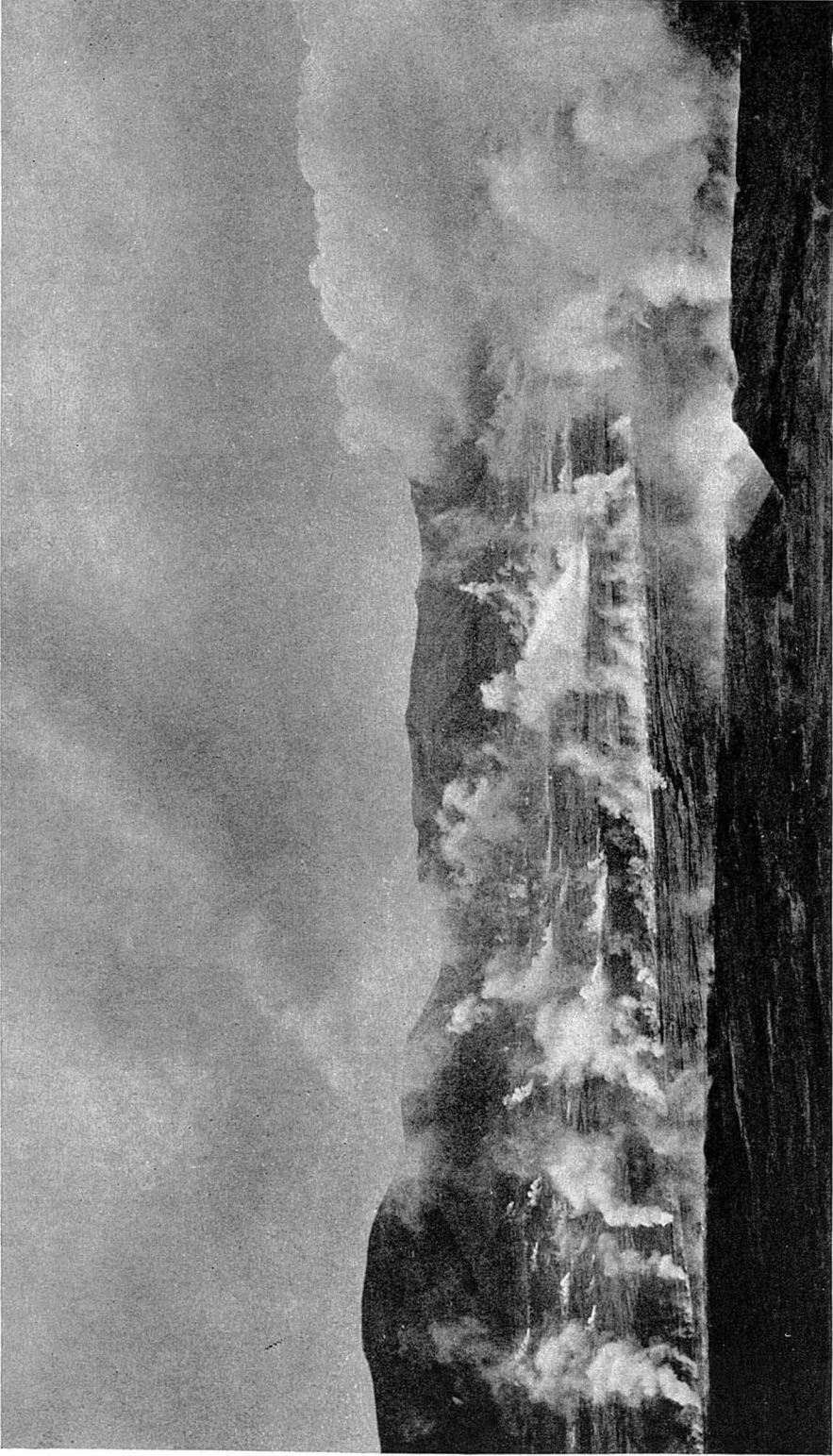


Fig.1.1

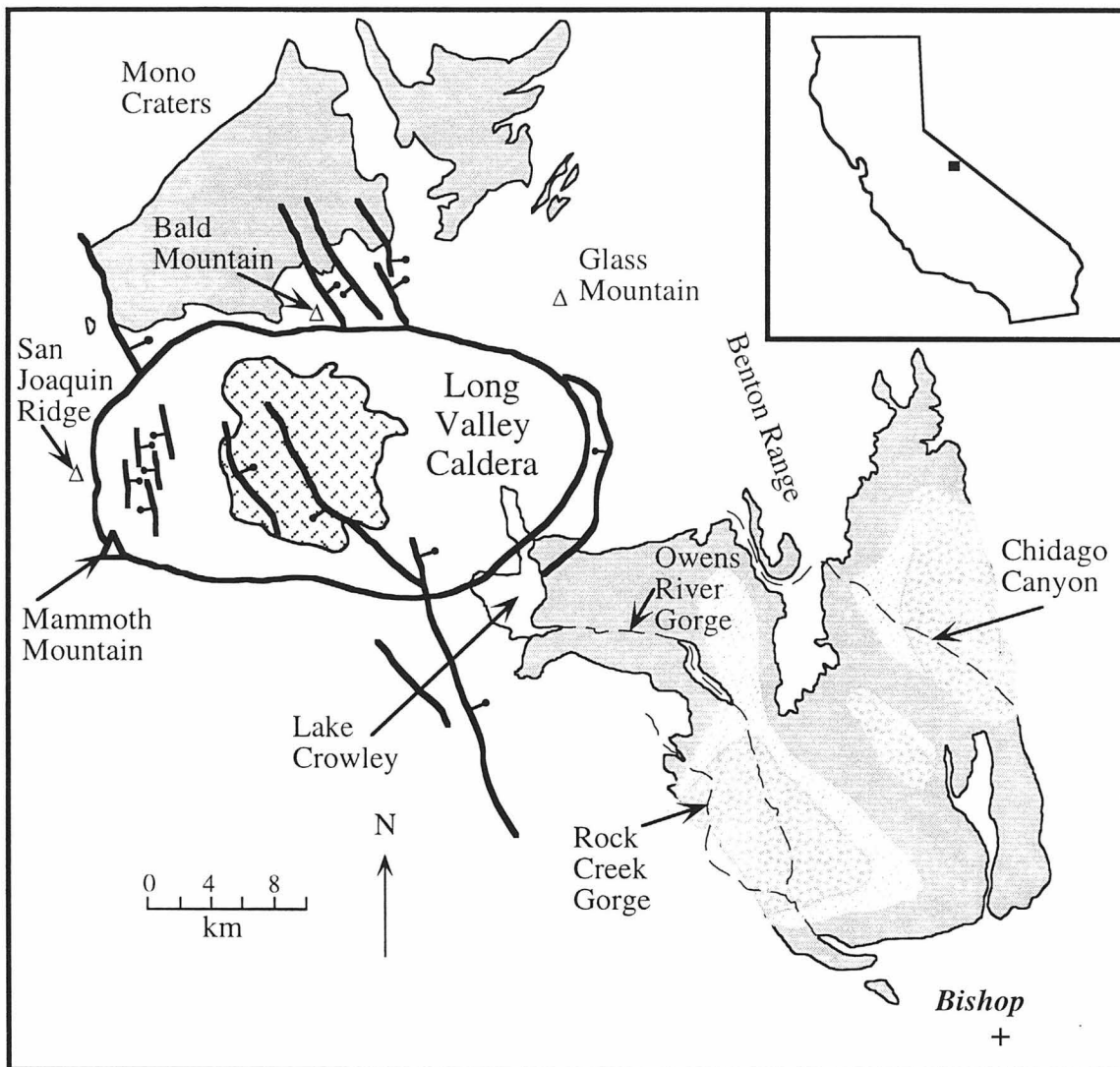


Fig. 1.2

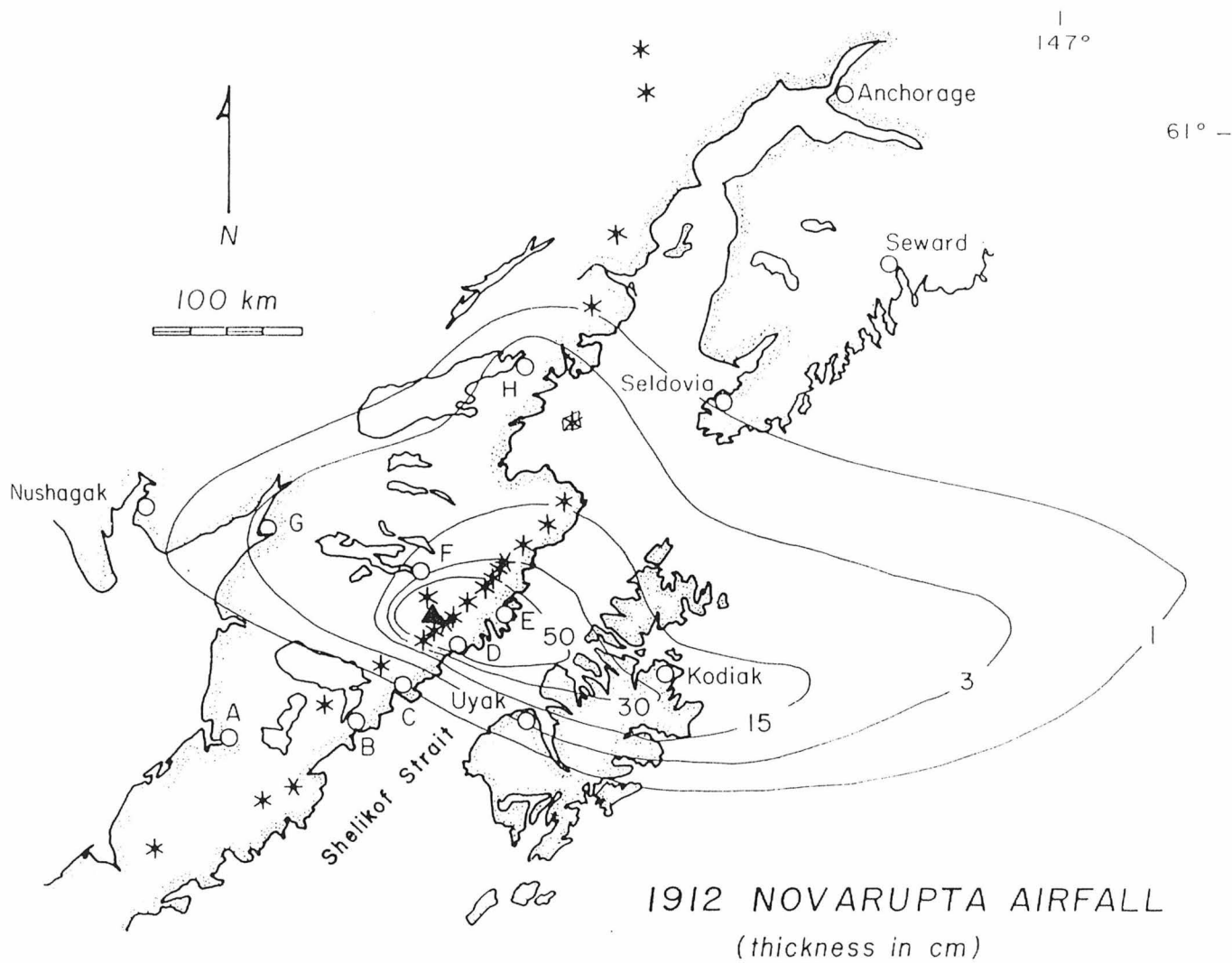


Fig. I.3

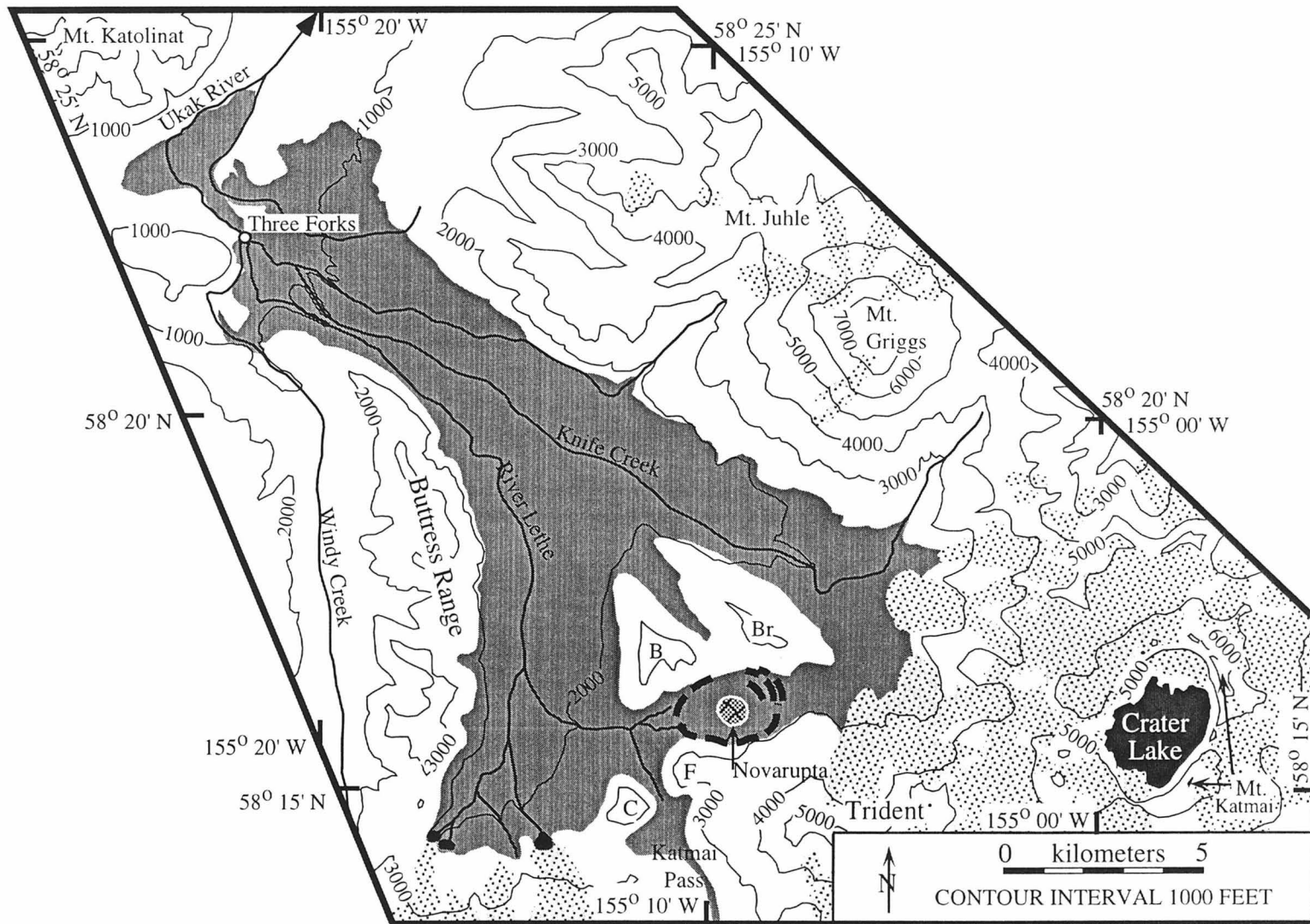


Fig. I.4

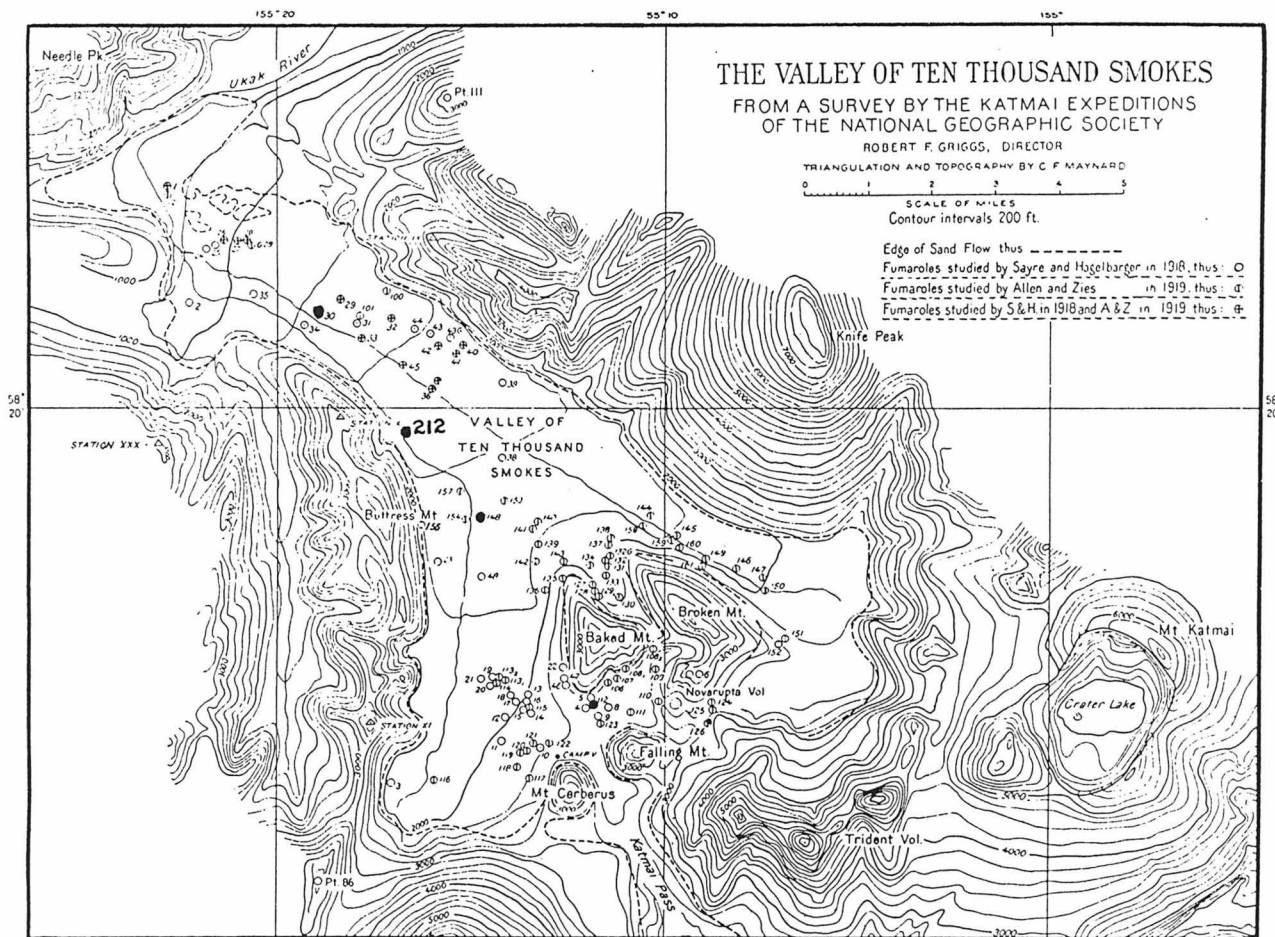


Fig. 1.5



**CHAPTER 2:  $^{18}\text{O}/^{16}\text{O}$  INVESTIGATIONS OF FUMAROLIC  
STRUCTURES IN THE 0.76 MA BISHOP TUFF OUTFLOW SHEET**

**2.1. Isotope systematics on  $\delta^{18}\text{O}$ - $\delta^{18}\text{O}$  diagrams**

Quartz and feldspar phenocrysts from the Bishop Tuff outflow sheet at several locations both within and outside the fumarole areas in the Bishop Tuff outflow sheet (Fig. 2.1; Table 2.1) all display very uniform  $^{18}\text{O}/^{16}\text{O}$ , with  $\delta^{18}\text{O}_{\text{qtz}} = +8.0$  to  $+8.7$  ( $n = 11$ ) and  $\delta^{18}\text{O}_{\text{feld}} = +6.9$  to  $+7.5$  ( $n = 10$ ). Phenocrysts with such  $\delta^{18}\text{O}$  values would be expected to have crystallized from a rhyolite magma having  $\delta^{18}\text{O} = +7.3$  to  $+7.9$  (e.g., Taylor and Sheppard, 1986), which in fact is very close to the range observed in unaltered samples of the Bishop Tuff (Halliday et al., 1984; Holt and Taylor, 1998; McConnell et al., 1997; see also below). The  $\Delta^{18}\text{O}_{\text{qtz-feld}}$  values ( $= \delta^{18}\text{O}_{\text{qtz}} - \delta^{18}\text{O}_{\text{feld}}$ ) are also very uniform ( $+0.8$  to  $+1.5\text{‰}$ ,  $n = 10$ ), with 7 of the 10 samples having values in the range 1.1 to 1.3‰; such  $\Delta^{18}\text{O}_{\text{qtz-feld}}$  values are appropriate for isotopic equilibrium at near-magmatic temperatures. This striking  $^{18}\text{O}/^{16}\text{O}$  uniformity in the phenocrysts is all the more remarkable considering the wide range in  $\delta^{18}\text{O}$  of coexisting groundmass/glass and pumice in the Bishop Tuff; for example whole-rock  $\delta^{18}\text{O}$  values of samples from which the above feldspars were separated vary by more than 15‰ (from  $-5.2$  to  $+9.2$ ), and the overall range in whole-rock  $\delta^{18}\text{O}$  for all analyzed samples of the Bishop Tuff outflow sheet is more than 23‰ (from  $-6.5$  to  $+16.7$ ; Table 2.2).

On a  $\delta^{18}\text{O}_{\text{qtz}}$  vs.  $\delta^{18}\text{O}_{\text{feld}}$  diagram (Fig. 2.2), data points from phenocryst pairs from the Bishop Tuff outflow sheet all plot very close to one another. This tight grouping of data points contrasts sharply with data on coexisting quartz and feldspar from previously studied, more "typical" meteoric-hydrothermal systems (Fig. 2.2) such as the Lake City, Colorado caldera (Larson and Taylor, 1986a; 1986b) and the subvolcanic Kumogi pluton, Japan (Matsuhisa et al., 1980). Those two fossil geothermal areas are representative of the

kinds of systems that characteristically exhibit steep disequilibrium arrays on  $\delta^{18}\text{O}_{\text{qtz}}-\delta^{18}\text{O}_{\text{feld}}$  diagrams (Fig. 2.2).

As shown by Gregory et al. (1989),  $\delta^{18}\text{O}_{\text{qtz}}-\delta^{18}\text{O}_{\text{feld}}$  diagrams can be used as "oxygen isotope clocks," because on such graphs the slopes and lengths of data-point arrays are mainly determined by (1) the length of time that hydrothermal exchange proceeds, and (2) the kinetic rate constant of the "slow-exchanging" mineral phase (quartz in the above examples). Thus, if large quantities of meteoric-hydrothermal fluids affected the groundmass/glass samples from the upper levels of the Bishop Tuff (and there are a number of compelling arguments for this, as indicated below), this must have taken place on a *much* shorter time scale ( $\ll 0.1$  Ma) and/or at *much* lower temperatures ( $\ll 300^\circ\text{C}$ ) than those that characterize "typical" hydrothermal systems, based on the fact that the feldspar phenocrysts have not undergone any significant  $^{18}\text{O}/^{16}\text{O}$  exchange. Lower temperatures can be immediately ruled out, because at such temperatures the equilibrium  $^{18}\text{O}/^{16}\text{O}$  fractionations are much too large to result in the observed whole-rock  $^{18}\text{O}$  depletions, even using meteoric waters with implausibly low  $\delta^{18}\text{O}$  values.

These types of isotopic contrasts are also well demonstrated on Fig. 2.3, which shows that the quartz-feldspar  $\Delta^{18}\text{O}$  values are extremely uniform ( $\Delta \approx 1.2\text{‰}$ ) for samples collected in the Bishop Tuff, as compared to the wide range (1.5 to 10.0‰) of quartz-feldspar  $\Delta^{18}\text{O}$  values obtained by Larson and Taylor (1986a, 1986b) for the hydrothermally altered rocks in and around Lake City caldera. It is thus clear that in the Bishop Tuff outflow sheet we are dealing with a unique kind of hydrothermal system, similar to the one that Gazis et al. (1996) inferred had operated in the Chegem caldera; as shown in Fig. 2 of Holt and Taylor (1998), both of these systems display  $^{18}\text{O}/^{16}\text{O}$  systematics that are considerably different from those in meteoric-hydrothermal systems heretofore described in the literature.

Whereas the  $\delta^{18}\text{O}$  values of phenocrysts from the Bishop Tuff are very uniform, the coexisting groundmass  $\delta^{18}\text{O}$  values are extremely variable (whole-rock  $\delta^{18}\text{O} = -5.2$  to

+9.2; Table 2.1 and Fig. 2.4). If we apply the concepts of Gregory et al. (1989) to the Bishop Tuff outflow sheet, for these short time scales it is appropriate to consider the groundmass/glass as the "fast-exchanging" phase and the feldspar phenocrysts as the "slow-exchanging" phase. By convention, we plot the "fast-exchanging" phase on the y-axis, and on such plots of  $\delta^{18}\text{O}_{\text{feld}}$  vs.  $\delta^{18}\text{O}_{\text{whole rock/groundmass}}$ , a steep disequilibrium array is observed for the Bishop Tuff outflow sheet (Fig. 2.4). The relatively rare high- $^{18}\text{O}$  samples that lie at the upper ends of the steep array are readily inferred to be the result of incipient weathering and/or low-temperature hydration processes, which are known to produce  $^{18}\text{O}$  enrichments in all volcanic glass that is exposed to meteoric water at the Earth's surface for more than a few thousand years (Taylor, 1968). In the much more common low- $^{18}\text{O}$  tuffs of this sample set, it is clear that the originally glassy, now pervasively devitrified groundmass (composed mainly of cristobalite and alkali feldspar) clearly must have exchanged oxygen to varying degrees with a low- $^{18}\text{O}$  fluid at high temperature ( $> 350^\circ\text{C}$ ). Meteoric water is the only fluid on Earth with a  $\delta^{18}\text{O}$  value low enough to cause the  $^{18}\text{O}$ -depletions observed in the 0.76-Ma Bishop Tuff.

According to the method of Gregory et al. (1989), by using the diffusion coefficient of feldspar and what we know about the temperature of fumarolic activity, the  $\delta^{18}\text{O}$  data from the Bishop Tuff outflow sheet can be used to estimate the duration of fumarolic water-rock interaction in the upper part of the Bishop Tuff. Because the diffusion of oxygen in feldspars is several orders of magnitude slower than in glass (Zhang et al., 1991), the measured slope of the data-point array on Fig. 2.4 ( $\approx 20\text{-}25$ ) can be shown to be equal to  $1/f$ , where  $f$  is the fractional approach of the feldspar to  $^{18}\text{O}/^{16}\text{O}$  equilibrium with the surrounding medium (Gregory et al., 1989). Combining this information with the oxygen diffusion coefficients in alkali feldspar as a function of temperature ( $D = 2.31 \times 10^{-9} \exp[-10,700/RT]$   $\text{cm}^2/\text{s}$ , as determined by Giletti et al., 1978), and with the equation relating the kinetic rate constant to the diffusion coefficient for fluid-buffered, open-system conditions ( $\exp[-kt] = 1 - f \approx \exp[-3.5(Dt/a^2)^{1/2}]$  for  $(Dt/a^2)^{1/2} < 0.1$ , as derived by Criss et al.,

1987), we can repeat the kinds of calculations done by Gazis et al. (1996) at Chegem, and thereby estimate the lifetime of the Bishop Tuff outflow sheet fumarole system (Holt and Taylor, 1998). Because we observe a fairly well-defined, very steep array for this meteoric-hydrothermal system, it is clear that it was active for only a short period of time. According to Holt and Taylor (1998), at temperatures of about 400°C, the lifetime calculated for the Bishop Tuff outflow sheet is  $\approx 10$  years, and at temperatures of about 500°C, this lifetime is even shorter at  $\approx 2$  years. Taking into account the observation that fumarolic activity probably did not begin and end simultaneously in all parts of the ash-flow sheet at once, fumarolic activity in the thickest parts of the ash-flow sheet may have continued for up to 25 years.

As will be shown in detail below, the observed  $^{18}\text{O}$ -depletions (whole-rock  $\delta^{18}\text{O}$  values  $< +7.6$ ) in the Bishop Tuff outflow sheet can be directly related to fumarole structure and morphology. Also, the *only* evidence for hydrothermal alteration in the large remnant of the Bishop Tuff outflow sheet lying southeast of Lake Crowley (Fig. 2.1) is that related to this fumarolic activity; there are no igneous rocks in this area younger than 0.76 Ma, and thus the only available heat to drive any type of hydrothermal circulation would have been simply the original heat content of the ignimbrite melt-crystal emulsion. This relatively straightforward situation in this southeastern lobe of the outflow sheet contrasts sharply with the more complex geologic history both to the northwest in the intracaldera Bishop Tuff and further north near remnants of the Bishop Tuff outflow sheet adjacent to the Holocene Mono Craters and Inyo Domes, where post-caldera igneous activity is well documented (Bailey et al., 1976). Isotopic evidence for such complications is shown by extremely low  $\delta^{18}\text{O}$  values from drill-core samples collected near the base of the intracaldera Bishop Tuff in the vicinity of the Long Valley resurgent dome (Holt and Taylor, 1998; McConnell et al., 1997). These kinds of  $^{18}\text{O}$ -depletions and alteration features observed in feldspars of the deep intracaldera Bishop Tuff (Smith and Suemnicht, 1991) are characteristic of the "typical" ( $\approx 300^\circ\text{C}$ ), long-lived meteoric-hydrothermal

systems associated with resurgent calderas elsewhere in the world (e.g., as at Lake City, see Fig. 2.2).

Thus, the data from Figs. 2.2 and 2.4 together demonstrate that the low- $^{18}\text{O}$  signature in the groundmass of the Bishop Tuff outflow sheet was formed during a short-lived, fumarolic meteoric-hydrothermal event, in which the convective circulation was driven solely by the original heat content of the newly deposited Bishop Tuff (i.e., its latent heat of crystallization or devitrification, its temperature, and its heat capacity); this conclusion (Holt and Taylor, 1996) was reached even before the detailed correlations between  $^{18}\text{O}/^{16}\text{O}$  and fumarolic structures discussed below were obtained. While this study is not the first to show that the fumarolic gases associated with ash-flow tuffs contain meteoric  $\text{H}_2\text{O}$  (e.g., Allen and Zies, 1923; Keith, 1991; Shevenell and Goff, 1995; Zies, 1929), together with Gazis et al. (1996) this is the first study to demonstrate that enormous amounts of heated meteoric  $\text{H}_2\text{O}$  have pervaded and interacted with the upper parts of these tuffs over a period of just a few tens of years following their eruption. Note that these conclusions are in conflict with the assertion of Sheridan (1970) that the fumarolic fluids in the Bishop Tuff outflow sheet were composed almost entirely of magmatic volatiles.

## **2.2. Geometry of $^{18}\text{O}/^{16}\text{O}$ distribution and fumarolic structures in the Bishop Tuff outflow sheet**

### *2.2.1. General Statement*

Fumarole morphology in the Bishop Tuff outflow sheet is evidenced most noticeably by prominent mounds and ridges on the surface of the tuff (see Figs. 2.5 and 2.6 and Sheridan, 1970). These formed both as primary geomorphic features and because such zones are more indurated and less subject to erosion than the surrounding tuff (as a result of interaction with fumarolic vapors). Spectacular examples of the inner workings of these mounds and ridges are exposed where erosion has cut down into the tuff, as in Owens River Gorge, Rock Creek Gorge, and Chidago Canyon. Steeply dipping, near-vertical

columnar joints are beautifully exposed in many of these cliff exposures. However, in the partially welded tuff below the fumarolic mounds, it is much more common to observe a great variety of curved and/or shallow-dipping columnar joints. Around tubular cavities in this part of the tuff, the jointing often has a radial orientation. Sheridan (1970) made compelling arguments that these zones of shallow-dipping columnar joints, which form perpendicular to isothermal surfaces while the tuff is cooling, all formed during fumarolic activity; the flow of fumarolic gases disturbed the conductive thermal regime of the tuff sufficiently to influence the directions of columnar joint growth and thereby caused them to grow in subvertical orientations.

At most of our sampling localities, the Bishop Tuff is composed largely of a single "ignimbrite sub-package" designated as Ig1E (e.g., see Wilson and Hildreth, 1997); this unit represents the greater part of the Gorges and Chidago Lobes of Hildreth (1979), with the samples from each of these lobes being designated respectively by "G" and "C" in the sample descriptions found in Tables 2.1 and 2.2. Throughout the text of this manuscript, the terminology of Hildreth (1979) will be used, i.e., the Gorges and the Chidago Lobes will refer to Unit Ig1E of Wilson and Hildreth (1997). In cases where it is necessary to distinguish eruptive Unit Ig1Ea from Ig1Eb, this will be noted in the text. Some of the samples collected for this study are from the Tableland Unit (Unit Ig2E of Wilson and Hildreth, 1997) and these are designated by a "T" in the sample descriptions in Tables 2.1 and 2.2. All of the samples from the tops of fumarolic mounds on the surface of the Bishop Tuff are from this Tableland Unit (Table 2.2).

As noted by Sheridan (1970), and as indicated by a comparison of our Figs. 2.1 and 2.6 with Fig. 6 in Wilson and Hildreth (1997), the region of most intense fumarolic activity coincides with the mapped areas of densely welded tuff from the Gorges and the Chidago Lobes. The Tableland Unit overlaps the Gorges and Chidago Lobes, thinning towards the caldera (see Fig. 8 in Wilson and Hildreth, 1997). Because there is a greater degree of welding, vapor-phase mineralization, and devitrification in the Tableland Unit where it

overlies the densely welded Gorges Unit, it is argued by Wilson and Hildreth (1997) that there could have been only a brief time break between the deposition of the Gorges and Tableland Units.

The relationships of the different fumarolic structures to one another and to the color and welding zonation in the Bishop Tuff beneath these fumarolic mounds are shown schematically in Fig. 2.7; this sketch is modeled from a photograph of the west side of Owens River Gorge about 75 m south of Site CG. Note that the shallow-dipping and radial columnar joints, the tubular conduit, and the steep fissures are all localized within the zone of partially welded, pervasively devitrified tuff, which is deep pink and well-indurated (see Tables 2.1 and 2.2). These geomorphic features and structures never extend downward for more than a few meters into the densely welded black tuff, which makes up the entire lower half of the exposed portion of the ash-flow sheet in the sampling localities in Rock Creek Gorge and in the middle part of Owens River Gorge. The horizon at the top of this 100-m-thick, densely welded black tuff is generally quite flat, but is slightly depressed and bowed downward in the vicinity of some of the tubular conduits and the zones of steep fissures. The patterns of the columnar joints in these localities indicate that cooling occurred along these steep fissures and at the axes of sets of radiating columnar joints. Sheridan (1970) suggests that these structures must have been the conduits for fumarolic fluids, and we concur. These two kinds of conduit structures are invariably found directly beneath fumarolic mounds and they are not present in areas of the Bishop Tuff where there is no evidence for fumarolic mounds and ridges on the surface.

### *2.2.2. Distribution of Sample Sites*

In the present study, the rocks associated with major fumarolic structures around the tubular conduits and zones of steep fissures were sampled in detail at two specific localities (Fig. 2.6): (1) a subhorizontal tubular cavity in the ash-flow tuff located along the central axis of a radiating pattern of columnar joints (Site HT); and about 3.5 m farther

downstream (2) a zone of steep, throughgoing, wide fissures, which are continuous along strike for several tens of meters and represent well-defined surfaces of termination for shallow-dipping columnar joints (Site LG).

In addition to the above samples that were specifically chosen to sample the inner workings of two important types of fumarolic conduits, samples were also collected from eight representative depth profiles of the outflow sheet that did not directly encompass any *major* fumarolic conduits (Figs. 2.1 and 2.6). Four of these depth profiles are from areas of relatively intense fumarolic activity and four others are from areas where the fumarolic activity was weak or non-existent. Of the four depth profiles that lie within the region of well-developed fumarolic mounds and ridges mapped by Sheridan (1970), three are in Owens River Gorge and one is in Chidago Canyon. In Owens River Gorge, these sampling localities are spaced about 0.5 - 2 km (Fig. 2.6) apart and consist of: a section that features shallow-dipping columnar joints beneath a large fumarolic mound (Site CG), a section located in an interval between fumarolic mounds in which the columnar joints are all nearly vertical (Site AG), and a section located in an interval between fumarolic mounds in which there are no well-developed columnar joints (Site LG-B). For direct comparison with Site CG, a suite of samples was also collected in Chidago Canyon at (Site CC-L), which is another section where shallow-dipping columnar joints are prominent beneath a fumarolic mound.

The four other depth profiles are all from regions of relatively weak or non-existent fumarolic activity, well away from the areas of prominent mounds. Sheridan (1970) mapped a zone of devitrified and vapor-phase altered Bishop Tuff (light stippled pattern on Fig. 2.1) that encompasses two of these profiles: a section in Rock Creek Gorge with nearly vertical columnar joints (Site RC), and a section in Owens River Gorge from just south of the basement high in which there are both crudely developed columnar joints and partially welded tuff exposed beneath the densely welded, devitrified tuff (Site UG). Another section in Chidago Canyon displays nearly vertical columnar joints (Site CC) and



lies just barely outside the area of weak fumarolic activity as mapped by Sheridan (1970). The final depth profile (Site CR) is from a section close to Lake Crowley that shows no evidence for columnar jointing; this locality lies well away from any area of fumarolic activity mapped by Sheridan (1970).

In addition to the depth profiles described above, surface outcrop samples were also collected from fumarolic mounds at several different locations on the surface of the Bishop Tuff. These surface sample localities include Sites LG, CG, and HT at the edge of Owens River Gorge and Site CC-L at the edge of Chidago Canyon, as well as localities lying in the area between Owens River Gorge and Rock Creek (Table 2.2). The upper part of the tuff that forms fumarolic mounds is characterized by highly variable whole-rock  $\delta^{18}\text{O}$  values that range from moderately  $^{18}\text{O}$ -depleted to extremely  $^{18}\text{O}$ -enriched (+2.7 to +16.7; Fig. 2.8). This contrasts with typical whole-rock  $\delta^{18}\text{O}$  values of samples from the surface of the tuff located away from the morphological effects of fumarolic activity; the latter samples are more uniform in  $\delta^{18}\text{O}$  and whole-rock  $\delta^{18}\text{O}$  values are only slightly perturbed from the original magmatic  $\delta^{18}\text{O}$  value of the Bishop Tuff (Fig. 2.8).

The characteristics of the surface of the Bishop Tuff associated with fumarolic mounds differ in several ways from the surface of the tuff away from fumarolic mounds. Thick (>1.5 mm)  $\text{SiO}_2$  and hematite coatings are commonly found in fractures near the surfaces of fumarolic mounds; coatings with similar mineralogy found within the fumarole areas away from fumarolic mounds are typically not as thick (<1 mm). "Arcuate roof joints" are joints in the upper part of the ash-flow sheet that are invariably associated with fumarolic mounds (Fig. 2.8). These joints form crude domes of indurated tuff that lie above a less indurated part of the tuff, which has commonly been eroded to form small hollows up to a few meters deep just underneath the surface of the ash-flow sheet. In the vicinity of the fumarolic mounds shown in Fig. 2.8, the surface of the ash-flow sheet is invariably unwelded. In contrast, except for samples AG-1 and AG-2, all of the samples collected from the surface of the ash-flow sheet away from fumarolic mounds exhibit a slightly

higher degree of welding than those collected from fumarolic mounds. As pointed out by Putnam (1960) and Sheridan (1970), because unwelded tuff near the surfaces of fumarolic mounds has been affected by the passage of abundant fumarolic vapors, it usually displays a greater degree of induration than tuff with a similar degree of welding away from fumarolic mounds. Thus the uppermost, unwelded part of the tuff away from fumarolic mounds and ridges has likely been more deeply eroded, exposing tuff having a slightly higher degree of welding than is observed in the more resistant tuff found directly on top of the fumarolic mounds.

### *2.2.3. Overall Pattern of Whole-Rock $^{18}\text{O}/^{16}\text{O}$ Values in the Bishop Tuff Outflow Sheet*

Taken together, we can make the following generalizations from  $^{18}\text{O}/^{16}\text{O}$  data obtained from the various kinds of sample sites throughout the Bishop Tuff outflow sheet. First, there is a widely varying pattern of whole-rock  $^{18}\text{O}$  depletion at depths of up to 60 to 80 meters in the upper part of the outflow sheet; in this zone the original  $\delta^{18}\text{O}$  value of the tuff (+7.6) has been locally lowered by as much as 14 per mil (Fig. 2.9). Superimposed upon this pattern of  $^{18}\text{O}$  depletion, there is also a general pattern of  $^{18}\text{O}$  enrichment of the near-surface portions of the tuff, particularly in the vicinity of fumarolic mounds and ridges, where whole-rock  $\delta^{18}\text{O}$  values have been elevated by as much as 9 ‰ (to whole-rock  $\delta^{18}\text{O}$  values as high as +16.7). Finally, extensive sampling indicates that the whole-rock  $\delta^{18}\text{O}$  of the lower half of the ash-flow sheet (the densely welded black tuff) is virtually unchanged from its original value at the time of eruption.

The above generalizations are put forth in a schematic fashion on the sketch in Fig. 2.9. The most prominent regional  $^{18}\text{O}/^{16}\text{O}$  feature in the tuff is a shallow zone of moderately  $^{18}\text{O}$ -depleted rock ( $\delta^{18}\text{O} \approx +2.5$  to  $+6.5$ ), which is located along a specific stratigraphic horizon in the upper part of much of the southeastern lobe of the Bishop Tuff outflow sheet, both inside and outside Sheridan's (1970) mapped fumarolic areas (Fig. 2.1). The general  $^{18}\text{O}/^{16}\text{O}$  features of this zone are shown on the far left side of Fig. 2.9. This low-

$^{18}\text{O}$  stratigraphic zone is up to 40 m thick, and it usually exhibits whole-rock  $\delta^{18}\text{O}$  values of about +5.5 to +6.0, except where it intersects major fumarolic features, in which case the  $\delta^{18}\text{O}$  values may be as low as -2.1. The maximum whole-rock  $^{18}\text{O}$ -depletions in this regional stratigraphic zone appear to be focused near the base of the Tableland Unit in cases where that unit is present in the sampled sections. In the discussion that follows, this feature will be referred to as the Upper Low- $^{18}\text{O}$  Zone (ULZ). The base of this Upper Low- $^{18}\text{O}$  Zone is not at a consistent depth within the Bishop Tuff outflow sheet, and its most consistent correlation with an observable geologic feature is that it is associated with the transition from light pink to dark pink groundmass. There is no evidence that the base of the ULZ ever lies closer than about 15-20 m to the upper boundary of the underlying densely welded black tuff.

As shown on the upper part of the sketch in Fig. 2.9, the fumarolic mounds on the surface of the tuff are characterized by extremely variable  $\delta^{18}\text{O}$  values ( $\delta^{18}\text{O} = +2.7$  to +16.7; see Table 2.2). The higher and lower whole-rock  $\delta^{18}\text{O}$  values are, respectively, interpreted to be mainly a function of the extremes of lower ( $\approx 50^\circ\text{C}$ ) and higher ( $\approx 650^\circ\text{C}$ ) temperatures of  $^{18}\text{O}/^{16}\text{O}$  exchange during the meteoric-hydrothermal activity. The surfaces of the fumarolic mounds are the only localities in the Bishop Tuff outflow sheet where the very high  $\delta^{18}\text{O}$  values and the presence of dark reddish-brown hematite coatings provide clear-cut  $^{18}\text{O}/^{16}\text{O}$  and/or mineralogical evidence for relatively low-temperature meteoric-hydrothermal (i.e., hot spring) activity.

The lowest whole-rock  $\delta^{18}\text{O}$  values ( $\delta^{18}\text{O} = -6.5$  to +1.6) in the Bishop Tuff outflow sheet are typically confined to a series of isolated zones that lie slightly deeper than the ULZ and directly atop the densely welded black tuff. These deep low- $^{18}\text{O}$  zones are always spatially associated with fumarolic structures such as tubular conduits, steep fissures, or shallow-dipping columnar joints, which are found only beneath fumarolic mounds and ridges. In the discussion that follows, these extremely  $^{18}\text{O}$ -depleted zones will be referred to as the Deep Fumarolic System (DFS).

The underlying densely welded tuff itself is characterized by  $\delta^{18}\text{O}$  values that are largely within the range expected for relatively unaltered Bishop Tuff ( $\delta^{18}\text{O} = +7.1$  to  $+8.4$ ), but some rare samples may be very slightly  $^{18}\text{O}$ -enriched ( $\delta^{18}\text{O} = +9.2$ ). Unwelded to partially welded units beneath the thick zone of densely welded tuff may locally be slightly  $^{18}\text{O}$ -depleted where the ash-flow tuff abuts against the underlying basement, as in the upper reaches of Owens River Gorge. However, for the most part, the densely welded lower part of the ash-flow sheet does not exhibit any  $^{18}\text{O}/^{16}\text{O}$  or morphological evidence for significant meteoric-hydrothermal fumarolic activity, and therefore it must be relatively impermeable to these fumarolic fluids. In the following discussions, this impermeable zone will be referred to as the Densely Welded Zone (DWZ).

The schematic diagram in Fig. 2.9 shows how the  $^{18}\text{O}/^{16}\text{O}$  values change in the Bishop Tuff outflow sheet as one approaches the structures beneath a fumarolic mound. It can be seen that the upper stratigraphic zone of  $^{18}\text{O}$  depletion (the ULZ) commonly merges into and overlaps with the somewhat deeper zone of more intense  $^{18}\text{O}$  depletion (the DFS) that lies directly beneath a fumarolic mound and above the densely welded black tuff (the DWZ). Whether these two distinct zones of  $^{18}\text{O}$  depletion do or do not physically overlap is mainly dependent upon how high the steep fissures penetrate upward into the overlying partially welded tuff. Nonetheless, even in cases where the two zones do not physically overlap, the  $\delta^{18}\text{O}$  values in the ULZ are usually strongly perturbed toward lower  $\delta^{18}\text{O}$  values directly over the deeper low- $^{18}\text{O}$  zones (i.e., beneath a fumarolic mound or ridge). This is surely in part the result of locally enhanced thermal gradients and fluid flow in the upper part of the sheet due to the presence of discrete fumarolic conduits such as tubular cavities or steep fissures. During the superposition of late-stage hot spring activity at lower temperatures, both of these zones of  $^{18}\text{O}$ -depletion may become locally elevated in  $\delta^{18}\text{O}$  as a result of continued fluid flow in the vicinity of the overlying fumarolic mound.

### 2.3. Temperatures and isotopic compositions of H<sub>2</sub>O involved in fumarolic activity

In the low-<sup>18</sup>O rocks of the Bishop Tuff outflow sheet, there is no evidence for formation of hydrous minerals, such as chlorite, sericite, and clay minerals, which should logically be formed as alteration products as the tuff cools through 350°C in the presence of abundant H<sub>2</sub>O. Because the hydrothermal system would necessarily be less vigorous at lower temperatures, this type of mineralogical alteration might not be expected everywhere in the tuff; however, local affects ought to be found along major fumarolic conduits, particularly where the <sup>18</sup>O/<sup>16</sup>O evidence requires that integrated water/rock ratios were very large. However, despite an extensive search of these low-<sup>18</sup>O zones at every sampling location, no significant amounts of hydrous minerals were found in these areas. In addition, in Sheridan's (1970) detailed study of the Bishop Tuff fumaroles, he does not report the occurrence of any of these kinds of low-temperature, OH-bearing minerals.

The presence of biotite, the absence of chlorite and sericite, and the fact that the sanidines do not exhibit any significant mineralogical or <sup>18</sup>O/<sup>16</sup>O alteration in the low-<sup>18</sup>O zone deep in the tuff, together imply that the minimum temperature at which significant meteoric-hydrothermal fluid/rock interaction took place in the vicinity of the Bishop Tuff fumarolic structures was probably around 400°C. Emplacement temperatures at least as high as 630-650°C are suggested by the degree of welding in the ash-flow sheet (Riehle et al., 1995), and Sheridan (1970) estimates temperatures of fluid/rock interaction as high as 650-750°C, based on welding temperatures (Smith et al., 1958) and on his identification of the fumarolic mineral marialite (a high-temperature form of scapolite). These estimates are similar to the maximum fumarole temperatures directly measured at Valley of Ten Thousand Smokes, Alaska (645°C, Zies, 1924).

Microscopic features in feldspar phenocrysts of ash-flow tuff samples located near fumarolic conduits support the idea that fumarolic temperatures were above ≈400°C. Exsolution lamellae and microstructures in sanidine phenocrysts (Or<sub>66</sub>Ab<sub>33</sub>An<sub>1</sub>) have been

studied by Snow and Yund (1988) from a profile through the Bishop Tuff along Middle Power Plant Road that coincides with Site LG. Their data include a set of samples collected within a fossil fumarole, which corresponds to the same section that is referred to below in Section 2.4.3 as a zone of steep fissures. Snow and Yund (1988) attribute the earliest stage of relatively patchy and irregular exsolution in these cryptoperthites to "a high flux of water associated with fumarolic activity." They also conclude that this high H<sub>2</sub>O flux continued as the tuff cooled below 460°C, but that the thermal anomaly caused by these fumarolic fluids "relaxed before the tuff cooled below 360°C." In any event, because our studies clearly show that these sanidines were not measurably depleted in <sup>18</sup>O by the fumarolic fluids (Table 2.1), any such effects on exsolution microstructures must have been produced by penetration of only tiny amounts of H<sub>2</sub>O into the sanidine phenocrysts.

There *is* evidence for significant hydrothermal circulation at lower temperatures (<250°C) in the Bishop Tuff outflow sheet, but this is observed only in the upper 10 to 20 meters of the tuff directly beneath some of the fumarolic mounds; here the tuff is mineralogically altered, and the groundmass locally contains amorphous silica and clay. Thick (≈2 mm) hematite and silica coatings on the walls of fissures in the fumarolic mounds also suggest that low-temperature fluids locally interacted with the uppermost portion of the tuff at those sites. As briefly mentioned in Section 2.2.3 and as explored in more detail below in Section 2.4.1, these mound samples exhibit a wide range in whole-rock δ<sup>18</sup>O values, including some that are very high and indicative of very low-temperature oxygen exchange, probably associated with late-stage hot-spring activity.

It is useful to use the <sup>18</sup>O/<sup>16</sup>O data to try to place some limited constraints on the temperatures and isotopic compositions of the fumarolic and hot-spring activity in the Bishop Tuff outflow sheet. Based upon a combination of experimental and theoretical determinations of the equilibrium <sup>18</sup>O/<sup>16</sup>O fractionations among the phases quartz, feldspar, and H<sub>2</sub>O, one can estimate the <sup>18</sup>O/<sup>16</sup>O fractionations between the groundmass of the Bishop Tuff and the associated fumarolic hydrothermal fluids as a function of

temperature (Fig. 2.10). For a specific  $\delta^{18}\text{O}_{\text{H}_2\text{O}}$ , there is a certain temperature below which  $\Delta^{18}\text{O}_{\text{groundmass-water}}$  becomes large enough to cause  $^{18}\text{O}$ -enrichment in the groundmass of the tuff and above which the groundmass becomes  $^{18}\text{O}$ -depleted as a result of exchange. These particular values of  $\Delta^{18}\text{O}_{\text{groundmass-water}}$  are referred to here as  $\Delta P$ . Assuming the groundmass of the tuff reaches isotopic equilibrium with the hydrothermal  $\text{H}_2\text{O}$ ,  $\Delta P$  is simply the difference between the  $\delta^{18}\text{O}$  of the hydrothermal  $\text{H}_2\text{O}$  of interest and the initial  $\delta^{18}\text{O}$  value of the Bishop Tuff groundmass (+7.6); therefore,  $\Delta P$  depends only on temperature and the  $\delta^{18}\text{O}$  of the  $\text{H}_2\text{O}$  (Fig. 2.10). For example, for a plausible range of  $\delta^{18}\text{O}_{\text{H}_2\text{O}}$  values in the Bishop Tuff fumarolic system (i.e., +3.5 to -13.0, see below),  $\Delta P$  ranges from +4.1 to +21.6‰, respectively, corresponding to a temperature range of 382°C to 86°C (Fig. 2.10).

The endmember values of  $\delta^{18}\text{O}_{\text{H}_2\text{O}}$  selected above (+3.5 to -13.0) are thought to encompass the range of  $\delta^{18}\text{O}$  values that might be observed in any significant volumes of hydrothermal  $\text{H}_2\text{O}$  involved in fumarolic activity in the Bishop Tuff outflow sheet 760,000 years ago. These values were chosen both by evaluating the  $\delta^{18}\text{O}$  of  $\text{H}_2\text{O}$  that could have been in equilibrium with selected portions of the ash-flow sheet in the first few years after eruption, and also by drawing analogy to the  $\delta^{18}\text{O}$  values of hydrothermal  $\text{H}_2\text{O}$  samples collected from present-day hot springs in Long Valley caldera.

The particular volume of rock chosen from the Bishop Tuff outflow sheet to estimate the upper limit of  $\delta^{18}\text{O}_{\text{H}_2\text{O}}$  is the  $\approx 20$ - to 40-m-thick stratigraphic zone designated above as the ULZ, which is inferred to extend over an area of at least 140 km<sup>2</sup>. Thus the ULZ represents the largest volume of  $^{18}\text{O}$ -depleted rocks in the Bishop Tuff outflow sheet ( $\approx 3 \times 10^9$  m<sup>3</sup>) that can be singled out as probably having formed over a specific range of temperatures ( $\approx 400^\circ$ -600°C); the ULZ also has a relatively narrow range of whole-rock  $\delta^{18}\text{O} = +4.5$  to +6.5 for samples collected well away from steep fissures, tubular conduits, and shallow-dipping columnar joints. For the purposes of this discussion, an average whole-rock  $\delta^{18}\text{O}$  value of +5.5 is assumed for the ULZ, and the temperature of exchange

is assumed to be  $\approx 500^{\circ}\text{C}$ . Using these parameters, the  $\delta^{18}\text{O}$  of  $\text{H}_2\text{O}$  in exchange equilibrium with the rocks in the ULZ would have been +3.5, which is the high- $^{18}\text{O}$  end member value for the fumarolic  $\text{H}_2\text{O}$  used in calculating  $\Delta P$  above. Although small amounts of meteoric-hydrothermal  $\text{H}_2\text{O}$  with  $\delta^{18}\text{O} > +3.5$  were certainly present locally in the ash-flow tuff fumarolic systems (e.g., where temperatures were higher than  $500^{\circ}\text{C}$ , or where the whole-rock  $\delta^{18}\text{O}$  value of the tuff was higher than +5.5), the value of +3.5 probably represents a fairly robust upper bound on the  $\delta^{18}\text{O}$  of any large volume of fumarolic  $\text{H}_2\text{O}$ . Note, however, that this estimate only applies to fumarolic fluids of meteoric derivation. There was undoubtedly some contribution as well from pure magmatic  $\text{H}_2\text{O}$  liberated from the silicate melt and hot glass originally present in the ash-flow sheet; such  $\text{H}_2\text{O}$  could have had a  $\delta^{18}\text{O}$  as high as +7 to +8 (See Section 2.7.1, below).

An analogous calculation can be done to estimate a lower bound for the  $\delta^{18}\text{O}$  of fumarolic  $\text{H}_2\text{O}$  by using some of the heaviest whole-rock  $\delta^{18}\text{O}$  values in the Bishop Tuff outflow sheet. These are from samples with orange, red, and black coloration collected on the surfaces of fumarolic mounds ( $\delta^{18}\text{O} = +7.4$  to +16.7). Allen and Zies (1923) observed that in the Valley of Ten Thousand Smokes, the low temperature ( $100^{\circ}$ - $125^{\circ}\text{C}$ ) vents were lined with a "metamorphosed pumice conspicuously colored by oxide of iron." Assuming that similar temperatures were present during hydrothermal activity around fumarolic mounds with similar coloration in the Bishop Tuff outflow sheet, the equilibrium  $\Delta^{18}\text{O}_{\text{groundmass-water}}$  values would have been about +17.0 to +19.5. Using an average of these two values (+18.3), this indicates that the  $\delta^{18}\text{O}$  of fumarolic  $\text{H}_2\text{O}$  in equilibrium with Bishop Tuff groundmass having  $\delta^{18}\text{O} = +7.4$  to +16.7 would have been between -1.6 and -10.9, respectively; these values lie well within the "low"-temperature rectangular envelope on Fig. 2.10.

Another way to estimate the  $\delta^{18}\text{O}$  of the low-temperature hot-spring waters in the Bishop Tuff 760,000 years ago is to make some inferences from the present-day situation.



The  $\delta^{18}\text{O}$  values of the hottest (91 $^{\circ}$ -201 $^{\circ}$ C) thermal waters collected during the period of 1984 to 1987 in Long Valley caldera range from  $\delta^{18}\text{O} = -12.9$  to  $-14.8$  (White et al., 1990); this range is only slightly heavier than that of cold surface waters collected during the same time period from the region surrounding Long Valley caldera ( $-13.9$  to  $-17.4$ ; White et al., 1990). Thus, the  $^{18}\text{O}$  shift observed in such thermal waters from Long Valley proper is at most only about 2 to 4 ‰, which is characteristic of many such lower temperature thermal waters observed throughout the world. This implies that, like most of these other thermal waters, hot springs in Long Valley emanate from hydrothermal systems with very high water/rock ratios.

The present-day precipitation in this region exhibits enormous variation in  $\delta^{18}\text{O}$  ( $-2.8$  to  $-20.6$ ), both on account of seasonal variations and because storm tracks approaching Long Valley from the west are affected by the Mammoth embayment, which refers to the north-trending valley cut by the San Joaquin River just southwest of Long Valley. As pointed out by White et al. (1990), storms from the Pacific Ocean that approach Long Valley by coming north up the San Joaquin River valley would contain  $\text{H}_2\text{O}$  with comparatively high  $\delta^{18}\text{O}$  values, because these storms have only to surmount elevations of  $\approx 2900$  m on the shoulders of Mammoth Mountain. Other storms approaching Long Valley will contain  $\text{H}_2\text{O}$  having much lower  $\delta^{18}\text{O}$  values, because these must cross over the crest of the Sierra Nevada Range, which in this area is at elevations of more than 4000 m. Although this wide range of  $\delta^{18}\text{O}$  values for precipitation in the Long Valley area is disconcerting with respect to deciding upon plausible  $\delta^{18}\text{O}$  values for the precipitation and groundwater 760,000 years ago, it is of note that these variations in the precipitation seem to be averaged out in both the thermal waters and cold surface waters of the present day, as these exhibit a comparatively narrow range of  $\delta^{18}\text{O}$  values ( $-12.9$  to  $-17.4$ ; White et al., 1990).

Bailey et al. (1976) report that, during its eruption, the Bishop Tuff ponded against glaciers present at elevations below 2300 m in Little Round Valley, which is located 2 km

south of the southern end of Lake Crowley. This observation implies that the Bishop Tuff was erupted during a time of cooler climate than today; in consequence, the  $\delta^{18}\text{O}$  values of surface water in this area could have been even lower than at present. However, this effect was probably at least in part counteracted by the fact that Mammoth Mountain had not yet formed; it is a much younger feature (215 to 52 ka; Bailey et al., 1976; Mankinen et al., 1986). Therefore, the topographic saddle in the Sierra Nevada west of Long Valley would have been even lower than it is today (probably about 2440 m), perhaps resulting in relatively higher  $\delta^{18}\text{O}$  values for precipitation from storms that migrated up the ancestral San Joaquin Valley. With all of the above arguments and qualifications, it is obvious that assigning a  $\delta^{18}\text{O}$  value to the meteoric ground waters in this area 760,000 years ago is a difficult task. However, assuming these values were comparable to what they are today, a reasonable estimate of the lower bound for fumarolic  $\text{H}_2\text{O}$  can be made by taking such waters and applying a moderate  $^{18}\text{O}$ -shift of a few per mil, giving us  $\delta^{18}\text{O} \approx -13$  for the  $^{18}\text{O}$ -shifted, late-stage,  $100^\circ\text{--}125^\circ\text{C}$  waters that flowed through the surface of fumarolic mounds on the Bishop Tuff outflow sheet; this value is plotted on Fig. 2.10 and used above in the calculation of  $\Delta P$ .

Using the calculations shown in Fig. 2.10 together with the estimated upper and lower bounds for the  $\delta^{18}\text{O}$  of the fumarolic  $\text{H}_2\text{O}$ , it is possible to calculate the range of possible  $\delta^{18}\text{O}$  values for the groundmass of the Bishop Tuff if the different kinds of hot-spring and fumarolic  $\text{H}_2\text{O}$  reached equilibrium with this fine-grained, fragmental tuffaceous groundmass (Fig. 2.11). The diagram in Fig. 2.11 is most useful in illustrating the constraints that the above arguments place upon the temperatures of exchange of the high- $^{18}\text{O}$  samples collected from the tops of fumarolic mounds. Under these assumptions, the sample (FM-21B) with the highest whole-rock  $\delta^{18}\text{O}$  value (+16.7) *must* have been hydrothermally altered at temperatures between  $45^\circ\text{C}$  and  $166^\circ\text{C}$  (Fig. 2.11). If instead of  $500^\circ\text{C}$ , the temperature of  $\text{H}_2\text{O}/\text{rock}$  interaction in the ULZ had been chosen to be  $400^\circ\text{C}$  or  $600^\circ\text{C}$ , the upper bounds on the temperature of exchange of sample FM-21B would

change from 166°C to 148°C or 184°C, respectively; these correspond to  $\delta^{18}\text{O}$  values of +1.8 and +4.7, respectively, for the upper bound on the  $\delta^{18}\text{O}$  of fumarolic  $\text{H}_2\text{O}$ .

These types of calculations do not substantially constrain the temperatures over which most of the low- $^{18}\text{O}$  rocks of the Bishop Tuff outflow sheet ( $\delta^{18}\text{O} = +2.0$  to  $-6.5$ ) were exchanged. Naturally, the low- $^{18}\text{O}$  rocks in the ULZ ( $\delta^{18}\text{O} \approx 5.5$ ) are assumed to have exchanged at temperatures of about 500°C, because these were the temperature and whole-rock  $\delta^{18}\text{O}$  values used to choose the value of the upper limit for the fumarolic  $\text{H}_2\text{O}$ . However, Fig. 2.11 shows clearly that the sample with the lowest whole-rock  $\delta^{18}\text{O}$  value *must* have formed above 300°C, even if the  $\delta^{18}\text{O}$  of the coexisting  $\text{H}_2\text{O}$  had the lowest plausible end-member  $\delta^{18}\text{O}$  value ( $-13$ ). Fig. 2.11 also demonstrates that for the very reasonable assumed range of  $\delta^{18}\text{O}$  for the  $^{18}\text{O}$ -shifted meteoric-hydrothermal fluids ( $-13$  to  $+3.5$ ), exchange temperatures of 450°-650°C are extremely plausible for all of the Bishop Tuff samples having whole-rock  $\delta^{18}\text{O}$  values between  $+5.5$  and  $-6.5$  (107 out of 191 samples).

## **2.4. Detailed $^{18}\text{O}/^{16}\text{O}$ relationships in and around the fumarolic conduits**

### *2.4.1. Fumarolic Mounds*

The samples with the highest whole-rock  $\delta^{18}\text{O}$  values found anywhere in the Bishop Tuff outflow sheet were all collected from the tops of the fumarolic mounds that dot the surface of the ash-flow sheet (Figs. 2.6 and 2.8). The mounds themselves are composed of sintered, unwelded Bishop Tuff of the Tableland Unit and all locally contain hydrous alteration minerals, such as sericite and clays, replacing the volcanic groundmass. Cooling fractures atop the mounds are arranged in roughly polygonal patterns, are typically less than a few meters deep, and are commonly coated with iron oxide minerals, primarily hematite. Sheridan (1970) gives a thorough description of the morphology and mineralogy of these fumarolic mounds, which are found in regions where fumarolic activity was presumably most intense. He reports: "Generally, fumarolic mounds stand 0.5 to 15 m

above the surrounding terrain. There are two main types: (1) domical mounds up to 60 m in diameter, and (2) straight or curved vertical joint ridges 1.5 to 5 m high and up to 600 m long." Both of these endmember types were sampled in this study. However, whereas many of the samples were collected from very elongate mounds, the only true ridge that was sampled was at Site HT.

As shown on Fig. 2.8, whole-rock  $\delta^{18}\text{O}$  values of samples collected from fumarolic mounds span a wide range ( $-2.5$  to  $+16.7$ ). Whereas two samples collected from Site HT in Owens River Gorge exhibit low  $\delta^{18}\text{O}$  values (NG-T2 and NG-T3), all of the remaining 10 samples from fumarolic mounds have either normal or elevated  $\delta^{18}\text{O}$  values (see also Table 2.2). The pumice and groundmass in these two low- $^{18}\text{O}$  samples (NG-T2 and NG-T3) are greyish-white to pink as opposed to the red, orange, and/or brown color of pumice or groundmass in the other 10 analyzed samples (Fig. 2.8). In general, the samples with higher  $\delta^{18}\text{O}$  values are from the larger mounds, and all but one of the mounds had at least one sample that was elevated in  $\delta^{18}\text{O}$ ; the single exception is the small mound from which sample FM-20C ( $\delta^{18}\text{O} = +7.4$ ) was collected, located just north and east of Rock Creek drainage.

Sample FM-21B ( $\delta^{18}\text{O} = +16.7$ ), which has the highest whole-rock  $\delta^{18}\text{O}$  value observed anywhere in the Bishop Tuff, was collected from a large mound directly adjacent to a cooling fracture coated with hematite. Both the high  $\delta^{18}\text{O}$  value and the presence of hematite are indicative of relatively low temperature. However, there is no obvious correlation between  $^{18}\text{O}$  enrichment and the presence of hematite coatings on fracture surfaces, because the four whole-rock samples collected adjacent to fractures with hematite or  $\text{SiO}_2$  coatings span the entire range of whole-rock  $\delta^{18}\text{O}$  values of samples from fumarolic mounds (Fig. 2.8).

Most of the fumarolic mounds sampled in this study had only crude, blocky joints preserved at the surface. However, well-developed, vertical columnar joints were partially exposed at the mound from which RB-4 ( $\delta^{18}\text{O} = +7.8$ ; Table 2.2) was collected, and

arcuate roof joints were present in the mounds sampled at Site CG and Site LG. Excluding sample FM-21B, the two samples collected from these areas of arcuate roof joints have the highest whole-rock  $\delta^{18}\text{O}$  values in the Bishop Tuff (+11.3 and +13.6). Arcuate roof joints may also be present in the mound from which the whole-rock sample with the highest  $\delta^{18}\text{O}$  value was collected (FM-21B), as it is possible that they have not yet been exposed by erosion.

These samples from fumarolic mounds, which represent only the uppermost expressions of the underlying fumarolic meteoric-hydrothermal systems, are also the only samples collected in this study that exhibit the significant  $^{18}\text{O}$ -enrichment and mineralogical alteration indicative of low-temperature hydrothermal exchange ( $\approx 100^\circ\text{C}$ ). As mentioned above in Section 2.3 and as will be explained in more detail below, samples from the underlying fumarolic plumbing system exhibit almost no evidence for low- or moderate-temperature ( $<400^\circ\text{C}$ ) mineralogical alteration, and no evidence for low-temperature  $^{18}\text{O}$ -exchange that cannot be accounted for by the minor effects of incipient weathering and/or hot-spring processes. The near-surface portions of the fumarolic mounds are thus the only places in the Bishop Tuff fumarolic meteoric-hydrothermal systems where we can identify from either isotopic or mineralogical evidence that there was any significant interaction with aqueous fluids at temperatures lower than  $400^\circ\text{C}$ .

#### 2.4.2. *An Isolated Tubular Fumarolic Conduit (Site HT)*

Holy Trinity conduit (Fig. 2.12, Site HT in Fig. 2.1) is exposed high up on a cliff face on the west side of Owens River Gorge beneath a fumarolic mound and directly above Holy Trinity climbing wall (a popular rock-climbing spot located just beneath the entrance to Upper Power Plant Road). This locality was chosen because it lies 40-50 m away from any other obvious fumarolic feature that conceivably could complicate the  $^{18}\text{O}/^{16}\text{O}$  pattern. The conduit itself is much smaller than the one illustrated in Fig. 2.7. Our isotopic measurements (Table 2.2) define a series of  $\delta^{18}\text{O}$  contours that form an oval-shaped "bulls-

eye" with  $\delta^{18}\text{O} < +3$  centered on the 2m x 6m cavity at the axis of this radiating set of columnar joints (Fig. 2.8), indicating that this  $^{18}\text{O}$ -minimum is the locus of maximum  $^{18}\text{O}/^{16}\text{O}$  exchange between rock and meteoric fluid at this locality (i.e., largest material-balance water/rock ratio). The  $^{18}\text{O}$ -depletions are greatest on the walls of the cavity (down to +1.3), which are a dark salmon-pink color in contrast to the immediately adjacent lighter pink tuff. The vertically elongate  $\delta^{18}\text{O}$  contours on Fig. 2.12 indicate that significant quantities of meteoric-hydrothermal fluids also exchanged oxygen with the rock directly above the cavity. However, the closely spaced  $\delta^{18}\text{O}$  contours both below and directly to the side of the central cavity imply that there was no major lateral or downward outflux of such fluids. The radiating pattern of columnar joints indicates that isothermal surfaces were curved around the central cavity, more or less subparallel to the surfaces of constant  $\delta^{18}\text{O}$ . This suggests that the gradients in  $^{18}\text{O}/^{16}\text{O}$  and temperature were coupled, and that both patterns were produced simultaneously as a result of subhorizontal fluid flow and heat transport through the tubular conduit in a direction approximately perpendicular to the cliff face.

Although the tubular conduit at Site HT in the Bishop Tuff outflow sheet is located at much greater depth than the shallow tunnels described by the early visitors to the Valley of Ten Thousand Smokes, the morphological and  $^{18}\text{O}/^{16}\text{O}$  evidence discussed above suggest that both types of conduits represented pathways for large-scale lateral transport of meteoric-hydrothermal fluids that locally disturbed the conductive thermal gradients in these ash-flow tuffs. For example, Shipley (1920) describes a possibly analogous situation in the Valley of Ten Thousand Smokes where a cave-in exposed a "subterranean, horizontal tunnel, 12 feet in diameter and 75 feet below the surface, the walls of which were baked a deep, brick red." Also, by lowering a plumb bob into the caved-in roof of another of these shallow tunnels at the Valley of Ten Thousand Smokes, Allen and Zies (1923) demonstrated conclusively that there was significant lateral transport of hot gases in the tunnel below.

Whereas it is certain that the whole-rock  $\delta^{18}\text{O}$  contours that are roughly concentric around the central cavity in the lower part of the section at Site HT must be the result of  $^{18}\text{O}$  exchange associated with flow of fumarolic gases through the tubular conduit, it is likely that the whole-rock  $\delta^{18}\text{O}$  values in the upper part of the Site HT profile were in part determined by overlapping  $^{18}\text{O}$  exchange effects associated with the independent meteoric-hydrothermal flow system in the Upper Low- $^{18}\text{O}$  Zone (ULZ) of the tuff. Fig. 2.12 illustrates that low- $^{18}\text{O}$  samples in the uppermost part of the tuff (NG-T2 and NG-T3) are physically separated from the low- $^{18}\text{O}$  samples in the vicinity of the central conduit by a zone of largely unwelded, white-colored Bishop Tuff that is not  $^{18}\text{O}$ -depleted (exemplified by sample NG-T1 on Fig. 2.12). There are several possible scenarios that can account for the geometry of  $^{18}\text{O}$ -depletion at Site HT, none of which are mutually exclusive. For example, these two systems may have both operated in the upper part of the tuff over different time intervals. Alternatively, it may be that during fumarolic activity, two different flow systems and geometries prevailed, and the meteoric-hydrothermal fluids in the ULZ were to a large degree physically separated from fumarolic fluids flowing through the underlying tubular conduit. A broader scale, shallow meteoric-hydrothermal circulation in the ULZ may have combined with a series of deeper, localized DFS circulation systems associated with structures analogous to the tubular conduit, and/or to the steep fissures described below, to create a composite low- $^{18}\text{O}$  signature in a 20- to 80-m-thick zone throughout the entire upper part of the tuff in the mapped fumarolic area. This early low- $^{18}\text{O}$  signature may have then been at least partially overprinted by a late-stage, lower-temperature  $^{18}\text{O}$  exchange event that locally raised the whole-rock  $\delta^{18}\text{O}$  values in the uppermost part of the tuff, particularly in the vicinity of the mounds.

Patterns of whole-rock  $^{18}\text{O}$ -depletion within the zone of columnar joints around the Site HT tubular conduit suggest that there was indeed a late-stage  $^{18}\text{O}$ -enrichment event near the top of the well developed columnar joints that are located directly over the tubular conduit. At the level of the tubular conduit, which is also at the base of the sampled profile shown in

Fig. 2.12, samples collected in a vertical traverse extending upward from the central cavity (right profile in Figs. 2.12 and 2.13; NG-3 samples in Table 2.2) have lower whole-rock  $\delta^{18}\text{O}$  values than those collected in a vertical traverse shown on the far left side of this zone of shallow-dipping columnar joints (left profile in Figs. 2.12 and 2.13; NG-1 samples in Table 2.2). In contrast, at the top of the well-developed columnar joints shown in Fig. 2.12, whole-rock  $\delta^{18}\text{O}$  values in the right profile are generally higher than those in the left profile (Fig. 2.13). The whole-rock  $\delta^{18}\text{O}$  values in the lower part of the section undoubtedly reflect the effects of enhanced high-temperature  $^{18}\text{O}$ -exchange directly adjacent to the conduit. Elevated whole-rock  $\delta^{18}\text{O}$  values near the tops of the columnar joints in the right profile, directly over the tubular conduit, may reflect the effects of the downward progression of late-stage low-temperature fluids along the extinct fumarolic conduits during the waning stages of fumarolic activity.

#### 2.4.3. *Fumarolic Zones Along Steep Fissures (Site LG)*

The Lower Gorge site (LG in Fig. 2.1) encompasses a zone containing the kinds of wide, steep fissures that in the Bishop Tuff are characteristically associated with extreme  $^{18}\text{O}$  depletions. At this site, these fissures are more than 30 m in length and typically 1-5 cm wide. The entire zone was sampled along a subhorizontal, 140-m-long, road-cut traverse on the west side of Middle Power Plant Road (Fig. 2.14); it includes a set of 32 samples (LG10-LG26, Table 2.2) collected from very fresh outcrops located along Middle Power Plant Road that straddle both sides of the main zone of fissures, which is about 40 m wide. This 40-m-wide zone at the center of the photograph in Fig. 2.14a exhibits the lowest  $\delta^{18}\text{O}$  values yet encountered in the Bishop Tuff outflow sheet. The range of  $\delta^{18}\text{O}$  values observed around the steep fissure shown in Fig. 2.14b indicates that the tuff in the vicinity of these fissures has been pervasively depleted in  $^{18}\text{O}$  by high-temperature fumarolic fluids ( $\delta^{18}\text{O} = +0.1$  to  $-6.5$ ). The samples collected farther than 10-15 m from either side of the zone of steep fissures are also  $^{18}\text{O}$ -depleted, but to a lesser degree ( $\delta^{18}\text{O} =$



+2.8 to +6.3; Fig. 2.14a). The fact that shallow-dipping columnar joints terminate at a high angle into these steep fissures implies that these columnar joints formed as a result of perturbations in the local thermal gradients in the tuff directly adjacent to the earlier-formed steep fissures. Thus, the steep, wide fissures clearly provided (1) a major focus for circulating meteoric-hydrothermal fluids during high-temperature fumarolic activity, and (2) a cooling surface from which sub-horizontal columnar joints could emanate.

Samples LG-R1 through LG-R5 were collected from the walls of Owens River Gorge on rappel down a 35-m-long traverse below Middle Power Plant Road directly beneath the rightmost steep fissure labeled on Fig. 2.14a. Proceeding downward, the  $\delta^{18}\text{O}$  values remain consistently low at  $-0.5$  to  $-2.6$  in the upper part of this traverse, and then they go up very slightly (to  $+0.7$  to  $+0.1$ ) before sharply increasing to a relatively high  $\delta^{18}\text{O}$  value at the point at which the tuff becomes densely welded (LG-R1,  $\delta^{18}\text{O} = +8.6$ ; compare Fig. 2.9 and Fig. 2.14a). As will be discussed in more detail below, these higher  $\delta^{18}\text{O}$  values are characteristic of the entire lower half of the ash-flow sheet, indicating that low- $^{18}\text{O}$  meteoric-hydrothermal fluids did not pervade the densely welded black tuff in any great quantities. Low- $^{18}\text{O}$  samples collected 15 and 30 m farther along the road to the north of this photograph (LG-27 and LG-28, respectively) indicate that the very sharp boundary between  $^{18}\text{O}$ -depleted rock ( $\delta^{18}\text{O} < +0.1$ ) above and normal- $^{18}\text{O}$  rock ( $\delta^{18}\text{O} > +7$ ) below can be traced laterally along the top of the dense, black tuff for at least 50 m. However, as at Site HT,  $^{18}\text{O}$  depletions are smaller in these marginal samples (LG23-LG28; Table 2.2), indicating that meteoric-hydrothermal circulation was less vigorous 50 m to the north of the steep fissures at Site LG than it was directly adjacent to these features.

While it is clear from the  $\delta^{18}\text{O}$  and field relations described above that the steep fissures are a locus for meteoric-hydrothermal fluid flow and  $^{18}\text{O}$ -exchange at high temperatures, it is interesting to note that the whole-rock samples with the lowest  $\delta^{18}\text{O}$  values within the zone of steep fissures (Fig. 2.14) are not those collected directly from the sides of these structures (e.g., Fig. 2.14b; see samples LG-15.15 and LG-20.5, Table 2.2). The rock

directly adjacent to the steep fissures themselves is extremely indurated, accounting for the smooth, relatively unbroken surfaces of the sides of these fissures exposed in the cliff face. It appears that silicification of the groundmass of the tuff in the vicinity of steep fissures, most especially within a few millimeters of their smooth surfaces, has both increased the strength of the rock and decreased its permeability out to a distance of a few tens of centimeters of the fracture surface. In addition, some of the surfaces of these fissures are encrusted with high- $^{18}\text{O}$  mineral deposits; two analyses of opal collected from a fracture at Site CG have  $\delta^{18}\text{O} = +10.3$  and  $+12.9$  (Table 2.3), suggesting that the opal was either deposited at low temperature or exchanged with a low temperature fluid or was deposited by a strongly  $^{18}\text{O}$ -shifted fluid (e.g., one with an end-member value for  $\delta^{18}\text{O} \approx +3.5$  at  $250^{\circ}\text{C}$ - $350^{\circ}\text{C}$ ). At Site LG, a white material (largely tridymite replaced by opaline silica?) coating a fracture surface in the partially welded tuff has an extremely high  $\delta^{18}\text{O}$  value of  $+17.9$  (Sample LG-coat; Table 2.3) and must have been deposited at very low temperatures ( $<100^{\circ}\text{C}$ , see Fig. 2.11). Further mineralogical evidence suggesting that late-stage, somewhat lower-temperature fluids ( $\approx 300^{\circ}\text{C}$ - $400^{\circ}\text{C}$ ) may have been important directly adjacent to main fumarolic conduits comes from rare deposits of epidote at Site LG, which are located in the groundmass of the tuff within 1.5 mm of the rightmost fissure surface shown in Fig. 2.14a.

Fractures along columnar joints adjacent to these main fumarolic fissures appear to have been less affected by late-stage, low-temperature processes. Within several meters of the steep fissure shown on the left of Fig. 2.14a, columnar joints are separated from one another by as much as 1 cm, and the outlines of individual columns can be observed on the otherwise smooth surface of one side of the fissure (Fig. 2.14b). The groundmass from samples collected along planes between joints (where extremely low- $^{18}\text{O}$  samples were collected) is less indurated than that of the interior of the column, and it is also more powdery and fractured to a greater degree (Fig. 2.14c). The samples with the lowest  $\delta^{18}\text{O}$  values in the Bishop Tuff outflow sheet were collected from such sites along the edges of

columnar joints that terminate into the steep fissure shown in Fig. 2.14b (Samples LG-15, LG-15.8, LG-15.9, LG-16, LG-16.21, LG-16.22, and LG-17; Table 2.2). Note, however, that the interior parts of some of these same columns are not as  $^{18}\text{O}$ -depleted as their margins (Samples LG-15.12, LG-15.17 and LG-16.19.5; Table 2.2). It is reasonable to infer that the interiors of the columns experienced lower  $\text{H}_2\text{O}/\text{rock}$  ratios during high-temperature fumarolic activity than the adjacent column margins, because column margins were very likely the local conduits for the fumarolic fluids. It is important to reiterate that none of the samples collected from the low- $^{18}\text{O}$  zone at Site LG contain feldspar or quartz phenocrysts that are mineralogically altered or  $^{18}\text{O}$ -depleted, indicating that the kind of high-temperature meteoric-hydrothermal activity under discussion must have been extremely short-lived (Gazis et al., 1996; Holt and Taylor, 1998).

What these  $^{18}\text{O}$ -data and mineralogical observations of the steep fissures seem to indicate is that whereas these steep fissures were clearly a major type of conduit for high-temperature meteoric fluids during DFS-type fumarolic activity (and also a great influence on the growth direction of adjacent columnar joints), the rock surfaces directly adjacent to these wide fissures also underwent: (1) silicification along the major conduits formed in the early stages of fumarolic activity (perhaps during a magmatic degassing stage), making the tuff less permeable and less susceptible to  $^{18}\text{O}/^{16}\text{O}$  exchange with the low- $^{18}\text{O}$  meteoric-hydrothermal fluids, and/or (2) later-stage meteoric-hydrothermal exchange, either at lower temperatures or with strongly  $^{18}\text{O}$ -shifted meteoric-hydrothermal fluids, that resulted in a local high- $^{18}\text{O}$  overprint upon the  $^{18}\text{O}$ -depleted rocks around the major fumarolic conduits. Deposits of very high- $^{18}\text{O}$  opaline silica directly on the surfaces of these fissures would argue for the latter scenario (Table 2.3). Silicification during the waning stages of fumarolic activity would likely decrease the permeability of the adjacent rocks, sealing the matrix of the tuff and protecting it from further exchange with any of the really low-temperature hot-spring fluids that would have appeared during the waning stages of fumarolic activity. In addition, this less-vigorous, very low-temperature hydrothermal

circulation would be more likely to affect the major, throughgoing fissures; the less accessible fractures along the margins of adjacent columnar joints would be correspondingly less affected by this process, perhaps explaining their retention of low whole-rock  $\delta^{18}\text{O}$  values. Somewhat similar features are observed in the shallow parts of the ash-flow sheet at the Valley of Ten Thousand Smokes (see Chapter 4).

Samples were also collected along Middle Power Plant Road at approximately 15 m intervals over a distance of approximately 150 m to the left (south) of the area shown in Fig. 2.14a all the way to where the road exits the gorge at the top of the tuff. This group of samples (LG-1 to LG-9) is from the Tableland Unit. Samples LG-1 to LG-6 are from the uppermost part of the Tableland Unit and for the most part have elevated whole-rock  $\delta^{18}\text{O}$  values (+7.7 to +10.0). The one exception is the locality where samples LG-3 and LG-3B ( $\delta^{18}\text{O} = +6.4$ ) were collected, which is located at the intersection of another, smaller set of steep fissures with Middle Power Plant Road. These samples are very slightly  $^{18}\text{O}$ -depleted, which indicates that the rocks adjacent to steep fissures may be  $^{18}\text{O}$ -depleted to very shallow levels in the tuff if these major hydrothermal conduits continue upward towards the surface, as they have at this locality. Samples LG-7 to LG-9 also have relatively low  $\delta^{18}\text{O}$  values (-2.1 to +3.9). Together with LG-10 and LG-11 (shown on Fig. 2.14a), these samples may represent the effects of the broadly based meteoric-hydrothermal circulation regime in the upper stratigraphic zone (ULZ). These samples straddle the base of the Tableland Unit, which is where the largest ULZ-type  $^{18}\text{O}$ -depletions are typically found.

#### *2.4.4. Fractures and Veins in the Densely Welded Zone (DWZ)*

Virtually the entire lower half of the Bishop Tuff outflow sheet beneath the areas of most intense fumarolic activity is made up of a densely welded black tuff having very uniform whole-rock  $\delta^{18}\text{O}$  values (+7.1 to +9.9) similar to the original Bishop Tuff magma, or just slightly  $^{18}\text{O}$ -enriched relative to that magma. In addition to the 9 samples discussed

below that were collected adjacent to steep fractures, 16 more-or-less random samples from the densely welded black tuff were analyzed from Sites CG, LG, AG, RC1, CC-L, and LG-B. Only two of these 25 samples have whole-rock  $\delta^{18}\text{O} < +7$ , and none have  $\delta^{18}\text{O} < +5.7$ , even though at each of these sites significant whole-rock  $^{18}\text{O}$ -depletions (down to  $\delta^{18}\text{O} = -6.5$ ) are observed higher up in the ash-flow sheet. This indicates that the black tuff in this Densely Welded Zone (DWZ) was probably hot, ductile, and locally unfractured, and thus essentially impermeable to the influx of significant amounts of low- $^{18}\text{O}$  meteoric-hydrothermal fluids during the lifetime of fumarolic activity, or else that magmatic gases escaping at lithostatic pressures blocked the influx of low- $^{18}\text{O}$  meteoric fluids, which would necessarily have been under hydrostatic pressures. Only very locally, and very rarely, did meteoric  $\text{H}_2\text{O}$  penetrate either downward into the hot, densely welded tuff or upward from the base of the ash-flow sheet.

The dominant type of jointing in the DWZ is a set of regularly spaced, narrow, steep fractures that commonly cut through the entire upper part of the section of densely welded black tuff at intervals of 3 to 10 m (see Figs. 2.7 and 2.9); these throughgoing fractures provide a sharp contrast with the overlying steep fissures in that they are much narrower (<0.5 cm wide), and they are not associated with either shallow-dipping columnar joints or  $^{18}\text{O}$ -depleted whole rock. The surfaces of these narrow fractures are typically coated with a thin ( $\approx 1$ -2 mm) white layer that may be similar in mineralogy to a material identified as dominantly tridymite in a couple of veinlet samples (see below). In one of the two steep fractures where it has been sampled, this white material exhibits a very high  $\delta^{18}\text{O}$  value (RC-WS,  $\delta^{18}\text{O} = +13.8$ ), suggesting deposition at relatively low temperatures (e.g., see Fig. 2.11). The other sample is isotopically similar to the surrounding tuff (LG-frac,  $\delta^{18}\text{O} = +8.6$ ; Table 2.3). A thin (< 1 mm) pink alteration selvage commonly separates the white coating from the adjacent black tuff.

Samples of the densely welded tuff were collected adjacent to the pink alteration selvages along the margins of nine of the steep fractures (CG-9, CG-L1, CG-L2, NG-L1,

NG-L2, AG-14, AG-16, LG-R1, and CC-L11); seven of these samples have remarkably uniform  $\delta^{18}\text{O}$  values (+8.2 to +9.9) that are slightly  $^{18}\text{O}$ -enriched relative to the original Bishop Tuff magma, but basically identical to the samples of densely welded black tuff collected well away from any of the steep fractures. Of the remaining two samples, one has a whole-rock  $\delta^{18}\text{O}$  value (+7.3, CG-L1) that is virtually unchanged from that of the original Bishop Tuff magma, and the other is only slightly  $^{18}\text{O}$ -depleted (+5.7, CG-L2). The relatively restricted range of  $\delta^{18}\text{O}$  values associated with these narrow steep fractures in the lower part of the ash-flow sheet (+5.7 to +9.9) is thus very different from the wide range of  $\delta^{18}\text{O}$  values (-6.5 to +4.4) associated with the much wider openings in the aforementioned steep fissures that are localized beneath fumarolic mounds and which cut the partially welded upper portion of the Bishop Tuff.

The only  $^{18}\text{O}$ -depleted sample (CG-L2) yet found in the DWZ was collected at the lowermost exposure of what appears to be a typical steep fracture in the densely welded tuff. However, this particular fracture can be traced upward to where it is connected to a steep fissure in the overlying,  $^{18}\text{O}$ -depleted, partially welded tuff. Thus, the slight degree of  $^{18}\text{O}$ -depletion observed adjacent to this fracture may indicate that this sample of densely welded black tuff underwent a very limited degree of exchange with the same types of downward-migrating meteoric-hydrothermal fluids that produced the much more striking  $^{18}\text{O}$ -depletions associated with the overlying, and directly connected, fumarolic structures.

In the present study, in addition to CG-L2, two other samples (NG-L1 and NG-L2) were collected from steep fractures in the densely welded black tuff that can be traced upward into a fumarolic structure, in this case, with the tubular conduit at Site HT. Samples CG-L2 and NG-L2 are also similar in that they are both cut by numerous veinlets containing identifiable tridymite. However, whereas CG-L2 is slightly  $^{18}\text{O}$ -depleted, samples NG-L1 and NG-L2 are both  $^{18}\text{O}$ -enriched (+8.8 and +9.9, respectively). These differences may be related to the fact that the volume of strongly  $^{18}\text{O}$ -depleted rock ( $\delta^{18}\text{O} < +2$ ) at Site HT is confined to within only a few meters of the central cavity of the

tubular conduit (see Fig. 2.12), and is therefore much smaller than the volume of low- $^{18}\text{O}$  rock associated with the broad zone of steep fissures at Site CG. Also, the depth profile at Site CG lies beneath the edge of the largest fumarolic mound sampled in this study. If we had *a priori* been asked to predict where in the Bishop Tuff outflow sheet we might expect to find at least some  $^{18}\text{O}$ -evidence for penetration of low- $^{18}\text{O}$  meteoric-hydrothermal fluids deep into the DWZ, it would have probably been at this location. Thus it was satisfying to discover that Site CG does indeed contain the lowest whole-rock  $\delta^{18}\text{O}$  value (+5.7) observed anywhere within the densely welded black tuff.

The normal to slightly  $^{18}\text{O}$ -enriched characteristics of virtually all of the samples of the densely welded black tuff collected adjacent to fractures indicate that for the most part, these types of narrow, steep fractures cannot have been conduits for any significant quantities of low- $^{18}\text{O}$  fluids at high temperature. If these fractures were formed soon after the emplacement of the ash-flow sheet, they can only have been conduits for magmatic fluids produced by degassing of the densely welded tuff (e.g., see Sheridan, 1970, and the discussion below in Section 2.7.1), or perhaps for small amounts of evolved (i.e., strongly  $^{18}\text{O}$ -shifted) meteoric  $\text{H}_2\text{O}$ .

In addition to the above-described steep fractures, one often observes a set of very well defined steep, continuous veins in the lower part of the DWZ in areas where the tuff is very thick (as in Owens River Gorge and Chidago Canyon, Fig. 2.15). These steep veins are typically: (1) 0.5 to 3 mm wide and coated with tridymite and small amounts of fayalite; (2) cross-cut by myriad, shallow-dipping, discontinuous veinlets of similar mineralogy; and (3) traceable continuously upward for 10-20 m, where they may merge into and connect with the aforementioned, narrow, steep fractures in the densely welded black tuff. The shallow-dipping veinlets associated with these veins commonly connect fiamme (Fig. 2.15), and some of the larger fiamme appear to have preserved pore spaces into which tridymite and fayalite have crystallized. Because the tridymite veinlets connect fiamme, and because their sub-horizontal orientations suggest that, like the fiamme, they have been

flattened during welding, it is probable that these veinlets formed before the densely welded tuff was fully compacted and welded. Their cross-cutting relationships to the steep veins indicate that those sets of steep veins could have formed even earlier than the veinlets; in this interpretation, the sets of narrow, steep fractures may connect to these steep veins simply because the veins represent earlier-formed planes of weakness in the densely welded tuff.

For the most part, these veins and veinlets exhibit  $\delta^{18}\text{O}$  values within the range observed in the densely welded black tuff itself (i.e., similar to or slightly higher than the  $\delta^{18}\text{O}$  value of the Bishop Tuff magma). For example, samples from a steep, continuous vein along Middle Power Plant Road and the fracture to which it connects have  $\delta^{18}\text{O}$  values of +8.8 and +8.6, respectively (Fig. 2.16, Table 2.3). Near the same locality, samples of a discontinuous, shallow tridymite veinlet and the glassy fiamme to which it connects both exhibit  $\delta^{18}\text{O}$  values of +9.1 (Fig. 2.16, Table 2.3). Two samples were collected specifically because they contain myriad tridymite veins and veinlets, but these also are isotopically similar to all the others (LG-34, whole-rock  $\delta^{18}\text{O} = +8.5$ , Fig. 2.16, Table 2.2; and CC-L10 from Lower Chidago Canyon, whole-rock  $\delta^{18}\text{O} = +7.1$ , Fig. 2.18). Samples CG-L2 and NG-L2 also contain tridymite veins and veinlets, but whereas the latter sample is elevated in  $\delta^{18}\text{O}$  (+9.9), CG-L2 is the  $^{18}\text{O}$ -depleted sample discussed in detail above ( $\delta^{18}\text{O} = +5.7$ ). Again, note that CG-L2 is the only veinlet-riddled sample with even a hint of an  $^{18}\text{O}$ -depleted signature; this slight  $^{18}\text{O}$ -depletion is perhaps a result of its fracture connection to the large overlying zone of strongly  $^{18}\text{O}$ -depleted rock (see above). The  $^{18}\text{O}/^{16}\text{O}$  data are thus all compatible with the idea that these tridymite veins and veinlets were formed early by degassing of magmatic  $\text{H}_2\text{O}$  from the ash-flow sheet, and that only locally, in rare samples such as CG-L2, were those  $^{18}\text{O}/^{16}\text{O}$  effects occasionally overprinted by interactions with meteoric-hydrothermal fluids.

Finally, we must address one of the most enigmatic samples collected in this study. Out of all of the veins in the densely welded tuff sampled in this work, only two tiny



samples have been found to be as strikingly  $^{18}\text{O}$ -depleted as those portions of the ash-flow sheet that contain the major fumarolic structures. Both of these unique low- $^{18}\text{O}$  samples were collected from a very thin, steep, tridymite vein (LG-vein1) located at least 10 m from any other veins or veinlets along Middle Power Plant Road; two analyses of this vein gave  $\delta^{18}\text{O} = -0.4$  and  $0.0$  (Table 2.3). Remarkably, the densely welded tuff within 2.5 cm of this vein is no way isotopically unusual; it has a slightly elevated whole-rock  $\delta^{18}\text{O}$  value of  $+8.4$  (LG-30, Fig. 2.16, Table 2.2), similar to all of the other samples of densely welded black tuff.

The very low  $\delta^{18}\text{O}$  value of this vein proves that it was formed from a low- $^{18}\text{O}$  meteoric-hydrothermal fluid at high temperature (see Fig. 2.11). However, there is no fumarolic mound in the Bishop Tuff above the exposure of veins and veinlets in the densely welded tuff along Middle Power Plant Road, nor is there any morphological evidence for fumarolic activity, such as shallow-dipping columnar jointing, in the overlying tuff. Samples LG-B1 to LG-B6 were collected in the Bishop Tuff above this location, and they show evidence for only a limited amount of meteoric-hydrothermal exchange, and that is seen very high up in the section, nearly 60 m above the LG-30 and LG-vein1 samples (Fig. 2.16).

Careful study was made of this site, and we found absolutely nothing unusual in the jointing pattern, the color, or the welding zonation of the tuff either below or above this particular vein. Because this low- $^{18}\text{O}$  vein represents only a very tiny volume, and because it is unique among our sampling set, it is perhaps appropriate to appeal to an unusual set of circumstances to explain the two LG-vein1 samples. One might speculate that this is perhaps a locality where the hot ash-flow tuff overrode a body of water (or ice?) during emplacement, resulting in phreatic activity that allowed transient fractures to form in the viscous, but still largely ductile, densely welded tuff. However, this would have had to happen very quickly in order that no  $^{18}\text{O}/^{16}\text{O}$  exchange occurred with the densely welded tuff 2.5 cm away from the vein. Because of the hot, ductile, glassy nature of the densely

welded black tuff, any steep veins that formed during such an event could have been closed and sealed off soon after their formation, before welding was complete (thereby protecting the vein from the  $^{18}\text{O}$ -exchange associated with degassing of higher- $^{18}\text{O}$  magmatic  $\text{H}_2\text{O}$ , and preserving the unique, low- $^{18}\text{O}$  signature). In any case, none of these putative meteoric fluids released during phreatic activity could have been abundant enough to fuel significant fumarolic activity or to strongly affect the  $\delta^{18}\text{O}$  signatures of either the adjacent densely welded black tuff or of the groundmass in the overlying ash-flow tuff. It is important to reiterate that this is the only one of these veins in the DWZ that can definitely be shown to have been deposited at high temperatures from a low- $^{18}\text{O}$  fluid, and it is located well away from (1) the areas where other veins and veinlets are abundant, and (2) the areas of intense fumarolic activity. This sample (LG-vein1) is clearly anomalous in its  $^{18}\text{O}/^{16}\text{O}$  pattern, and even though a search was specifically undertaken to try to find another vein with similar low- $^{18}\text{O}$  values, none was located in the limited time available.

Mineralogical and structural evidence strongly suggest that the tridymite veins and veinlets in the densely welded tuff formed at very high temperatures and very early, perhaps before welding was complete. The  $^{18}\text{O}/^{16}\text{O}$  evidence in general supports this conclusion, because it is clear that no significant quantities of meteoric-hydrothermal fluids penetrated the densely welded black tuff during the first few years after eruption. Virtually all of the  $^{18}\text{O}/^{16}\text{O}$  phenomena in the lower half of the ash-flow sheet (i.e. the DWZ) can be explained by degassing of magmatic volatiles that had  $\delta^{18}\text{O}$  values similar to the original Bishop Tuff magma. However, there are a couple of  $^{18}\text{O}$ -depleted samples (particularly LG-vein1) that seem to require a special explanation involving local influx of small amounts of a high-temperature meteoric-hydrothermal fluid, and there is also evidence for local overprinting by high- $^{18}\text{O}$  materials deposited at much lower temperatures. Thus, although precipitation of minerals in these veins and veinlets typically seems to have involved either magmatic gases, and/or small amounts of highly  $^{18}\text{O}$ -shifted meteoric  $\text{H}_2\text{O}$ , it may also be that, very rarely, some of these veinlets formed from larger amounts of low-

$^{18}\text{O}$  meteoric  $\text{H}_2\text{O}$  during local, pre-welding phreatic events at the base of the Bishop Tuff. Sorting out these unique low- $^{18}\text{O}$  events in the densely welded tuff will require a good deal of careful sampling and much more  $^{18}\text{O}/^{16}\text{O}$  data.

#### 2.4.5. $^{18}\text{O}/^{16}\text{O}$ -Depth Profiles Beneath Fumarolic Mounds (Sites CG and CC-L)

The Central Gorge traverse (Site CG, Fig. 2.1) includes 30 samples collected along a steep side gully on the west side of Owens River Gorge. This site is located beneath the margin of a very large (>100 m diameter) fumarolic mound, well away from any major fumarolic structures, but containing a broad, well-defined zone of shallow-dipping columnar joints that cut the pervasively devitrified, partially welded tuff (Fig. 2.17). Whereas the upper 1/3 of this traverse is strongly  $^{18}\text{O}$ -depleted, the lower 2/3 has very uniform  $\delta^{18}\text{O}$  values (+6.1 to +9.2), which are largely unchanged from the original  $\delta^{18}\text{O}$  value of the Bishop Tuff magma. The major change in  $^{18}\text{O}/^{16}\text{O}$  occurs at the base of a 40-m-thick, low- $^{18}\text{O}$  zone, within a transition interval where the  $^{18}\text{O}/^{16}\text{O}$  gradient is extremely sharp (change in whole-rock  $\delta^{18}\text{O}$  of about 3 per mil per meter). The steepest part of this  $^{18}\text{O}$ -gradient can be exactly placed between two very closely spaced samples collected 2 m apart: CG-5.62 ( $\delta^{18}\text{O} = -1.1$ ) and CG-5.64 ( $\delta^{18}\text{O} = +4.8$ ). Beneath this sharp transition there is no  $^{18}\text{O}/^{16}\text{O}$  evidence for any significant meteoric-hydrothermal interaction in the underlying,  $\approx 100$ -m-thick densely welded black tuff.  $^{18}\text{O}/^{16}\text{O}$  analyses of pink, devitrified groundmass and dense black fiamme from 3 samples of densely welded tuff (Tables 2.1 and 2.2) collected immediately above the upper boundary of the densely welded black tuff indicate that: (1) both the groundmass ( $\delta^{18}\text{O} = -3.0$  to  $-3.1$ ) and fiamme (+4.7 to +5.8) exchanged with meteoric-hydrothermal fluids, and (2) these hot fluids penetrated downward at least 5 meters into the densely welded tuff at this location.

Within the 40-m-thick interval where the upper part of the ash-flow sheet at Site CG is pervasively  $^{18}\text{O}$ -depleted, and where the whole-rock  $\delta^{18}\text{O}$  values of a continuous profile of 20 samples are all lower than +5.2, there is also a continuous, 15-m-thick, extremely  $^{18}\text{O}$ -

depleted interval where the whole-rock  $\delta^{18}\text{O}$  values all lie between 0.0 and  $-2.5$ . Except for the LG traverse along Middle Power Plant Road, this is the largest zone of intensely  $^{18}\text{O}$ -depleted tuff (i.e.,  $\delta^{18}\text{O} < 0$ ) found anywhere in the Bishop Tuff outflow sheet. This is probably because the samples in the depth profile at Site CG were collected along a side gully that cuts through the margin of the biggest fumarolic mound sampled in this study. Beneath this fumarolic mound, there are at least four steep fissures of the type sampled at Site LG and which are shown in Fig. 2.14a. There is also at least one tubular conduit beneath this gigantic ( $\approx 100$ -m-across) fumarolic mound. In addition, the shallow-dipping columnar joints shown in Fig. 2.17, with which the 20 extremely low- $^{18}\text{O}$  samples mentioned above exactly coincide, are at the same stratigraphic horizon as the fumarolic conduits exposed beneath the center of this fumarolic mound 40 to 120 m to the south of Site CG. Thus the large zone of extremely low- $^{18}\text{O}$  samples at Site CG is readily inferred to be due to: (1) the high temperatures associated with proximity to numerous fumarolic conduits beneath a very large fumarolic mound; and (2) the exact coincidence in space with a package of shallow-dipping columnar fractures that would have provided an appropriately high permeability. Also, it may be conjectured that there is in fact an unexposed steep fissure buried beneath the talus in the steep gully located just 3 to 5 m south of the Site CG depth profile, because, as discussed in more detail in Chapter 3, these kinds of large zones of shallow-dipping columnar joints are almost invariably juxtaposed against such a fissure.

Site CC-L, located in Lower Chidago Canyon, is also located directly beneath a fumarole mound, and although the mound is much smaller than at Site CG (only  $\approx 10$  m in diameter), the relationship of whole-rock  $^{18}\text{O}$ -depletions to welding zonation in the tuff is virtually the same as it is at Site CG (Fig. 2.18). At Site CC-L, about 20 m of densely welded black tuff is exposed; however, it is not clear how thick the densely welded black tuff is in this location, because its base is not exposed. The partially welded to unwelded upper part of the tuff is approximately 85 m thick, which is very similar to the thickness of the upper part of the ash-flow sheet at Site CG. Although shallow-dipping columnar joints

are nicely exposed in the partially welded tuff just below the surface expression of the fumarolic mound, talus covers a good portion of the rest of the cliff face. Therefore, if any fumarolic conduits of the type observed at Site CG are present at Site CC-L, they could not be identified (Fig. 2.18).

As was *a priori* expected, samples collected from the depth profile at Site CC-L show an  $^{18}\text{O}$ -depleted whole-rock pattern analogous to that observed at Site CG, but one in which the magnitude of these  $^{18}\text{O}$ -depletions is much less ( $\delta^{18}\text{O} = +4.5$  to  $+5.2$  vs.  $\delta^{18}\text{O} = -2.6$  to  $+3.4$ , respectively). The three samples from the lowest part of this profile (CC-L3, CC-L10, and CC-L11; Fig. 2.18) have normal to high whole-rock  $\delta^{18}\text{O}$  values ( $+7.1$  to  $+8.4$ ). Higher up, samples collected from the zone of shallow-dipping columnar joints in the overlying partially welded tuff are all  $^{18}\text{O}$  depleted ( $+4.5$  to  $+5.2$ ; Fig. 2.18), whereas samples collected from even higher up in the section and atop the fumarolic mound are either normal or slightly  $^{18}\text{O}$ -enriched ( $+7.7$  to  $+8.9$ ; Fig. 2.18). Samples CC-L3 ( $+8.1$ ) and CC-L4 ( $+4.7$ ) straddle the zone where there is a sharp gradient in whole-rock  $\delta^{18}\text{O}$  values ( $\approx 1.7$  per mil per meter) that is again completely analogous, but less steep, than the  $^{18}\text{O}/^{16}\text{O}$  gradient observed at Site CG. Also, as at Site CG, this sharp transition is located at a similar horizon, namely at the base of the shallow-dipping columnar joints and about 10 m above the top of the densely welded black tuff.

The very complete, and extensively sampled Central Gorge (Site CG) profile (Fig. 2.17) provides a framework upon which we can compare the  $^{18}\text{O}/^{16}\text{O}$  data obtained from the vicinity of various kinds of conduits beneath fumarolic mounds at other localities in the Bishop Tuff outflow sheet (Sites HT, LG, and CC-L). Although the base of the tuff is not exposed here, Site CG provides a virtually complete section through the Gorges Lobe of the ash-flow sheet, which constitutes our major sampling unit in the Bishop Tuff at Sites HT, LG, and CG. At CC-L, the major sampling unit is the Chidago Lobe. However, this unit, together with the Gorges Lobe, corresponds to eruptive Unit Ig1Eb of Wilson and Hildreth (1997), making the CC-L profile very analogous to the others. The section of the

ash-flow sheet at Site CG is also fairly representative of the welding, devitrification, and jointing variations with depth that are observed at all four of these sample localities.

A composite diagram comparing the  $^{18}\text{O}/^{16}\text{O}$  data at all four sampling sites can be readily constructed by plotting the positions of each of these samples relative to the top of the zone of densely welded black tuff; this horizon is significant not only because it is laterally continuous and easily mapped in the field, but also because it corresponds closely to the base of the fumarolic system, where whole-rock  $\delta^{18}\text{O}$  values change rapidly over short vertical distances. Thus whole-rock  $^{18}\text{O}/^{16}\text{O}$  data from all sites beneath fumarolic mounds can be readily compared on Fig. 2.19. This plot clearly shows the consistent and very intense  $^{18}\text{O}$  depletions that are present in the vicinity of the fumarolic conduits that lie beneath well-developed fumarolic mounds throughout the  $\approx 40\text{-m}$ -thick zone of partially welded tuff that lies directly above the densely welded black tuff.

## **2.5. The Bishop Tuff outflow sheet away from fumarolic conduits**

### *2.5.1. Two $^{18}\text{O}/^{16}\text{O}$ -Depth Profiles in Areas Located Between Fumarolic Mounds*

The sample locality at Abandoned Gorge (Site AG) lies within the region of fumarolic mounds and ridges along Owens River Gorge mapped by Sheridan (1970), but it is not directly beneath a fumarolic mound (Fig. 2.1). The closest identifiable fumarolic structures are (1) a single tubular conduit exposed at Site HT, 500 m to the north-northwest; (2) a group of large, steep fissures and tubular conduits located 500 m to the north, directly across the Owens River Gorge from Site HT; and (3) steep fissures exposed on the west side of the Owens River Gorge about 250 m downstream of Site AG. A photograph of Site AG illustrates the set of steep, well-developed columnar joints that were sampled along this depth profile (Fig. 2.20).

Although there are no obvious fumarolic conduits exposed in the cliff face at Site AG, there are two shallow-dipping discontinuities that separate the columnar joints into three tiers; these discontinuities are marked by very slight changes in whole-rock  $\delta^{18}\text{O}$  (Fig.

2.21). In the upper two tiers, whole-rock samples are slightly  $^{18}\text{O}$ -depleted ( $\delta^{18}\text{O} = +5.3$  to  $+7.0$ ), and our interpretation is that this stratigraphic horizon represents a portion of the region-wide Upper Low- $^{18}\text{O}$  Zone (ULZ). The maximum whole-rock  $^{18}\text{O}$ -depletions at Site AG are located at the base of the Tableland Unit (Ig2E), which corresponds to the uppermost, subhorizontal discontinuity (Figs. 2.20 and 2.21). At the discontinuity between the lower two sets of columnar joints shown on Fig. 2.20, there is a sharp transition from the slightly  $^{18}\text{O}$ -depleted rocks of the ULZ to the slightly elevated  $\delta^{18}\text{O}$  values ( $+7.5$  to  $+8.9$ ) that are typical of the densely welded lower part of the Bishop Tuff (i.e., the DWZ) at other sampling sites. This discontinuity at Site AG is located about 20 m above the top of the densely welded black tuff. Thus, even though the  $^{18}\text{O}$ -depletions are, overall, much less pronounced here, the data at Site AG again confirm the existence of a sharp  $^{18}\text{O}$ -gradient just above the top of the densely welded black tuff. It is clear that this sharp gradient in whole-rock  $\delta^{18}\text{O}$  values at this stratigraphic horizon can be observed at a variety of localities in the ash-flow sheet, both directly beneath fumarolic mounds and in areas where there are no mounds (compare with Fig. 2.19).

The Lower Gorge profile (samples LG-B1 through LG-B6) was collected from the Bishop Tuff along the steep old road intersecting Middle Power Plant Road approximately 750 m northwest of the steep fissures shown in Fig. 2.14. This depth profile is also within the region of fumarolic mounds and ridges, although, like Site AG, it is not located directly beneath a fumarolic mound. In contrast to Site AG, however, there are no well-developed columnar joints anywhere within this entire profile (Fig. 2.16). Samples were collected at regular intervals along the steep road beginning near the top of the densely welded black tuff (LG-B1, Table 2.2) and continuing up to the top of the Bishop Tuff (LG-B6, Table 2.2). Only the top two samples are even slightly  $^{18}\text{O}$ -depleted ( $+4.7$  to  $+6.3$ ), and the uppermost of these ( $+6.3$ ) is from the Tableland Unit (Fig. 2.16).

In conjunction with the  $^{18}\text{O}/^{16}\text{O}$  data from other sites in the regions of intense fumarolic activity (Sites HT, LG, CG, and CC-L), the  $\delta^{18}\text{O}$  values from these two depth profiles

located well away from fumarolic mounds (Site AG and Site LG-B) allow us to draw some important conclusions. Taken together, these data show that within the broad region of intense fumarolic activity, which is indicated by the heavy stippled pattern on Fig. 2.1 and by the density of fumarolic mounds on Fig. 2.6, deep ( $\approx 60$  to 80 m) circulation of large amounts of meteoric  $\text{H}_2\text{O}$  into the Bishop Tuff was confined to the areas directly beneath the fumarolic mounds. Only where there are steep fissures and tubular conduits to carry the fumarolic fluids do we find extensive zones of  $^{18}\text{O}$ -depletion impinging upon and extending down into the densely welded tuff. Nevertheless, the consistent patterns of moderate  $^{18}\text{O}$ -depletion in the upper parts of both the Site AG and the Site LG-B depth profiles, within a stratigraphic zone that typically lies near the contact with the Tableland Unit, indicate that there was a pervasive zone of meteoric-hydrothermal exchange in the uppermost parts of the Bishop Tuff outflow sheet throughout the broad region of mapped fumarolic activity on Fig. 2.1. In the present study, we have been referring to this moderately  $^{18}\text{O}$ -depleted stratigraphic horizon as the ULZ (Upper Low- $^{18}\text{O}$  Zone). The ULZ is also interpreted to be present beneath the fumarolic mounds, but at those localities, its  $^{18}\text{O}/^{16}\text{O}$  pattern is complicated by the more intense  $^{18}\text{O}$ -depletions associated with the fumarolic structures themselves. The results from Site AG and Site LG-B are important in another way, because they demonstrate that we can discern the effects of the weak fumarolic activity associated with the ULZ by means of  $^{18}\text{O}/^{16}\text{O}$  analyses alone, even in areas where there is no obvious textural, mineralogical, or geomorphological evidence for such activity, and well away from any fumarolic mounds or ridges.

#### *2.5.2. $^{18}\text{O}/^{16}\text{O}$ -Depth Profiles from Regions of Weak and/or Non-Existent Fumarolic Activity (Sites RC, CC, and UG)*

Site RC is located in Rock Creek Gorge within Sheridan's (1970) mapped region of vapor phase alteration associated with weak fumarolic activity (light stippled pattern in Fig. 2.1), but outside his mapped region of intense fumarolic activity associated with mounds



and ridges. In the partially welded tuff at Site RC, the outflow sheet exhibits very well developed, steeply dipping columnar joints that form a colonnade above a section of densely welded black tuff that is at least 50 m thick (Fig. 2.22). At this site, no fumarolic conduits (i.e., tubular conduits, steep fissures, or shallow-dipping columnar joints) were observed in the ash-flow tuff. Eight samples were collected along a vertical profile through this zone of steeply dipping columnar joints in the partially welded tuff at intervals of 5 to 15 m on the west side of Rock Creek Gorge (Table 2.2); these are numbered in order from RC2-1 at the top to RC2-8 at the bottom of the cliff face (Fig. 2.22). All but one of the samples are within or slightly above the  $\delta^{18}\text{O}$  range of unaltered Bishop Tuff ( $\delta^{18}\text{O} = +7.6$  to  $+8.9$ ). The single exception is the near-surface sample RC2-2, which is slightly  $^{18}\text{O}$ -depleted ( $\delta^{18}\text{O} = +5.2$ ), and which is located just above the base of the Tableland Unit (Ig2E) about 15 m above the top of the colonnade of well-developed columnar joints shown in Fig. 2.22.

On the east side of Rock Creek Gorge (Fig. 2.23) at Site RC, a 20-m-thick lower colonnade of large (1-m-diameter) columnar joints is exposed at the base of the densely welded black tuff. Two samples (RC1-2 and RC1-5; Table 2.1) from the lower colonnade at Site RC are slightly  $^{18}\text{O}$ -enriched relative to the original Bishop Tuff magma ( $+8.5$  and  $+8.2$ ); thus, in spite of their association with good-sized columnar fractures that could have provided permeable conduits, it is clear that these samples cannot have undergone any significant exchange with a low- $^{18}\text{O}$  fluid during high-temperature meteoric-hydrothermal activity. This does not preclude the possibility of exchange with magmatic  $\text{H}_2\text{O}$ , or of meteoric-hydrothermal exchange at low to moderate temperatures. As discussed above in Section 2.4.4, such columnar joints elsewhere in the densely welded black tuff are commonly coated with a white substance having  $\delta^{18}\text{O}$  values as high as  $+13.8$ , indicating that such coatings probably formed at relatively low temperatures ( $\approx 100^\circ\text{--}200^\circ\text{C}$ , see Fig. 2.11).

Site CC is located in Chidago Canyon, just outside Sheridan's (1970) mapped region of weak fumarolic activity (Fig. 2.1). The entire thickness of the tuff at Site CC is composed of the Chidago Lobe (Unit Ig1Eb of Wilson and Hildreth, 1997); the Tableland Unit is not present. At Site CC, several tiers of steeply dipping columnar joints in the partially welded tuff are exposed above a thick zone of densely welded black tuff (Fig. 2.24). Here, three samples were collected about 15 m apart; CC-2 is the lowermost sample collected about 25 m above the transition to densely welded black tuff, CC-3T is the uppermost sample collected in unwelded tuff at the top of the cliff, and CC-4T was collected from partially welded tuff halfway between those two samples (Fig. 2.24). All three of these samples have very uniform whole-rock  $\delta^{18}\text{O}$  values (+7.7 to +7.9) that are virtually identical to the  $\delta^{18}\text{O}$  value of the Bishop Tuff magma. Thus there is no morphological or  $^{18}\text{O}$ -evidence for any kind of meteoric-hydrothermal activity at Site CC.

Site UG is located in a region of weak fumarolic activity just south of the granitic basement high exposed in Owens River Gorge and about 1.25 km south of the Upper Power Plant (Fig. 2.1). The Bishop Tuff at this location is composed almost entirely of the Gorges Unit (Ig1Eb of Wilson and Hildreth, 1997), except for the uppermost 10 m, which is comprised of the Tableland Unit. Here, where the Bishop Tuff laps up against the granitic basement high (Fig. 2.6), partially welded tuff is exposed beneath a steep, 50-m-high cliff composed of densely welded black tuff. Crudely developed columnar joints are found in densely welded tuff both above and below the uppermost section of densely welded black tuff in this cliff face (Fig. 2.25). Again, in spite of the association with columnar jointing, the  $\delta^{18}\text{O}$ -depth profile from this location shows no major whole-rock  $^{18}\text{O}$ -depletion anywhere in the section. However, there is a slight decrease in whole-rock  $\delta^{18}\text{O}$  values (down to  $\delta^{18}\text{O} = +5.8$  to +6.3) near the very top of the Gorges Unit and at the base of the Tableland Unit, just as we saw at the ULZ horizon in other  $\delta^{18}\text{O}$ -depth profiles that contain the Tableland Unit (i.e., Sites AG, LG-B, HT and RC).

Thus it appears that in the vicinity of the Tableland Unit, the whole-rock  $\delta^{18}\text{O}$  values throughout the mapped area of weaker fumarolic activity in the Bishop Tuff outflow sheet are very similar to the whole-rock  $\delta^{18}\text{O}$  values from this same horizon within the region of intense fumarolic activity. This is the basis for assigning the whole-rock  $^{18}\text{O}$ -depletions associated with the base of the Tableland Unit to a region-wide, stratigraphic zone of  $^{18}\text{O}$  depletion that is here termed the Upper Low- $^{18}\text{O}$  Zone or ULZ. The characteristic features of the ULZ are well documented at Sites HT, LG, AG, RC, UG and LG-B. However, no evidence for the ULZ has been observed in either of the two sampling sites in Chidago Canyon (CC and CC-L). The absence of the ULZ at Site CC may be a local phenomenon related to the absence of the Tableland Unit at this location. However, because the ULZ is also not observed at Site CC-L, where the Tableland Unit *is* present, there is also a possibility that the ULZ is simply not present anywhere in the fumarole area along Chidago Canyon (see discussion in Section 2.4.5). The uppermost sample from the surface of the fumarolic mounds, which is  $^{18}\text{O}$ -enriched, was collected from the Tableland Unit (CC-L9); however, the critical part of such a depth profile, namely the lower part of the Tableland Unit, was not sampled at Site CC-L. Therefore, the present density of sampling really does not allow us to determine conclusively whether or not the ULZ is present in Chidago Canyon.

### 2.5.3. An $^{18}\text{O}/^{16}\text{O}$ -Depth Profile near Lake Crowley (Site CR)

At Site CR (Fig. 2.1), the Bishop Tuff is less than 2/3 the thickness of the tuff at Sites CG, LG, AG, and HT, and the thickness of the densely welded zone is proportionally even smaller ( $\approx 40$  m as compared to  $\approx 100$  m, compare Fig. 2.26 with Fig. 2.17). Site CR lies about 10 km outside of the area of weak fumarolic activity mapped by Sheridan (1970). The Site CR profile is within the Gorges Lobe, and it includes both eruptive units Ig1Ea and Ig1Eb of Wilson and Hildreth (1997). Although sampling at Site CR is sparse (Fig. 2.26), there is definitely a zone of  $^{18}\text{O}$ -depletion and hydrothermal exchange within

the upper, partially welded tuff. Although the existence of this zone of  $^{18}\text{O}$ -depletion is based upon analyses of only one whole-rock sample and two pumice separates (whole-rock  $\delta^{18}\text{O} = +2.5$ ; Tables 2.1 and 2.2), this strongly  $^{18}\text{O}$ -depleted sample lies very close to the projected position of the ULZ horizon. Nevertheless, as was *a priori* expected for a depth profile located well outside the mapped fumarolic areas, the extent of  $^{18}\text{O}$ -depletion is overall much less at this locality than at the localities closer to the fumarolic mounds and ridges mapped by Sheridan (1970). Note that the pumice and whole-rock  $\delta^{18}\text{O}$  values of this single low- $^{18}\text{O}$  sample at Site CR are nowhere near as low as at Site CG ( $\delta^{18}\text{O} = +2.5$  compared to  $\delta^{18}\text{O} = -2.6$ ). Obviously, meteoric-hydrothermal fluid/rock activity was much less vigorous at Site CR than within the area of fumarolic mounds (compare with Fig. 2.19).

None of the samples from the underlying densely welded tuff at Site CR are discernibly depleted in  $^{18}\text{O}$  (Fig. 2.26). This is compatible with the concept that here, as at sites within the mapped fumarole area, the hot, ductile, densely welded black tuff was relatively impermeable to influx of meteoric fluids. The unwelded ash-flow tuff and the pumice fall deposit at the bottom of the section also have essentially pristine  $\delta^{18}\text{O}$  values, indicating that in spite of their relatively permeable appearance, neither of these underlying units could have interacted appreciably with low- $^{18}\text{O}$  hydrothermal fluids.

Although the data involve only a single low- $^{18}\text{O}$  sample, it is nevertheless interesting to speculate why the observed degree of  $^{18}\text{O}$ -depletion at Site CR is slightly greater than for other sites that are also not located directly beneath fumarolic mounds ( $\delta^{18}\text{O} = +2.5$  compared to  $\delta^{18}\text{O} > +4.5$ , Fig. 2.27). This conceivably could be because there was a greater supply of surface water at this location, which is directly adjacent to the ancestral Long Valley Lake that filled the caldera shortly after eruption (Smith and Bailey, 1976; Putnam, 1960). Indeed, although Site CR lies well outside of Sheridan's (1970) region of weaker fumarolic alteration in the Bishop Tuff outflow sheet (Fig. 2.1) and shows no evidence whatsoever for the types of fumarolic conduits typically observed beneath

fumarolic mounds, there are a series of prominent, roughly east-west striking ridges that are visible on air photos (see Fig. 3.5) and that cover the surface of the Bishop Tuff outflow sheet directly south of the current position of Lake Crowley and the paleo-position of the southern shore of ancestral Long Valley Lake (Smith and Bailey, 1976). Thus it may be that Site CR is actually within a region densely populated with a group of somewhat "anomalous" fumarolic ridges, whose features have been partially obscured by weathering and forestation (see Chapter 3).

## **2.6. The Deep Fumarolic System (DFS) and the Upper Low-<sup>18</sup>O Zone (ULZ)**

A common attribute can be discerned in the combined set of whole-rock  $\delta^{18}\text{O}$  values from nearly all of the sample sites that are not directly beneath fumarolic mounds (Sites AG, LG-B, RC, UG, and CR), including a series of  $\delta^{18}\text{O}$ -depth profiles, both from regions of intense fumarolic activity as well as from regions of weak and/or no fumarolic activity. This feature that is common to all of these sites is the presence of a stratigraphic horizon of  $^{18}\text{O}$ -depleted rock ( $\delta^{18}\text{O} = +2.5$  to  $+6.8$ ) in a characteristic position at the base of the Tableland Unit in the upper part of the Bishop Tuff outflow sheet (Fig. 2.27). This low- $^{18}\text{O}$  stratigraphic zone has been termed the ULZ (Upper Low- $^{18}\text{O}$  Zone); it is present throughout the region of fumarolic mounds and ridges surrounding Owens River and Rock Creek Gorges, and it extends locally into regions exhibiting little or no morphological evidence for past fumarolic activity.

Every sampling locality except for Site CC (and possibly Site CC-L) shows some evidence for this low- $^{18}\text{O}$  horizon, including the sites located directly beneath or adjacent to fumarolic mounds at Sites HT, LG, and CG. Although Site CC-L does not show any evidence for the ULZ at the stratigraphic position seen at the other sites, there is a somewhat analogous zone of  $^{18}\text{O}$  depletions (whole-rock  $\delta^{18}\text{O} = +4.5$  to  $+5.2$ ) in the upper part of the tuff in that profile. At both Site CC and Site CC-L, the absence of such a

low- $^{18}\text{O}$  zone may be the result of insufficient sampling. This is because the base of the Tableland Unit, which is where the maximum  $^{18}\text{O}$ -depletions in the ULZ typically occur, was not sampled at Site CC-L, and at Site CC, only three samples were collected. Additionally, the Tableland Unit was apparently not deposited at Site CC, and therefore any low- $^{18}\text{O}$  zone associated with this stratigraphic horizon might not be expected to be present. We cannot conclude with any certainty that the ULZ is present in Chidago Canyon, and more sampling is required to answer this question.

By comparing all of the  $^{18}\text{O}/^{16}\text{O}$  data from samples located beneath fumarolic mounds and ridges (depth profiles from Sites HT, LG, CG, CC-L; Fig. 2.19) with all of the data from samples located well away from fumarolic conduits (depth profiles from Sites AG, LG-B, RC, CC, UG, and CR; Fig. 2.27), it becomes obvious that low- $^{18}\text{O}$  meteoric-hydrothermal fluids circulated deeper into the tuff in the vicinity of fumarolic conduits (e.g., tubular conduits, steep fissures, and shallow-dipping columnar joints) than they did away from these structures. In general, in the vicinity of tubular conduits, steep fissures and shallow-dipping columnar joints, the whole-rock low- $^{18}\text{O}$  signatures associated with meteoric-hydrothermal circulation in the tuff are much lower ( $\delta^{18}\text{O} = -6.5$  to  $+5.2$ ) than in the ULZ, and the zone of  $^{18}\text{O}$ -depletion extends much deeper (down to the level of the densely welded black tuff). Away from fumarolic conduits, the whole-rock  $^{18}\text{O}$  depletions are less intense ( $\delta^{18}\text{O} = +2.5$  to  $+6.5$ ) and are confined to the ULZ horizon, which extends down to a level no closer than about 20 m above the upper boundary of the densely welded black tuff (compare Figs. 2.19 and 2.27). These  $^{18}\text{O}/^{16}\text{O}$  data strongly suggest that the structures found beneath fumarolic mounds, such as steep fissures and tubular conduits, provide the necessary permeability for large amounts of high-temperature low- $^{18}\text{O}$  meteoric  $\text{H}_2\text{O}$  to penetrate and exchange with the deeper portions of the ash-flow sheet. This series of zones, which are together referred to as the Deep Fumarolic System (DFS), is associated with the lowest  $\delta^{18}\text{O}$  values and the highest water/rock ratios in the Bishop Tuff outflow sheet, and is confined to the volume of rock located directly beneath each of the more than

1000 fumarolic mounds that pepper the surface of large portions of the outflow sheet (Fig. 2.6). The shallow meteoric-hydrothermal circulation associated with the Upper Low- $^{18}\text{O}$  Zone (the ULZ) is a region-wide stratigraphic phenomenon in the upper part of the ash-flow tuff, and hence involves a much greater volume of rock than the DFS.

## **2.7. Volatile Sources for the Bishop Tuff Outflow Sheet Fumaroles**

### *2.7.1. Magmatic vs. Meteoric H<sub>2</sub>O Sources*

The role of primary magmatic gases in the fumarolic activity associated with cooling ash-flow tuffs is difficult to discern using oxygen isotopes, because any magmatic H<sub>2</sub>O evolved at near magmatic temperatures (>600°C) would have about the same  $\delta^{18}\text{O}$  value as the hosting ash-flow tuff (i.e., +7 to +8). If the glass in the Bishop Tuff outflow sheet contained about 3.0 wt % water, then magmatic H<sub>2</sub>O conceivably could have constituted at most about 16% to 22% of the total H<sub>2</sub>O in the fumarolic fluids; this is almost certainly an over-estimate, because much of the original magmatic H<sub>2</sub>O was likely lost during the eruption and emplacement of the tuff. Possible evidence for influx of such magmatic water is provided by our observation that the boundary between the dense black tuff and the overlying pervasively devitrified zone is commonly marked by intense shattering of the tuff, particularly in the vicinity of the steep fumarolic fissures and tubular conduits. We suggest that this may be the result of explosive interactions between hot magmatic gases emanating from the lower, densely welded part of the tuff and cooler meteoric fluids percolating through the more permeable upper zone.

At the Valley of Ten Thousand Smokes, it has been suggested that mixing of magmatic volatiles and meteoric waters did occur (Allen and Zies, 1923; Papike et al., 1991), forming halogen acids that leached soluble elements from the upper part of the tuff, depositing them as fumarolic encrustations at the surface. Although surface manifestations of fumarolic minerals in the Bishop Tuff are sparse, there is a 30-m-thick bleached horizon at the top of the outflow sheet, and iron oxide encrustations are preserved at the tops of

some of the fumarolic mounds and ridges. Many fumarolic minerals are metastable in the weathering environment, and the same processes of erosion that have beautifully exposed the fumarolic mounds and ridges have probably also destroyed much of the evidence for fumarolic minerals deposited along exposed joints and fissures on the surface of the tuff. For example, in the 85 years since they were deposited, erosion has already stripped away virtually all of the minerals deposited at the tops of fumarolic mounds at the Valley of Ten Thousand Smokes (Keith, 1991; Zies, 1929).

### 2.7.2. *Meteoric H<sub>2</sub>O Beneath the Bishop Tuff Outflow Sheet*

Maps of fumaroles on the surface of the Bishop Tuff indicate that there is a rough correlation between the density of fumarolic mounds and ridges on the surface of the ash-flow sheet and the regional drainage pattern as defined by gullies and canyons that have cut into the Bishop Tuff. This relationship between fumarolic activity and drainage pattern conceivably could be interpreted to mean that meteoric water flowed underneath the outflow sheet, perhaps feeding the overlying fumaroles through the widely spaced, throughgoing fractures that are prominent in the densely welded tuff. Further, the observation that some of these steep fractures terminate upwards into fumarolic fissures and tubular conduits might suggest that the fumaroles were indeed supplied by meteoric fluids from below. However, as discussed previously, samples from the only likely conduits for such fluids, namely the regularly spaced, narrow, steep fractures in the densely welded tuff, are not significantly <sup>18</sup>O-depleted. Thus our <sup>18</sup>O/<sup>16</sup>O data rule out these fractures as major conduits for meteoric-hydrothermal fluids derived from the base of the tuff. Moreover, in 16 additional samples collected from the densely welded black tuff at 6 different localities where there *are* significant whole-rock <sup>18</sup>O-depletions higher up in the ash-flow sheet, not a single whole-rock sample has  $\delta^{18}\text{O} < +6$ . Although, as discussed in Section 2.4.4, there may locally be evidence for some type of phreatic interaction between the Bishop Tuff and H<sub>2</sub>O overridden during emplacement, it is clear even in that instance that phreatic fluids



could not have been a significant source of H<sub>2</sub>O for any of the overlying fumarolic systems.

Another hypothesis is that perhaps fumaroles were supplied by groundwater that flowed beneath the Bishop Tuff outflow sheet, as there is indeed some evidence for meteoric H<sub>2</sub>O recharge to the lower part of the Bishop Tuff at Site UG. There is a slight <sup>18</sup>O depletion in one of the samples from the partially welded tuff near the base of the profile at Site UG (UG-2,  $\delta^{18}\text{O} = +6.8$ , Table 2.2; UG-2-groundmass,  $\delta^{18}\text{O} = +6.6$ , Table 2.1), indicating that these rocks probably underwent limited oxygen exchange with meteoric H<sub>2</sub>O at high temperature. This part of the tuff is also a burnt orange in color, which is much different from the typical unwelded to partially welded units seen at the base of the tuff in other locations; for example, at Site CR, the partially welded to unwelded units underneath the densely welded zone are grey to white in color.

This zone of <sup>18</sup>O-depletions at the base of the outflow sheet cannot be very extensive however, because sample UG-3 was collected only 10 m above UG-2 at the base of the cliff of densely welded black tuff, which exhibits a  $\delta^{18}\text{O}$  value (+7.9) within the range expected for unexchanged Bishop Tuff. As discussed in Section 2.4.4, the Densely Welded Zone (DWZ) typically does not show *any* evidence for exchange with significant amounts of low-<sup>18</sup>O meteoric H<sub>2</sub>O, indicating that the DWZ was basically impermeable during fumarolic activity. Thus any meteoric fluids that exchanged with sample UG-2 could not have come through the DWZ from the top of the ash-flow sheet, and by process of elimination they therefore *must* have been supplied from below. In areas where the DWZ is thin or absent, it is possible that meteoric H<sub>2</sub>O could have penetrated down through the permeable partially welded tuff. This very likely occurred atop the fractured, granitic-basement high that projects upward into the base of the outflow sheet to the north of Site UG. By this groundwater pathway, meteoric fluids might have had access to the lower, partially welded tuff at Site UG.

An alternative explanation is that sample UG-2 exchanged with water derived from streams, snow, or ice overridden by the Bishop Tuff during emplacement. Arguing against this is the fact that Site UG is located on the shoulder of a basement high, an unlikely location for water to collect. However, the hot Bishop Tuff interacted with glaciers located 13 km NNW and only  $\approx 500$  m higher in elevation than Site UG (Bailey, 1989). In the present-day climatic regime, mid-winter snow frequently blankets the area of the tuff around Site UG, and therefore it is not unreasonable that ice and snow could have been overridden by the Bishop Tuff at Site UG.

The above observations are all compatible with the idea that magmatic volatiles with  $\delta^{18}\text{O} = +7$  to  $+8$  were the dominant fluids passing through the lower part of the tuff during the fumarolic stage, and that there was no significant meteoric water recharge to the overlying fumaroles from streams or rivers flowing beneath the base of the Bishop Tuff.

## **2.8. Summary**

The data in the present chapter confirm the discovery by Gazis et al. (1996) that welded ash-flow tuffs may commonly preserve a heretofore unrecognized type of  $^{18}\text{O}/^{16}\text{O}$  signature, namely a strongly  $^{18}\text{O}$ -depleted groundmass and fiamme coexisting with phenocrysts of quartz and feldspar that have closely preserved their magmatic  $\delta^{18}\text{O}$  values. This type of  $\delta^{18}\text{O}$  signature can be shown to be a result of short-lived (10-25 year) fumarolic meteoric-hydrothermal activity in the upper parts of such ash-flow sheets, and this interpretation is much more clear in the Bishop Tuff outflow sheet than it is in the intracaldera tuff at either the Chegem caldera (Gazis et al., 1996) or in Long Valley caldera (Holt and Taylor, 1998), because the  $^{18}\text{O}/^{16}\text{O}$  effects can be directly related to obvious fumarolic features (see Section 5.6).

Directly beneath fumarolic mounds in the Bishop Tuff, fumarolic activity involved vigorous, high-temperature circulation of meteoric-hydrothermal fluids through the  $\approx 80$ -m-thick, partially welded upper part of this ash-flow sheet. These fluids cannot have been

dominantly composed of magmatic H<sub>2</sub>O as proposed by Sheridan (1970). They are clearly derived from local surface waters, either rain and snow falling directly on the tuff or discharge from the surrounding lakes and streams. The Densely Welded Zone (DWZ), which makes up the lower 1/2 to 2/3 of the outflow sheet, is pristine and not measurably <sup>18</sup>O-depleted, indicating that during the fumarolic activity much of this hot, ductile, densely welded tuff was impermeable to meteoric fluids. There is evidence for small amounts of water/rock interaction near the base of the Bishop Tuff, involving both H<sub>2</sub>O overridden during eruption and groundwater from adjacent country rocks, but these are not significant sources of H<sub>2</sub>O to the overlying fumaroles.

The patterns of mineralogy and whole-rock <sup>18</sup>O-depletion in the Bishop Tuff outflow sheet delineate the geometric boundaries of fumarolic meteoric-hydrothermal activity and show that deep circulation of large amounts of very high-temperature (>400°C) meteoric fluids into the Bishop Tuff was localized directly beneath fumarolic mounds and ridges, in what we here term the Deep Fumarolic System (the DFS). Also, a broader, but shallower penetration of high-temperature meteoric fluids occurred in the upper part of the partially welded ash-flow sheet in a stratigraphic zone (the ULZ) that can be observed everywhere at a relatively uniform depth of 5 to 50 m throughout the fumarolic areas mapped by Sheridan (1970) as well as at other locations outside the mapped areas, even where there is no morphological or structural evidence for past fumarolic activity.

The tops of fumarolic mounds and ridges are the only locations at which there is <sup>18</sup>O/<sup>16</sup>O and mineralogical evidence for low-temperature (<200°C) meteoric-hydrothermal circulation. At all other locations studied, and especially within the low-<sup>18</sup>O zones beneath fumarolic mounds, little or no evidence was found for extensive low-temperature oxygen exchange or moderate-temperature (≤300°C) mineralogical alteration of the tuff.

The present study has also shown that fumarolic zones can be identified solely by means of <sup>18</sup>O/<sup>16</sup>O analyses, even in cases where such activity was too weak to allow fumarolic morphological features to develop (e.g., Site CR in the Bishop Tuff outflow

sheet), or where fumarolic morphological features are not exposed or have been largely destroyed by tectonism and erosion. This has important implications with regard to studies of all large welded ash-flow tuff sheets, particularly where outcrop exposures are poor and where morphological evidence for fumarolic activity is not apparent. Thus, the data in this chapter, together with the pioneering work of Gazis et al. (1996), represent the first set of studies to demonstrate that detailed mapping of isotopic stratigraphy, combined with analyses of phenocryst mineral separates, can be used to identify fossil fumarolic activity and distinguish it from the effects of other types of meteoric-hydrothermal systems that typically form at lower temperatures (<400°C).

**Table 2.1.** Oxygen isotope analyses ( $\delta^{18}\text{O}$  values) of mineral separates, pumice, and groundmass (gmass) from the Bishop Tuff outflow sheet.

Sample No.	Description††	Whole-rock	Feldspar#	Quartz	Pumice*	gmass
CG-2	G, PW, lpk, p	2.73	7.40†	8.73†		
CG-3	G, PW, dpk, k, cj-sh	4.51		8.37		
CG-4	G, PW, dpk, k, cj-sh	-1.05	7.25†	7.99†, 8.20		
CG-5	G, PW, dpk, k, cj-sh	-1.14	6.88†	8.15†	4.70**	-3.05
CG-5.62	G, DW, dpk, k, cj-sh	-1.12			5.82**	-3.09
CG-5.64	G, DW, dpk, k, cj-sh	4.09			6.88**	
CG-7	G, DW, ypk, g	7.94	7.17†	8.43†		
CG-10	G, DW, blk, g	6.12	7.44†	8.73†		
CG-13	G, DW, blk, g	9.21	7.49	8.59		
NG-A	G, DW, ypk, g, cav	4.58	6.98†	8.29†		
NG-B	G, DW, ypk, g, cav	1.31	7.28†	8.44†		
LG-2	T, PW, dpk, k				10.00 (o)	
LG-17	G, PW, dpk, k, cj-sh,	-5.2	6.94†	8.36†		
AG-1	T, UW, wht, p, cj-vr				5.41 (w)	
AG-5	G, UW, pur, k, cj-vr				6.45 (w)	
RC1-2	G, DW, gry, g, cj-vr				8.54**	
RC1-5	G, DW, gry, g, cj-vr				8.22**	
UG-2	G, DW, brn, k					6.58
LC-6	G, PW, brn, p	2.48	7.04	8.55	2.19 (y) 2.52 (b)	

† Oxygen was liberated from these samples using a laser fluorination technique (see text).

\* These samples are pumice lapilli (y=yellow; b=brown; w=white; o=orange; \*\*=fiamme).

\*\* These are black, glassy fiamme (flattened lapilli).

# Feldspar phenocrysts in all samples are pristine, colorless, transparent sanidine.

†† In the sample descriptions in this table and in Table 2.2, "G" refers to the Gorges Unit, "T" to the Tablelands Unit, and "C" to the Chidago Lobe of Hildreth (1979). Welding zonation is indicated by (UW) unwelded, (PW) partially welded, and (DW) densely welded. Groundmass coloring is indicated by (wht) white, (lpk) light pink, (dpk) dark pink, (ypk) yellowish pink, (gry) grey, (blk) black, (pur) purple, (ong) orange, and (brn) brown. The style of columnar jointing is indicated as follows: (cj-sh) shallow-dipping columnar joints, (cj-vr) near-vertical columnar joints; absence of coding indicates lack of columnar joints. Samples from well-developed fumarolic structures are identified either as frac = well-defined steep fracture zones, cav = cavities at the axis of radial columnar joints, or mound = conical hills and ridges on the surface of the ash-flow sheet. The texture of the tuff is designated as (p) powdery, (k) indurated, or (g) granular. Powdery (p) indicates unwelded or partially welded tuff that is poorly indurated, crumbly, and porous. Indurated (k) refers to a type of tuff that is well-indurated and makes a sharp, metallic "klink" when struck with a hammer. Granular (g) typically refers to densely welded tuff that makes a dull "thud" when struck with a hammer, readily breaking up into smaller pieces.

**Table 2.2.** Whole-rock oxygen isotope analyses and sample descriptions from the Bishop Tuff outflow sheet (see Table 2.1 for description of abbreviations).

Sample No.	Description	$\delta^{18}\text{O}$	Sample No.	Description	$\delta^{18}\text{O}$
<i>Holy Trinity Fumarole (Site HT)</i>			<i>Central Gorge Gully (Site CG)</i>		
NG-A	G, DW, ypk, g, cav	4.6	CG-1	G, UW, wht, p	8.2
NG-B	G, DW, ypk, g, cav	1.3	CG-2	G, PW, lpk, p	2.7
NG-D	G, DW, ypk, g, cav	4.6	CG-3	G, PW, dpk, k, cj-sh	4.5
NG-3-1	G, PW, lpk, k	5.0	CG-3.425	G, PW, dpk, k, cj-sh	3.2
NG-3-2	G, PW, lpk, k	5.7	CG-3.44	G, PW, dpk, k, cj-sh	4.2
NG-3-4	G, PW, lpk, k	5.4	CG-3.45	G, PW, dpk, k, cj-sh	4.0
NG-3-5	G, PW, lpk, k	5.2	CG-3.46	G, PW, dpk, k, cj-sh	3.4
NG-3-6	G, PW, lpk, k	5.3	CG-3.48	G, PW, dpk, k, cj-sh	1.1
NG-3-7	G, PW, lpk, k, cj-sv	6.0	CG-3.49	G, PW, dpk, k, cj-sh	-2.6
NG-3-8	G, PW, lpk, k, cj-sv	6.1	CG-4	G, PW, dpk, k, cj-sh	-1.1
NG-3-9	G, PW, dpk, k, cj-sv	4.3	CG-3.505	G, PW, dpk, k, cj-sh	-1.1
NG-3-10	G, PW, dpk, k, cj-sv	1.6	CG-3.52	G, PW, dpk, k, cj-sh	-1.3
NG-3-11	G, PW, dpk, k, cj-sv	2.0	CG-3.56	G, PW, dpk, k, cj-sh	-1
NG-2-1	G, PW, lpk, k	5.8	CG-3.58	G, DW, dpk, k, cj-sh	-2.5
NG-2-2	G, PW, lpk, k	4.0	CG-3.59	G, DW, dpk, k, cj-sh	0.0
NG-2-3	G, PW, lpk, k	3.9	CG-5	G, DW, dpk, k, cj-sh	-1.1
NG-2-4	G, PW, lpk, k, cj-sh	6.0	CG-5.61	G, DW, dpk, k, cj-sh	-1.0
NG-2-5	G, PW, lpk, k, cj-sh	5.8	CG-5.62	G, DW, dpk, k, cj-sh	-1.1
NG-2-6	G, PW, lpk, g, cj-sh	6.1	CG-5.64	G, DW, dpk, k, cj-sh	4.8
NG-2-7	G, PW, lpk, g	6.6	CG-5.65	G, DW, dpk, k, cj-sh	5.2
NG-2-8	G, PW, dpk, g	7.0	CG-5.66	G, DW, dpk, k, cj-sh	5.8
NG-2-9	G, PW, dpk, g	4.4	CG-6	G, DW, ypk, g, cj-sv	4.6
NG-2-10	G, PW, dpk, g	6.0	CG-7	G, DW, ypk, g	7.9
NG-1-1	G, PW, lpk, k	4.3	CG-8	G, DW, blk, g	7.1
NG-1-2	G, PW, lpk, k	5.1	CG-9	G, DW, blk, g	9.1
NG-1-3	G, PW, lpk, k	3.8	CG-10	G, DW, blk, g	6.1
NG-1-4	G, PW, lpk, k, cj-sh	4.9	CG-11	G, DW, blk, g	7.8
NG-1-5	G, PW, lpk, k, cj-sh	5.9	CG-12	G, DW, blk, g	8.4
NG-1-6	G, PW, lpk, k, cj-sh	6.3	CG-13	G, DW, blk, g	9.2
NG-1-7	G, DW, dpk, k, cj-sh	6.7	CG-14	G, DW, blk, g	8.3
NG-1-8	G, DW, dpk, g, cj-sh	7.5	CG-L1	G, DW, blk, g, frac	7.3
NG-1-9	G, DW, dpk, g, cj-sh	7.4	CG-L2	G, DW, blk, g, frac	5.7
NG-1-10	G, DW, dpk, g, cj-sh	7.8	CG-T1, surface	T, UW, wht, p, mound	11.3
NG-L1	G, DW, blk, g, frac	8.8	CG-T2, surface	T, UW, wht, p, mound	8.6
NG-L2	G, DW, blk, g, frac	9.9			
NG-T1, surface	G, UW, wht, p, mound	7.7			
NG-T2, surface	G, UW, wht, p, mound	5.0			
NG-T3, surface	T, UW, wht, p, mound	2.7			

Table 2.2 (cont.)

Sample No.	Description	$\delta^{18}\text{O}$	Sample No.	Description	$\delta^{18}\text{O}$
<i>Middle Power Plant Road (Site LG)</i>					
LG-1	T, PW, dpk, k	10.0	LG-18.4	G, PW, dpk, k, cj-sh, frac	-0.9
LG-3	T, UW, wht, p	6.4	LG-18.8	G, PW, dpk, k, cj-sh, frac	-0.8
LG-3B	T, UW, wht, p	6.4	LG-20	G, PW, dpk, k, cj-sh, frac	0.3
LG-4	T, UW, wht, p	9.6	LG-20.1	G, PW, dpk, k, cj-sh, frac	-1.2
LG-5	T, UW, wht, p	7.7	LG-20.5	G, PW, dpk, k, cj-sh, frac	-1.4
LG-6	T, UW, wht, p	8.8	LG-21	G, PW, dpk, k, cj-sh	-1.9
LG-7	T, UW, wht, p	3.9	LG-22	G, PW, dpk, k, cj-sh	3.4
LG-8	T, UW, wht, p, cj-sh	3.2	LG-23	G, PW, dpk, k, cj-vr	5.5
LG-9	T, UW, wht, p, cj-sh	-2.1	LG-24	G, PW, dpk, k, cj-vr	6.3
LG-10	T, UW, wht, p	-1.3	LG-25	G, DW, dpk, k, cj-vr	3.4
LG-11	G, UW, pur, p	-0.2	LG-26	G, DW, dpk, k	5.2
LG-12	G, UW, pur, p	3.3	LG-27	G, DW, dpk, k	6.5
LG-13	G, PW, pur, k	2.8	LG-28	G, DW, dpk, k	8.1
LG-14	G, PW, dpk, k, cj-sh, frac	-0.7	LG-29	G, DW, gry, g	8.6
LG-15	G, PW, dpk, k, cj-sh, frac	-3.3	LG-30	G, DW, gry, g	8.4
LG-15.8	G, PW, dpk, k, cj-sh, frac	-2.3	LG-34	G, DW, blk, g	8.5
LG-15.9	G, PW, dpk, k, cj-sh, frac	-1.7	LG-R1	G, DW, ypk, g, frac	8.6
LG-15.12	G, PW, dpk, k, cj-sh, frac	-0.2	LG-R2	G, PW, dpk, k, frac	1.0
LG-15.15	G, PW, dpk, k, cj-sh, frac	-1.7	LG-R3	G, PW, dpk, k, frac	0.7
LG-15.17	G, PW, dpk, k, cj-sh, frac	-1.1	LG-R4	G, PW, dpk, k, frac	-2.6
LG-16	G, PW, dpk, k, cj-sh, frac	-3.7	LG-R5	G, PW, dpk, k, frac	-0.5
LG-16.19.5	G, PW, dpk, k, cj-sh, frac	0.1	LG-B1	G, DW, gry, g	8.7
LG-16.21	G, PW, dpk, k, cj-sh, frac	-6.2, -6.5	LG-B2	G, DW, ypk, k	8.6
LG-16.22	G, PW, dpk, k, cj-sh, frac	-4.2	LG-B3	G, DW, dpk, k	8.4
LG-17	G, PW, dpk, k, cj-sh, frac	-5.2	LG-B4	G, PW, dpk, k	7.9
LG-17.36	G, PW, dpk, k, cj-sh, frac	2.8	LG-B5	G, PW, pur, k	4.7
LG-18	G, PW, dpk, g, cj-sh, frac	4.1	LG-B6	T, UW, wht, p	6.3
LG-18B	G, PW, dpk, g, cj-sh, frac	4.0	LG-T1, surface	T, UW, wht, p, mound	8.9
LG-18C	G, PW, dpk, g, cj-sh, frac	4.2	LG-T2A, surface	T, UW, wht, p, mound	13.6
LG-18.2	G, PW, dpk, k, cj-sh, frac	0.1	LG-T3, surface	T, UW, wht, p, mound	9.8
<i>Abandoned Gorge (Site AG)</i>					
AG-1, surface	T, UW, wht, p, cj-vr	5.6	AG-10	G, PW, dpk, k, cj-vr	7.5
AG-2, surface	T, UW, wht, p, cj-vr	5.3	AG-11	G, PW, ypk, g, cj-vr	8.3
AG-3	T, UW, wht, p, cj-vr	6.4	AG-12	G, DW, ypk, g, cj-vr	8.5
AG-4	G, UW, wht, p, cj-vr	6.8	AG-13	G, DW, ypk, g	8.6
AG-5	G, UW, pur, k, cj-vr	6.8	AG-14	G, DW, blk, g	8.2
AG-6	G, PW, pur, k, cj-vr	7.0	AG-15	G, DW, blk, g	8.8
AG-7	G, PW, lpk, k, cj-vr	6.9	AG-16	G, DW, blk, g	8.4
AG-8	G, PW, lpk, k, cj-vr	6.8	AG-17	G, DW, blk, g	8.1
AG-9	G, PW, dpk, k, cj-vr	6.5			

Table 2.2 (cont.)

Sample No.	Description	$\delta^{18}\text{O}$	Sample No.	Description	$\delta^{18}\text{O}$
<i>Upper Power Plant Road (Site UG)</i>			<i>Rock Creek (Site RC)</i>		
UG-1	G, PW, ong, p	7.7	RC2-1, surface	T, PW, brn, k	8.0
UG-2	G, DW, brn, k	6.8	RC2-2, surface	T, PW, wht, k	5.2
UG-3	G, DW, brn, g	7.9	RC2-3	G, PW, wht, p, cj-vr	7.6
UG-4	G, DW, ypk, g	7.1	RC2-4	G, PW, wht, p, cj-vr	8.1
UG-5	G, DW, dpk, k	8.9, 8.4	RC2-5	G, PW, lpk, k, cj-vr	8.3
UG-6	G, PW, lpk, k	7.3	RC2-6	G, PW, lpk, k, cj-vr	8.9
UG-7	G, PW, pur, k	5.9, 5.7	RC2-7	G, PW, lpk, k, cj-vr	8.3
UG-8	G, PW, pur, k	6.0	RC2-8	G, PW, lpk, k, cj-vr	8.6
UG-9, surface	T, UW, pur, k	6.3			
UG-10, surface	T, UW, pur, p	7.3			
<i>Lake Crowley South (Site CR)</i>			<i>Lower Chidago Canyon (Site CC-L)</i>		
LC-2	G, UW, wht, p	8.2	CC-L10	C, DW, blk, g	7.1
LC-3C	G, UW, wht, p	7.9	CC-L11	C, DW, blk, g	8.4
LC-4	G, DW, gry, k	8.1	CC-L3	C, PW, lpk, k, cj-sh	8.1
LC-5	G, DW, brn, k	7.8	CC-L4	C, PW, lpk, k, cj-sh	4.7
LC-6	G, PW, brn, p	2.5	CC-L5	C, PW, lpk, k, cj-sh	5.2
LC-7, surface	G, PW, brn, p	7.1	CC-L6	C, PW, lpk, k, cj-sh	4.5
			CC-L7	C, UW, wht, k	7.7
			CC-L9, surface	C, UW, wht, p, mound	8.9
<i>Fumarole Mounds (T, UW, wht, p)</i>			<i>Upper Chidago Canyon (Site CC)</i>		
	<u>Location (Lat., Long.)</u>		CC-2	G, DW, dpk, k	7.7
FM-20C, surface	37°36.16', 118°36.16'	7.4	CC-4T	G, PW, dpk, k	7.9
FM-21B, surface	37°31.05', 118°36.05'	16.7	CC-3T, surface	G, UW, lpk, p	7.7
RB-4, surface	37°31.28', 118°34.92'	7.9			



**Table 2.3.** Oxygen isotope analyses ( $\delta^{18}\text{O}$  values) of mineral coatings, veins, and veinlets in the Bishop Tuff outflow sheet

Sample No.	Description: Collection location	$\delta^{18}\text{O}$
CG-HQ	Opaline silica coating collected from a fracture in partially welded tuff: near sample CG-5.64	10.3, 12.9
RC-WS	White mineral coating collected from a fracture in densely welded tuff: near sample RC1-2	13.8
LG-coat	White mineral coating collected from a fracture in partially welded tuff: see Fig. 2.13a for location	17.9
LG-frac	Tridymite coating collected from a fracture in densely welded tuff: see Fig. 2.15 for location	8.6
LG-vein1	Tridymite from a steep, continuous veinlet in densely welded tuff: see Fig. 2.15 for location	-0.4, 0.0
LG-vein2	Tridymite from a steep vein that merges upward with the fracture in LG-frac see Fig. 2.15 for location	8.80
LG-31	Tridymite from a shallow, discontinuous veinlet in densely welded tuff: see Fig. 2.15 for location	9.1
LG-32	Glass collected from a fiamme connected to the veinlet in LG-31: see Fig. 2.15 for location	9.1

## Figure Captions

Fig. 2.1. Map of Long Valley caldera and vicinity showing the principal sampling sites in this work from the outflow sheet of Bishop Tuff (open circles). The outcrop area of the Bishop Tuff is shown by dark grey shading (Hildreth and Mahood, 1986) and that of the Early Rhyolites in the resurgent dome of the caldera is shown by the hatched pattern (Bailey et al., 1976). The areas of extensive fumarolic mounds and ridges (dark stippled regions), surrounded by zones of weaker fumarolic alteration (light stippled regions), are based on mapping by Sheridan (1970). Crowley Dam Road (**CR**), Upper Gorge (**UG**), Holy Trinity Conduit (**HT**), Abandoned Gorge (**AG**), Central Gorge (**CG**), and Lower Gorge (**LG**) are sampling sites in Owens River Gorge. Site **LG-B** is not shown, but is located about 1/4 mile north of Site **LG** on the west side of Owens River Gorge along an old road above Middle Power Plant Road. Sampling Site **RC** is located in Rock Creek Gorge and sampling sites **CC** and **CC-L** are located in Chidago Canyon. A few other samples were collected from surface outcrops in the area between Sites **RC** and **UG**.

Fig. 2.2. Plot of  $\delta^{18}\text{O}$  quartz vs.  $\delta^{18}\text{O}$  feldspar, showing the data points (cluster of black dots) for all analyzed quartz-feldspar phenocryst pairs from the Bishop Tuff outflow sheet. This tight grouping of data points from the Bishop Tuff may be compared with the much different situations shown by the 3 shaded fields that encompass the steep data-point arrays for quartz-feldspar pairs from two classic areas of relatively long-lived ( $\approx 0.1$  Ma), moderate temperature ( $\approx 300^\circ\text{C}$ ), sub-volcanic meteoric-hydrothermal systems: The horizontally striped field on the right represents data from outcrops of hydrothermally altered Precambrian Cataract Gulch Granite just outside the southern edge of the Lake City caldera in Colorado (Larson and Taylor, 1986b); the stippled field in the middle represents data from units within this same caldera (the 23 Ma intracaldera Sunshine Peak Tuff and its associated resurgent intrusion, Larson and Taylor, 1986a); and the dark shaded field on

the left represents data from the Kumogi pluton in the Hamada cauldron, Japan (Matsuhisa et al., 1980). Diagonal lines at  $\Delta^{18}\text{O}_{\text{qtz-feld}} = 0$  and 1.5 encompass the expected range of equilibrium  $\Delta^{18}\text{O}_{\text{qtz-feld}}$  values at magmatic temperatures and are shown for reference only ( $\Delta^{18}\text{O}_{\text{qtz-feld}} = \delta^{18}\text{O}_{\text{qtz}} - \delta^{18}\text{O}_{\text{feld}}$ ).

Fig. 2.3. A set of three histograms showing the distribution of  $\Delta^{18}\text{O}_{\text{qtz-feld}}$  values ( $\delta^{18}\text{O}_{\text{qtz}} - \delta^{18}\text{O}_{\text{feld}}$ ) for mineral pairs from the Bishop Tuff outflow sheet, the Sunshine Peak Tuff, and the Cataract Gulch Granite. These histograms illustrate the stark contrast between the very uniform quartz-feldspar fractionations from the Bishop Tuff outflow sheet (0.8 to 1.5‰, n=10, with 7 of 10 samples having  $\Delta^{18}\text{O}_{\text{qtz-feld}}$  values of 1.1 to 1.3‰) and the widely variable  $\Delta^{18}\text{O}_{\text{qtz-feld}}$  values typically observed in hydrothermally altered rocks from the vicinity of most fossil hydrothermal systems, as exemplified by whole-rock  $^{18}\text{O}$  data shown here from Lake City caldera in Colorado (1.1 to 9.8 ‰ for the Sunshine Peak Tuff and 1.9 to 8.5 ‰ for the Cataract Gulch Pluton; Larson and Taylor, 1986a).

Fig. 2.4. Plot of  $\delta^{18}\text{O}$  feldspar vs.  $\delta^{18}\text{O}$  groundmass/whole rock, showing that these data points from the Bishop Tuff outflow sheet plot along a steep, near-vertical array (solid circles, this study; open circles, Halliday et al., 1984). The shaded region encompasses all of the  $^{18}\text{O}$ -data points from this study; note that the  $\delta^{18}\text{O}$  values from Halliday et al. (1984) also plot along this same steep array. Most of the  $\delta^{18}\text{O}$ -data from the Bishop Tuff outflow sheet are from whole-rock analyses; however, because these rocks are composed primarily of groundmass and because the only remaining significant components are quartz and feldspar phenocrysts, which have very uniform  $\delta^{18}\text{O}$  values (see Table 2.1 and Fig. 2.2), one can use simple material-balance to calculate the groundmass  $\delta^{18}\text{O}$  value from the whole-rock  $\delta^{18}\text{O}$  value. Also note that groundmass separates were analyzed for three different samples from the Bishop Tuff outflow sheet (Table 2.1), and in each case material-balance calculations of the whole-rock  $\delta^{18}\text{O}$  values are indistinguishable from the

measured  $\delta^{18}\text{O}$  values. Diagonal lines for  $\Delta^{18}\text{O}_{\text{feld-wholerock}}$  at  $\Delta = 0$  and 1.0 encompass the expected range of equilibrium values at magmatic temperatures and are shown for reference only.

Fig. 2.5. Photograph of fumarolic mounds on the surface of the Bishop Tuff. The photograph was taken from a vantage point about 3 km due south of Site LG (Fig. 2.1); the view is to the northwest. The Sierra Nevada escarpment is shown on the left-hand side of the photograph, and Rock Creek Gorge is shown in the upper center. The distance along the prominent wash in the foreground is about 350 m.

Fig. 2.6. Map of the southeastern lobe of the Bishop Tuff outflow sheet showing the location of the larger fumarole mounds and ridges on the surface of the ash-flow sheet and the positions of Owens River Gorge, Rock Creek Gorge, and Chidago Canyon. Site locations are as in Fig. 2.1. The large, sinuous white area outlined in Owens River Gorge and three smaller areas to the north and east represent exposures of basement rock. Together with the two much larger areas of basement rock exposed near Casa Diablo Mountain and on the west side of the Bishop Tuff, these mark the position of a basement high (BH) extending northeast and southwest from Owens River Gorge (Bailey, 1989; Wilson and Hildreth, 1997). Fumarole mounds were identified using 1:46,500 scale aerial photographs, and all identifiable fumarolic features were transferred to the map. Although these features, where they are present, are readily identifiable over most of the ash-flow sheet, it is possible that erosion of the tuff along ephemeral tributary drainages of the ancestral Owens River may have destroyed some of the topographic expressions of fossil fumaroles in the blank areas just to the south of Casa Diablo Mountain. Also, subdued features near the basement high were more difficult to identify because of heavier forest cover in that area.

Fig. 2.7. Sketch illustrating how various fumarolic structures (i.e., shallow-dipping columnar joints, fumarolic conduits, and steep fissures) underneath fumarolic mounds in the Bishop Tuff outflow sheet relate to stratigraphic position, welding zonation, groundmass coloration and devitrification, and texture/induration. This sketch is based on observations of cliffs on the the west side of Owens River Gorge about 75 m south of Site CG (Fig. 2.6). The white background indicates the zone of dark-pink, pervasively devitrified, well-indurated tuff that characteristically surrounds and encompasses all major fumarolic structures exposed on the cliff face; other types of groundmass coloration and texture are indicated by the patterns described in the legend. Columnar joints are outlined by the light black lines; two of the steep fissures are indicated by the heavy vertical lines; and a large, tubular, subhorizontal conduit is indicated by a dark oval at the central axis of radiating columnar joints. Blocky, jointed tuff without columnar structure is shown on the left side of the diagram and is indicated by irregularly crossing black lines. Also shown are the widely spaced (20-30 m), steep fractures that are common in the densely welded black tuff; locally, these fractures can be traced upward into the pervasively devitrified zone where they merge with the steep fissures or tubular conduits.

Fig. 2.8. Plot of whole-rock  $\delta^{18}\text{O}$  values from all analyzed samples collected in the upper 5 m of the Bishop Tuff outflow sheet. Eleven of these samples were collected from the tops of fumarolic mounds at seven different locations: NG-T2, NG-T3, CG-T1, CG-T2, LG-T1, LG-T2A, LG-T3, CC-L9, FM-20C, FM-21B, and RB-4 (Fig. 2.1; Table 2.2). The other eight samples were collected from the upper 5 m of the tuff at five different locations well away from any fumarolic mounds: RC2-1, RC2-2, CC-3T, LC-7, UG-9, UG-10, AG-1, and AG-2 (Fig. 2.1; Table 2.2). Samples were collected from outcrops with well-developed, vertical columnar joints (diamonds), arcuate roof joints (squares), and either crudely developed columnar jointing or no jointing at all (circles). For samples collected from the margins of fissures coated with  $\text{SiO}_2$  or hematite, the symbols are filled with

either an "x" or a "+", respectively. For samples that contain groundmass and/or fiamme with a deep orange, brown, or red coloration, the symbols are marked by a vertical line (or tail) extending downward from the symbol. The symbols without a tail contain groundmass and fiamme with a pink, grey, or white coloration. The grey vertical band represents the original  $\delta^{18}\text{O}$  value of the Bishop Tuff ( $+7.6 \pm 0.5$ ).

Fig. 2.9. A diagrammatic illustration showing the generalized  $\delta^{18}\text{O}$  contours that might be expected around various fumarolic structures typically found beneath a fumarolic mound; the positions of the  $\delta^{18}\text{O}$  contours are mainly based on  $^{18}\text{O}$  data obtained near Site CG, but they also represent inferences and extrapolations based upon all of the isotopic data collected from the vicinity of fumarolic structures throughout the Bishop Tuff outflow sheet. Note that in place of a contour for  $\delta^{18}\text{O} = +8$ , a contour for  $\delta^{18}\text{O} = +7.6$  is shown, because this is the original whole-rock  $\delta^{18}\text{O}$  value of the Bishop Tuff, and as such represents the  $\delta^{18}\text{O}$  value to which all whole-rock  $^{18}\text{O}$  enrichments or depletions should be compared. The left side of the diagram illustrates the situation at some distance from any major fumarolic features; here, a moderately  $^{18}\text{O}$ -depleted stratigraphic zone with  $\delta^{18}\text{O} = +2.5$  to  $+6.5$  is typically observed in the upper part of the tuff. This stratigraphic zone (termed the Upper Low- $^{18}\text{O}$  Zone or ULZ) is inferred to underlie much of the heavily stippled region shown in Fig. 2.1, but it is also known to extend outward beyond the fumarolic areas mapped by Sheridan (1970). The maximum  $^{18}\text{O}$ -depletions in the ULZ characteristically occur near the base of the Tableland Unit, which corresponds on the diagram to the whitish, poorly indurated unit shown by the diagonal-line pattern. The base of the ULZ is located at the transition from light pink, moderately indurated tuff to dark pink, well-indurated tuff, which typically occurs about 20 m above the top of the densely welded black tuff. Fumarolic features in the form of steep fissures, tubular conduits, and shallow-dipping columnar joints are commonly located just above the upper contact of this densely welded black tuff; these are invariably spatially associated with zones of very low

$\delta^{18}\text{O}$  values ( $< +2$ ). As shown in this cross section, these low- $^{18}\text{O}$  zones commonly coalesce into a deep, 20- to 40-m-thick,  $^{18}\text{O}$ -depleted zone ( $\delta^{18}\text{O} < +4$ ) located directly beneath the fumarolic mound. The base of this composite low- $^{18}\text{O}$  zone is extremely sharp and typically bowed downward, forming a local depression of 3-5 m of the  $\delta^{18}\text{O}$  contours at the transition from densely welded tuff with pink groundmass and black fiamme to the densely welded black tuff; this depression in  $^{18}\text{O}$ -contours follows a similar depression of the level of this transition. DWZ = Densely Welded Zone (see text).

Fig. 2.10. Plot of the variation of the estimated equilibrium value of  $\Delta^{18}\text{O}_{\text{groundmass-water}}$  for the Bishop Tuff as a function of temperature, calculated by combining the feldspar/water  $^{18}\text{O}/^{16}\text{O}$  fractionations from O'Neil and Taylor (1967) with the quartz/feldspar fractionations from Clayton and Kieffer (1991), and assuming that the groundmass is made up of 2/3 alkali feldspar and 1/3 quartz. The tick marks show the points on the curve that mark 4 different values of  $\Delta\text{P}$  (defined as  $\Delta\text{P} = +7.6 - \delta^{18}\text{O}_{\text{H}_2\text{O}}$ ) for particular  $\delta^{18}\text{O}$  values of the hydrothermal  $\text{H}_2\text{O}$  (see text). The shaded grey box represents the temperature range below which the  $\delta^{18}\text{O}$  value of the groundmass will become enriched in  $\delta^{18}\text{O}$  as a result of  $^{18}\text{O}/^{16}\text{O}$  exchange assuming the  $\delta^{18}\text{O}$  of the fumarolic  $\text{H}_2\text{O}$  is between +3.5 and  $-13\text{‰}$ . Above this temperature range, the  $\delta^{18}\text{O}$  value of the groundmass decreases during  $^{18}\text{O}/^{16}\text{O}$  exchange. "Low" temperature and high-temperature regimes are shown on either side of this zone.

Fig. 2.11. Plot of temperature as a function of the  $\delta^{18}\text{O}$  value of the groundmass of the Bishop Tuff, calculated using the equilibrium  $\Delta^{18}\text{O}_{\text{groundmass-water}}$  values shown in Fig. 2.10, and assuming that the tuff is in isotopic equilibrium with two endmember fumarolic waters having  $\delta^{18}\text{O}$  values of +3.5 (upper boundary of shaded region) and  $-13$  (lower boundary of shaded region). The vertical dashed line pinpoints the  $\delta^{18}\text{O}$  value of unaltered Bishop Tuff (+7.6). Also shown are four bold vertical lines within the shaded region; two

of these span the range of whole-rock  $\delta^{18}\text{O}$  values actually observed in the Bishop Tuff outflow sheet, and the other two are representative whole-rock  $\delta^{18}\text{O}$  values of the ULZ (+5.5) and of the DFS zones around the main high-temperature fumarolic conduits (0.0).

Fig. 2.12. Photograph of Holy Trinity tubular conduit (Site HT) in the upper part of the Gorges Lobe on the west side of Owens River Gorge, illustrating  $\delta^{18}\text{O}$  contours of the left-hand portion of this bilaterally symmetrical feature (see illustrative sketch of an analogous feature in Fig. 2.7). These  $\delta^{18}\text{O}$  contours are based on whole-rock analyses of 34 samples taken from this cliff exposure. Sample locations are shown by the white dots. Whole-rock  $\delta^{18}\text{O} < +2$  characterizes the zone around the subhorizontal, oval-shaped, 6-m-wide cavity centered along the axis of this radiating pattern of columnar joints. Samples NG-T2 and NG-T3 were collected from the upper 5 m of the tuff about 50 m to the north (right) of the area shown in this photograph; sample NG-T2 was collected from the base of the Tableland Unit, and Sample NG-T3 was collected 2.5 m above Sample NT-T2. Both of these samples are  $^{18}\text{O}$ -depleted relative to the original magmatic  $\delta^{18}\text{O}$  value of the Bishop Tuff (Table 2.2). Sample NG-T1 has a normal  $\delta^{18}\text{O} = +7.7$ , and its sample location is shown by a single white dot located approximately 60 m above the central cavity and 20 m below the surface of the tuff.

Fig. 2.13. Whole-rock  $\delta^{18}\text{O}$  values of samples from Site HT, plotted as a function of distance above the top of the dense black tuff. The tubular conduit is located about 10 m above the transition to densely welded black tuff at the position shown by the dotted line. Open circles are data points from a linear traverse (referred to as the right profile in the text) lying directly above the central cavity (samples NG-3; Table 2.2). Filled circles are data points from the sample traverse on the far left side of the sampling area shown on the photograph in Fig. 2.8 (i.e., the south side of the sampled cliff face); these are referred to as the left profile in the text (samples NG-1; Table 2.2).



Fig. 2.14. (a) Photograph of a zone of steep fissures along Middle Power Plant Road (Site LG), showing  $\delta^{18}\text{O}$  values of whole-rock samples (small white dots). There are three fissures shown in this cliff face: the one on the far left is sub-parallel to the road and the two on the right are at an angle to the road and hence have a smaller exposure.

(b) Inset from (a) showing a steep fissure and the  $\delta^{18}\text{O}$  values of samples collected from columnar joints on either side of it. The lowest  $\delta^{18}\text{O}$  values are from samples collected along the highly fractured margins of columnar joints. See hammer (circled) for scale.

(c) Photograph of the space between two columnar joints shown in 2.14b illustrating the crumbly and fractured nature of the tuff. See sample tag (7 cm in length) for scale.

Fig. 2.15. Photograph of tridymite and fayalite veins and veinlets along Middle Power Plant Road below Site LG-B. White veins and veinlets about 0.5 mm wide are bordered by a selvage of pink, devitrified tuff up to 1 mm thick. Steep, continuous veins are cross-cut by discontinuous shallow-dipping veinlets, which connect fiamme in the densely welded tuff. Pore spaces into which tridymite and fayalite have crystallized are preserved in some of the larger fiamme.

Fig. 2.16. Photograph of the tuff along Middle Power Plant Road just north of the location shown in Fig. 2.14a. The steep old road along which samples LG-B1 through LG-B6 were collected is also shown. The distance along Middle Power Plant Road shown here is  $\approx 200$  m. Note the conspicuous lack of well developed columnar jointing or recognizable fumarolic conduits exposed in the sides of the gorge. The upper, white part of the tuff from which sample LG-B6 was collected belongs to the Tableland Unit. The lower part of the tuff belongs to the Gorges Unit. Sample locations and corresponding  $\delta^{18}\text{O}$  values are shown by the white dots.

Fig. 2.17. Variations of  $\delta^{18}\text{O}$  with depth and welding zonation in the Bishop Tuff along the Central Gorge profile (Site CG in Fig. 2.1). All samples are from the Gorges Unit, and the dotted pattern indicates that portion of the top of the section that is from the Tableland Unit. Low- $^{18}\text{O}$  rocks are observed throughout a 40-m-thick interval that coincides with the zone of shallow-dipping columnar joints, which at this locality is confined to the pervasively devitrified tuff directly above a thick zone of black, densely welded tuff. In this upper zone, both the dense black fiamme and the pervasively devitrified groundmass are depleted in  $^{18}\text{O}$  and are out of isotopic equilibrium with coexisting quartz and feldspar phenocrysts, indicating that both the fiamme and the groundmass have selectively undergone exchange with a low- $^{18}\text{O}$  fluid at high temperature, whereas the quartz and feldspar phenocrysts have not. The latter have  $\delta^{18}\text{O}$  values consistent with equilibrium attained at magmatic temperatures, maintaining a constant  $\Delta^{18}\text{O}_{\text{qtz-feld}} = 1.2$  with depth (shown by the vertical band 1.2 per mil in width that straddles the  $\delta^{18}\text{O} = +8$  coordinate).

Fig. 2.18. Photograph of Site CC-L in Chidago Canyon showing shallow-dipping columnar joints exposed between a small fumarolic mound on the surface of the tuff and a steep cliff of densely welded black tuff at the bottom of the canyon. This cliff of densely welded tuff is approximately 15 m high, and the base of the Bishop Tuff is not exposed in this location. The sample from the top of the tuff at Site CC-L (CC-L9; Table 2.2) was collected from the unwelded Tableland Unit, which comprises the uppermost part of the ash-flow sheet in this location. All of the other samples are from the Chidago Lobe (IglEb eruptive Unit). As indicated by the arrow in the lower right of the photograph, two samples (CC-L10 and CC-L11) were collected from a location directly beneath the sampling locations of CC-L3 to CC-L4 at the base of the steep cliff of densely welded black tuff. The pattern of  $^{18}\text{O}$  depletion in the upper part of the tuff at Site CC-L is analogous to that at Site CG, but less intense. Just as at Site CG, the lowest  $\delta^{18}\text{O}$  values

in the profile (+4.5 to +5.2) occur in the zone of shallow-dipping columnar joints directly above the densely welded tuff.

Fig. 2.19. Variations of whole-rock  $\delta^{18}\text{O}$  with distance above (–) and below (+) the top of the dense black tuff (indicated by the zero on the y-axis) for samples collected beneath fumarolic mounds exposed in Owens River Gorge and Chidago Canyon. The plot includes *all* samples from Sites HT, CG, LG, and CC-L (Fig. 2.1, Table 2.2), including data from samples collected on the surfaces of the mounds at these sites. In spite of the fact that both the intensity of fumarolic activity and thickness of the Bishop Tuff vary markedly among the four sampling sites, the  $^{18}\text{O}$ -depleted zone is consistently located in a similar position directly above the zone of densely welded black tuff. The shaded vertical band has the same significance as in Fig. 2.17.

Fig. 2.20. Photograph of columnar joints at Site AG, which is located on the west side of Owens River Gorge about 500 m downstream (south-southeast) of Site HT. Two shallow-dipping discontinuities in the columnar joints are marked; the upper discontinuity separates the Tableland Unit (Ig2E) from the underlying Gorges Unit. For scale, see Fig. 2.21.

Fig. 2.21. Variations of whole-rock  $\delta^{18}\text{O}$  values with depth and welding zonation in the Bishop Tuff along the Abandoned Gorge profile (Site AG in Fig. 2.1), which is located 500 m south of the fumarolic mound at Site HT. Whole-rock samples are only very slightly  $^{18}\text{O}$ -depleted throughout this depth profile ( $\delta^{18}\text{O} > +5$ ), which was sampled at 5 m intervals above the dense black tuff and at 10 m intervals below this boundary. There are no fumarolic conduits or shallow-dipping columnar joints present in the sampled cliff face. Two shallow-dipping discontinuities divide the steeply dipping columnar joints into three tiers. The uppermost discontinuity separates the Gorges Lobe (Ig1Eb of Wilson and Hildreth, 1997) from the overlying Tableland Unit, and above this horizon (in the

uppermost tier of columnar joints), the tuff is slightly more  $^{18}\text{O}$ -depleted (average  $\delta^{18}\text{O}_{\text{whole-rock}} = +5.8$ ,  $n = 3$ ) than it is below. The middle tier of columnar joints contains six samples and is also slightly  $^{18}\text{O}$ -depleted (although not as much as in the upper tier) with an average whole-rock  $\delta^{18}\text{O} = +6.7$ . The lower discontinuity marks the transition to  $\delta^{18}\text{O}_{\text{whole-rock}}$  values that are characteristic of the densely welded black tuff (average whole-rock  $\delta^{18}\text{O} = +8.3$ ,  $n = 8$ ); these values are typically slightly elevated relative to the  $\delta^{18}\text{O}$  value of the original Bishop Tuff magma (+7.6). The subhorizontal discontinuity between the two lower tiers of columnar joints is located about 20 m above the transition to densely welded tuff, which is where the sharp  $\delta^{18}\text{O}$  gradient occurs in depth profiles beneath the fumarolic mounds (compare Fig. 2.19). The dotted pattern and the shaded vertical band have the same significance as in Fig. 2.17.

Fig. 2.22. Photograph of the upper colonnade at Site RC on the west side of Rock Creek Gorge, showing whole-rock  $\delta^{18}\text{O}$  values for samples collected from this cliff face. The small white dots are sampling locations. Columnar joints are 25 m high and are composed of the Gorges Lobe (IglEb of Wilson and Hildreth, 1997). The small cliff at the top of the gorge is about 7 m high and is composed of the Tableland Unit.

Fig. 2.23. Photograph of the east side of Rock Creek Gorge illustrating the lower colonnade of steeply dipping columnar joints at the base of the densely welded black tuff. Columnar joints are about 1 m in diameter. The locations from which samples RC1-2 and RC1-5 were collected are shown by the upper and lower white dots, respectively. A fumarolic mound overlies this exposure, but the view of it in this photograph is obscured by the upper edge of the steep cliff of densely welded tuff.

Fig. 2.24. Photograph of Site CC in the upper part of Chidago Canyon, showing whole-rock  $\delta^{18}\text{O}$  values for samples collected from this site. The small white dots are sampling

locations. This section is from the Chidago Lobe (Ig1Eb of Wilson and Hildreth, 1997). Note the steeply dipping columnar joints in the upper partially welded tuff.

Fig. 2.25. Variations in whole-rock  $\delta^{18}\text{O}$  values with depth and welding zonation at Site UG. Site UG is outside the mapped region of fumarolic mounds and ridges (Fig. 2.1) but within the region of vapor phase fumarolic alteration as mapped by Sheridan (1970). The base of the tuff is not exposed at this location, and it is unclear whether the tuff is welded below the lowest exposed part, which is only partially welded. The dotted pattern and shaded vertical band have the same significance as in Fig. 2.17.

Fig. 2.26. Variations in whole-rock  $\delta^{18}\text{O}$  values with depth and welding zonation in the Bishop Tuff at Site CR (Fig. 2.1), which is located outside Sheridan's (1970) mapped fumarolic area. Designated units of Wilson and Hildreth (1997) are, from bottom to top: Ig1Ea (lower, unwelded ignimbrite), F6 (unwelded, intervening pumice fall), and Ig1Eb (upper, unwelded to densely welded ignimbrite). The shaded vertical band has the same significance as in Fig. 2.17.

Fig. 2.27. Variations of whole-rock  $\delta^{18}\text{O}$  with distance above (–) and below (+) the top of the densely welded black tuff (indicated by the zero on the y-axis) for all depth profiles not located beneath fumarolic mounds. The plot includes all samples from Site AG, Site LG-B, Site UG, Site RC, Site CC, and Site CR (Fig. 2.1, Table 2.2). Open symbols indicate sampling sites that exhibit well-developed, steeply dipping, columnar joints. Closed symbols indicate sampling sites without well-developed columnar joints of any kind. None of the plotted depth profiles pass adjacent to or through any obvious fumarolic feature (e.g., a steep fissure or a tubular conduit). As stated previously and as shown in Fig. 2.1, Sites AG and LG-B are located in regions where there is morphological evidence for intense fumarolic activity; sites RC, CC, UG, and CR are located in regions where there is

little or no evidence for fumarolic activity. There does not appear to be any relationship between the degree of  $^{18}\text{O}$ -depletion and the presence of columnar jointing at any of these sites, although as observed at Site AG (Fig. 2.21), slight  $^{18}\text{O}$ -changes within a single  $\delta^{18}\text{O}$ -depth profile appear to be related to shallow-dipping discontinuities in the vertical columnar jointing pattern.

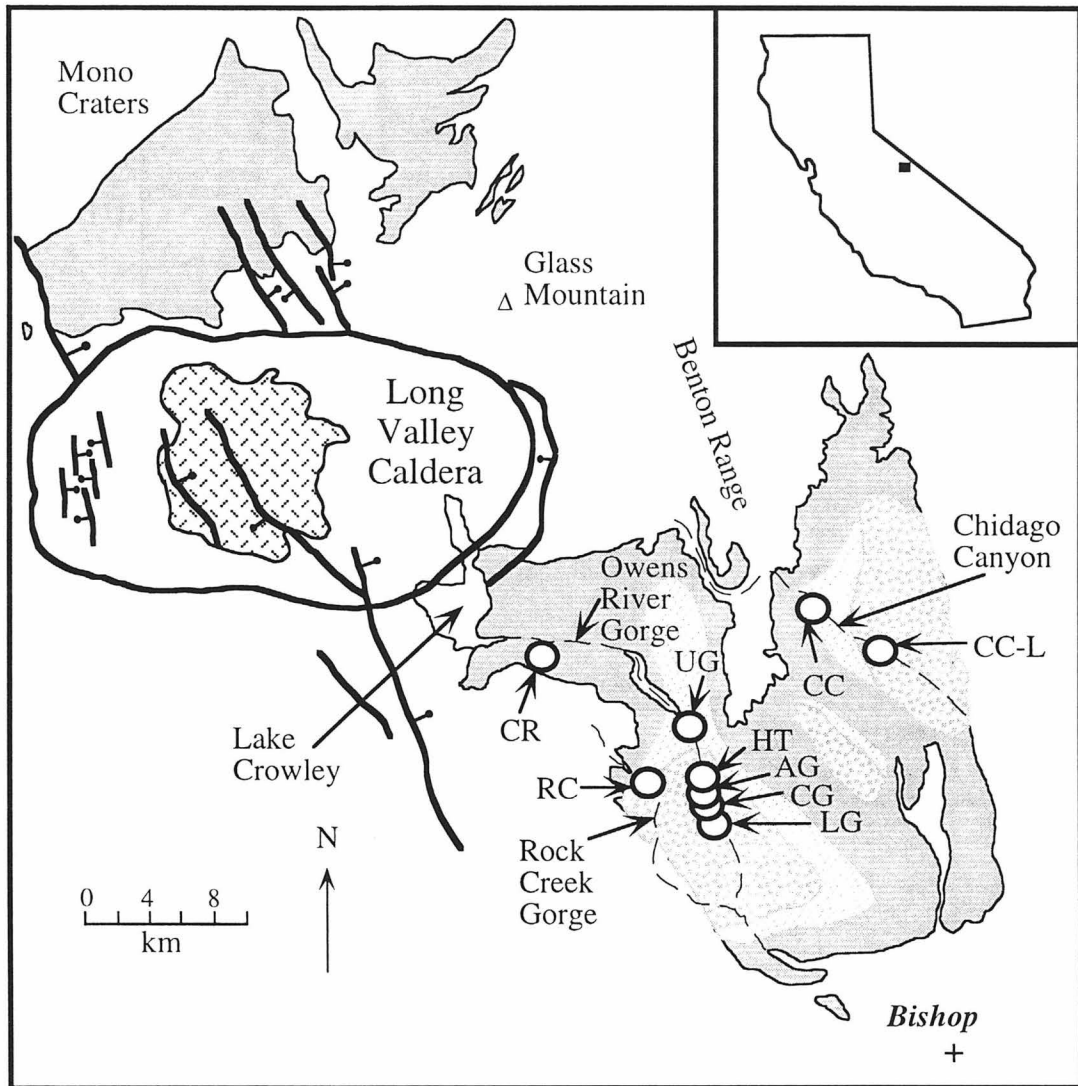


Fig.2.1

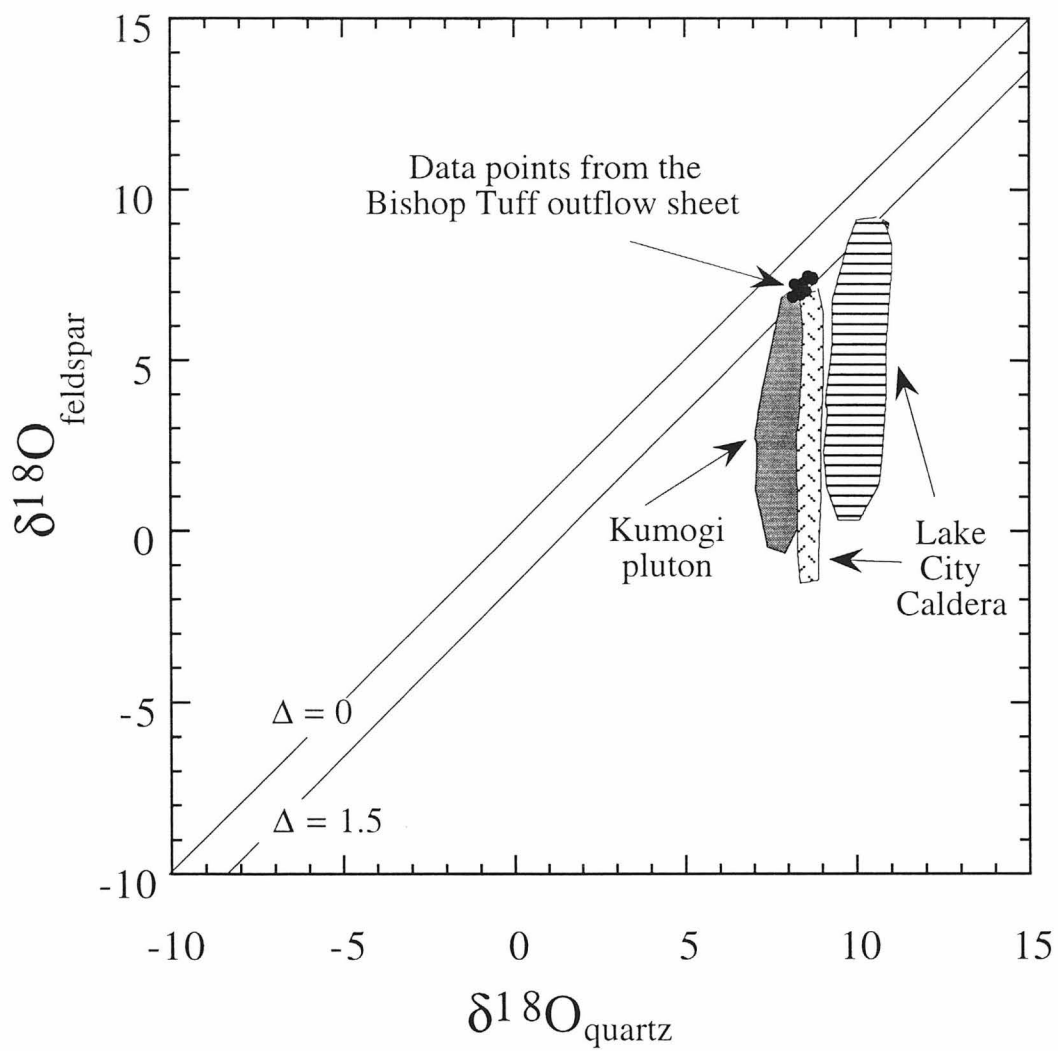


Fig. 2.2



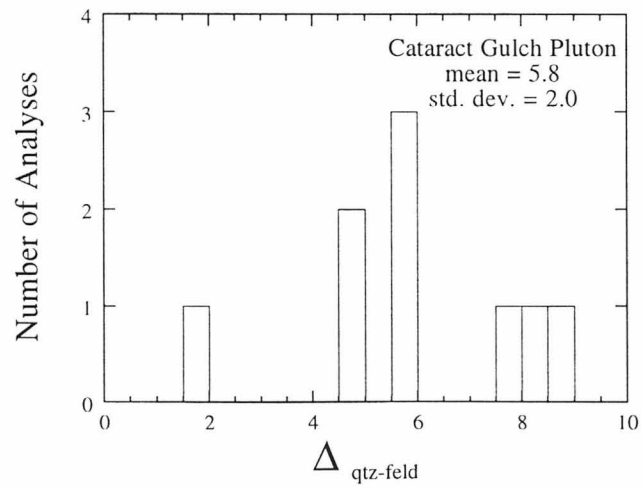
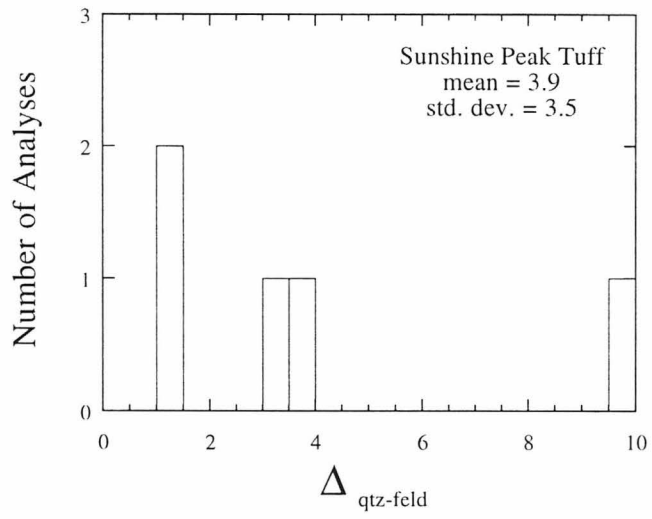
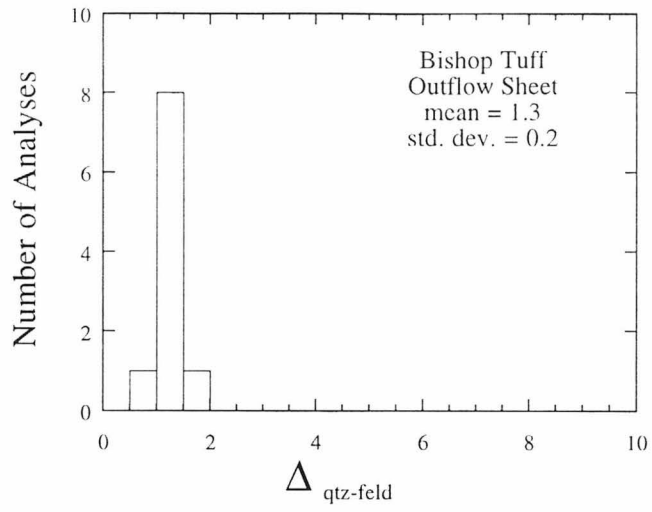


Fig. 2.3

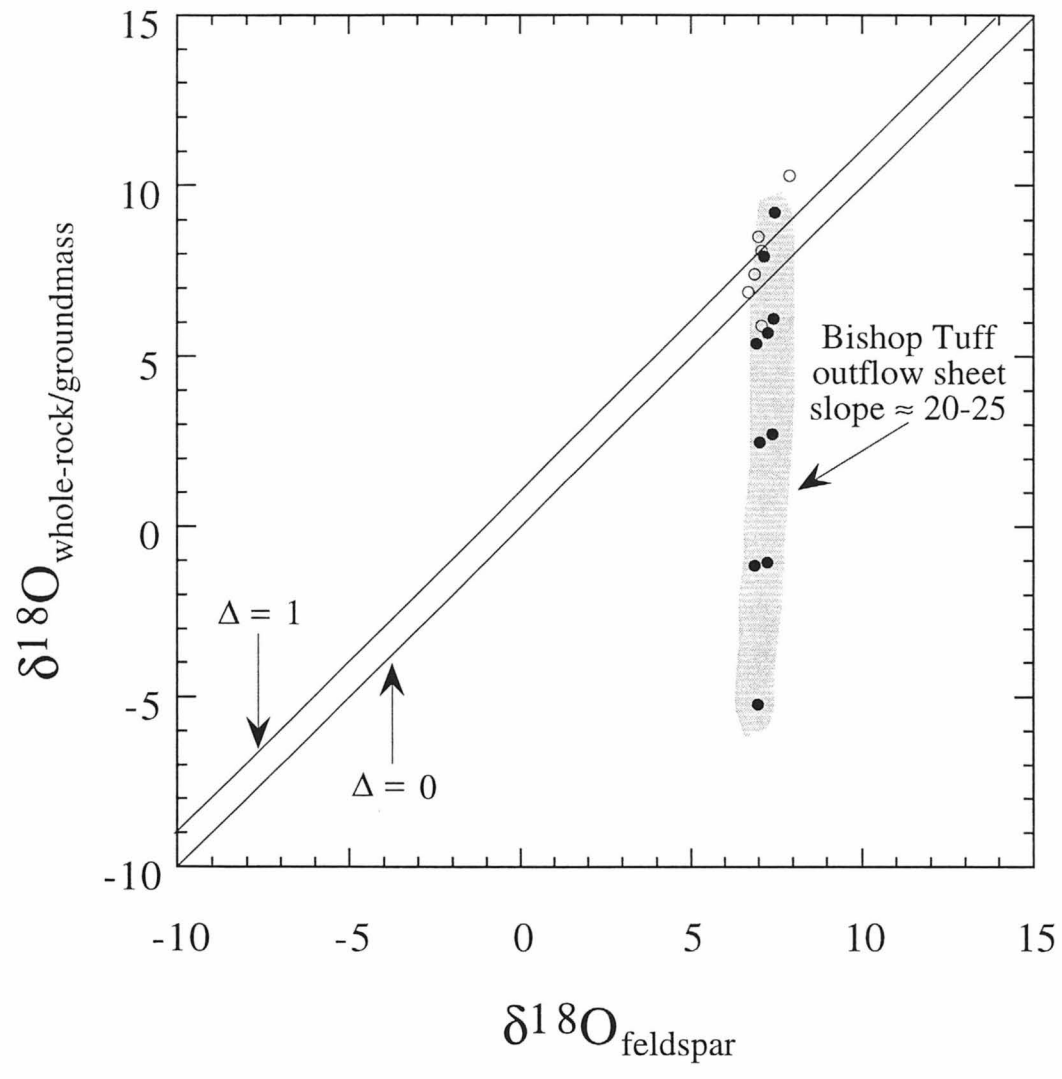


Fig. 2.4

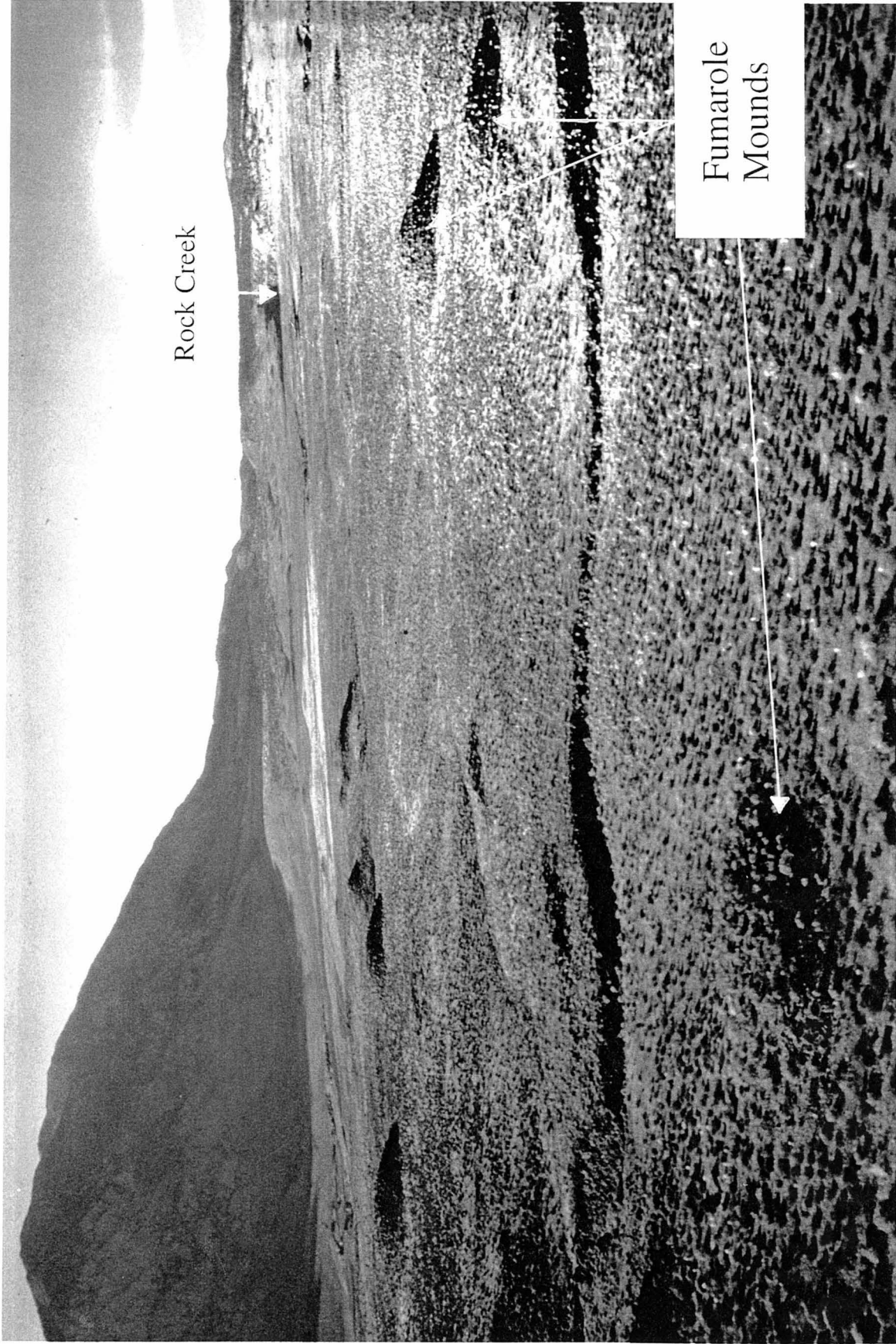
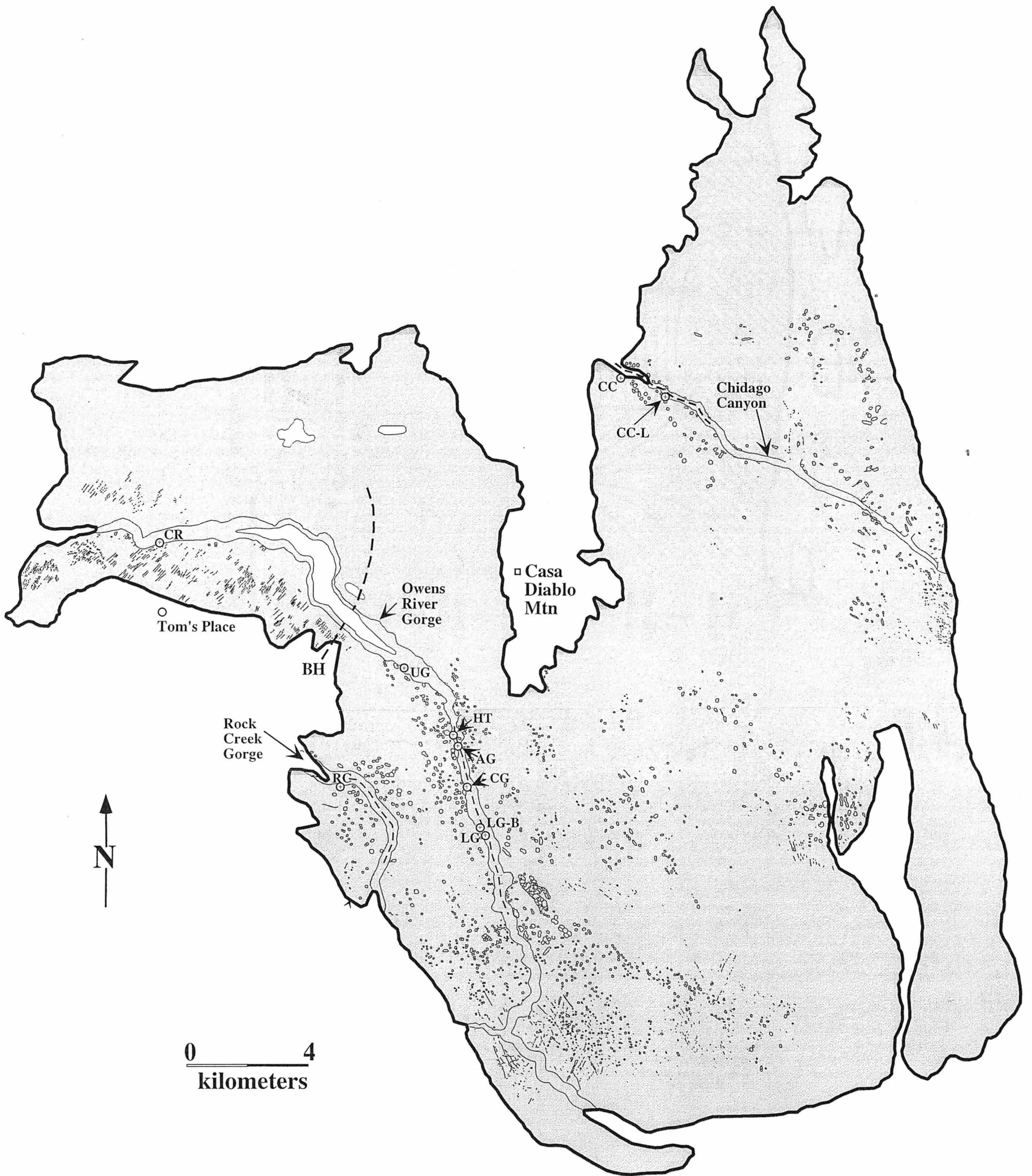


Fig. 2.5



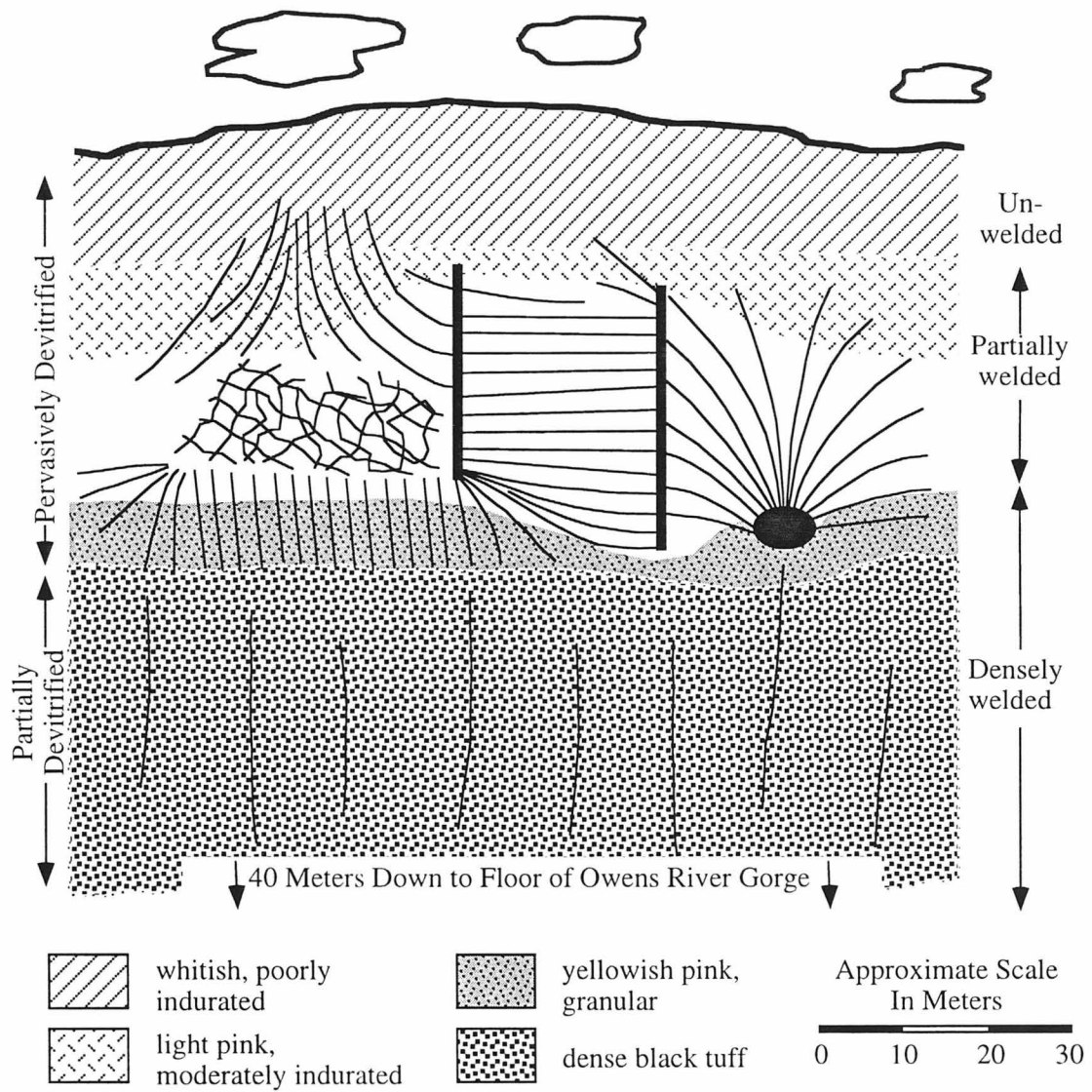


Fig.2.7

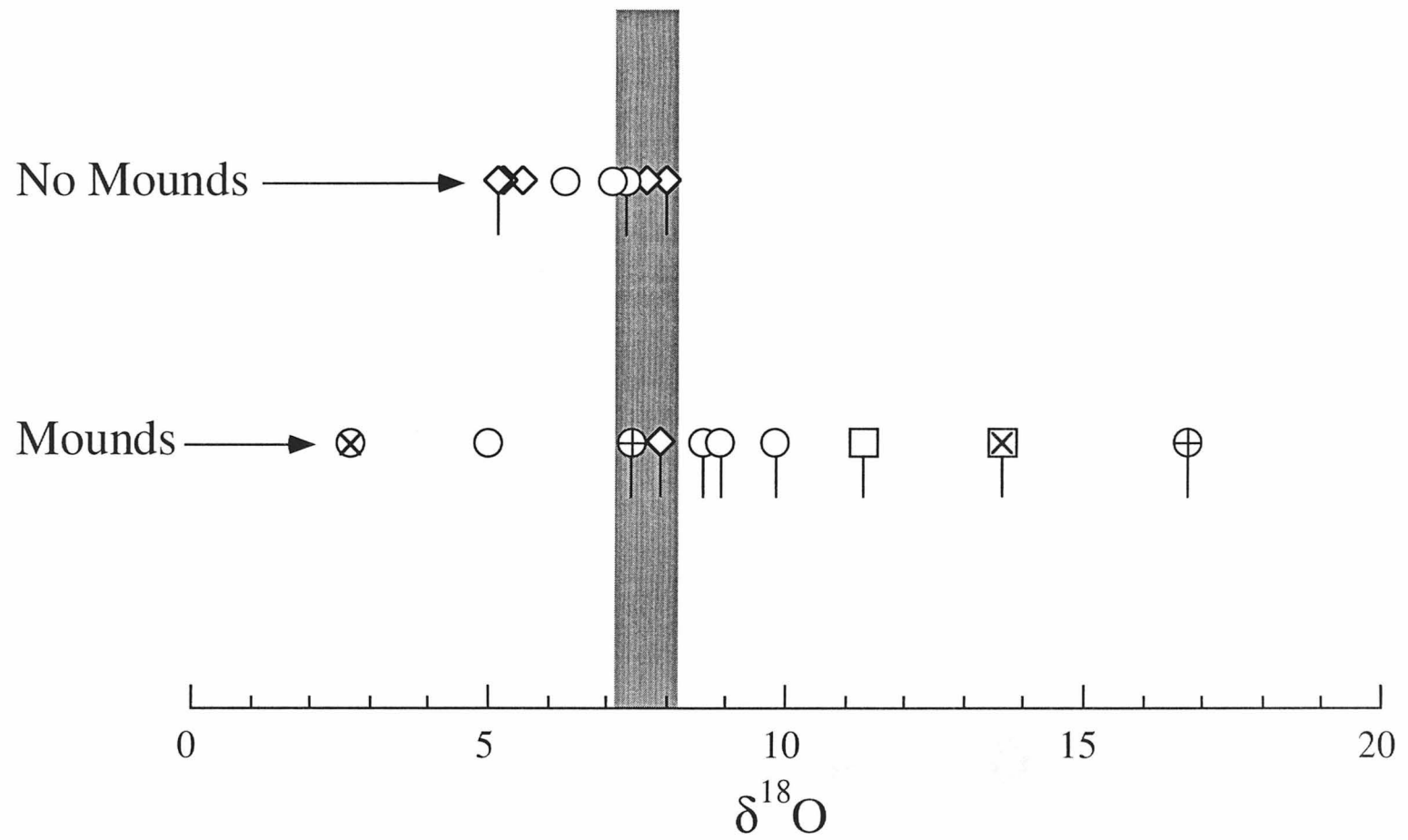


Fig. 2.8

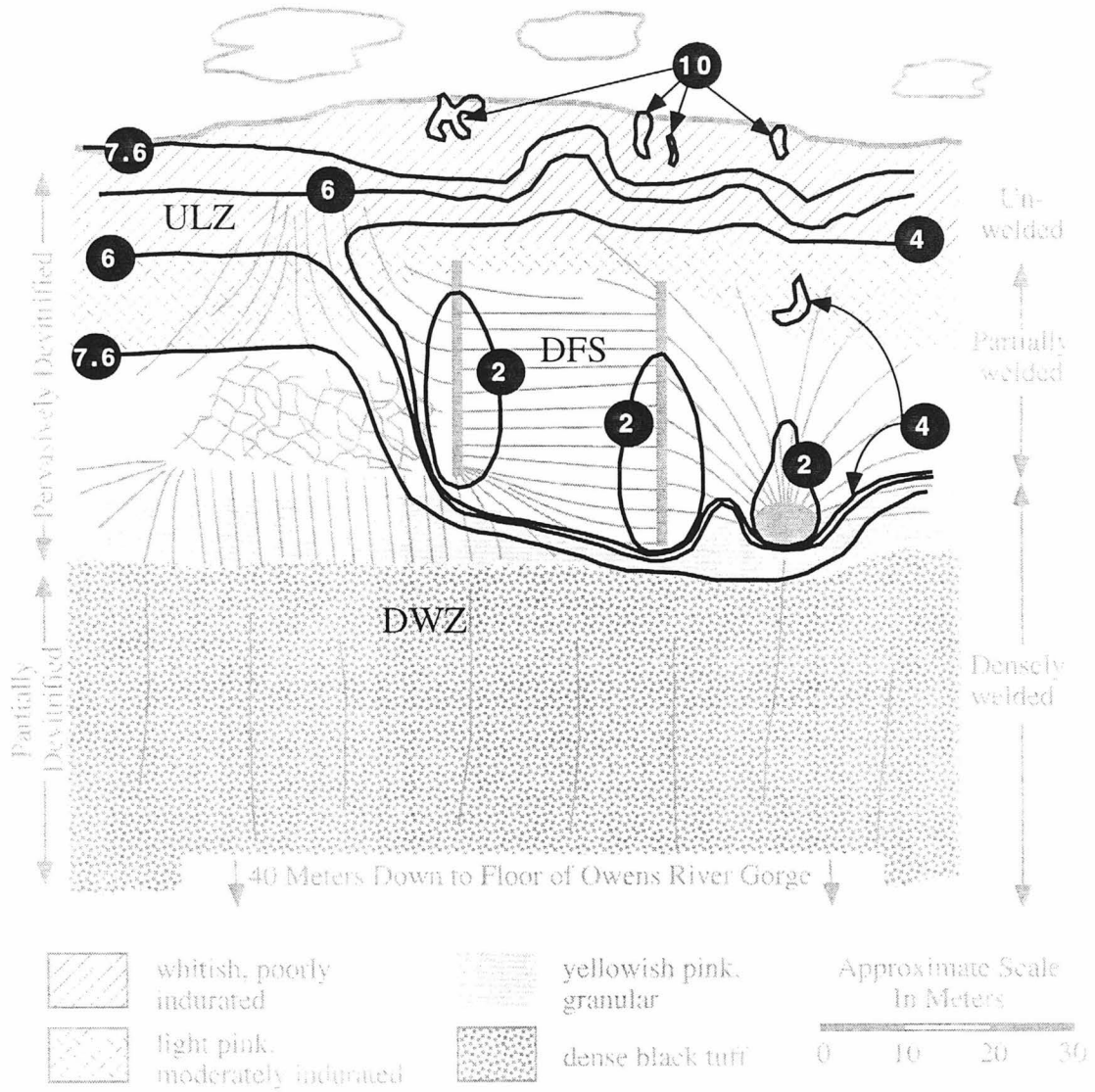


Fig.2.9

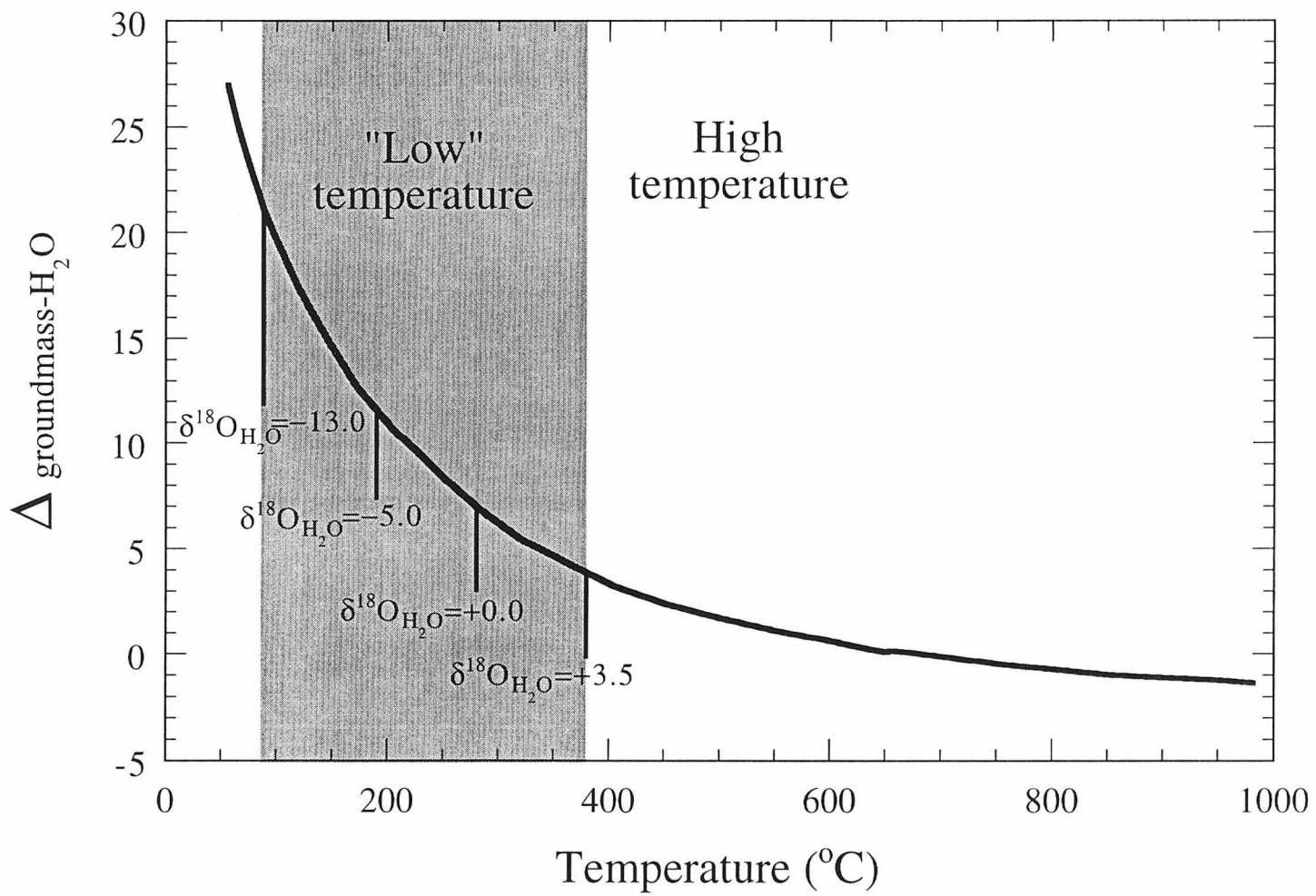


Fig. 2.10



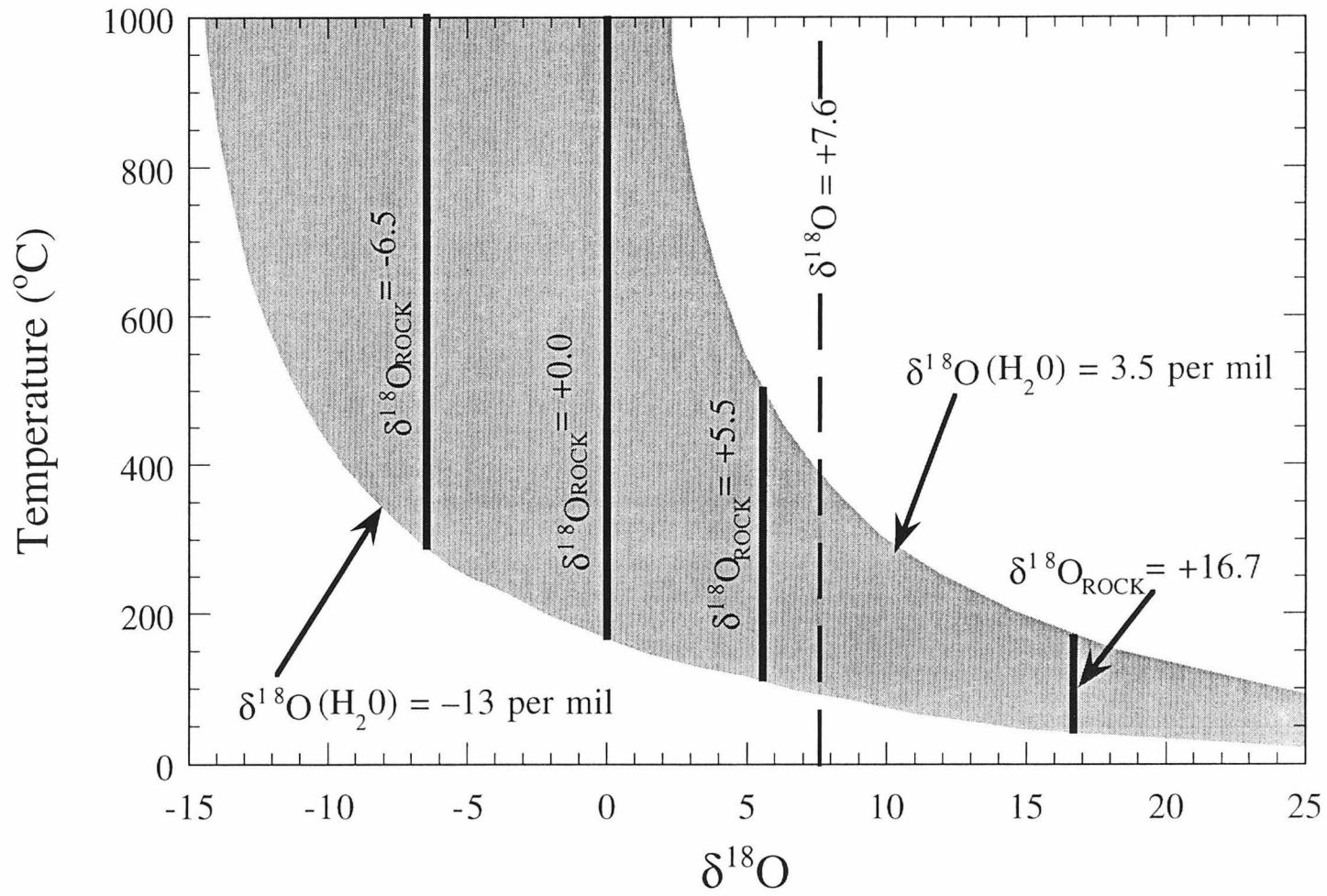


Fig. 2.11

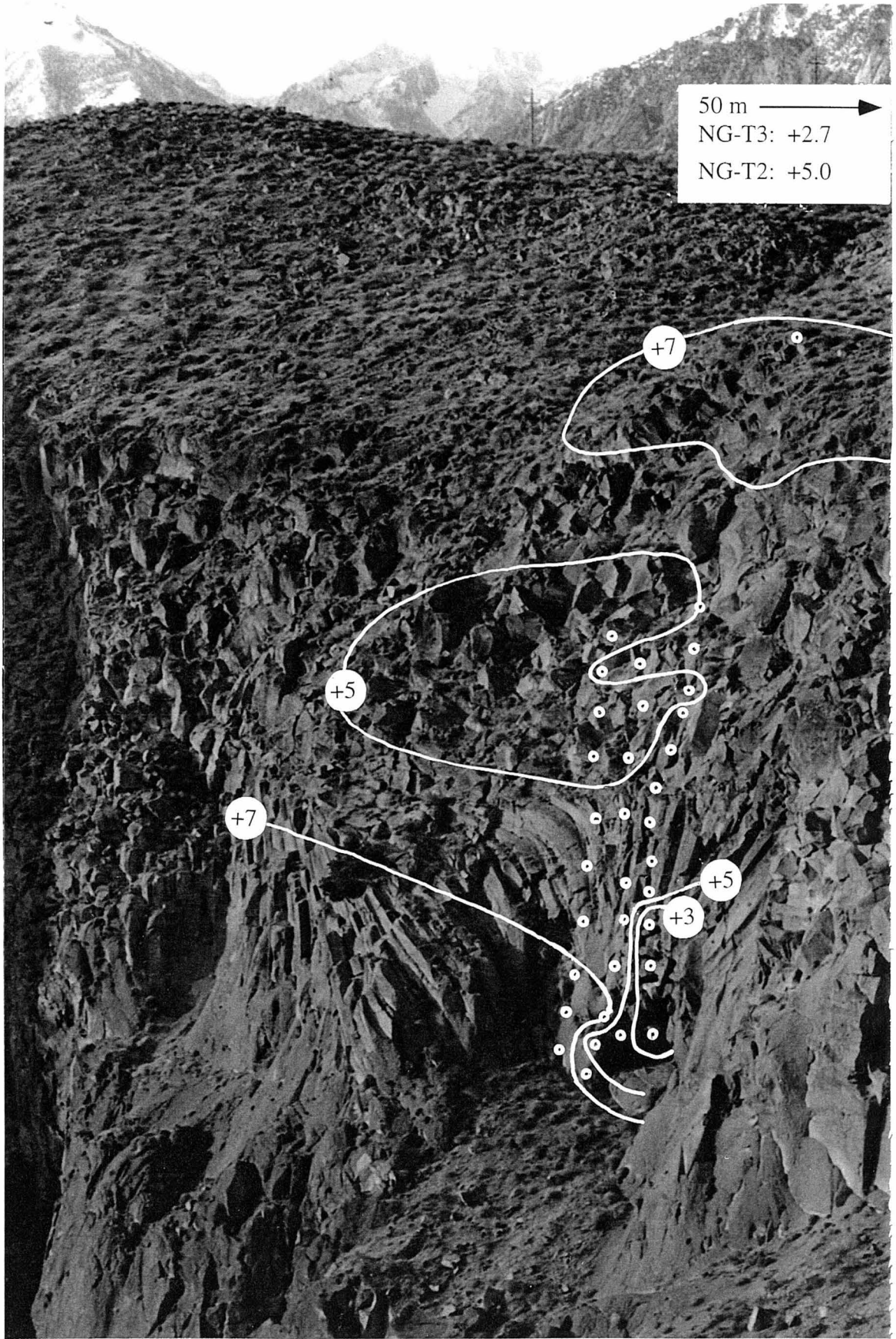


Fig.2.12

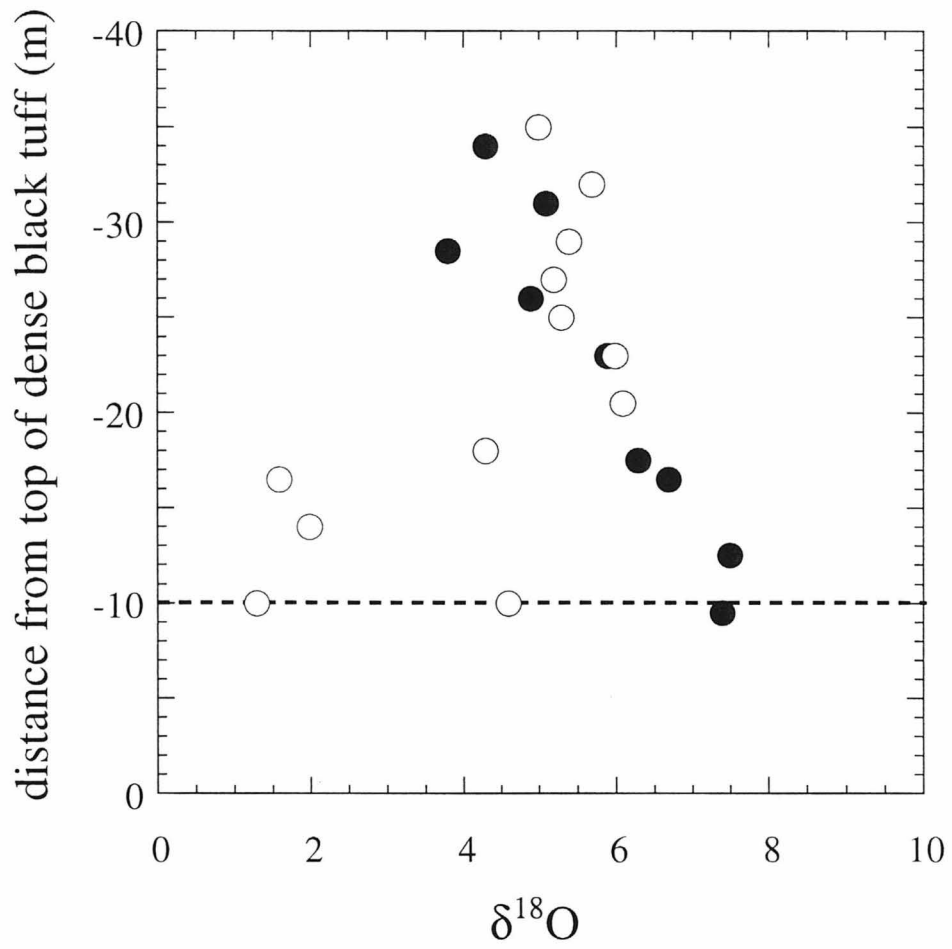


Fig. 2.13

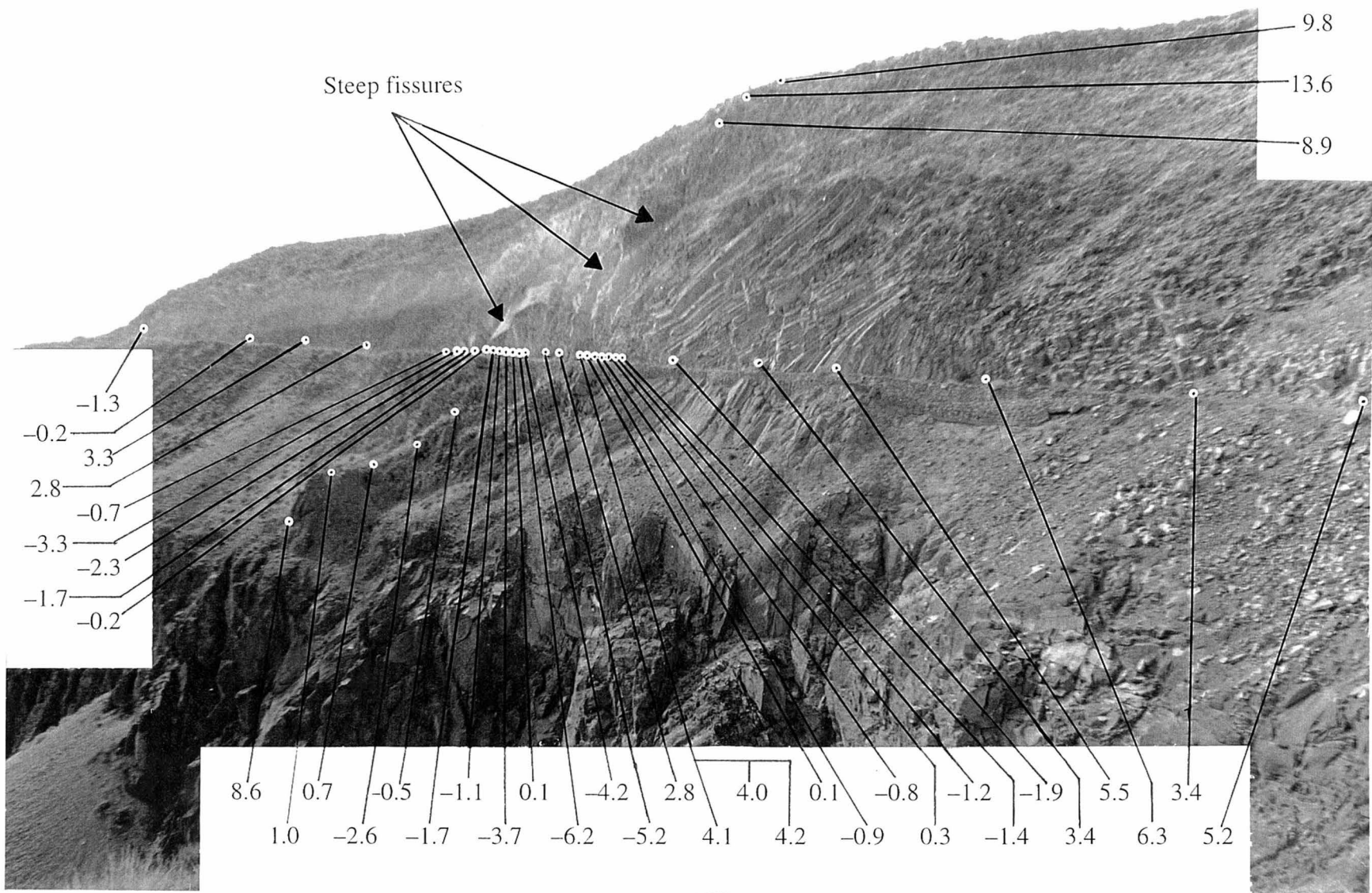


Fig. 2.4a

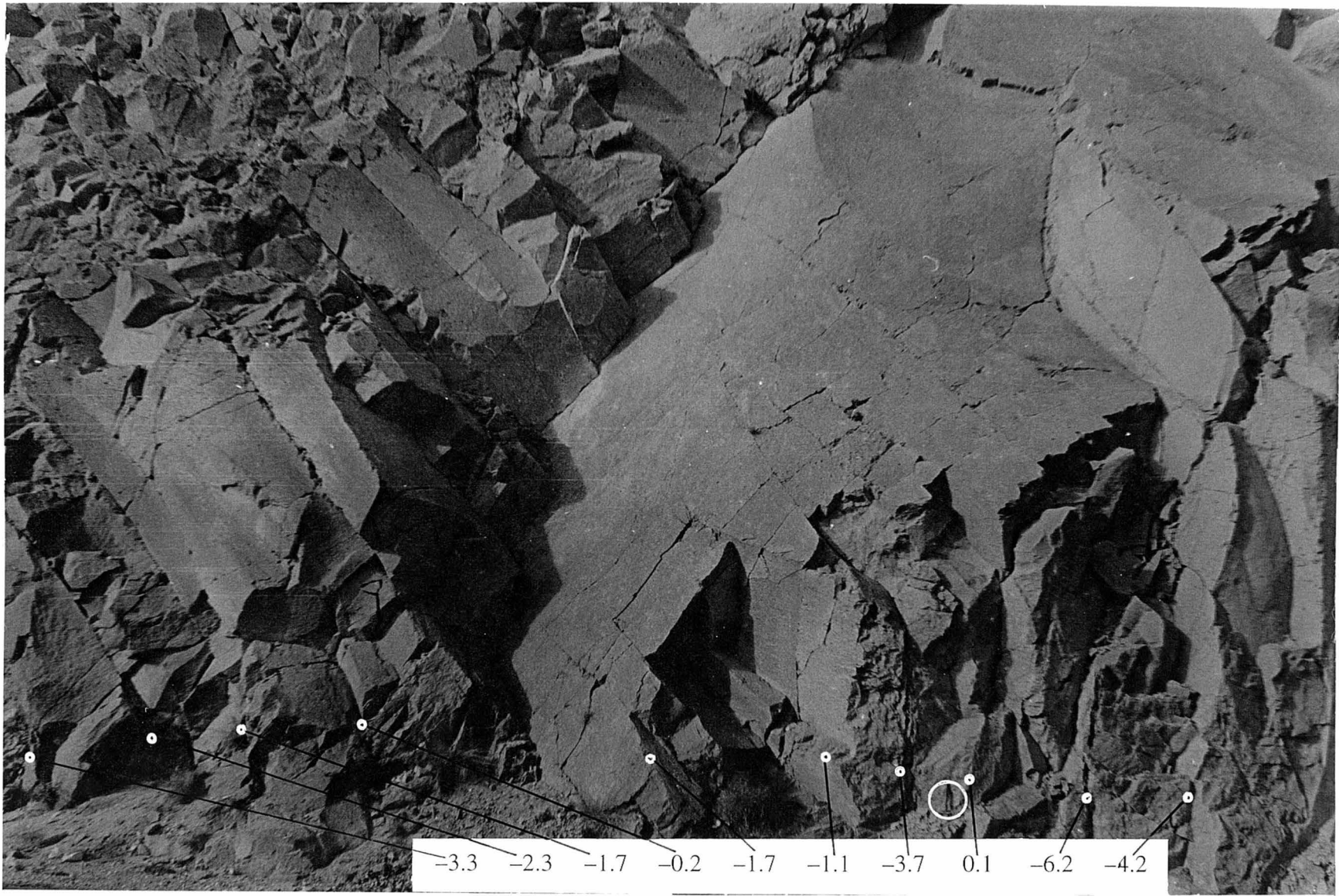


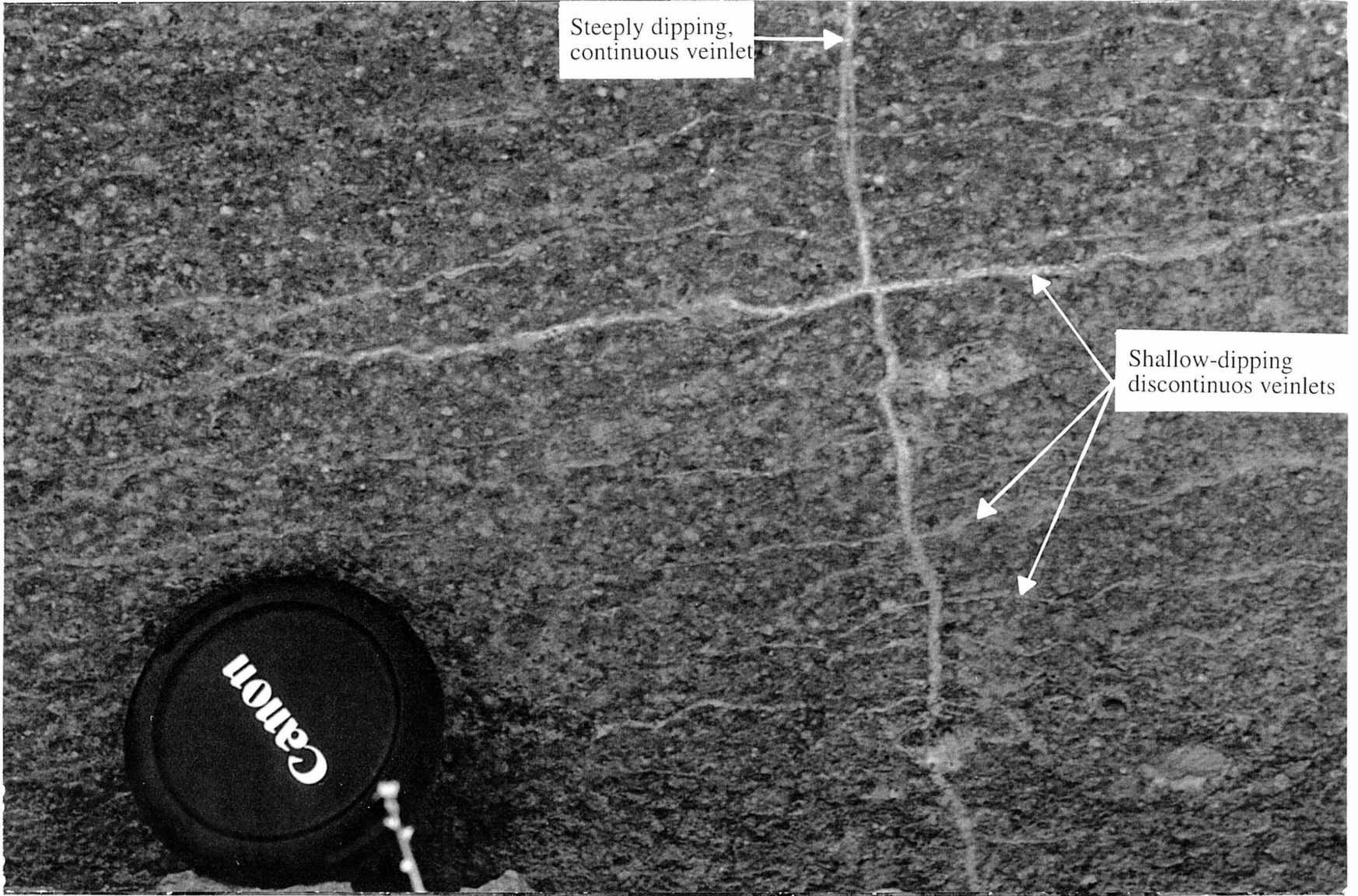
Fig. 2.146



Sample LG-16

$\delta^{18}\text{O} = -3.7$

Fig. 2.14c

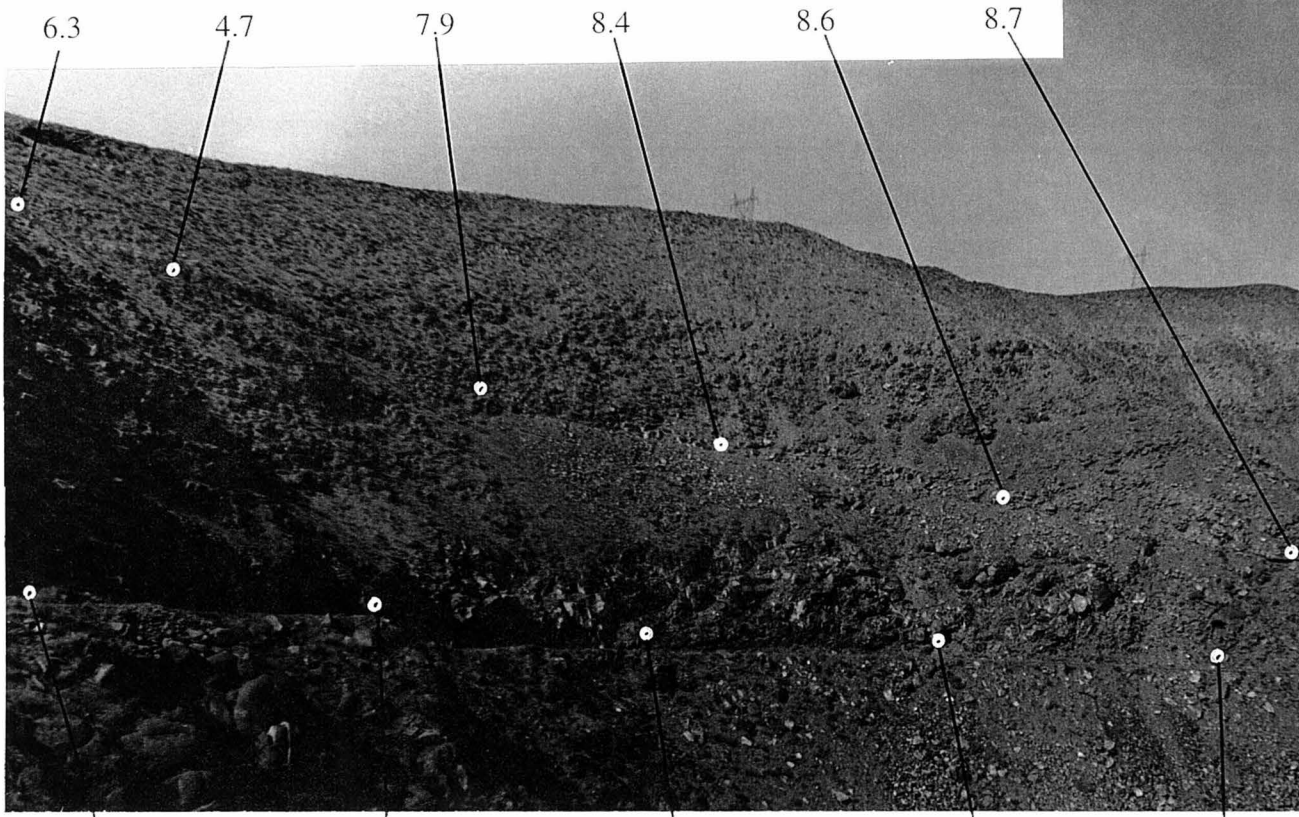


Steeply dipping,  
continuous veinlet

Shallow-dipping  
discontinuous veinlets

Fig. 2.15

Steep Old Road



Samples LG-31 (9.1) and LG-32 (9.1) were collected a few meters around the corner on Middle Power Plant Road

8.1                      8.6                      8.4                      LG-frac: 8.6                      8.5  
(LG-vein1: -0.4, 0.0)                      LG-vein2: 8.8

Middle Power Plant Road



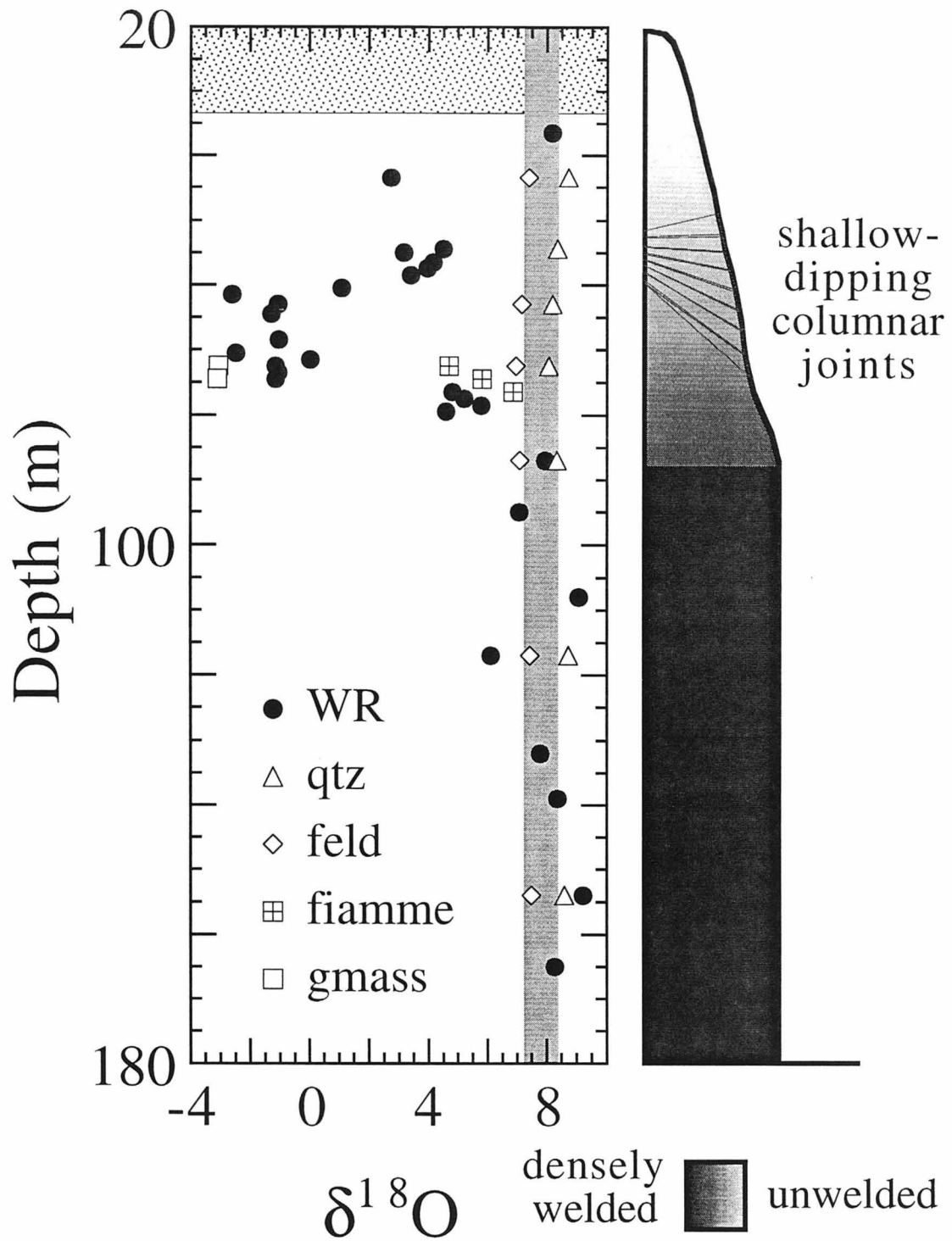


Fig.2.17

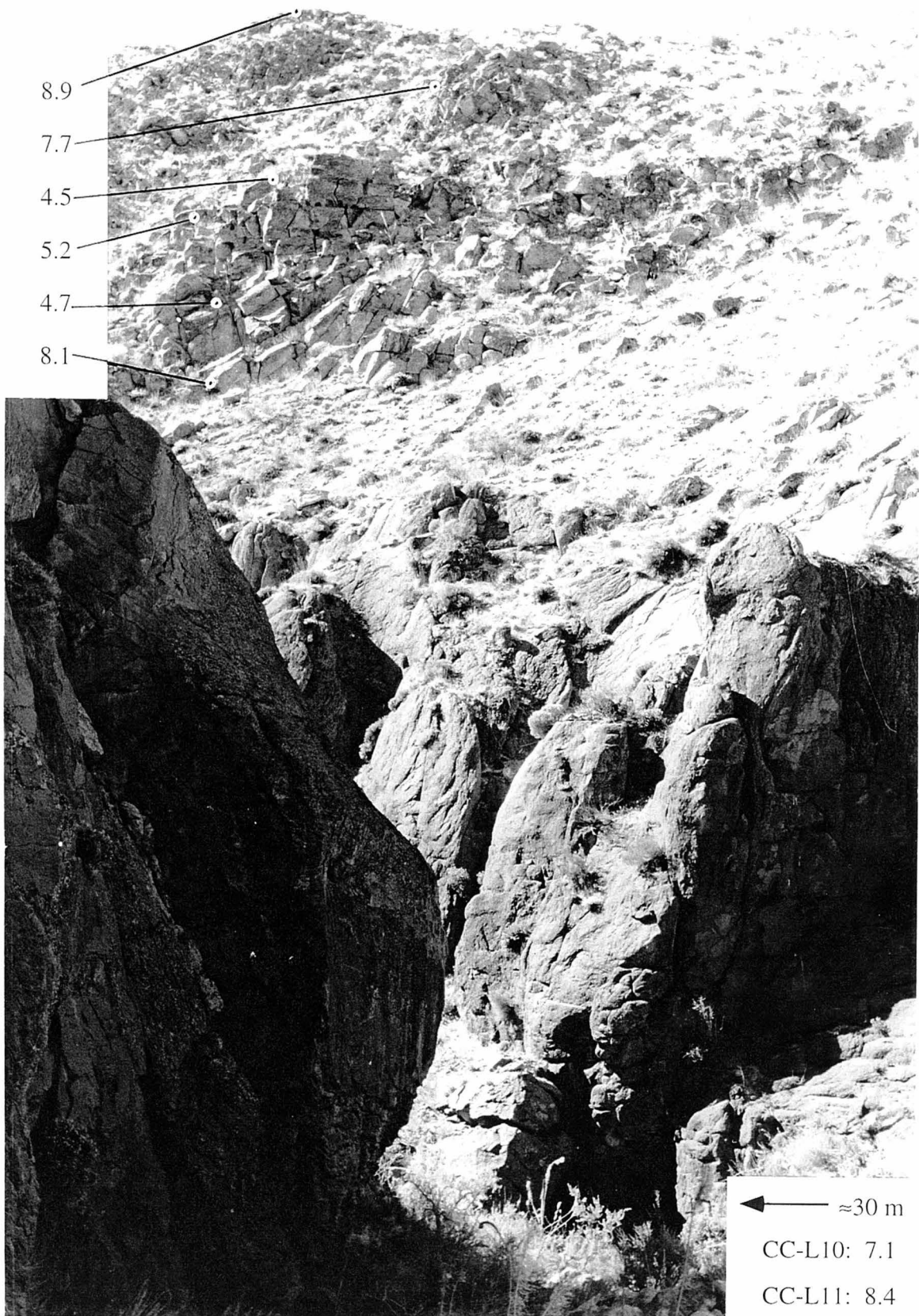


Fig. 2.18

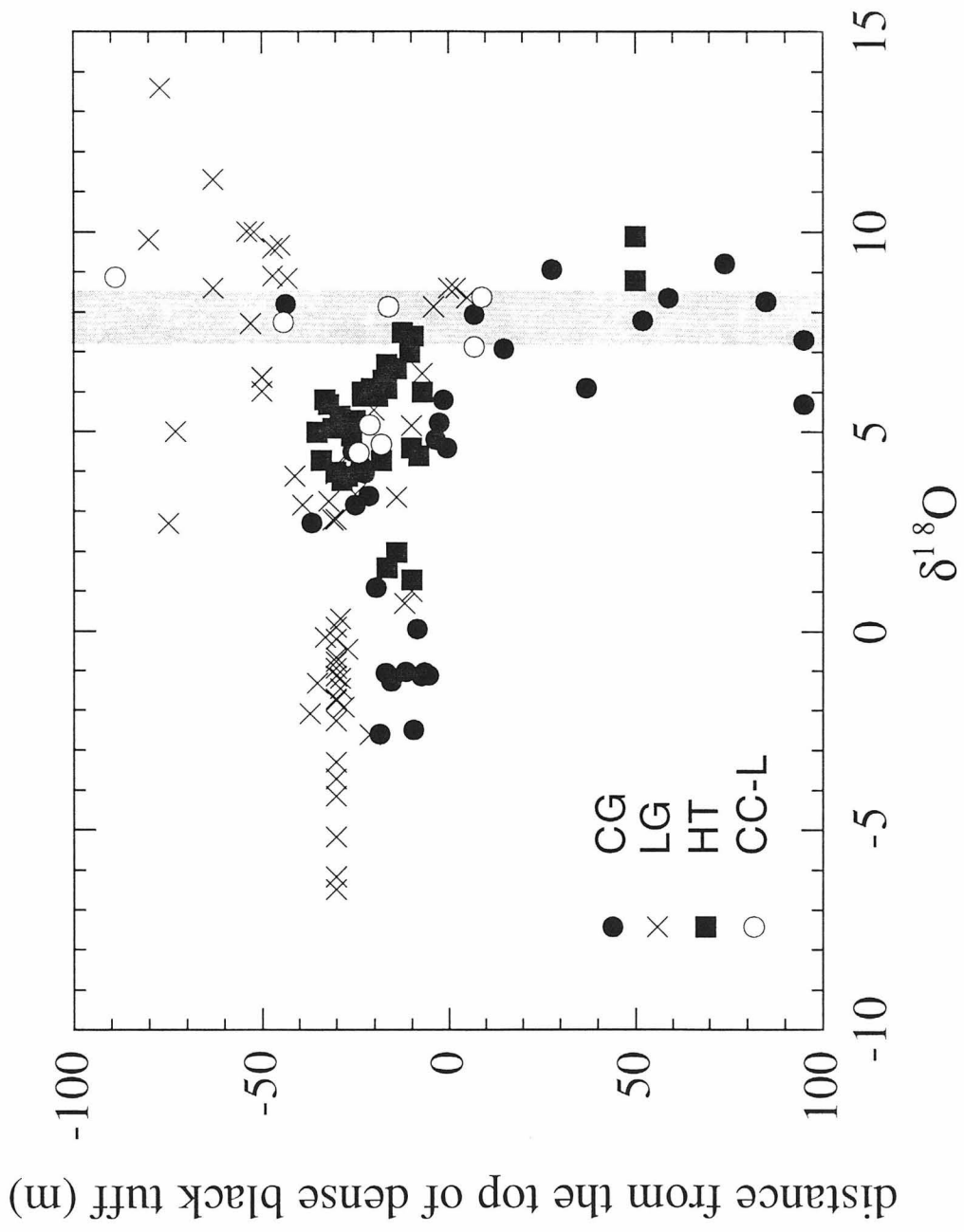


Fig. 2.19

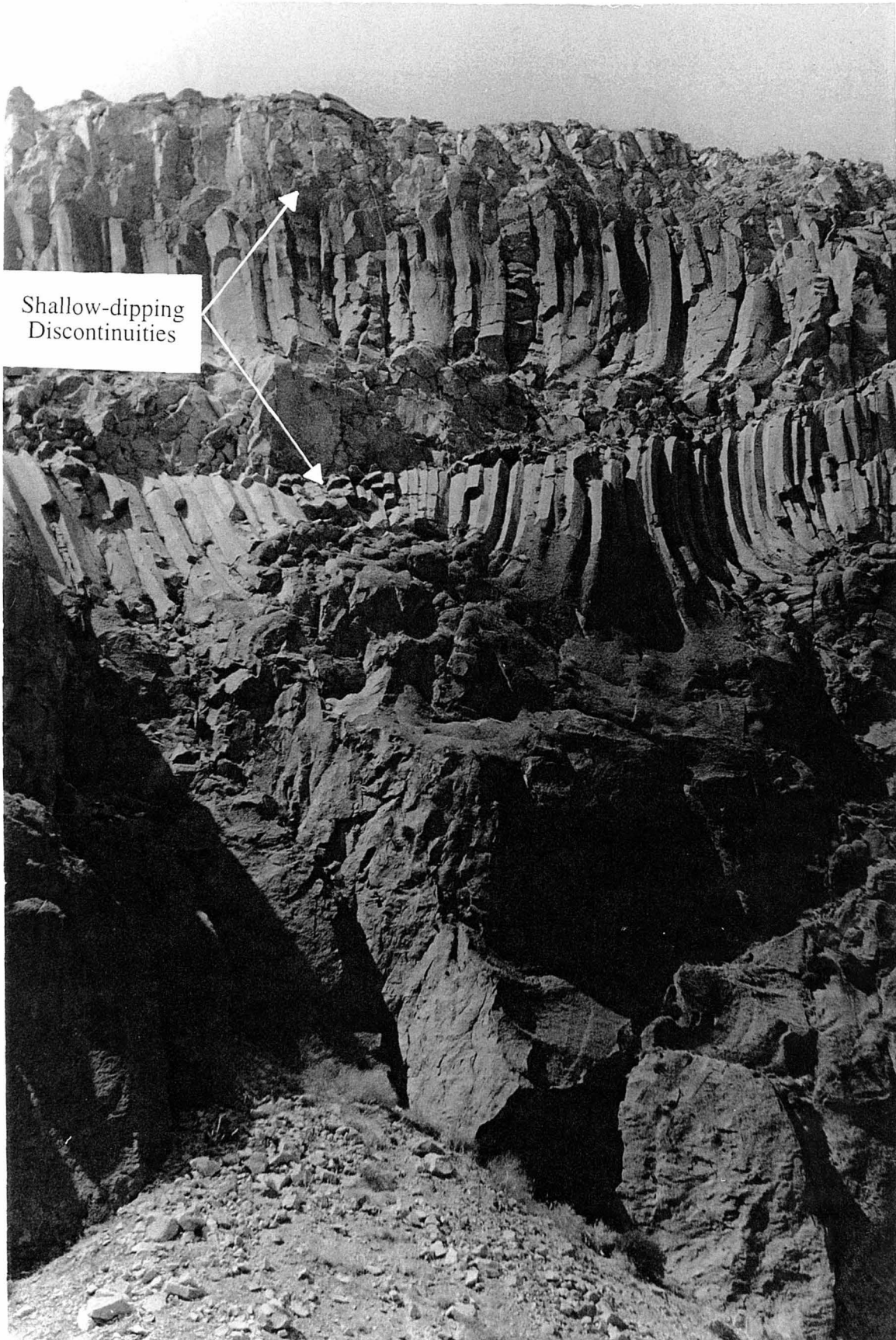


Fig. 2.20

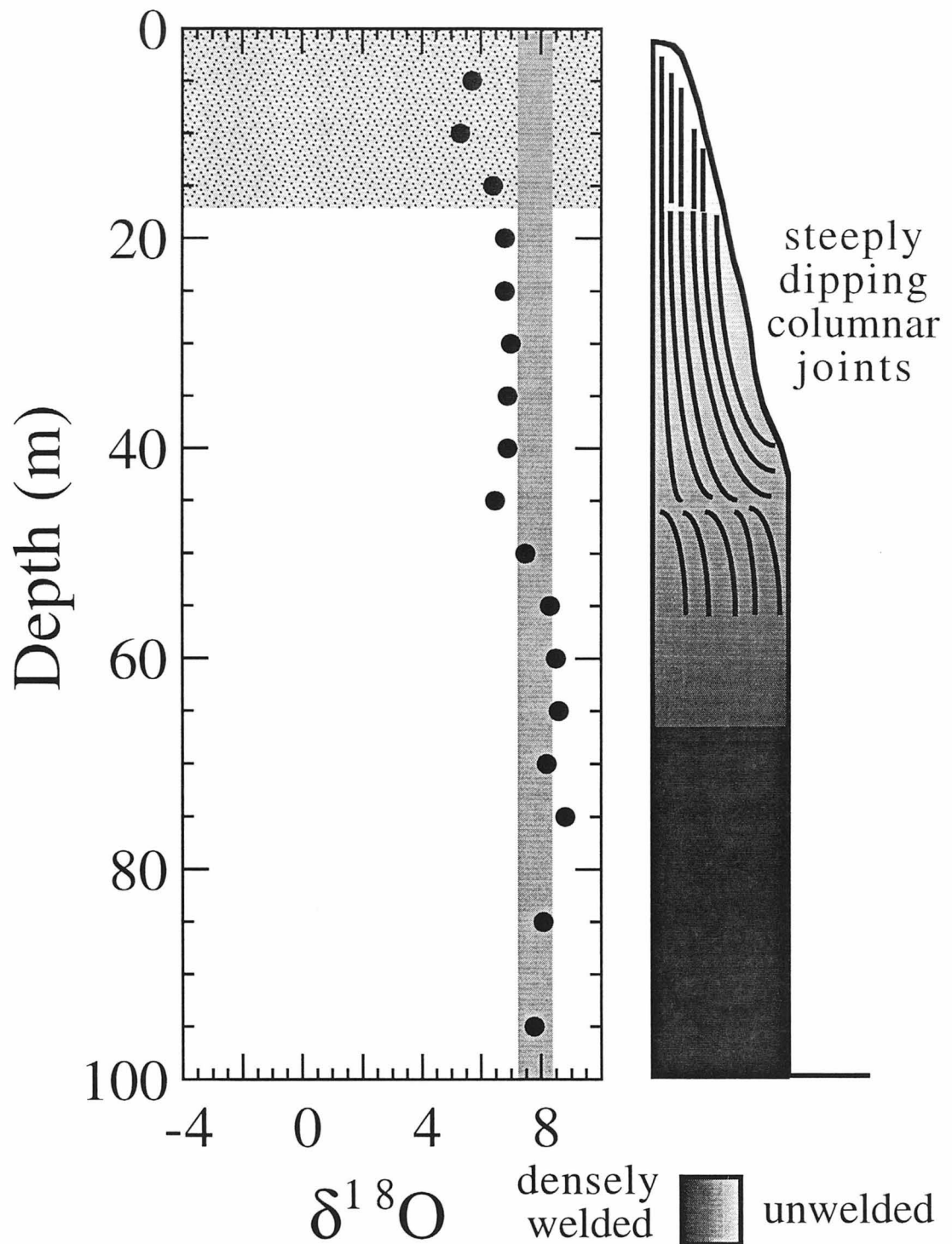


Fig.2.21

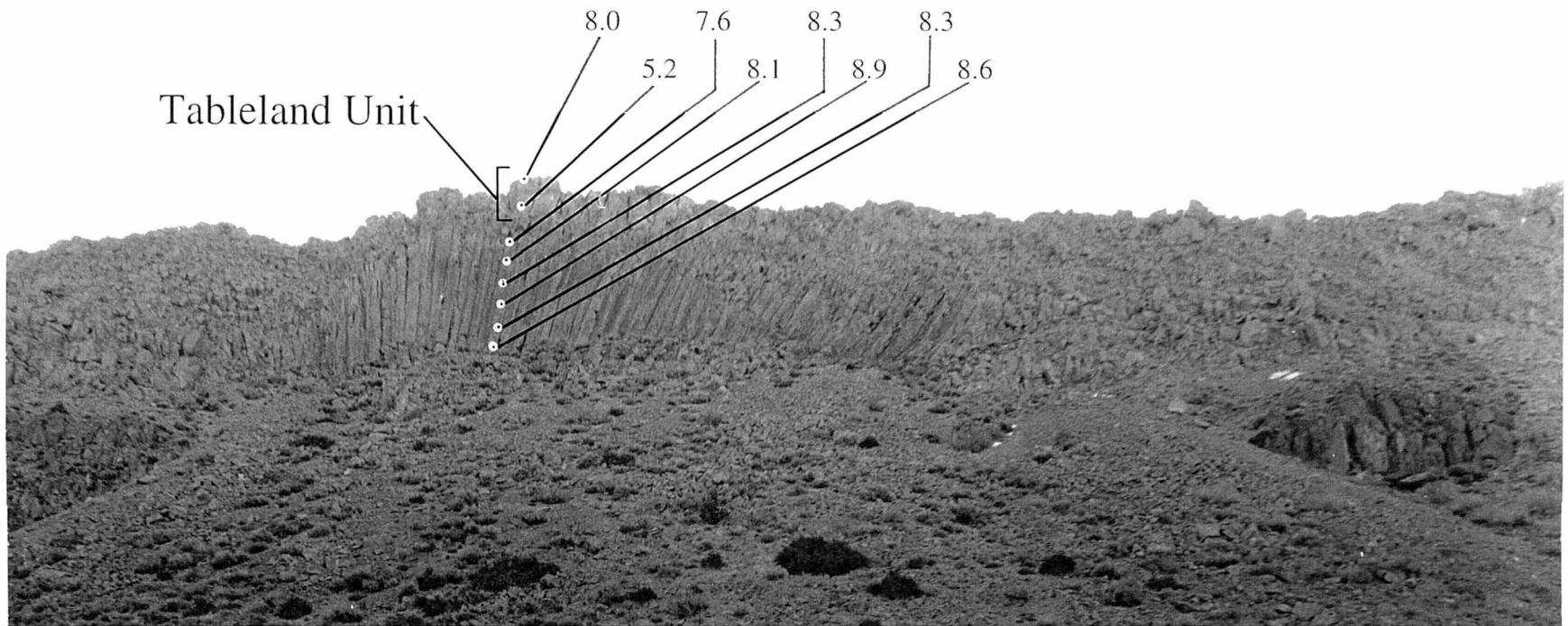


Fig. 2.22



Fig. 2.23



RC1-2: +8.5

RC1-5: +8.2

Fig. 2.24



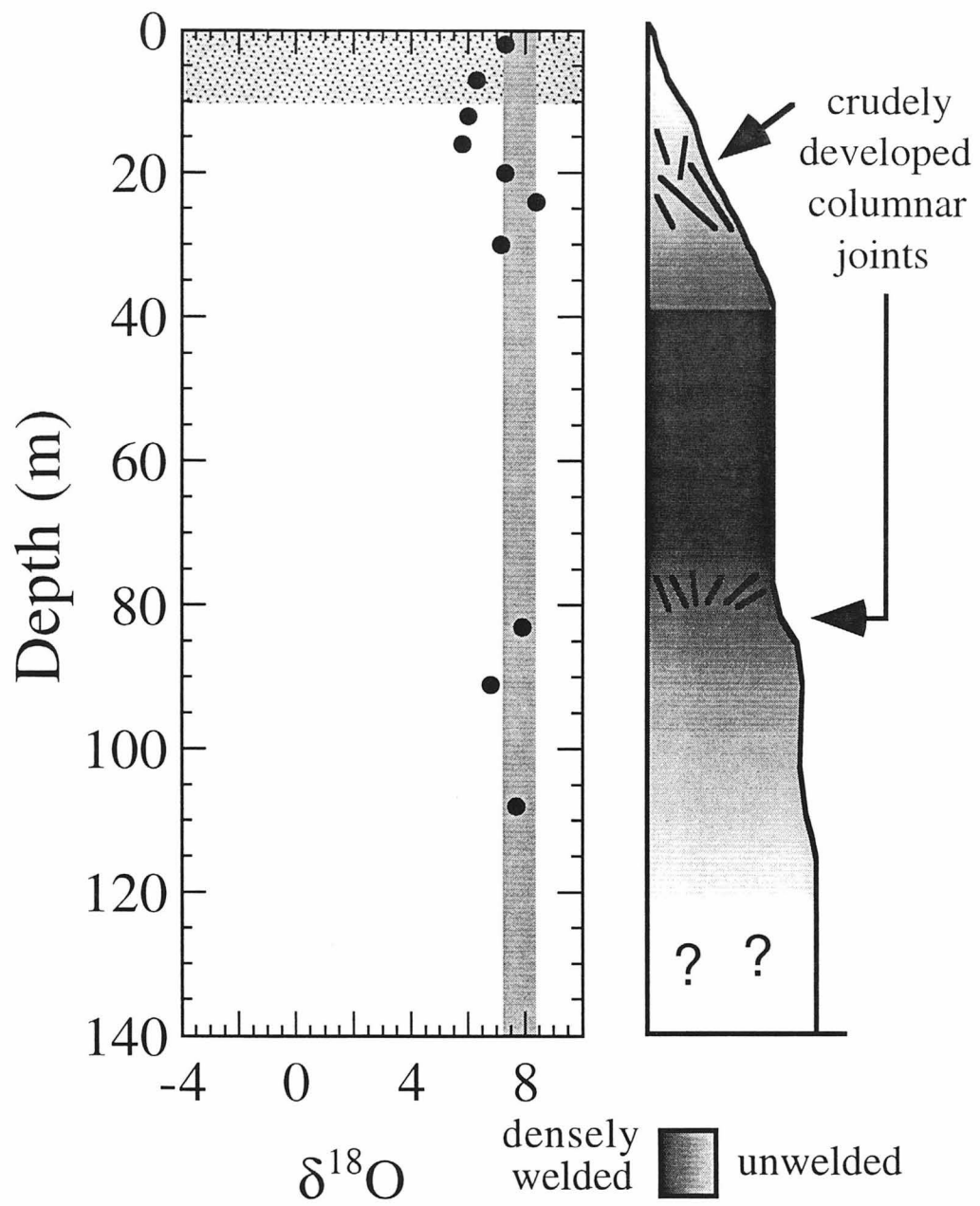


Fig.2.25

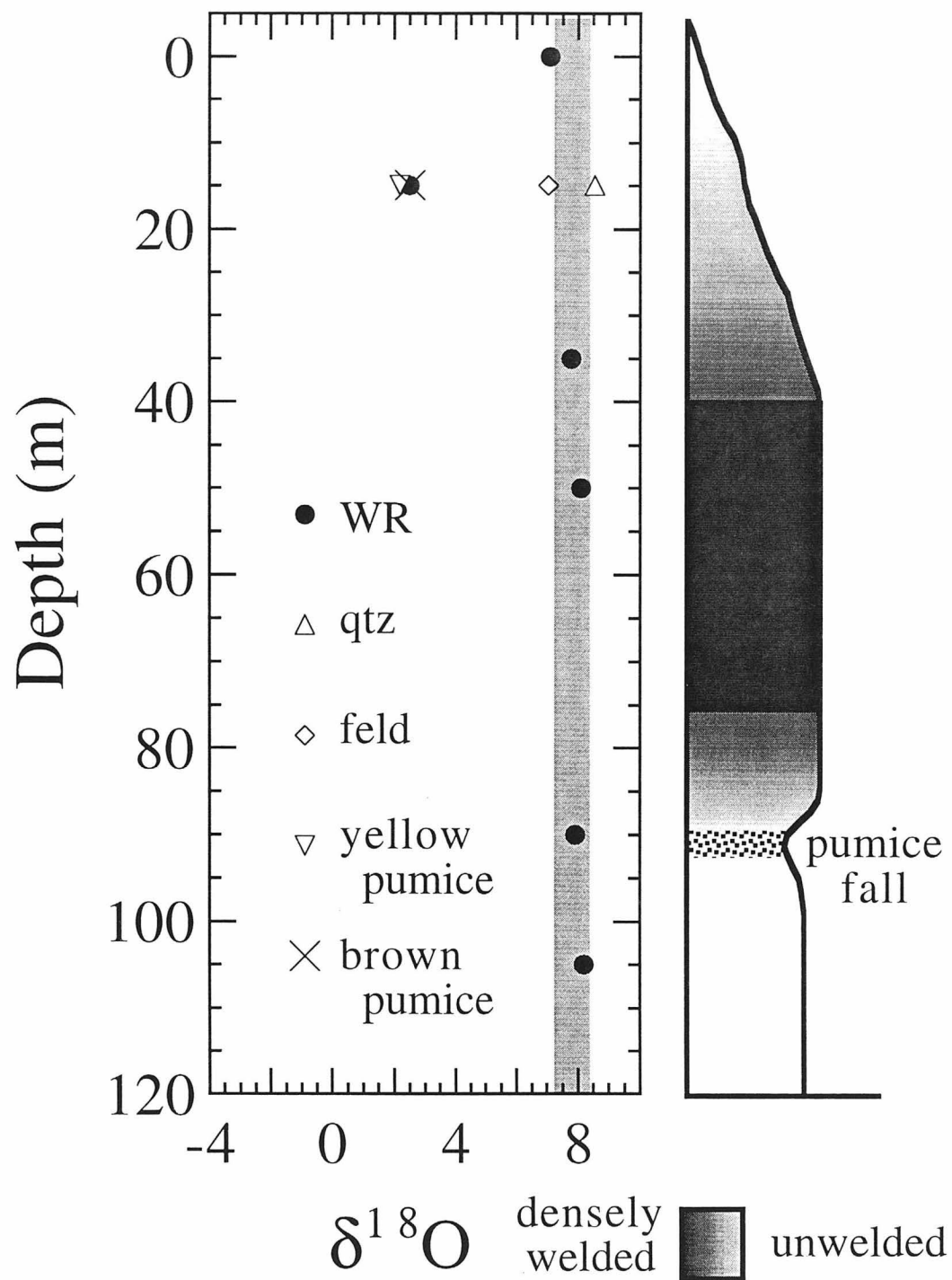


Fig. 2.26

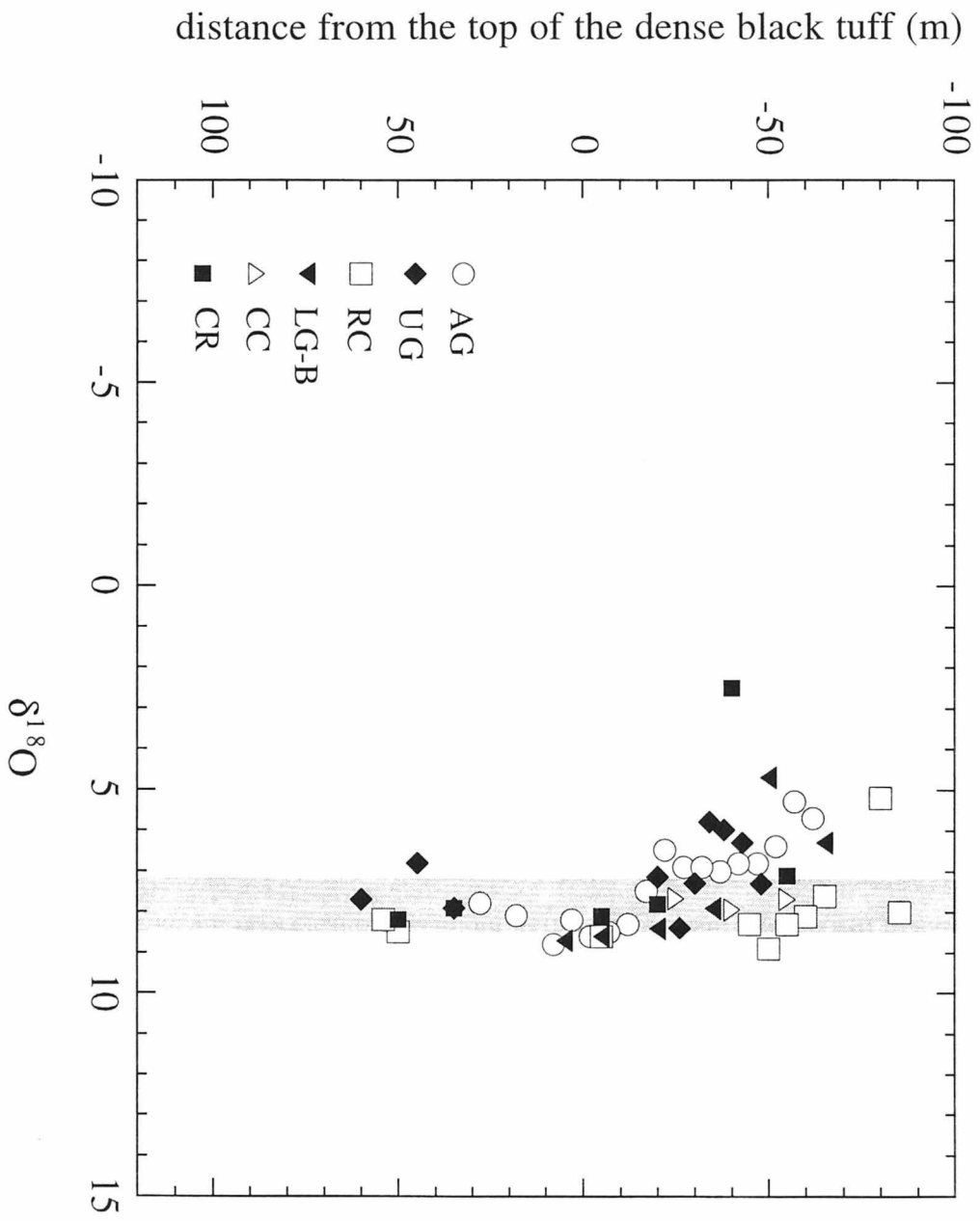


Fig. 2.27

## CHAPTER 3: HYDROGEOLOGY OF FOSSIL FUMARoles IN THE SOUTHEASTERN LOBE OF THE BISHOP TUFF OUTFLOW SHEET

### 3.1 Fossil fumarole distribution and morphology

The most prominent morphological features of the Bishop Tuff fumarole area are the mounds and ridges that dot the surface of the southeastern lobe of the Bishop Tuff outflow sheet just north of Bishop, California (Figs. 3.1 and 3.2). These mounds and ridges are composed of Bishop Tuff that was sintered during the escape of fumarolic vapors shortly after the tuff was emplaced, making these areas more indurated and less susceptible to erosion than surrounding unwelded Bishop Tuff (Putnam, 1960; Sheridan, 1970). For purposes of discussion, the distribution of mounds and ridges on the surface of the Bishop Tuff can be conveniently divided into four geographic regions: the Gorges Area, the Southeast Area, the Chidago Area, and the Crowley Area (Fig. 3.2). As described previously by Sheridan (1970), fumarole mounds in the Gorges, Southeast, and Chidago Areas are up to 60 m in diameter, and ridges are 1.5 to 5 m high and up to 600 m long. The fumarolic surface features in the Crowley Area exhibit a heretofore unrecognized, but markedly different morphology than those in the other three fumarolic areas; as shown on Fig. 3.2, mounds are very rare, and the abundant ridges are much more regular in length ( $\approx$ 400-600 m) and orientation (trending approximately N40E).

Whole-rock  $^{18}\text{O}/^{16}\text{O}$  data from the Bishop Tuff outflow sheet reported in Chapter 2 demonstrate that there is a correlation between  $\delta^{18}\text{O}$  and spatial position within the fumarolic plumbing system. Broadly speaking, it was found that at least two kinds of meteoric-hydrothermal circulation systems were active during fumarolic activity (see Figs. 2.19 and 2.27 and discussion in Chapter 2): (1) A shallow, less vigorous hydrothermal circulation regime (the ULZ) that produced modest  $^{18}\text{O}$  depletions in the tuff, and whose effects are seen throughout an areally extensive stratigraphic horizon in the uppermost part of the ash-flow sheet; and (2) A set of deeper, much more vigorous hydrothermal

circulation systems (the DFS) that produced extreme  $^{18}\text{O}$  depletions in the tuff, and whose effects are directly associated with fumarolic structures (tubular conduits and steep fissures; see Fig. 3.3) that fed very large amounts of hot, buoyant  $\text{H}_2\text{O}$  into the directly overlying fumarolic mounds and ridges on the surface of the tuff. Mapping of the exposures of Bishop Tuff in the Gorges, Southeast, and Chidago Areas indicates that the tubular conduits and steep fissures, together with their associated shallow-dipping columnar joints, are found *only* beneath fumarolic mounds, and that in these three areas, fumarolic mounds always have at least one of these kinds of structures beneath them.

The inferred areal extent and volumes of rock involved in both the ULZ and the DFS can be estimated by determining the distribution of mounds and ridges on the surface of the Bishop Tuff from aerial photographs, and by mapping the associated fumarolic conduits along the three canyons that cut deeply into the tuff (i.e., Owens River Gorge, Rock Creek Gorge, and Chidago Canyon; Fig. 3.2, Tables 3.1 and 3.2). Using this information and the  $\delta^{18}\text{O}$ -depth profiles determined for various locations in the Bishop Tuff outflow sheet (see Chapter 2), the three-dimensional geometry of both the ULZ and the DFS can be approximated, and material-balance water/rock ratios and heat-balance constraints can be calculated for both of these kinds of meteoric-hydrothermal systems (Tables 3.1 and 3.2).

In several ways, the characteristics of the fumaroles in the Crowley Area are distinct from those of the fumaroles in the Gorges, Southeast and Chidago Areas. For example, in the Crowley Area there are very few fumarolic mounds on the surface of the tuff, and these few are located only along the edge of Owens River Gorge east of Crowley Dam (Fig. 3.2). In fact, this entire area was considered by Sheridan (1970) to be a zone of weak or non-existent fumarolic activity (see Fig. 2.1), and Site CR was initially chosen as an example of a depth profile through a part of the tuff where there had been little or no fumarolic activity (Holt and Taylor, 1998). However, significant  $^{18}\text{O}$  depletions were observed in the upper part of the Site CR depth profile (Fig. 2.26), and it was also noticed that in this area there is a plethora of regularly spaced fumarolic ridges, all about 400-600 m

long and oriented roughly N40E (Fig. 3.2). Forestation, as well as topographic relief in this area, makes identification of these ridges more difficult on the ground, but they are clearly visible on aerial photographs (Fig. 3.4 and 3.5). These fumarolic ridges in the Crowley Area are far more regular in orientation and size than any located in the other three fumarole areas (see Fig. 3.2). More importantly, in contrast to the less well-defined, irregular fumarolic ridges in the other three areas, no major fumarolic conduits (e.g., tubular conduits or steep fissures) were observed beneath the ridges in the Crowley Area. Because there are abundant exposures of the tuff below the fumarolic ridges where they cross Owens River Gorge and where the ridges intersect cliffs along the southern margin of the Crowley Area, we must conclude that in the Crowley Area, these ridges are not associated with the types of fumarolic conduits observed in the Gorges and Chidago Areas. It thus seems probable that these morphologically distinct fumarolic ridges were formed by a different mechanism. Considerations of the hydrogeology of this region immediately after eruption of the Bishop Tuff suggest that fumaroles in the Crowley Area may have been supplied directly by groundwater from ancestral Long Valley Lake.

In large part, the following discussions (Sections 3.3 to 3.7) refer only to the Gorges, Southeast, and Chidago Areas. The unique characteristics of the Crowley Area are discussed separately in Section 3.8.

### **3.2. Shallow meteoric-hydrothermal circulation in the ULZ**

Whole-rock  $^{18}\text{O}/^{16}\text{O}$  data from various sampling sites from both inside and outside the fumarole areas shown in Fig. 3.2 indicate the existence of a ubiquitous, relatively weak, shallow type of fumarolic activity throughout the upper part of the Bishop Tuff, irrespective of the location of fumarolic mounds and ridges (see Fig. 2.27). Of the sampling sites for which  $\delta^{18}\text{O}$  data are shown on Fig. 2.27, two (Sites AG and LG-B) are located away from any fumarolic mounds, but still in the region where there is abundant nearby morphological evidence for intense fumarolic activity. Three other sampling sites

shown on Fig 2.27 (Sites UG, RC, and CC) are from regions along the margins of the Gorges and Chidago Areas, where there is very little morphologic evidence for any nearby fumarolic activity. The single remaining sampling site (CR) in Fig. 2.27 is from outside the regions of fumarolic activity mapped by Sheridan (1970) but from inside the Crowley Area as mapped in this study. It is apparent from Fig. 2.27 that, with the exception of Site CC, all of these sites display a shallow 20-to 40-m-thick zone of whole-rock  $^{18}\text{O}$ -depletion, which is referred to as the ULZ. The base of the ULZ typically lies about 20 to 40 m above the upper contact of the densely welded black tuff. As is also apparent from Fig. 2.27, there is no simple relationship between the presence or absence of vertical columnar joints and the extent of  $^{18}\text{O}$  depletion in the ULZ.

Shallow meteoric-hydrothermal exchange in the ULZ appears to have been focused along a stratigraphic horizon located at the base of the Tableland Unit. Although  $^{18}\text{O}$  depletions are characteristically observed both above and below this contact, as shown in Fig. 3.6, the largest volume of  $^{18}\text{O}$ -depleted tuff is generally associated with the lower part of the Tableland Unit itself. Fig. 3.6 shows how whole-rock  $\delta^{18}\text{O}$  values change as a function of position within the upper parts of several depth profiles in the Gorges and Chidago Areas that contain the Tableland Unit. This portion of the upper part of the Bishop Tuff outflow sheet exhibits measurable whole-rock  $^{18}\text{O}$ -depletions at every site in which the base of the Tableland Unit was sampled, and this statement also applies to samples collected at sites lying beneath fumarolic mounds. The maximum whole-rock  $^{18}\text{O}$ -depletions in the upper parts of each of these depth profiles are invariably located near the base of the Tableland Unit.

The  $^{18}\text{O}/^{16}\text{O}$  characteristics of the ULZ are best isolated in those depth profiles from areas located well away from fumarolic conduits (Sites AG, UG, RC, and LG-B; see Figs. 2.27, 3.2, and 3.6). At Sites RC and LG-B, the  $^{18}\text{O}$ -depleted samples are largely confined to the Tableland Unit, whereas at Sites UG and AG, samples from well below the base of the Tableland Unit are also very slightly  $^{18}\text{O}$ -depleted (see also Figs. 2.21 and

2.25). However, as discussed in Chapter 2 and as shown in Fig. 2.27, these  $^{18}\text{O}$ -depletions in the ULZ are never observed to penetrate downward below a level about 20 m above the boundary with the densely welded black tuff.

Because the sampling sites shown on the composite  $\delta^{18}\text{O}$ -depth profile in Fig. 2.27 are well away from fumarolic mounds or any types of fumarolic conduits, the ULZ might be considered to be a phenomenon that is independent of the type of fumarolic process that produced the numerous prominent mounds on the surface of the tuff. Nevertheless, there is evidence that the ULZ can indeed be traced into the zones directly beneath fumarolic mounds, suggesting that it is truly a region-wide stratigraphic phenomenon. While there are no samples from the base of the Tableland Unit at Site CG, whole-rock samples near fumarole mounds at Sites LG and HT both exhibit a pronounced dip in whole-rock  $\delta^{18}\text{O}$  values near the base of the Tableland Unit (Fig. 3.6). As discussed in Chapter 2, there are undoubtedly some overlapping  $^{18}\text{O}/^{16}\text{O}$  effects from the nearby, vigorous, meteoric-hydrothermal activity associated with the Deep Fumarolic System (DFS) beneath the fumarolic mounds at Sites LG and HT. However, at least in and around the Gorges Area, the shallow meteoric-hydrothermal circulation associated with the ULZ appears to have produced  $^{18}\text{O}/^{16}\text{O}$  effects that are independent of those associated with the type of localized, intense vapor-phase activity responsible for formation of fumarolic mounds and ridges. This may be because the  $^{18}\text{O}/^{16}\text{O}$  effects observed in the ULZ formed at an earlier time than those in the DFS.

The formation of a ULZ was undoubtedly well under way very soon after eruption of the Bishop Tuff, during the time that the uppermost part of the ash-flow sheet was still hot enough to produce  $^{18}\text{O}$ -depletions (with much of the  $^{18}\text{O}$  depletion occurring within the first few months?). As shown in Fig. 3.6, meteoric  $\text{H}_2\text{O}$  percolating down through fractures and along columnar joints in the Tableland Unit would have exchanged with the groundmass to produce  $^{18}\text{O}$  depletions in the tuff. The orderly fluid flow paths shown in the sketch on the right-hand side of Fig. 3.6 are drawn in an attempt to explain the currently



observed pattern of  $^{18}\text{O}$  depletion, and therefore might better represent the later stages of hydrologic evolution in the ULZ. The earlier hydrologic situation was probably much more chaotic, perhaps involving some amount of phreatic explosive activity, because meteoric  $\text{H}_2\text{O}$  would have flashed to steam as it entered newly-formed fractures over the entire surface of the very hot ash-flow sheet. Much of the  $^{18}\text{O}$ -depletion in the ULZ may have occurred during this early period, before meteoric-hydrothermal circulation stabilized around the high-heat-flow areas associated with fumarolic conduits in the DFS.

The observation that  $^{18}\text{O}$  depletions in the ULZ are focused at the base of the Tableland Unit indicates that during fumarolic activity, this discontinuity must have marked a sharp permeability boundary, with the underlying Gorges Unit being decidedly less permeable than the overlying Tableland Unit (see Fig. 3.6). As shown in the sketch on the right-hand side of Fig. 3.6, in order to explain the measurable  $^{18}\text{O}$  depletions in the underlying Gorges Unit (see also Fig. 2.21), small amounts of meteoric  $\text{H}_2\text{O}$  must have percolated into the Gorges Unit below the discontinuity at the base of the Tableland Unit; however, the lowest  $\delta^{18}\text{O}$  values associated with the ULZ are all located above this horizon. Thus, in the early stages of fumarolic activity, the boundary between the Tableland Unit and the Gorges Unit may have been somewhat analogous to the boundary between the DFS and the DWZ that was important later, during DFS-type fumarolic activity (although the permeability contrast between the Tableland Unit and the Gorges Unit was undoubtedly much less than between the DFS and the initially ductile DWZ). The actual discontinuity at the base of the Tableland Unit was almost certainly a zone of relatively high permeability, because it is associated with a break in deposition of the fragmental ash-flow material, as well as with a sharp change in the degree of welding associated with such a depositional hiatus; there is also the possibility that small amounts of phreatic activity occurred at the base of the Tableland Unit, triggered by the presence of surface  $\text{H}_2\text{O}$  on top of the Gorges Unit.

It is worth noting that neither of the sampling localities along Chidago Canyon shows any evidence for the event that produced the shallow zone of meteoric-hydrothermal exchange. This may be because the Tableland Unit is not present at Site CC, and because, although it is present at Site CC-L, the lower part of the Tableland Unit was not sampled there. Therefore, either the ULZ is not present in the Chidago Area, or it is present locally but was not detected in the present study due to insufficient sampling density in the upper parts of these Chidago Area depth profiles.

Although the  $^{18}\text{O}$  depletions associated with the relatively weak hydrothermal circulation in the ULZ are small, the significant lateral extent of this stratigraphic horizon makes it very important with regard to the water budget for the Bishop Tuff fumarolic system as a whole. For example, the areal extent of the ULZ appears to have included the entire Gorges Area, which extends over  $140\text{ km}^2$ . Using an average thickness of 20 m for the low- $^{18}\text{O}$  zone in the upper part of the tuff (which is also close to the average thickness of the Tableland Unit; see Wilson and Hildreth, 1997), this means that in the Gorges Area alone, at least  $3 \times 10^9\text{ m}^3$  of the Bishop Tuff were hydrothermally exchanged by fumarolic activity in the ULZ. While there is not enough evidence presented in this work to prove it, is likely that a similar low- $^{18}\text{O}$  stratigraphic horizon exists in the Southeast and Chidago Areas.

### **3.3. Relationship of deep hydrothermal circulation in the DFS to the ULZ and the DWZ**

#### *3.3.1. Extent and General Characteristics of the Deep Fumarolic System (DFS)*

Extreme whole-rock  $^{18}\text{O}$ -depletions in the lower part of the partially welded Bishop Tuff are spatially coincident with fumarolic structures (i.e., steep fissures, tubular conduits, and shallow-dipping columnar joints), and are confined to the volumes of rock that lie directly beneath the fumarolic mounds (see discussion of the DFS in Chapter 2). The morphology of the fumarolic conduits indicates that they formed fairly early in the

cooling history of the Bishop Tuff outflow sheet, but possibly after the ULZ had begun to form (see below). The edges of the steep fissures in the DFS are smooth, curvilinear surfaces into which shallow-dipping columnar joints terminate, and these columnar joints can never be traced across one of these fissures from one side to the other (Fig. 3.7). In the case of both steep fissures and tubular conduits, it is clear that the fumarolic conduits were heat sinks during cooling of the Bishop Tuff, and that the columnar joints (which grow perpendicular to cooling surfaces; DeGraff et al., 1989), nucleated around these conduits and propagated outward from them. Sheridan (1970) took note of this two-part morphology and suggested that it resulted from a two-stage degassing of the Bishop Tuff, the second stage being one associated with magmatic gases released during devitrification of glassy parts of the tuff. However, the  $^{18}\text{O}/^{16}\text{O}$  evidence presented in Chapter 2 demonstrates conclusively that these columnar joints nucleated at and grew outward away from the fumarolic conduits in response to advective cooling by low- $^{18}\text{O}$  meteoric  $\text{H}_2\text{O}$  that had somehow penetrated down to this level in the tuff and then had been focused along these high-permeability channels in the partially welded tuff (Fig. 3.8).

In this study, the fumarolic conduits and their associated  $^{18}\text{O}$  depletions are together referred to as the Deep Fumarolic System (DFS). The DFS is inferred to include well over a thousand roughly cylindrical or dike-shaped volumes of strongly  $^{18}\text{O}$ -depleted rock that lie directly beneath each of the mounds and ridges shown on Fig. 3.2. Because most of the very small mounds are not indicated on Fig. 3.2, this number might easily be a factor of 10 higher if one includes all of the very tiny fossil fumaroles scattered across the surface of the Bishop Tuff ash-flow sheet. In the areas that could be sampled, the volumes of the most strongly  $^{18}\text{O}$ -depleted rock in the DFS are generally confined to a 40- to 65-m-thick zone of the partially welded tuff; these volumes typically extend down to, and locally impinge upon, the underlying densely welded black tuff. At that boundary, there is typically an extremely steep  $\delta^{18}\text{O}$  gradient (2-3 per mil per meter) that marks the very sharp base of the DFS.

The structures associated with the fumarolic features in the DFS are beautifully exposed in the Gorges and Chidago Areas along Owens River Gorge, Rock Creek Gorge, and Chidago Canyon, and they can be conveniently characterized by two end-members here referred to as the steep fissures and the tubular conduits. A continuum of sizes and morphologies exists between these two end-member types (Figs. 3.9, 3.10, 3.11, and 3.12), indicating that both types of DFS conduits were probably formed at about the same time and by similar mechanisms. The main difference between the two is that the tubular conduits (Fig. 3.10) display a radial set of columnar joints, whereas the steep fissures are accompanied by two sets of sub-horizontal columnar joints on either side (3.12). Intermediate structures are fissures that close up and terminate before they reach the surface of the tuff; these typically have two sets of shallow-dipping columnar joints on either side, combined with a radiating set of columnar joints at their tops (Fig. 3.11).

The steep fissures commonly range in width from less than 1 cm up to a few meters, and the tubular conduits can be less than a meter wide to up to 6 m across. The widest openings in each particular structural type are usually found deep in the partially welded tuff between about 15 and 20 m above the top of the densely welded tuff; this is also the zone where the longest and best-developed columnar joints are typically located. Steep fissures in many cases narrow upward, and when they neck down to a width of less than 5 cm, they may be indistinguishable from other randomly oriented fractures in the uppermost part of the tuff. Sheridan (1970) noted that fractures on the surface of the tuff that connect to steep fissures at depth are commonly coated with Fe-oxide minerals.

Tubular conduits range in size from gigantic features with a 6-m-wide cavity at the center of 40-m-long columnar joints, such as is observed at Site HT, to very small features, which are barely recognizable as any type of conduit, and that are accompanied by only incipient columnar joints less than a few meters in length that surround a central depression in the side of the cliff face (Fig. 3.13). Only a couple of these smaller features have been analyzed for  $^{18}\text{O}/^{16}\text{O}$ , and none have yet been found to be associated with any recognizable

$^{18}\text{O}$ -depletions; these features may represent under-developed tubular conduits that never carried significant amounts of a meteoric-hydrothermal fluid, or they may possibly have been escape pathways for magmatic gases derived from the underlying Densely Welded Zone (DWZ).

### 3.3.2. *Comparison with Features in the Valley of Ten Thousand Smokes*

The fumarolic mounds and ridges and their associated underlying fumarolic conduits clearly represent zones of buoyant upflow of large amounts of very hot fumarolic gases during the main part of fumarolic activity in the Bishop Tuff outflow sheet. The fumarolic mounds and ridges that are now present on the surface of the tuff formed as a result of a preferential induration of the tuff during water/rock interactions associated with the upward passage of these fumarolic exhalations.

The above situation is exactly what was observed by scientists who visited the Valley of Ten Thousand Smokes (VTTS) from 1916-1919, where thousands of high-velocity steam jets and myriad, smaller fumaroles emanated from fumarolic mounds and ridges on the surface of the 1912 ash-flow sheet. At the VTTS, individual fumaroles were stable in the same location over the same vent for many years; these larger fumaroles had individual characteristics, and they were numbered, described, and monitored as they were observed from year to year (see Fig. 1.5; Allen and Zies, 1923; Shipley, 1920; Griggs, 1920). Thus it can be readily inferred that the zones of upflow of hot gases beneath fumarolic mounds in the Valley of Ten Thousand Smokes became established relatively early after the 1912 eruption (i.e., probably before the summer of 1916 when the fumaroles were first discovered by Robert Griggs, and certainly prior to the summer of 1917, when the first serious scientific studies of the fumaroles were carried out; see Shipley, 1920). These  $\text{H}_2\text{O}$  circulation patterns persisted as the fumarolic activity eventually waned and died out during the following 10-20 years. Unfortunately, there were no observers in the VTTS before 1916, and therefore we have no record of the characteristics of fumarolic activity

during the first 4 years after eruption, which is the time period over which fumarolic activity was probably most intense and may have exhibited the highest temperatures. It would be very useful to know if these myriad "permanent" fumaroles became fixed in position after a few months, or whether it took a year or more. In any case, once the major fumarole vents and lines of fumaroles became established at the VTTS, these zones of major discharge would have then controlled the overall circulation geometry of meteoric-hydrothermal fluids in the upper part of the ash-flow sheet. Recharge by cold meteoric water at the VTTS was clearly both by precipitation falling directly on the ash-flow sheet and by the numerous streams and rivers that flowed out onto the tuff (Allen and Zies, 1923).

Using these extremely important observations of active fumaroles in the VTTS together with what we have discovered from our own studies of the underlying fumarolic plumbing systems in the Bishop Tuff, we postulate that once these zones of upflow along steep fissures and tubular conduits were established and stabilized, from that time forward fumarolic fluids would have been continuously drawn into these conduit zones from the surrounding ash-flow tuff. Movement of the cold recharge H<sub>2</sub>O would have been generally downward in the intervening areas between the mounds, and then laterally toward the major fumarolic conduits, where the H<sub>2</sub>O was then channeled upward through vents on the surfaces of the fumarolic mounds (Fig. 3.14). At the Valley of Ten Thousand Smokes, Allen and Zies (1923) describe a situation in which rivers that flowed out over the surface of the ash-flow sheet completely disappeared into the sheet within a distance of less than a kilometer, presumably to emerge in the form of fumarolic vapors farther down-gradient. As remarked by Allen and Zies (1923) in their study of the active fumaroles at the VTTS, "steam enveloping one of these chimneys would inevitably be drawn into it by the suction of the rising gases". With the aid of a plumb bob, Allen and Zies (1923) were able to determine that shallow tunnels in the upper part of the 1912 ash-flow sheet had significant lateral currents of hot fumarolic gases moving through them. Also, scientists who visited

the active fumaroles in the VTTS from 1916 to 1919 concurred that, notwithstanding many differences with regards to the velocities and temperatures of the fumarolic exhalations, as well as the individual morphologies of the fumarolic vents, all fumarole types were considered to be part of a single, interconnected, fissure-type geometry at depth (Allen and Zies, 1923; Shipley, 1920; Griggs, 1920).

### *3.3.3. Tentative Hydrothermal Models for the DFS and the ULZ*

With the aid of the 3-dimensional exposure of the fumarolic plumbing systems in the Bishop Tuff outflow sheet afforded by spectacular exposures of fumarolic mounds and ridges in Owens River Gorge, we are able to construct a tentative model of fumarolic flow through the upper part of the Bishop Tuff outflow sheet, and to relate it to the  $^{18}\text{O}/^{16}\text{O}$  measurements. Cross section Y-Y' in Fig. 3.14 shows how a continuum of shapes and sizes for tubular conduits and steep fissures means that they could represent different parts of a single elongate permeability structure in three dimensions. Obviously, columnar joints would have still been forming during at least the earlier stages of fumarolic activity (refer back to Fig. 3.8), but for clarity, they are shown only in their final, fully grown state on Fig. 3.14. The pathways of meteoric  $\text{H}_2\text{O}$  moving into the established zones of upflow through steep fissures beneath fumarolic mounds are shown by the arrows on the diagrams in Fig. 3.14. Thus recharge of meteoric  $\text{H}_2\text{O}$  to the deep fumarolic system (DFS) would have occurred over wide areas in the upper part of the tuff; because this water had to pass through the part of the tuff that had evolved into the ULZ, it is logical to attribute at least part of the development of the ULZ to exchange with these recharge fluids, at least during the earlier stages of fumarolic activity.

As discussed previously in Section 3.2, it is probable that some of the  $^{18}\text{O}$  depletions associated with meteoric-hydrothermal circulation in the ULZ represent an earlier, and perhaps more chaotic, stage of fumarolic activity in the first few months after eruption. At this hypothetical early stage, which was not observed in the VTTS, it seems likely that the

entire upper part of the ash-flow sheet may have been exhaling fumarolic gases, and that the individual vents and local circulation systems numbered in the tens of millions rather than a few thousand. Even in 1916 and 1917, when the VTTS was first examined, it was noted that enormous numbers of smaller, transient fumarolic vents were emitting gases throughout the intervening areas between the major fumaroles. In fact, Griggs (1920) stated that the area probably should have been called the "Valley of Ten Million Smokes" rather than the Valley of Ten Thousand Smokes.

Once the upper part of the tuff had sufficiently cooled and fractured, it may have provided numerous pathways for significant amounts of cooler meteoric H<sub>2</sub>O to penetrate into the Deep Fumarolic System (the DFS). The interconnected network of steep fissures and tubular conduits that is part of the DFS taps heat from a deeper, thicker part of the ash-flow sheet than does the ULZ; therefore the zones of upflow associated with the DFS have the potential to drive fumarolic activity for a longer time span ( $\approx$ 10-25 years) than the lifetime of meteoric-hydrothermal circulation in the ULZ, where the hypothetical, early, "chaotic" stage may have lasted only a few months. The heat stored in the underlying, Densely Welded Zone (DWZ) would probably also have helped to sustain fumarolic activity in the steep fissures and tubular conduits that directly overlie and impinge upon this zone, thereby facilitating the establishment of these areas as zones of upflow that thereafter dominate the remainder of fumarolic meteoric-hydrothermal activity.

The above models make some predictions about the kinds of <sup>18</sup>O-depletions we should see associated with various parts of the underlying fumarolic plumbing systems. First, during the cooling of the upper 40-50 m of partially welded tuff from its initial temperature of about 700°C, there would have been sufficient heat to form a broad, but relatively thin, low-<sup>18</sup>O zone in the zone of recharge over the entire upper part of the ash-flow sheet, even outside the areas that overlie what would later become the DFS; this is probably the region-wide, stratigraphically bound zone of <sup>18</sup>O-depletion we observe as the ULZ. Next, as <sup>18</sup>O/<sup>16</sup>O exchange continued and the circulation system in the upper part of the ash-flow



sheet became more organized and more permanent, we should expect that the largest  $^{18}\text{O}$ -depletions would be associated with the fumarolic conduits in the DFS, which are zones of relatively long-lasting upflow of meteoric-hydrothermal fluids where the integrated material-balance water/rock ratios in the ash-flow sheet can build up to much higher values ( $\approx 0.5$ , see Table 3.2) than those required to explain the ULZ data ( $\approx 0.2$  or less, see Table 3.2). This is exactly the pattern of  $^{18}\text{O}$ -depletion observed in the Bishop Tuff outflow sheet, as exemplified by Sites LG and HT, and also as shown in Figs. 2.19 and 2.27. Additionally, we might expect that tubular conduits would not exhibit such extreme  $^{18}\text{O}$ -depletions as those observed in nearby steep fissures, because the former "see" a smaller quantity of the meteoric-hydrothermal fluids that are ultimately focused towards the vents above fissures (See Fig. 3.14). There is some preliminary evidence for this in the Bishop Tuff. Site HT, which is a very large, subhorizontal tubular conduit in Owens River Gorge, shows only moderate  $^{18}\text{O}$  depletions (down to  $\delta^{18}\text{O} = +1.3$ ) relative to the zone of steep fissures at Site LG (down to  $\delta^{18}\text{O} = -6.5$ ). Even at Site CG, which lies beneath the outer edge of a fumarolic mound, and which may or may not be adjacent to a steep fissure, the rocks are significantly more depleted in  $^{18}\text{O}$  (down to  $\delta^{18}\text{O} = -2.6$ ) than those at Site HT.

#### *3.3.4. Distribution of the DFS in the Bishop Tuff Outflow Sheet*

Mapping of exposures of the Bishop Tuff in Rock Creek Gorge, Owens River Gorge, and Chidago Canyon shows clearly that DFS fumarolic conduits occur beneath fumarolic mounds and ridges. In addition, nearly every exposure of the partially welded Bishop Tuff beneath a fumarolic mound contains evidence for the presence of one or more of these structures at depth. In many cases, while steep fissures or tubular conduits may have been removed by erosion or obscured by debris, the presence of well-developed shallow-dipping columnar joints in the partially welded tuff beneath fumarolic mounds and ridges attests to the nearby presence of one or more of these conduits. Figs. 3.15 and 3.16 show examples of these observations from portions of each of the three gorges that were

mapped. The entire length of the cliff exposures in all three gorges was inspected and photographed with the use of a small aircraft flown at low altitude. The above criteria that fumarolic conduits are invariably associated with fumarolic mounds on the surface of the ash-flow sheet was found to be true for the entire length of all three canyons, with the exception of that portion of Owens River Gorge within the Crowley Area that intersects the "anomalous" N40E fumarolic ridges. Thus the entire DFS as exposed in the Gorges and Chidago Areas appears to be confined to the roughly cylindrical or dike-like volumes of rock lying beneath fumarolic mounds and ridges, and its distribution is probably coincident with the mapped distribution of fumarolic mounds and ridges shown on Fig. 3.2.

Fumarolic mounds and ridges, and by inference their directly underlying fumarolic conduits, are concentrated over the area of the Bishop Tuff that contains the densely welded Gorges and Chidago Lobes (Fig. 3.17). This also corresponds to areas of known paleobasins and paleodrainages, because it is over these areas that the tuff is thickest (Sheridan, 1970; Wilson and Hildreth, 1997). Comparing Fig. 3.2 to Fig. 3.17a, it is apparent that, for the most part, the Gorges, the Southeast, and the Chidago Areas are all located over parts of the Bishop Tuff that Wilson and Hildreth (1997) have mapped as containing the densely welded Ig1E unit, which corresponds with the Gorges and Chidago Lobes of Hildreth (1979). The only real exception to this correlation is in the southeast corner of the Gorges Area. However, because the lower part of the tuff is not exposed in that region, it is possible that the densely welded tuff is, in fact, also present there. According to Bateman (1965), the southern limit of fumarolic mounds and ridges in the vicinity of cross section G-G' is located at the transition from a thick section of densely welded tuff to largely unwelded tuff (compare Figs. 3.2 and 3.17b).

It is the combination of fumarolic conduits and a thick densely welded zone that best explains the distribution of fumarolic mounds and ridges atop the Bishop Tuff outflow sheet. The existence of the Densely Welded Zone (DWZ), which is dominantly composed of a very thick (>100 m) layer of densely welded black tuff, is obviously essential to the

establishment of the DFS type of fumarolic activity; the DWZ can be thought of as a wide, thick "frying-pan" that underlies the zone of meteoric-hydrothermal circulation in the overlying tuff. During welding, the DWZ was undergoing ductile deformation, and thus it constituted an impermeable zone preventing surface H<sub>2</sub>O from flowing downward through the ash-flow sheet; this zone would also have been the source of much of the heat driving meteoric-hydrothermal circulation in the directly overlying DFS. However, there are numerous sections of partially welded tuff located over the thickest parts of the DWZ in which the only whole-rock <sup>18</sup>O depletions observed in the upper part of the ash-flow sheet are those associated with the ULZ (Fig. 2.27). Thus, although heat energy was available everywhere beneath this broad area, it seems clear that, at least as a generalization, this heat energy was largely utilized in heating the meteoric H<sub>2</sub>O that ultimately became focused into the DFS. Thus, the mounds on the surface of the tuff represent areas where intense, buoyant upflow and discharge of H<sub>2</sub>O from the DFS was occurring during fumarolic activity; recharge to the DFS would have occurred across the much larger intervening areas between the fumarolic mounds.

In addition to noting that the regions of most intense fumarolic activity in the Bishop Tuff correspond with both the thickest zones of densely welded tuff and the positions of the pre-Bishop Tuff paleobasins, Sheridan (1970) also pointed out that the orientations of the steep fissures in the upper, partially welded tuff are "correlated with basin radials". Therefore, another reason why fumarolic activity may have been more intense in these regions is simply because surface waters and groundwaters were focused toward these broad areas. It is likely that the formation of fumarolic conduits and the existence of a thick densely welded zone are interdependent, and that as long as there is sufficient H<sub>2</sub>O recharge, semi-permanent fumarolic conduits must ultimately form over thick zones of hot, welded tuff. These will then persist as stable features for the lifetime of fumarolic activity (≈10-20 years). Perhaps sagging of the tuff over variable gradients in the basement topography result in the formation of fractures in the brittle, upper part of the tuff during

welding and compaction, which later widen as they become part of the DFS. Alternatively, fumarolic conduits may have initially formed explosively, by the escape of magmatic gases from the densely welded tuff as it devitrified at high temperatures, or even locally, by phreatic activity at the base of the densely welded tuff involving meteoric waters or ice overridden during emplacement. We probably cannot know exactly how, or why, a specific part of the partially welded upper part of the ash-flow sheet is singled out to become a future DFS site; however, it is very likely that this is a result of some favorable combination of the timing of welding and the onset of brittle fracturing in the upper part of the ash-flow sheet at points just above the Densely Welded Zone. In any case, from the time of fracturing forward, these sites would tend to become "permanent", because the influx of H<sub>2</sub>O toward those sites would continue to produce the cooling that causes these fumarolic conduits to widen.

### *3.3.5. Relationship of the DFS to the Densely Welded Zone (DWZ)*

As defined in this thesis, the Densely Welded Zone (DWZ) refers to that part of the tuff that, during fumarolic activity, was largely impermeable and did not undergo significant amounts of exchange with any low-<sup>18</sup>O meteoric fluids. Initially, the entire densely welded part of the tuff was hot, ductile, and impermeable, and thus was part of the DWZ; as fumarolic activity progressed, however, the parts of the densely welded tuff that were directly adjacent to or actually penetrated by DFS fumarolic conduits underwent <sup>18</sup>O-exchange with large amounts of low-<sup>18</sup>O meteoric fluids, which would have been channeled into these zones of upflow in the upper part of the ash-flow sheet. In regions of the tuff that did not contain a DFS (i.e., the intervals between fumarolic mounds), the entire thickness of densely welded tuff was probably impermeable during the lifetime of fumarolic activity and was therefore always part of the DWZ.

As fumarolic activity progressed, local dimples and elongate depressions in the DWZ would have formed as meteoric-hydrothermal circulation around fumarolic conduits in the

overlying DFS impinged upon the initially impermeable densely welded tuff. These dimples and depressions are observed in the DWZ, and they are defined by  $^{18}\text{O}$ -depletions in the upper 5-10 m of the densely welded tuff; they are also associated with spatially correlative 5-10 m depressions in the top of the densely welded *black* tuff, which, in the regions of intense fumarolic activity, is typically located between 10 and 20 m below the top of the densely welded tuff. The depression of the top of the densely welded black tuff underneath fumarolic mounds was previously described by Sheridan (1970), who attributed it to magmatic volatiles and to a so-called downward expansion of the "vapor phase zone", in which flattened black fiamme are contained within a pink groundmass that contains vapor phase minerals.

As a result of enhanced cooling in the numerous, scattered, cylindrical volumes that make up the DFS, we would expect that vertical fractures in the densely welded tuff might form in greater density beneath the fumarolic conduits that form each of these dimples and depressions in the top of the DWZ. This is in fact actually observed in the Bishop Tuff outflow sheet, where vertical fractures in the densely welded black tuff are more closely spaced beneath the fumarolic mounds (3 to 5 m) than they are outside those areas (10-20 m). As discussed in more detail in Section 5.8.2, the final extensions of such fractures throughout the entire thickness of the densely welded black tuff may result in the downward flow and consequent removal of the  $\text{H}_2\text{O}$  from what is essentially a perched hydrothermal aquifer in the upper part of the tuff; this could be the event that results in the termination of fumarolic activity in the DFS and the ULZ. If this very speculative argument has some resemblance to what actually happened, then the only place in which we ought to find evidence for high-temperature, meteoric-hydrothermal exchange with low- $^{18}\text{O}$  fluids in the densely welded black tuff would be along closely spaced, vertical fractures that cut through the densely welded tuff below fumarolic conduits. In fact, there is some small amount of evidence for this process in the form of sample CG-L2 ( $\delta^{18}\text{O} = +5.7$ ), which was collected at a depth of  $\approx 150$  m along a vertical fracture in the densely welded black tuff

that connects directly to a fumarolic conduit beneath the largest fumarolic mound sampled in this study (see also Section 2.4.4).

### 3.4. Water/Rock ratios

The minimum amount of water necessary to supply fumarolic meteoric-hydrothermal circulation in the Bishop Tuff outflow sheet can be estimated in the following way. First, the material-balance water/rock (W/R) ratio integrated over the lifetime of fumarolic activity is calculated, by assuming an open system in which the fine-grained or glassy groundmass reaches near-equilibrium with the interacting water (e.g., Taylor, 1977; Gazis et al., 1996), and by using  $\delta^{18}\text{O}$  data from as many areas in the ULZ and the DFS as it takes to get a some idea of the average W/R ratio applicable to each of these systems as a whole. Calculated material-balance W/R ratios depend on the actual size of the considered portion of the hydrothermal system, and are only equal to the actual W/R ratios when that size is large enough to encompass the entire hydrothermal system (e.g., see Criss and Taylor, 1986). Thus, as long as we deal with these larger entities, we can calculate the amount of  $\text{H}_2\text{O}$  necessary to account for this average W/R ratio over the entire volume of rock occupied by each of these kinds of hydrothermal systems. The ULZ and the DFS are considered separately, not only because they occupy rock volumes that are for the most part physically separated, but also because they probably formed at different times and by different mechanisms (see above). In addition, the disparate  $\delta^{18}\text{O}$  values and significantly different permeabilities within the different rock volumes that make up the ULZ and the DFS make it necessary to consider each system separately. W/R ratios for the Crowley Area are also discussed separately, because the mechanism by which fumaroles in the Crowley Area were supplied with  $\text{H}_2\text{O}$  was probably very different than it was for the Gorges, Southeast, and Chidago Areas.

The material-balance W/R ratio applicable to the entire ULZ can be estimated by determining an average  $^{18}\text{O}$  depletion for this  $\approx 20\text{-m}$ -thick zone in the upper part of the

ash-flow sheet. An example of a typical profile of W/R ratios from this zone is shown for Site AG in Fig. 3.18 (top). Site AG isolates the  $^{18}\text{O}/^{16}\text{O}$  characteristics of the ULZ, because it is not located very close to a fumarolic mound or to any high-permeability structures in the partially welded tuff, such as steep fissures or tubular conduits (Figs. 2.20 and 2.21). The W/R ratio applicable to the entire ULZ can be roughly estimated by using the mean  $^{18}\text{O}$ -depletion within the ULZ to calculate a W/R ratio for its entire thickness. For an average  $^{18}\text{O}$ -depletion of 2.5 ‰ in the ULZ (see Fig. 3.6), calculated W/R ratios are 0.17 and 0.21 for temperatures of 600°C and 400°C, respectively, or 0.09 to 0.12 in weight units (i.e., grams of  $\text{H}_2\text{O}$ /grams of rock). These 400°-600°C temperatures are chosen for this calculation, because they probably encompass the temperatures of most of the fumarolic meteoric-hydrothermal activity in the Bishop Tuff (see Chapter 2).

By extrapolating the average thickness for the ULZ over the entire area of interest to obtain the total volume of rock involved in shallow meteoric-hydrothermal exchange (Table 3.1), the minimum amount of water necessary to account for the oxygen isotope compositions of the Bishop Tuff outflow sheet can be calculated, if we assume an average W/R ratio as estimated above, a realistic value for the average density of the uppermost part of the outflow sheet ( $1.75 \text{ g cm}^{-3}$ ; Ragan and Sheridan, 1972), and an appropriate value for the atomic oxygen content of the Bishop Tuff (as measured in the course of our oxygen isotope analyses, this turns out to be  $30 \mu\text{mol mg}^{-1}$ ). Proceeding with this calculation, the water requirements for the entire ULZ in the Gorges, Southeast, and Chidago Areas are on the order of  $10^{14}$  g; the requirements in each area range in mass in proportion to the area of each (Table 3.1).

W/R ratios calculated for the DFS are necessarily much higher than those calculated for the shallow ULZ system, because the  $^{18}\text{O}$ -depletions are greater (an average of  $\approx 5.5$  ‰ in contrast to 2.5 ‰ for the shallow system). The average W/R ratios calculated for Site CG (Fig. 3.18, bottom) are 0.51 and 0.42 for 400°C and 600°C, respectively, within the  $\approx 40$ -m-thick zone that lies directly above the densely welded black tuff. Because the deep

hydrothermal system for the Gorges Area is for the most part physically separated from the shallow hydrothermal system, and because  $^{18}\text{O}$ -depletions in the  $\approx 40\text{-m}$ -thick zone are of similar magnitude throughout the Gorges Area, a rough estimate of the W/R ratio for the entire DFS in the Gorges Area can be made by taking the average of W/R ratios in the 40-m-thick zone at Site CG (i.e., 0.51 and 0.42). Then, these average W/R ratios for deep hydrothermal circulation are extrapolated to the Southeast and Chidago Areas by assuming that the  $^{18}\text{O}$ -depletions in these areas are analogous in both geometry and magnitude to those in the Gorges Area. Clearly, these calculations are much more robust for the Gorges Area than for the other two areas.

As discussed in Chapter 2, the conclusions drawn from  $^{18}\text{O}$  data in Chidago Canyon are in general agreement with those drawn from  $^{18}\text{O}$  studies in the Gorges Area: (1) that the most vigorous meteoric-hydrothermal circulation was associated with fumarolic conduits located directly beneath fumarole mounds, and (2) that the geometry of whole-rock  $^{18}\text{O}$ -depletion is also analogous to the DFS in the Gorges Area, in that there is also a  $\approx 40\text{-m}$ -thick zone of  $^{18}\text{O}$ -depleted tuff located directly above the densely welded black tuff in the Chidago Area. Nonetheless, conclusions regarding water budget calculations made using  $^{18}\text{O}$  data from analogous rocks in the Gorges Area may not be strictly valid in the Chidago Area. Samples collected from shallow-dipping columnar joints beneath a fumarole mound in Chidago Canyon are less  $^{18}\text{O}$ -depleted (by  $\approx 2.5$  ‰; Fig. 2.18) than those collected in the Gorges Area, and therefore it is possible that the strength of the DFS hydrothermal circulation may vary considerably between fumarole areas, perhaps because of differences in the initial heat content of the ash-flow sheet or because of lateral variations in permeability or  $\text{H}_2\text{O}$  supply. Also, no evidence for the ULZ was found in the Chidago Area (see Fig. 3.6). Thus the limited  $^{18}\text{O}$  data available suggest that the magnitude of  $^{18}\text{O}$  depletion observed in fumarolic meteoric-hydrothermal systems in the Chidago Area is less than in the Gorges Area. If this is the case, then smaller W/R ratios may be sufficient to account for  $\delta^{18}\text{O}$  values of the Bishop Tuff in the Chidago Area. Only further sampling



along Chidago Canyon will be able to resolve this question. Until more information on the magnitude of  $^{18}\text{O}$  exchange is obtained, these water budget calculations for the Chidago Area represent at best a crude estimate.

With the above caveat in mind, by extrapolating material-balance W/R ratios determined for the Gorges Area to include the Southeast and Chidago Areas (Table 3.2), the amount of  $\text{H}_2\text{O}$  necessary to supply the total volume of the DFS in the Gorges, Southeast, and Chidago Areas can be estimated by a calculation analogous to that described for the ULZ. The amount of  $\text{H}_2\text{O}$  required for the DFS is between  $2.3 \times 10^{14}$  g and  $2.7 \times 10^{14}$  g for the largest area (Gorges), and between  $2.8 \times 10^{13}$  g and  $3.4 \times 10^{13}$  g for the smallest area (Southeast), and in both cases this constitutes about 25% of the  $\text{H}_2\text{O}$  required for the ULZ in each of these areas. Therefore the amount of water involved in shallow hydrothermal circulation in the ULZ is, overall, actually much greater than that required for the DFS; W/R ratios, however, are comparatively lower in the shallow system. This is because, even though material-balance W/R ratios are smaller in the ULZ, the DFS contains less than 20 volume % of the total quantity of hydrothermally exchanged rock, compared to the more than 80% contained in the much more broadly distributed ULZ (compare Tables 3.1 and 3.2).

### **3.5 Heat balance**

A heat balance calculation is an independent check on whether the material-balance W/R ratios calculated above are reasonable for meteoric-hydrothermal circulation in the Bishop Tuff outflow sheet, because the only heat source for meteoric-hydrothermal circulation in the southeastern lobe of the Bishop Tuff outflow sheet is that of the tuff itself. In the relatively short lifetime of fumarolic activity (10-25 years), the amount of conductive heat transfer from parts of the tuff not directly in contact with circulating meteoric fluids would be relatively small. Thus we would expect that fumarolic meteoric-hydrothermal circulation ought to be driven mainly by the heat initially contained within the volume of rock involved

in meteoric-hydrothermal circulation itself. The following calculations were made using the same thermal parameters employed in analogous calculations by Gazis et al. (1996) and Holt and Taylor (1998) (i.e., heat capacities of 0.22 and 0.6 cal g<sup>-1</sup> °C<sup>-1</sup> and latent heats of 30-70 cal/g and 540 cal/g for tuff and water, respectively), and assuming the tuff cooled from 750°C to 450°C while the required amount of meteoric water was raised from 25°C to 450°C and vaporized.

The amount of heat available in the 20-m-thick ULZ is more than enough to heat the H<sub>2</sub>O and drive meteoric-hydrothermal circulation in this zone, and to account for the observed amount of <sup>18</sup>O-exchange. Indeed, the excess of heat (13 to 53 cal/g of rock in the 20-m-thick zone) suggests that the amount of heat contained in the rock was not the limiting factor driving meteoric-hydrothermal circulation in the ULZ. Instead, either the supply of meteoric H<sub>2</sub>O (i.e., direct precipitation or run-off) or low permeabilities in the ash-flow tuff itself must have been the controlling factor with regards to the vigor of meteoric-hydrothermal circulation in the upper ≈20 m of the Bishop Tuff. This idea is supported by the observation that while there is an identifiable drop in δ<sup>18</sup>O near the base of the Tableland Unit, whole-rock δ<sup>18</sup>O values vary widely over distances as small as a few meters (e.g., see Fig. 2.12), presumably in response to slight changes in permeability in the upper part of the tuff.

Analogous heat-balance calculations for the DFS indicate that 203 cal/g of rock in the 40-m-thick zone of rock beneath fumarolic mounds are required to account for observed material-balance W/R ratios. This is 67-107 cal/g in excess of what can be supplied solely by the rock involved in meteoric-hydrothermal exchange. However, there are two other obvious sources of heat for the DFS that seem to be more than adequate to account for this "thermal deficiency". For example, the amount of conductive heat transfer into the 40-m-thick DFS from the underlying DWZ during the lifetime of fumarolic activity can be calculated and taken into account. The addition of this heat to the DFS results in a slight heat excess of 40-80 cal/g. Also, however, still another source of heat is provided by the

still-hot upper portion of the ash-flow sheet in the recharge areas that surround each individual DFS feature ( $\approx$ 60- to 80-m-thick section of partially welded tuff). Thus this H<sub>2</sub>O would have been "pre-heated" prior to reaching the DFS fumarolic conduits themselves. Regardless of the complications described above in establishing the exact sources of heat for the DFS, there is clearly no unresolved heat-balance problem for the DFS, and there is sufficient energy available to provide all of the heat necessary to raise the temperature of enough H<sub>2</sub>O to satisfy the calculated W/R ratios.

### **3.6. Fluid fluxes**

As alluded to previously, in contrast to the straightforward, readily calculated, non-dimensional material-balance W/R calculations, any attempt to calculate the actual W/R ratios on an outcrop scale or to translate these into true fluid fluxes along the fumarolic channelways requires a complete, three dimensional map of whole-rock <sup>18</sup>O/<sup>16</sup>O and a detailed knowledge of the geometry and flow pattern for the entire hydrothermal system. Such a set of computer simulations was in fact attempted with some success by Norton and Taylor (1979) for the 55 Ma fossil hydrothermal system associated with the Skaergaard layered gabbro, but there are very few examples in nature where the data base is sufficient to do this, or where the geometry of meteoric-hydrothermal circulation is so simple. It would be very interesting to attempt a calculation of this sort for the Bishop Tuff outflow sheet. The relatively uniform mineralogy, the spectacular exposure, the short lifetime of fumarolic activity, and the consequent simplicity with regard to the clear association of particular areas of <sup>18</sup>O-depletion to each fumarolic mound, all make the Bishop Tuff fossil fumarole area an ideal location to study the effects of size and shape of high-permeability pathways on thermally driven circulation of H<sub>2</sub>O through rock. A preliminary attempt of this sort has been made by Keating (1998), in which the limited knowledge of meteoric-hydrothermal circulation in the Bishop Tuff fumarole area published by Holt and Taylor (1998) was used to construct a finite-difference model to describe the positions of

isotherms in the Bishop Tuff during advective cooling. With the more refined knowledge of the three dimensional geometry and extent of fumarolic meteoric-hydrothermal circulation discussed above, future calculations of this sort should give an even better idea of cooling timescales and outcrop-scale permeabilities of the Bishop Tuff. In the meantime, the flux of meteoric H<sub>2</sub>O through the ash-flow tuff during fumarolic activity can only be crudely estimated using the W/R ratios calculated for the ULZ and the DFS (Tables 3.1 and 3.2), together with the limited amount of <sup>18</sup>O-mapping that has been done in the Bishop Tuff fossil fumarole area, most particularly in the Gorges Area.

A rough estimate of the minimum fluid fluxes required to produce the shallow (ULZ) and deep (DFS) hydrothermal systems may be made by defining appropriate length scales for the hydrothermal flow paths. For example, at Chegem caldera, Gazis et al. (1996) chose a length scale of  $\approx 750$  m, which is the depth to the top of the <sup>18</sup>O-depleted zone in the intracaldera fill. In this type of admittedly crude calculation, the hydrothermal flow path refers to the general direction and distance that a packet of H<sub>2</sub>O travels through a zone of hydrothermally exchanged rock. For the DFS, it is probably appropriate to choose a length scale of about 60 m, which is a plausible length for the upward flow path taken by the hot, buoyant H<sub>2</sub>O moving through these cylindrically shaped volumes. The flow paths in the ULZ are less well defined, but they are surely shorter than in the DFS, and the average distance to the base of the Tableland Unit (20 m) would appear to be a plausible length scale to choose.

The flux (F) of a fluid along a linear flow path through a stacked set of elemental cubes (with side b and volume b<sup>3</sup>) is determined by the average water/rock ratio (W/R), the ratio of the total flow length to the distance across each elemental volume ( $\lambda/b$ ), the cross-sectional area of the elemental volume (b<sup>2</sup>), and the length of time that the flow system operated; the time duration of flow for both the ULZ and the DFS is taken to be 10 years (see discussion in Section 2.1). A conversion factor (m) is equal to the moles of rock

oxygen in an elemental volume divided by the number of moles of water oxygen per mole of H<sub>2</sub>O, giving a fluid-flux value (F) in moles of H<sub>2</sub>O per unit area (Taylor, 1997):

$$F = \frac{m(\lambda/b)(W/R)}{(b^2t)}$$

Because the W/R ratios are only minimum values, using the above equation also gives the minimum values for H<sub>2</sub>O flux. For the time scales and length scales chosen above, these calculated fluid flux values are 4.2x10<sup>-7</sup> to 5.1x10<sup>-7</sup> mol s<sup>-1</sup> cm<sup>-2</sup> for the DFS and 5.7x10<sup>-8</sup> to 7.1x10<sup>-8</sup> mol s<sup>-1</sup> cm<sup>-2</sup> for the ULZ. The cumulative flux values for the total amount of H<sub>2</sub>O per unit cross sectional area that flowed through each of these systems can be derived directly from the above equation, simply by removing t from the denominator on the right-hand side. These cumulative values are 161 to 132 mol/cm<sup>2</sup> for the DFS and 18 to 22 mol/cm<sup>2</sup> for the ULZ, which are equivalent to 2.4 to 2.9 kg H<sub>2</sub>O/cm<sup>2</sup> and 0.32 to 0.40 kg H<sub>2</sub>O/cm<sup>2</sup>, respectively. These calculated cumulative flux values are enormously smaller than the values calculated for typical long-lived 250<sup>o</sup>-350<sup>o</sup>C meteoric-hydrothermal systems associated with shallow plutons. Because of the much longer fluid flow paths (on the order of kilometers) and the long lifetimes (≈100,000 years), those kinds of systems typically display values of cumulative flux in the range of 200 to 1000 kg H<sub>2</sub>O/cm<sup>2</sup> (Norton and Taylor, 1979; Taylor, 1997), even though the calculated material-balance water/rock ratios and the magnitudes of the <sup>18</sup>O depletions are very similar to the Bishop Tuff systems. It is thus very important to make the point that the very significant <sup>18</sup>O depletions seen in the DFS of the Bishop Tuff outflow sheet can be produced by a *much* smaller cumulative flux of H<sub>2</sub>O than can similar <sup>18</sup>O depletions in the larger, longer-lived, meteoric-hydrothermal systems associated with igneous intrusions.

Values of fluid flux in the Bishop Tuff fumaroles cannot be used to calculate Darcy-law type permeabilities of the rocks involved in fumarolic meteoric-hydrothermal circulation, because this calculation requires knowledge of the hydrostatic head (Freeze and Cherry, 1979). Also, given the sizes of the apertures of many of these conduits, it is unlikely that

Darcy flow applies to these flow patterns anyway. However, fracture permeability associated with these fumarolic structures (steep fissures and tubular conduits) clearly controlled much of the lateral movement of fumarolic gases through the tuff. An estimate of fracture permeability ( $k$ ) along any given rock face can be made using an equation relating the number of joints per unit distance across the rock face ( $N$ ) to the aperture ( $d$ ) of each joint (Freeze and Cherry, 1979).

$$k = \frac{N \sum d_i^3}{12}$$

Fracture permeabilities associated with steep fissures and tubular conduits beneath fumarolic mounds are extremely high ( $\approx 2 \text{ cm}^2$ ), simply because these structures are gigantic open fractures (see Figs. 3.3, 3.7, 3.11 and 3.12). These values of fracture permeability in the Bishop Tuff outflow sheet are far greater than permeabilities measured for the matrix of ash-flow tuff with a similar degree of welding at Yucca Mountain (0.01-1 mdarcy; Nelson and Anderson, 1992).

While these steep fissures and tubular conduits provide abundant lateral permeability in the ash-flow sheet, they are clearly not the rate-controlling step in the advection of fumarolic fluids through the DFS. Observations of active fumaroles at the Valley of Ten Thousand Smokes and of fumarolic conduits in the Bishop Tuff outflow sheet indicate that these high-permeability structures are, for the most part, capped at the top by a zone of tuff with myriad smaller fractures (see Figs. 3.3 and 3.12); fumarolic gases emanating from the underlying conduits were forced to traverse a tortuous path through these smaller fractures to the surface, explaining the high-velocities with which they exited the surface vents in the ash-flow sheet that filled the Valley of Ten Thousand Smokes.

An interesting aspect of the fumarolic circulation patterns is that the DFS-type of fumarolic hydrothermal system may generate its own permeability during the cooling of the ash-flow sheet. As meteoric fluids abstract heat from the tuff on either side of fumarolic conduits, tensile stresses generated within the rock by advective cooling would cause

formation of shallow-dipping columnar joints and widening of the conduits. Once a single fracture became significantly wider than its neighbors, fumarolic fluids would quickly concentrate along its length at the expense of fluid supply to the other fractures, because of the dependence of permeability on the cube of the fracture width. The resulting increase in advective cooling along the length of the fissure surface would cause the conduit to open still further in a positive feedback effect that would tend to concentrate fumarolic fluid flow along a few major conduits rather than along many smaller fractures, thus stabilizing the zones of upflow over these major conduits. This effect would be intensified in the hotter part of the ash-flow sheet, where the release of tensile stresses during cooling would be largest; this may help to explain the observation that the widest parts of fumarolic conduits are located deep within the partially welded tuff.

### **3.7. Sources of meteoric H<sub>2</sub>O for fumaroles in the Gorges, Southeast and Chidago Areas**

Considering the very short time-scale of fumarolic activity and the position of Long Valley caldera in the rain shadow of the Sierra Nevada mountains, there is some question as to whether precipitation on the surface of the tuff would be sufficient to supply fumarolic meteoric-hydrothermal circulation. Previous estimates of the amount of precipitation per year required to supply fumaroles, assuming fumaroles were supplied only by precipitation upon the fumarole area itself, in both the intracaldera Bishop Tuff and the Bishop Tuff outflow sheet seemed unreasonably high (>120 inches/year and >135 inches/year for the intracaldera Bishop Tuff and the Bishop Tuff outflow sheet, respectively; Holt and Taylor, 1998). The estimate for the Bishop Tuff outflow sheet was made using a crude, preliminary estimate of the size of the fumarolic meteoric-hydrothermal system in the Bishop Tuff outflow sheet (which has been significantly revised in this chapter), and the estimate for the intracaldera Bishop Tuff was made using  $\delta^{18}\text{O}$  values from drill holes into the intracaldera Bishop Tuff (Holt and Taylor, 1998; McConnell et al., 1997; Smith and

Suemnicht, 1991). While the Pleistocene era was undeniably wetter than the present day (average precipitation in the area today is 5 inches/year in Bishop and 11 inches/year in the Long Valley area), the geographic position of the Bishop area was still in the rain shadow of the Sierra Nevada Range. In order to account for this seeming discrepancy in the amount of water required to supply the fumarole system in the Bishop Tuff outflow sheet, it was suggested by Holt and Taylor (1998) that intracaldera fumaroles were supplied by H<sub>2</sub>O from Pleistocene Long Valley Lake, and that fumaroles in the Bishop Tuff outflow sheet were at least partially supplied by groundwater flow from the lake, down along the top of the densely welded tuff.

The new estimates in this thesis of the amount of H<sub>2</sub>O needed to supply fumaroles in the Bishop Tuff outflow sheet, which utilize the refined knowledge of the size and geometry of the ULZ and the DFS presented in this chapter, are more compatible with the idea that fumaroles in the Bishop Tuff outflow sheet could have been supplied solely by precipitation and local runoff onto the surface of the ash-flow sheet. Certainly this is true for the ULZ, which requires a total of only 12 inches per year of precipitation on the surface of the fumarole areas. However, with the addition of the H<sub>2</sub>O requirement of the DFS, this value increases by an amount depending on how much lateral transport and focusing of meteoric H<sub>2</sub>O occurs both on the surface and in the upper part of the Bishop Tuff. A realistic size for the watershed feeding the DFS might be the whole of each respective fumarole area, (i.e., Gorges, Southeast, and Chidago). Assuming that precipitation over these entire areas is the only supply of H<sub>2</sub>O to both the ULZ and the DFS, an average precipitation of about 19 inches per year is required for the Gorges Area and about 16.5 inches per year for the Southeast and Chidago Areas. It is easy to imagine that this area had at least that amount of precipitation (rainfall and snowfall) 760,000 years ago.

The slightly higher H<sub>2</sub>O requirement calculated for the Gorges Area compared to the other two areas reflects the greater density of mounds and ridges in the Gorges Area.



Present-day average precipitation in the Long Valley area is about 11 inches per year, and in the vicinity of the Benton Range, average precipitation is about 8 inches per year. Therefore the Gorges Area might have received more precipitation than the Southeast and Chidago Areas because of its slightly higher average elevation and its position to the west (windward) side of Casa Diablo Mountain. Alternatively, any surface runoff from topographic highs on Casa Diablo and the area southeast of Tom's Place or groundwater from Long Valley Lake would have contributed to the H<sub>2</sub>O supply of fumaroles in the Gorges Area, whereas fumaroles in the Southeast and Chidago Areas would have only received runoff from the east side of Casa Diablo Mountain.

A portion of the precipitation would probably have flowed across the surface of the Bishop Tuff without becoming entrained in the hydrothermal system. Allen and Zies made a very conservative estimate of the amount of H<sub>2</sub>O that drained the Valley of Ten Thousand Smokes relative to the water that flowed into it, and they determined that at least 89% of the water that flowed into the valley was diverted into the active fumaroles. Assuming that a similar value applies to the Bishop Tuff fumaroles, the above precipitation requirements for the Gorges, Southeast, and Chidago Areas increase to about 21 inches/year and 18 inches/year, respectively, which is still well within a reasonable upper limit for precipitation in this region.

Thus, in contrast to preliminary suggestions of Holt and Taylor (1998), while there is no reason why groundwater flow from outside the three fumarole areas could not have contributed to fumarolic meteoric-hydrothermal activity, it is not *necessary* for the survival of the fumaroles in the Gorges, Southeast, and Chidago Areas. The suggestion made by Holt and Taylor (1998) regarding the necessity of focused sources of H<sub>2</sub>O supply to fumarolic mounds and ridges in the form of rivers or groundwater flow is still valid, but these H<sub>2</sub>O sources need only originate in each fumarole area itself rather than from the surrounding area. Conclusions made by Holt and Taylor (1998) regarding the probable geometry of intracaldera fumarolic meteoric-hydrothermal systems using <sup>18</sup>O/<sup>16</sup>O data from

drill holes into the intracaldera tuff (McConnell et al., 1997) are unchanged by the results of this chapter. As discussed by Holt and Taylor (1998), the fumarolic meteoric-hydrothermal systems in the intracaldera tuffs at Chegem and Long Valley calderas did indeed require an enormous amount of meteoric H<sub>2</sub>O during the lifetime of fumarolic activity, but all of the required H<sub>2</sub>O could readily have been supplied from the overlying caldera lakes.

### **3.8. Crowley Area**

Fossil fumaroles in the Crowley Area have a very different morphology than in the other fumarole areas in the Bishop Tuff outflow sheet. There are very few fumarolic mounds in the form of conical hills, and those that are present are located directly adjacent to Owens River Gorge. Fumarolic ridges are abundant and more regular in length ( $\approx$  600 m) and orientation (trending roughly N40E) than in the other three fumarole areas (Figs. 3.4 and 3.5). Although a steep, N40E-trending sheet-like system of fractures is exposed along the southern edge of the Crowley Area and the upper part of the tuff in this area is known to be very permeable (see below), no structures analogous to tubular conduits or steep fissures were observed anywhere in the Crowley Area. In addition, columnar joints are not as common nor as well-developed in the Crowley Area as they are in the other fumarole areas.

These differences in fumarole morphology suggest that fumarolic meteoric-hydrothermal circulation may have been fundamentally different in the Crowley Area than it was in the Gorges, Southeast, and Chidago Areas. The <sup>18</sup>O/<sup>16</sup>O evidence, together with the absence of any fumarolic conduits like those that are present in the other three areas, clearly indicates that the Crowley Area could not have hosted any deep hydrothermal systems analogous to the DFS. Because both the fumarolic ridges and the sheet-like fracture system in the Crowley Area trend roughly N40E, it is probable that they are related, with the fractures acting as pathways for fumarolic fluids. These N40E fractures

trend roughly parallel to the margin of the caldera in the Crowley Area, and therefore it is plausible that they formed in response to subsidence of the adjacent caldera very soon after eruption, while the Bishop Tuff was still very hot.

The  $\delta^{18}\text{O}$  data from Site CR in the Crowley Area, which is not located directly adjacent to any of these NE-trending fractures or NE-trending fumarolic ridges, or in fact to any other type of fumarolic structure, indicate that perhaps as much as a 40-m-thick zone of partially welded tuff has exchanged oxygen with meteoric fluids at high temperature (see Fig. 2.26). Thus it appears that the upper part of the tuff in the Crowley Area may have been thoroughly "soaked" by fumarolic fluids. That is, it may be that significant  $^{18}\text{O}$  depletions are present well away from the main conduits for meteoric fluids, because meteoric-hydrothermal circulation was pervasive throughout this upper zone in the tuff.

Certainly, even the very limited amount of  $^{18}\text{O}/^{16}\text{O}$  data available from the Crowley Area (i.e., just from Site CR) demonstrates that meteoric-hydrothermal activity was much less vigorous than it was in the DFS. In the other fumarolic areas, the nearest analogy for the meteoric-hydrothermal activity in the Crowley Area is that associated with the formation of the ULZ. However, judging by the abundance of fumarolic ridges and the lower  $\delta^{18}\text{O}$  values, fumarolic activity was even more vigorous in the Crowley Area than it was in the ULZ of the Gorges Area. Material-balance W/R ratios calculated for the upper part of the tuff at Site CR are almost twice those for the ULZ in the Gorges Area (0.35 to 0.41, or 0.19 to 0.22 in weight units, at 600°C and 400°C, respectively). On the other hand, because the tuff is thinner at Site CR, the amount of heat available to drive meteoric-hydrothermal circulation was less than the heat available in the Gorges Area. Below, we suggest that one reason why ULZ-type fumarolic activity in the Crowley Area was more vigorous may be because there was a greater  $\text{H}_2\text{O}$  supply to the fumaroles in this area.

While precipitation could conceivably have supplied all of the  $\text{H}_2\text{O}$  necessary to account for W/R ratios in the Crowley Area, there are several reasons why it seems more likely that the fumaroles in this area were supplied by groundwater flow from surrounding areas, in

particular from the adjacent ancestral Long Valley Lake. Assuming that at least a 20-m-thick stratigraphic zone in the upper part of the tuff in the Crowley Area is  $^{18}\text{O}$ -depleted by an average of 5 ‰, calculations analogous to those performed earlier for the Gorges Area indicate that an average of 26 inches of precipitation per year are required to supply fumaroles in the Crowley Area. This is not an unreasonable figure, but it is considerably higher than that required to explain the combined ULZ and the DFS systems in the Gorges Area, suggesting that the "anomalous" fumarolic ridges in the Crowley Area may indeed have had an additional source of meteoric  $\text{H}_2\text{O}$ .

Another reason to suspect that fumaroles in the Crowley Area must have been supplied by groundwater from the surrounding area is that fumarolic ridges blanket the Crowley Area rather than being located preferentially along paleodrainages. If fumaroles in the Crowley Area were fed by precipitation on the surface of the tuff, might we not expect fumarolic ridges to be located preferentially along present-day drainages? That is certainly the case in the Gorges, Southeast, and Chidago Areas. In contrast, the fumarolic ridges in the Crowley Area transect substantial topographic changes (over 80 m elevation differences) on the surface of the Bishop Tuff with no apparent regard to the present-day drainage pattern (Fig. 3.2).

Finally, hydrogeologic arguments give support to the idea that fumarolic meteoric-hydrothermal circulation in the Crowley Area had a significant groundwater component. The history of discussion regarding the hydrogeology of this region began 65 years ago, when Mayo (1934) first remarked that he considered it likely that Owens River Gorge formed by the capture of the Owens River, which previously flowed into Long Valley. This idea was later opposed by Francois Matthes, who for various reasons stated that he believed that Owens River Gorge formed by overflow of Long Valley Lake (Putnam, 1960). This lake formed within the caldera, in the vicinity of the present-day Lake Crowley (Fig. 3.19), behind a dam of Bishop Tuff created at the time of eruption (Bailey et al., 1976; Mayo, 1934; Putnam, 1960). Putnam (1960) and Mayo (1934) asserted that

there was no significant overflow of Long Valley Lake to the southeast, because neither lake gravels nor shorelines can be traced up to 7,280 feet, the current elevation of the "drainage divide". Bailey et al. (1976) disagreed with Putnam (1960) and Mayo (1934), restating the assertion of Matthes (see Putnam, 1960, p. 248) that overflow did occur. Bailey et al. (1976) state that "the lake probably rose rapidly", and they also point out that immediately following eruption the highest lake gravel deposits (currently at an elevation of 7000 ft. in the southern portion of the caldera) were at the same elevation as the top of the densely welded tuff, suggesting to them that erosional downcutting was sufficiently slowed at that resistant horizon to stabilize the lake level. Holt and Taylor (1998) remarked that while Long Valley Lake probably did not overflow over the *surface* of the tuff while the tuff was still very hot, there may have been significant subsurface groundwater flow from Long Valley Lake down through the very permeable, uppermost stratigraphic zone of partially welded ash-flow tuff, and this would in consequence have stabilized the lake level at the elevation of the top of the impermeable densely welded tuff (i.e., 7000 feet), exactly as noted by Bailey et al. (1976). One might question whether such a large lake could have formed so rapidly (i.e., within the first 10 years after formation of Long Valley caldera). However, it is known that there were numerous glaciers in the surrounding catchment area at the time of eruption, and these are likely to have undergone catastrophic melting as they were blanketed by hot ash (Bailey, 1989; Bailey et al., 1976).

For the duration of fumarolic activity (i.e., while the hot, ductile, densely welded tuff was still impermeable), groundwater would have been confined to that portion of the tuff located above the top of the densely welded zone. Indeed, the observation of Bailey et al. (1984) that the elevation of the top of the densely welded tuff is at 7000 feet was at the heart of the argument by Holt and Taylor (1998) that groundwater flow out along the top of the densely welded tuff stabilized the lake level at 7000 feet. However, the elevation of the top of the densely welded tuff is not a constant, but changes with both the total thickness of the outflow sheet and with changes in the elevation of the contact with basement rock. The

top of the densely welded tuff is actually at an elevation of about 6870 feet at the point where the ancient shoreline (Fig. 3.19) intersects Owens River Gorge; the elevation of this boundary increases moving north and south away from this area as the contact between the Bishop Tuff and the underlying basement rises away from the ancestral drainage. A cross section drawn along tunnel no. 1 of the Owens Gorge water project and another drawn along the trace of the basement high in the vicinity of the bend in Owens River Gorge (Figs. 3.19 and 3.20; Putnam, 1960) illustrate that before Owens River Gorge was cut, groundwater in the Bishop Tuff would have been confined within a perched paleobasin lying upon the upper contact of the densely welded tuff. At the location of the drainage divide, the thickness of the Bishop Tuff is about 308 feet (or 94 m), and the top of the impermeable part of the tuff would have been at a depth between 66-131 feet (20-40 m ; compare Site CR) or, in other words, at an elevation of 6950-7010 feet.

Because the contact with the densely welded tuff is between 20 and 40 m below the surface of the tuff in this area, we expect that the outline of the perched paleobasin described above might be somewhat larger than the area outlined by the 7000 ft. elevation contour on the top of the tuff. The edge of the Crowley Area as drawn on Fig. 3.2 is, in fact, just slightly larger than the outline of the present-day 7000 ft. elevation contour on the upper surface of the densely welded tuff. Thus we infer that the boundary of the Crowley Area on Fig. 3.2 closely corresponds to the area of this perched paleobasin, as defined by the above-described topographic low in the upper contact of the densely welded tuff. This coincidence of the 6950-7010 ft. elevation of the top of the densely welded tuff with the ancient 7000-foot shoreline of Long Valley Lake strongly suggests that fumaroles in the Crowley Area were supplied by groundwater that became trapped in this hypothetical perched paleobasin when Long Valley Lake filled up to that level after eruption of the Bishop Tuff. Fumarolic ridges are evenly distributed over nearly the entire area of the perched paleobasin, which narrows to a width of about 400 m at the ancestral drainage divide near the basement high at the sharp bend in Owens River Gorge (Fig. 3.19).

Even today, this area displays a very high permeability and evidence for abundant groundwater. During construction of tunnel no.1 of the Owens Gorge Project, construction was seriously delayed near this location, because of massive flooding by H<sub>2</sub>O underflow from Rock Creek through the ash-flow tuff as the water traveled toward springs at the base of the tuff in Owens River Gorge (Fig. 3.20; Putnam, 1960). Water had to be pumped out of the tunnel at a rate of almost 1000 liters/minute. Thus, even under the present semi-arid conditions in this area, groundwater flow through the Bishop Tuff outflow sheet near this basement high is an important component of the hydrology of the region.

If fumaroles in the Crowley Area were supplied by confined groundwater within a perched paleobasin, or in other words, within a hydrothermal aquifer, they may represent a better analogue for intracaldera fumaroles, which are probably supplied by an overlying lake, than do the fumaroles in the Gorges, Southeast, and Chidago Areas. The regular orientation of the steep fractures in the Crowley Area is in fact reminiscent of the sheet-like fractures commonly observed in intracaldera tuffs, and which were in fact observed at Chegem caldera by Lipman et al. (1993). These kinds of sheet-like fractures might be the permeable pathways that host fumarolic meteoric-hydrothermal circulation both in the Crowley Area and in most intracaldera tuffs (e.g., in the intracaldera tuff of Long Valley; see Section 5.6 and Holt and Taylor, 1998).

Fumaroles in the Gorges Area extend northward nearly to the position where the perched paleobasin narrows to a width of 400 m, near the sharp bend in Owens River Gorge. Thus, whereas fumaroles in the Crowley Area were almost certainly supplied by groundwater connected directly to Long Valley Lake, the Gorges Area probably received little, if any, contribution of fresh, unexchanged meteoric H<sub>2</sub>O from this source. The only such groundwater that could have reached the Gorges Area from Long Valley Lake would have had to travel nearly 10 km through the upper part of the hot Bishop Tuff and over the drainage divide. Hence any groundwater that spilled over into the Gorges Area while the

tuff was still hot would doubtless have thoroughly exchanged with the intervening hot tuff in the Crowley Area.

### **3.9. Hydrogeology and drainage capture in the vicinity of Tom's Place**

The preceding discussion does not preclude the possibility that, long after the Bishop Tuff had fractured and cooled, Long Valley Lake may have overflowed at some point early in its history. However, in contrast to what was suggested by Bailey et al. (1976), there are several lines of evidence that suggest that any overflow from Long Valley Lake would have likely taken place along the Rock Creek drainage rather than along the Owens River. Characteristics of these two drainages indicate that Owens River drainage was more likely to have been cut by headward erosion, rather than overflow. First, the Owens River has several deeply dissected tributary drainages between the area of the pre-gorge drainage divide with Long Valley and its intersection with Rock Creek in Birchim Canyon, supporting the idea that significant downcutting occurred along all of these drainages, including Owens Gorge. Also, Owens River drainage follows the path of least resistance along a basement fault trace in the area of the basement high in Owens Gorge (Putnam, 1960; Bailey, 1989), as we would expect for a drainage cut by headward erosion. In addition, the walls of Owens Gorge form at least two prominent meander bends, one of which is active, the other of which has been cut off and abandoned on the cliff wall of Owens Gorge opposite Site HT. It seems unlikely that these erosional features would have been formed or preserved in the event that Owens Gorge formed by catastrophic overflow of Long Valley Lake as suggested by Bailey et al. (1976).

The geometry of the Owens River and Rock Creek drainages in the vicinity of Birchim Canyon suggests that Rock Creek drainage was cut deeply before Owens River became a high-discharge watercourse. Rock Creek runs from the low-relief Round Valley eastward through steep-sided Birchim Canyon, where Owens River intersects it at a right angle. Because the trend of Rock Creek is undiverted, whereas the Owens River makes a right-



angle bend at the intersection of the two watercourses in Birchim Canyon, it appears most likely that Rock Creek was the older and larger drainage and that the Owens River began as a tributary to Rock Creek. In support of this, while Owens River is cut primarily into ash-flow tuff (except for near the sharp bend at the basement high), much of Rock Creek is carved into metamorphic basement, which is more resistant to erosion than ash-flow tuff; this suggests that Rock Creek Gorge is older than Owens River Gorge and/or that Rock Creek once had a much greater discharge, relative to the Owens River, than it does today.

While the above arguments contraindicate the hypothesis that Owens Gorge was incised by catastrophic overflow of Long Valley Lake, there are several arguments that suggest that ancestral Long Valley Lake may have been drained by Rock Creek. It is suspiciously serendipitous that Rock Creek takes a sharp, right angle bend in the vicinity of Tom's Place (see Fig. 3.19), because this is also the location that we would expect to find the spillover point in the event that Rock Creek were the drainage emptying ancestral Long Valley Lake. The exact position of the putative spillover point is buried by younger alluvium, but the elevation of the spillover point below the alluvium at about 7000 feet and corresponds exactly to the elevation of the highest, most well-developed terraces (Unit Qtg, 600-50 ka; Bailey, 1989) of ancestral Long Valley Lake. In addition, Crooked Creek, which is a small stream that currently drains the valley to the west of Tom's Place, occupies an anomalously deep gorge cut into the Bishop Tuff on the southern edge of Lake Crowley (Bailey, 1989). It is far more likely that this gorge and the 70- to 120-m-high escarpment of Bishop Tuff directly to the east of it were downcut by a high-discharge stream from Pleistocene Long Valley Lake as it emptied down Rock Creek Gorge than that it was carved by the tiny Crooked Creek that flows through it in the opposite direction today.

By the above arguments, Long Valley Lake was probably first drained by Rock Creek. Eventually, Owens River captured Long Valley Lake and outflow was diverted along its length, where it remains today. Capture of the Long Valley drainage by Owens River probably occurred near the sharp bend in Owens River Gorge, where a stream flowing

west into Long Valley Lake was captured and diverted to flow the opposite direction down the Owens River (Putnam, 1960). Stream capture may have been facilitated by enhanced groundwater flow over the low point on the basement high at this particular location, which would have preferentially increased the discharge to the ancestral Owens River relative to other streams draining the southeastern Lobe of the Bishop Tuff. At the spillover point, this stream would quickly have eroded to the elevation of the top of the densely welded tuff, as the upper part of the tuff was washed away by the resulting accelerated discharge due to capture of the Long Valley Lake drainage. A second, smaller set of terraces for Long Valley Lake are present at an elevation of about 6880 ft. (Unit Q1, 600-50 ka, Bailey, 1989), which corresponds to the elevation of the top of the densely welded tuff near the bend in Owens River Gorge. These terraces were probably formed when the lake level was stabilized at the elevation of the top of the less erodable, densely welded tuff. Once capture by the Owens River occurred, the outlet of Long Valley Lake through Pleasant Valley and down along Rock Creek Gorge would have been abandoned.

### **3.10. Summary**

Mapping of the distribution of fumarolic mounds and ridges shows that evidence for fumarolic activity on the surface of the Bishop Tuff outflow sheet can be divided into four geographic areas, which also represent pre-Bishop Tuff basins: the Gorges Area, the Southeast Area, the Chidago Area, and the Crowley Area. It is probably the presence of thick sections of densely welded tuff in these paleobasins that accounts for this correlation, because it would have provided a hot, impermeable base for the fumarolic fluids circulating through the upper part of the tuff. Fumarolic morphology and  $^{18}\text{O}$  systematics in the Crowley Area are distinct from those in the other three areas, suggesting that they formed by a different mechanism. This, combined with material-balance water/rock and hydrogeologic arguments suggests that whereas the fumaroles in the Gorges Area, the Southeast Area, and the Chidago Area could have been wholly supplied just by rainfall on

the surface of the ash-flow sheet, fumaroles in the Crowley Area may also have been supplied by groundwater from ancestral Long Valley Lake.

In the Gorges, Southeast, and Chidago Areas, the  $^{18}\text{O}/^{16}\text{O}$  data show that fumarolic activity involved both shallow and deep hydrothermal circulation. Shallow hydrothermal circulation occupied a stratigraphic horizon located in the upper part of the tuff in the vicinity of the boundary between ignimbrite Units Ig1E and Ig2E of Wilson and Hildreth (1997). Deep hydrothermal activity was localized around high-permeability structures, such as steep fissures and tubular conduits, which occur directly below fumarolic mounds and ridges. High-permeability structures formed early in the cooling history of the tuff, probably as a result of accelerated thermal contraction along conduits through which fumarolic fluids first gained access. Heat balance calculations show that for the shallow system, there is sufficient heat within the hydrothermally exchanged rocks themselves to account for the heating of all of the  $\text{H}_2\text{O}$  required by material-balance water/rock calculations. For the deep system, an additional 67 to 107 cal/g of heat is required, but heat-flow calculations from Chapter 5 indicate that this can easily be delivered (1) by conductive heat flow from the underlying densely welded tuff during the estimated lifetime of fumarolic activity ( $\approx 10\text{-}25$  years), and (2) from continued flow of  $\text{H}_2\text{O}$  through the still hot, partially welded tuff in the upper part of the ash-flow sheet.

**Table 3.1.** Calculated hydrogeologic parameters for the upper meteoric-hydrothermal regime (ULZ) for three fumarolic areas in the Bishop Tuff outflow sheet. (See text for explanation of terms.)

	Gorges Area	Southeast Area	Chidago Area
Total Area (km <sup>2</sup> )	139.9	23.8	59.6
Volume of 20-m-thick stratigraphic zone (km <sup>3</sup> )	2.8	0.48	1.19
Mass of 20-m-thick stratigraphic zone (g)	4.9x10 <sup>15</sup>	8.4x10 <sup>14</sup>	2.1x10 <sup>15</sup>
Material-balance H <sub>2</sub> O requirement (g) calculated for: W/R = 0.17, and W/R = 0.21	4.40x10 <sup>14</sup> , 5.88x10 <sup>14</sup>	7.56x10 <sup>13</sup> , 1.01x10 <sup>14</sup>	1.89x10 <sup>14</sup> , 2.52x10 <sup>14</sup>
Heat Required (cal.) (see text for explanation)	4.09x10 <sup>17</sup>	7.02x10 <sup>16</sup>	1.76x10 <sup>17</sup>
Heat Available (cal.) Latent heat = 30 cal/g, Latent heat = 70 cal/g	4.70x10 <sup>17</sup> , 6.66x10 <sup>17</sup>	8.06x10 <sup>16</sup> , 11.40x10 <sup>16</sup>	2.02x10 <sup>17</sup> 2.86x10 <sup>17</sup>
Heat balance (cal.) (Heat Available – Heat Required)	0.61x10 <sup>17</sup> , 2.57x10 <sup>17</sup>	1.04x10 <sup>16</sup> , 4.38x10 <sup>16</sup>	0.26x10 <sup>17</sup> , 1.10x10 <sup>17</sup>

**Table 3.2.** Calculated hydrogeologic parameters for the lower meteoric-hydrothermal regime (DFS) for three fumarole areas in the Bishop Tuff outflow sheet. (See text for explanation of terms.)

	Gorges Area	Southeast Area	Chidago Area
Total area of fumarole mounds on the surface of the Bishop Tuff (km <sup>2</sup> )	13.91	1.84	3.44
Volume of 40-m-thick zone beneath fumarole mounds (km <sup>3</sup> )	0.56	0.07	0.14
Mass of 40-m-thick zone beneath fumarole mounds (g)	9.8X10 <sup>14</sup>	1.23X10 <sup>14</sup>	2.45x10 <sup>14</sup>
Material-balance H <sub>2</sub> O requirement (g) calculated for: W/R = 0.42, and W/R = 0.51	2.25x10 <sup>14</sup> , 2.74x10 <sup>14</sup>	2.83x10 <sup>13</sup> , 3.44x10 <sup>13</sup>	5.64x10 <sup>13</sup> , 6.86x10 <sup>13</sup>
Heat Required (cal.) (see text for explanation)	19.9x10 <sup>16</sup>	2.50x10 <sup>16</sup>	4.97x10 <sup>16</sup>
Heat Available (cal.) Latent heat = 30 cal/g, Latent heat = 70 cal/g	9.41x10 <sup>16</sup> , 13.3x10 <sup>16</sup>	1.18x10 <sup>16</sup> , 1.67x10 <sup>16</sup>	2.35x10 <sup>16</sup> 3.33x10 <sup>16</sup>
Heat balance (cal.) (Heat Required – Heat Available)	-10.5x10 <sup>16</sup> , -6.6x10 <sup>16</sup>	-1.32x10 <sup>16</sup> , -0.83x10 <sup>16</sup>	-2.62x10 <sup>16</sup> -1.64x10 <sup>16</sup>
Heat Available (cal.) from conductive cooling of lower, densely welded Bishop Tuff	14.4x10 <sup>16</sup>	1.80x10 <sup>16</sup>	3.6x10 <sup>16</sup>
Heat Balance (cal.) corrected for the effects of conductive heat transfer from lower, densely welded Bishop Tuff (see text)	3.9x10 <sup>16</sup> 7.8x10 <sup>16</sup>	0.48x10 <sup>16</sup> 0.97x10 <sup>16</sup>	0.98x10 <sup>16</sup> 1.96x10 <sup>16</sup>

## Figure Captions

Fig. 3.1. Photograph of an area of coalesced fumarole mounds on the surface of the Bishop Tuff about 2-3 km SE of Site LG. View is to the southeast from highway 395, and the White Mountains are in the distance. The edge of Owens River Gorge is visible in the middleground. Large transmission line poles are also visible on the surface of the ash-flow sheet.

Fig. 3.2. Map of the southeastern lobe of the Bishop Tuff outflow sheet showing the location of the larger fumarole mounds and ridges on the surface of the ash-flow sheet and the positions of Owens River Gorge, Rock Creek Gorge, and Chidago Canyon. Site locations are as in Fig. 2.1. Fumarole mounds were identified using 1:46,500 scale aerial photographs. Four main fumarole areas on the surface of the tuff are outlined; the Gorges Area, the Southeast Area, the Chidago Area, and the Crowley Area. Whereas the first three fumarole areas roughly correspond to the regions identified by Sheridan (1970), the Crowley Area is first described in this study. The large, sinuous, white area outlined in Owens River Gorge and three smaller areas to the north and east represent exposures of basement rock, and together with the two much larger areas of basement rock exposed near Casa Diablo Mountain and on the west side of the Bishop Tuff, they mark the position of a basement high (BH) extending northeast and southwest from Owens River Gorge (Bailey, 1989; Wilson and Hildreth, 1997). Heavy dashed lines in each of the canyons indicate the portion of each canyon that is included in Fig. 3.15. The rectangular outline indicates the area of this figure shown in Fig. 3.19. The location of cross section G-G' from Bateman (1965), which is reprinted in Fig. 3.17b, is also shown.

Fig. 3.3. (a) Photograph of structures beneath a fumarole mound on the west side of Owens River Gorge. The Site CG depth profile (Fig. 2.17) is located at the northern

margin of this mound, about 75 m to the north of the view shown in this photograph. The cliff face shown is about 80 m high. Prominent shallow-dipping columnar joints and steep fissures are shown in the center part of the photo, and a tubular conduit is displayed on the right side of the photo. This tubular conduit is of the large type; the size of the central cavity ( $\approx 5$  m) and the length of radiating columnar joints ( $\approx 40$  m) is analogous to the size of the tubular conduit at Site HT. (b) Photograph of structures beneath a fumarole mound on the east side of Owens River Gorge across from Site HT. It is about 150 m from the base of the cliff at the level of the Owens River to the top of the ash-flow sheet. Note two prominent tubular conduits as well as shallow-dipping columnar joints. The tubular conduit on the right is of the large type, with an oblong central cavity having a long axis of more than 10 m and radiating columnar joints in excess of 40 m long. The tubular conduit on the left is of the smaller type, and is only about 1/5 of the size of the tubular conduit exposed at Site HT.

Fig. 3.4. This is an oblique aerial photograph taken from above the Owens River Gorge looking to the south toward Tom's Place, showing the uniformly oriented N40E-trending ridges on the surface of the Bishop Tuff in the Crowley Area. The base of the Sierran escarpment is in the background.

Fig. 3.5. Vertical aerial photograph of the uniformly oriented N40E-trending ridges on the surface of the Bishop Tuff in the Crowley Area. The margins of the Crowley Area are outlined in black (see also Fig. 3.2). Scale = 1:46,500.

Fig. 3.6. The right-hand diagram is a sketch illustrating probable pathways for meteoric  $\text{H}_2\text{O}$  in the Upper Low- $^{18}\text{O}$  Zone (ULZ). The left-hand diagram shows whole-rock  $\delta^{18}\text{O}$  values for all sampling sites that include the Tableland Unit. The  $\delta^{18}\text{O}$  values are plotted in their appropriate stratigraphic positions for each site relative to the right-hand diagram. For

Depth Profiles CG, LG, HT, and CC-L, each of which is located beneath a fumarole mound, only those data points are shown for samples not collected directly adjacent to shallow-dipping columnar joints. This is done in order to isolate the effects of the ULZ from local effects associated with the shallow-dipping columnar joints. Relatively weak meteoric-H<sub>2</sub>O circulation in the permeable, uppermost part of the Bishop Tuff (locally containing sets of vertical columnar joints) results in a stratigraphic horizon of low-<sup>18</sup>O whole rock, here referred to as the ULZ. Away from fumarole mounds, the maximum <sup>18</sup>O-depletions are ≈2.5 ‰ and occur near the base of the Tableland Unit, where there is a discontinuity in the sets of vertical columnar joints. Below this discontinuity, there was probably a sharp increase in permeability that would explain why the rocks above this horizon are always more <sup>18</sup>O-depleted than those below. As shown in the sketch on the right and as reflected by the δ<sup>18</sup>O data shown in Chapter 2 (e.g., Fig. 2.27), small amounts of meteoric H<sub>2</sub>O are assumed to penetrate down along fractures into the underlying Gorges Lobe.

Fig. 3.7. Photograph of steep (≈70°-dipping) fissure along Middle Power Plant Road. The tuff from the edge of the fissure has a whole-rock δ<sup>18</sup>O value of -1.2, and it is the one located farthest to the right in the photograph in Fig. 2.14a. This fissure shows the typical situation in which columnar joints cannot be traced from one side to the other. The hammer located just to the left of the fissure in the lower middle part of the photograph is 38 cm long.

Fig. 3.8. Cross sections of the thick Bishop Tuff outflow sheet illustrating the probable sequence of formation of fractures and joints as determined by cross-cutting relationships in the upper part of the tuff. The complications that might be associated with the deposition of the Tableland Unit are ignored in this sketch. (a) Hot Bishop Tuff is emplaced at about 750°C. (b) A 100-m-thick zone of densely welded tuff forms in the lower portion of the



ash-flow sheet (dark grey shading). Fractures form in the upper part of the tuff as it begins to cool. (c) Those fractures that connect to shallow sources of meteoric H<sub>2</sub>O become fumarolic conduits, and columnar joints begin to grow outward from these structures. These fumarolic conduits probably widen as cooling progresses (see text). Vertical columnar joints also grow downward from the surface as heat is removed from the top of the tuff. (d) Columnar joints and other fractures continue to grow during cooling of the tuff.

Fig. 3.9. Sketch illustrating the continuum in morphology that exists between steep fissures and tubular conduits. Steep fissures are accompanied by shallow-dipping joints on either side, whereas tubular conduits display radiating columnar joints. Intermediate structures have two sets of shallow-dipping columnar joints on either side and a zone of radiating columnar joints at the top.

Fig. 3.10. Photograph of a tubular conduit on the west side of Owens River Gorge at Site HT. This is the same tubular conduit that is shown in Fig. 2.12, the left side of which was sampled in detail in order to determine the <sup>18</sup>O-systematics of the groundmass in the ash-flow tuff in the immediate vicinity of this feature. The cavity located at the axis of radiating columnar joints is 6 m wide.

Fig. 3.11. Photograph of an ≈80-cm-wide tube/fissure at the axis of radiating columnar joints on the west side of Owens River Gorge along Upper Power Plant Road. The hammer balanced on the lowermost ledge to the left of this tube/fissure is 38 cm long.

Fig. 3.12. Photograph of a ≈60-m-tall steep fissure exposed in the east wall of Owens River Gorge along Upper Power Plant Road. The light-colored splotches in the cliff face in the center of the photograph are sunlight reflections. The steep fissure is located about

halfway between the sunlight reflections and the left side of the photograph. The fissure is several meters wide at its center, thinning upward as it continues through highly fractured tuff to the surface of the overlying mound. It is clear that from the surface of the tuff, and without the exposure in the gorge, it would be impossible to pick out which of the fractures was most directly connected to the underlying fissure.

Fig. 3.13. Photograph of an underdeveloped tubular conduit (circled) at Site CG that probably would have had little access to meteoric H<sub>2</sub>O from the surface of the tuff. Note incipient radial jointing pattern in the tuff around this feature. See hiker at lower center for scale.

Fig. 3.14. Sketch of probable fluid-flow paths (shown by the dark arrows) deep into the partially welded tuff beneath a fumarole mound. Thicker arrows represent a greater flux of fluid. X-X' is a cross section through the tuff oriented roughly at right angles to a steep fissure and a tubular conduit; this drawing is patterned after the sketch in Fig. 2.6 and the photograph in Fig. 3.3a of the cliff face under the fumarolic mound near Site CG. Y-Y' represents a cross section oriented orthogonally to X-X' and along the plane of a tube/fissure, indicating a possible interpretation whereby a steep fissure gradually narrows down to become a tubular conduit at depth. Fluid flux is greatest in a direction parallel to Y-Y' and perpendicular to X-X'. Whole-rock  $\delta^{18}\text{O}$  values as a function of depth are shown for Site CG and Site HT on the left-hand and right-hand sides of Y-Y', respectively, to illustrate the  $\delta^{18}\text{O}$  profile expected at each end of Y-Y'. Small amounts of meteoric H<sub>2</sub>O percolating into the upper part of the tuff (as described in Fig. 3.6) are also shown, and this upper hydrothermal system locally overlaps with the deeper, more vigorous hydrothermal circulation associated with high-permeability fumarolic conduits formed just above the top of the densely welded tuff.

Fig. 3.15. Maps of portions of (a) Owens River Gorge and (b) Chidago Canyon and Rock Creek Gorge. These maps show the positions of fumarole mounds on the surface of the tuff relative to steep fissures and tubular conduits exposed on the walls of the respective canyons. The positions of tubular conduits (black ovals) and steep fissures (heavy black lines) are drawn schematically between the topographic edges of each canyon. The portions of each canyon shown here are indicated in Fig. 3.2 by a heavy dashed line down the centers of the respective canyons. Some mounds shown on these diagrams are not shown on Fig. 3.2, because they are not visible on the aerial photographs from which Fig. 3.2 was derived. In every instance, fumarolic conduits exposed in the walls of the canyons were observed to be associated with an overlying fumarolic mound. Conversely, every mound exposed on the edge of one of the canyons was observed to display a high-permeability structure beneath it.

Fig. 3.16. Oblique aerial photograph of the west wall of Owens River Gorge along Middle Power Plant Road (Site LG), showing steep fissures exposed beneath a small fumarole mound on the surface of the tuff. Areas directly to the south (left) and to the north (right) exhibit neither fumarolic conduits in the west wall of the gorge nor mounds on the surface of the tuff. Samples from Site LG-B were collected along the old road shown in the right-hand portion of this photograph. The area of this photograph is shown as a rectangle on Fig. 3.15a.

Fig. 3.17. (a) Distribution and welding zonation of eruptive unit Ig1E from Wilson and Hildreth (1997), which consists of the Gorges and Chidago Lobes of Hildreth (1979). The diagonal lines indicating the extent of Unit Ig1Ea roughly demarcate the paleovalley occupied by the ancestral Owens River before eruption of the Bishop Tuff (Wilson and Hildreth, 1997). The location of the axis of the basement high (BH) is indicated by the northeast-trending dashed line. (b) Cross section modified from Bateman (1965), which

illustrates the welding zonation in the Bishop Tuff outflow sheet in the southeast portion of the Gorges Area. The welded Bishop Tuff corresponds with Bateman's (1965) "hard agglutinated tuff", and is shown by the dark grey shading. Unwelded Bishop Tuff is shown by the light grey shading, and is designated as "soft tuff with rounded pumice fragments" by Bateman (1965). The edge of the volcanic Tableland is shown by a prominent scarp to the right of the Owens River drainage. Left of the scarp, the unwelded Bishop Tuff is buried by younger alluvium in Owens Valley. This cross section shows that the transition from mostly unwelded tuff to welded tuff occurs at a distance of about 4 km north of the southern edge of the volcanic Tableland at about the same latitude as the southern limit of large concentrations of fumarolic mounds on the surface of the Bishop Tuff outflow sheet.

Fig. 3.18. Water/Rock (W/R) ratios for (top) Site AG and (bottom) Site CG in the Bishop Tuff outflow sheet. These and all following W/R ratios were calculated in the same general manner as was done for Fig. 2 of Gazis et al. (1996), namely: (1) using the equation of Taylor (1977) for the material-balance water/rock ratio (i.e., the ratio of the amount of water oxygen to the amount of rock oxygen) for an open system, in which the fine-grained, devitrified groundmass/glass is assumed to have reached approximate  $^{18}\text{O}/^{16}\text{O}$  equilibrium with the interacting water, integrated over the lifetime of the hydrothermal system; (2) using an initial meteoric water  $\delta^{18}\text{O} = -16$ ; and (3) using an initial  $\delta^{18}\text{O}$  value for the Bishop Tuff groundmass of  $+7.6$ . The latter is the value appropriate for equilibrium between melt and phenocrysts at magmatic temperatures. For the calculations, groundmass  $\delta^{18}\text{O}$  values are estimated from whole-rock  $\delta^{18}\text{O}$  values (Table 2.2) assuming 80% groundmass and 20% phenocrysts as done in Holt and Taylor (1998). Fractionations between water and groundmass at  $600^\circ\text{C}$  and  $400^\circ\text{C}$  are calculated (1) using feldspar/water  $^{18}\text{O}/^{16}\text{O}$  fractionations from O'Neil and Taylor (1967), (2) combining the latter with the quartz/feldspar fractionations from Clayton and Kieffer (1991) to calculate quartz/water

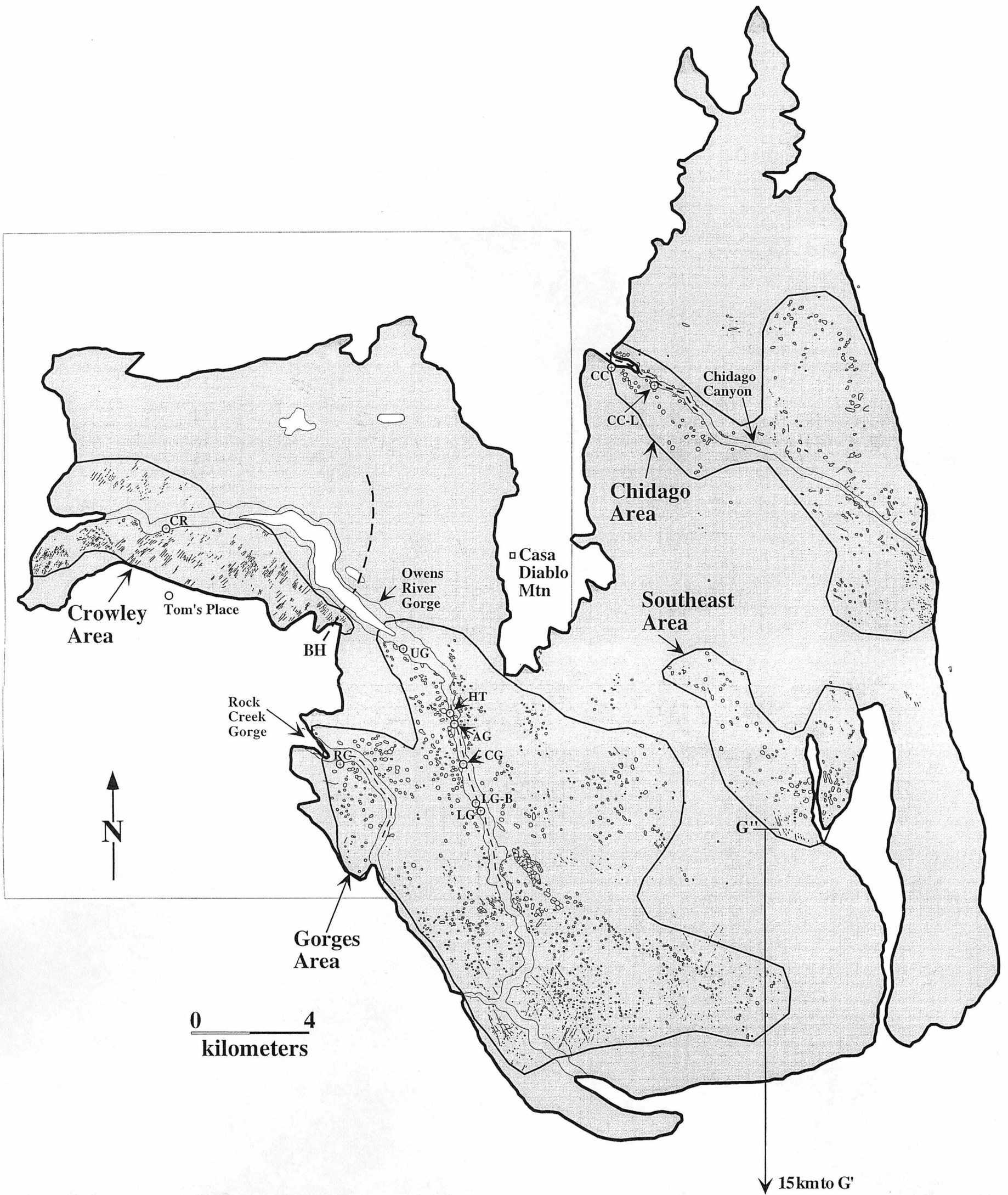
fractionations, and finally, by (3) assuming that the groundmass is made up of 2/3 alkali feldspar and 1/3 quartz.

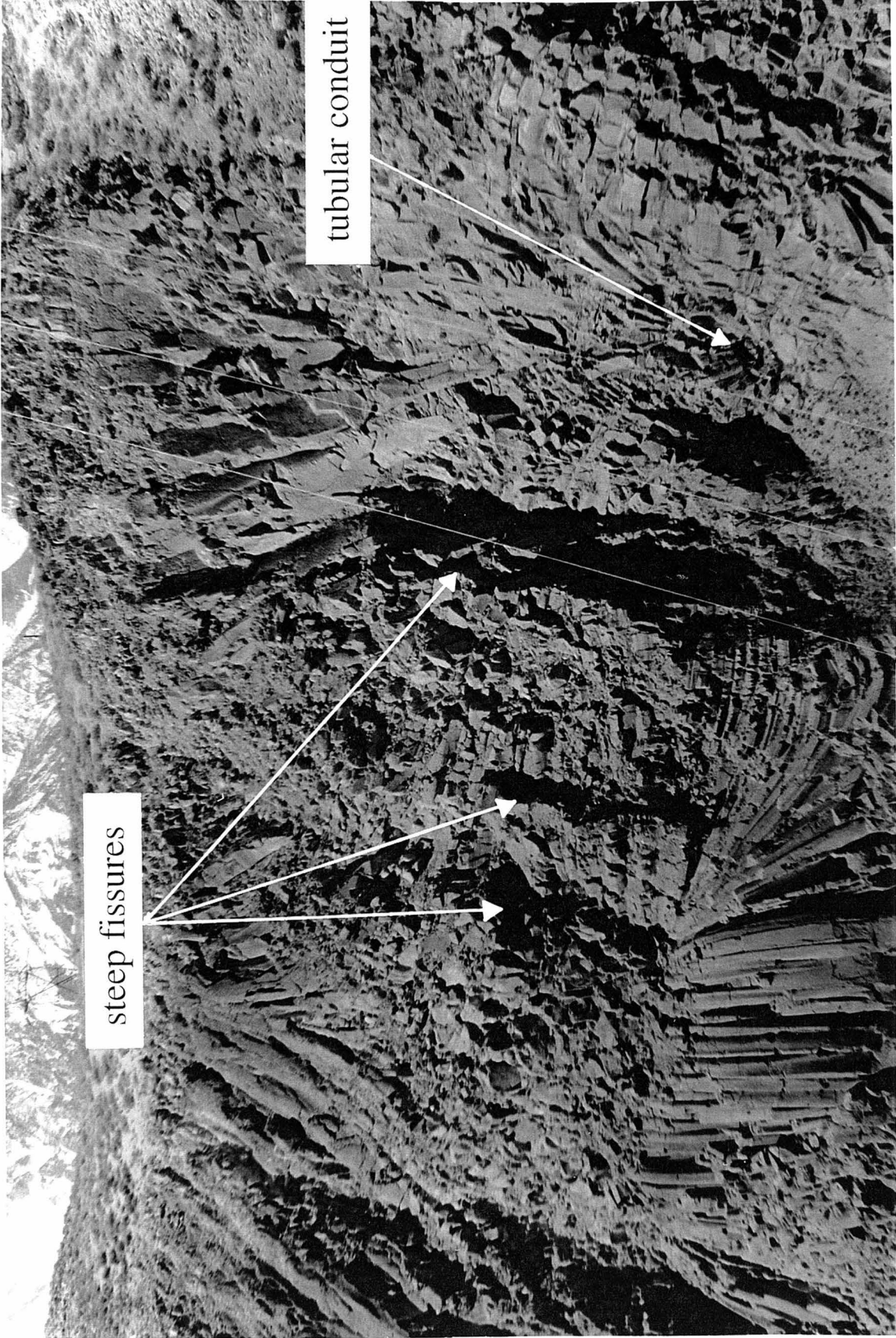
Fig. 3.19. Map of hydrogeologic features in the vicinity of the Crowley Area in the Bishop Tuff outflow sheet. Area shown is within the rectangle identified on Fig. 3.2. Dark shading indicates outcrops of basement rock within the outline of the Bishop Tuff outflow sheet. Lighter shading indicates the area of the paleovalley (see Fig. 3.17) defined by eruptive Unit Ig1Ea of Wilson and Hildreth (1997). The heavy dashed line is the shoreline of ancestral Long Valley Lake from Bailey et al. (1976). The shoreline is defined by the highest and most incised lake terraces, which are at an elevation of 7000 feet along this southeast margin of Long Valley caldera (Bailey, 1989). A-A' and tunnel no.1 are shown in Putnam (1960) and a cross section drawn along the length of this tunnel is shown in Fig. 3.20.

Fig. 3.20. Cross sections taken from Putnam (1960) drawn (1) along tunnel no. 1 of the Owens Gorge water project and (2) parallel to the basement high exposed in Owens River Gorge. A map view of this cross section line is shown in Fig. 3.19.



Fig. 3.1





steep fissures

tubular conduit

Fig. 3.3a



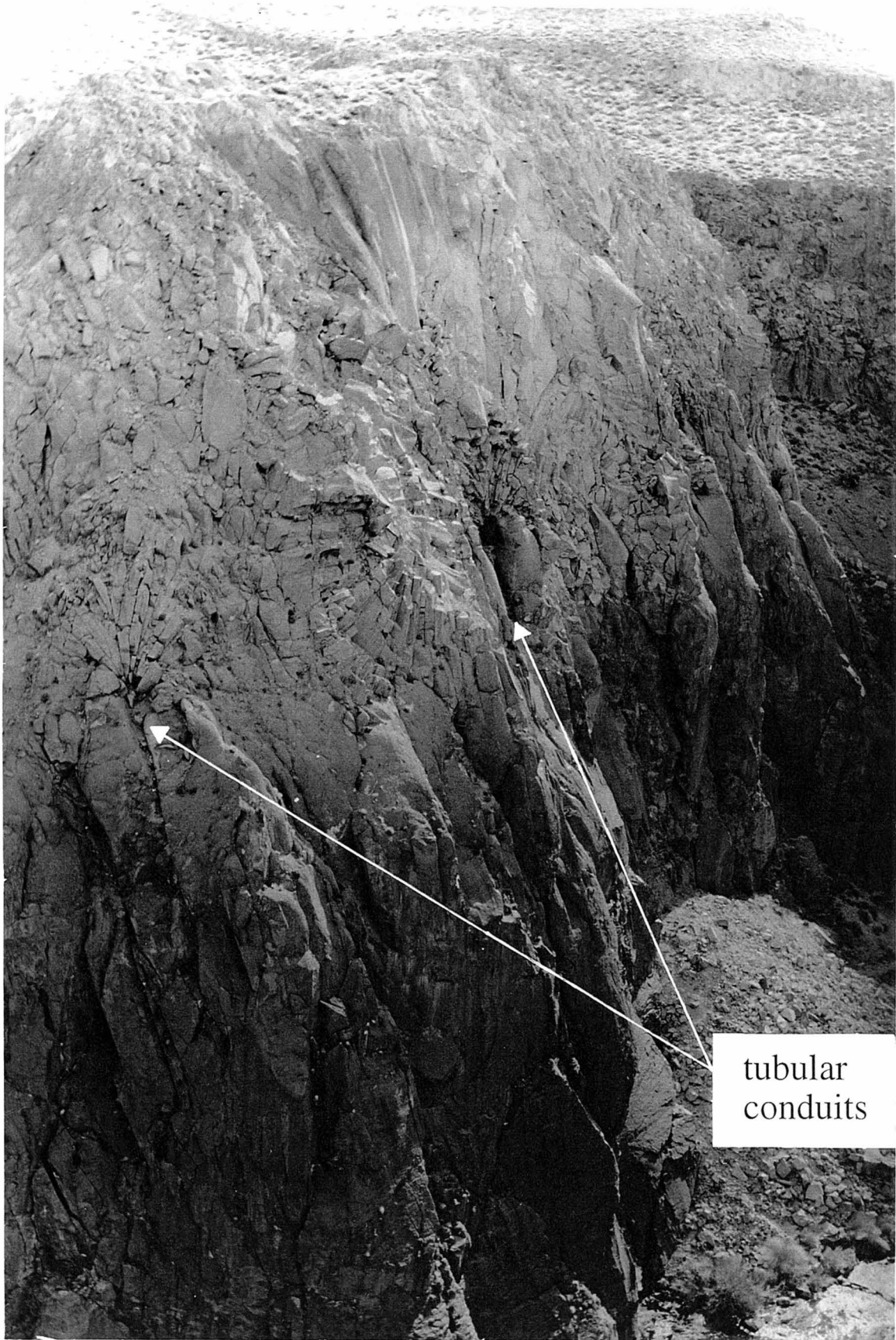


Fig.3.3b

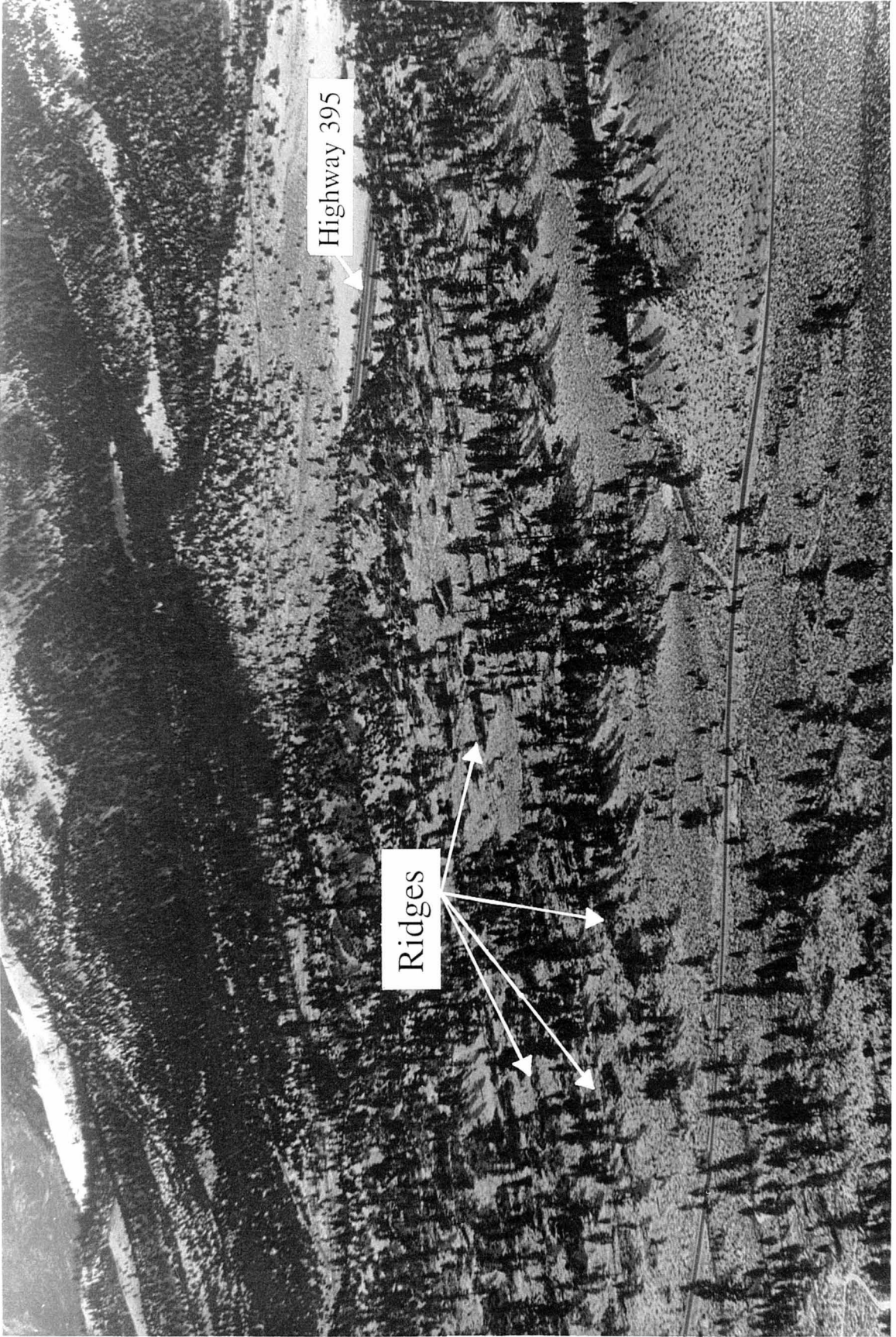


Fig. 3.4

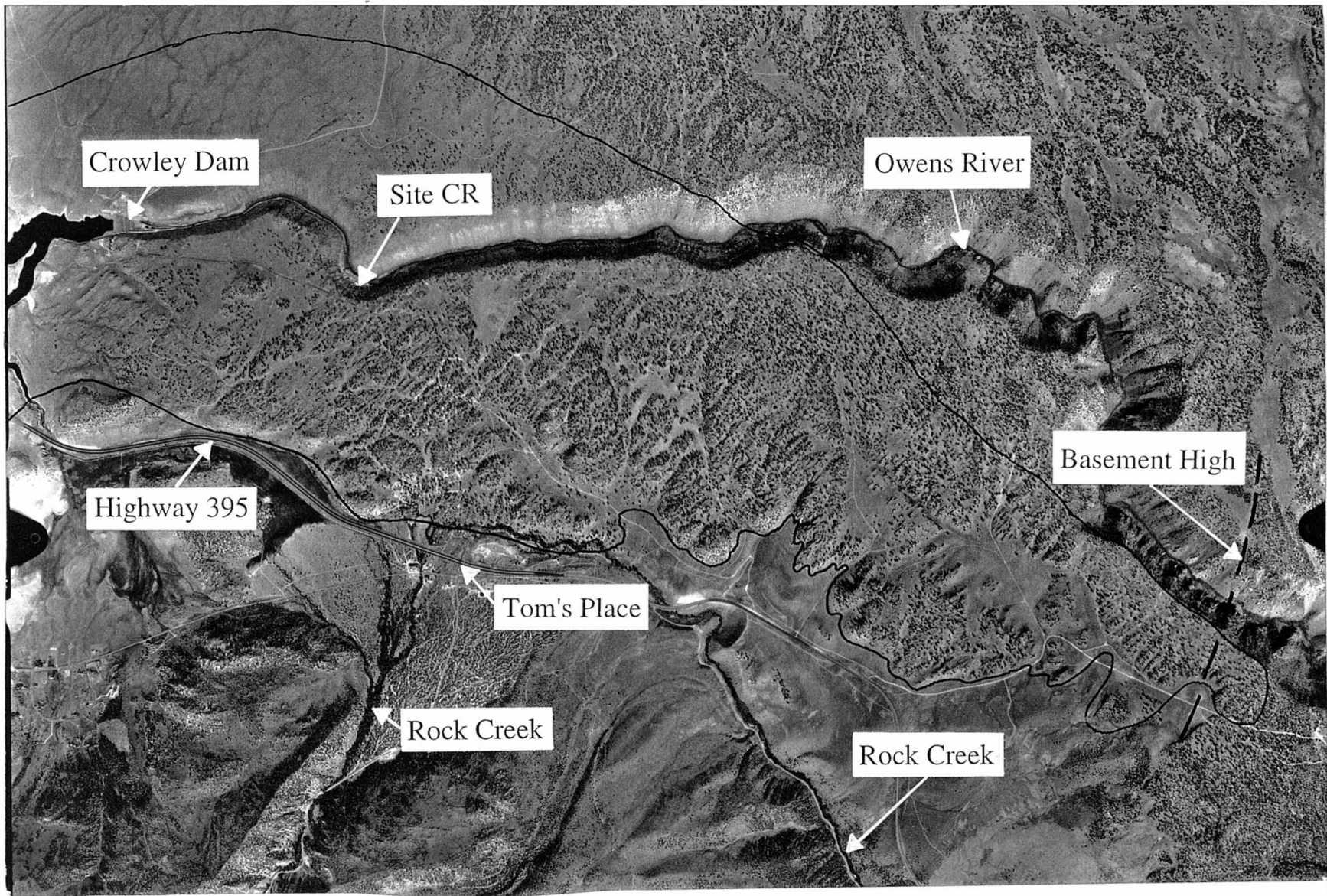


Fig. 3.5

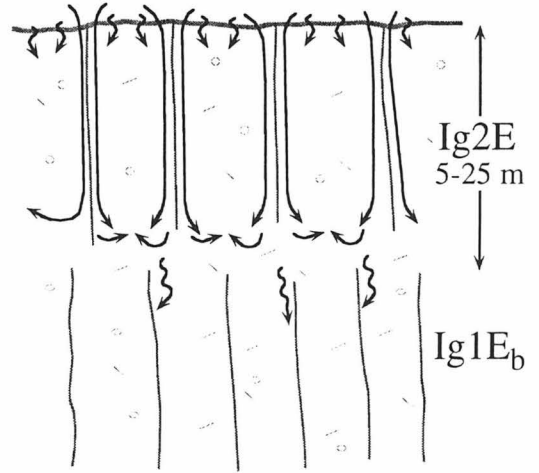
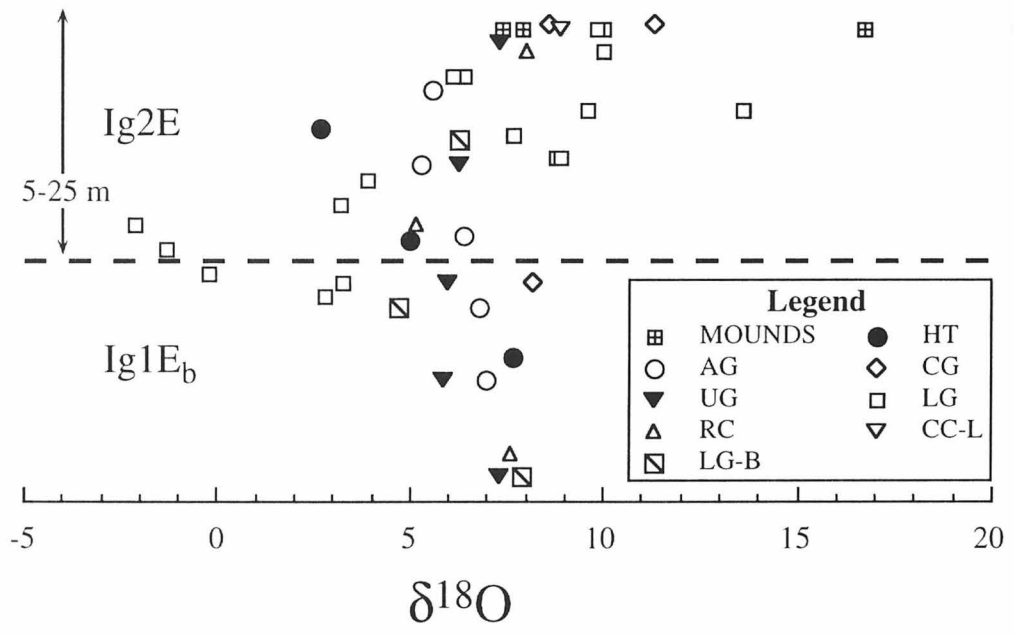




Fig. 3. <sup>7</sup>/<sub>6</sub>

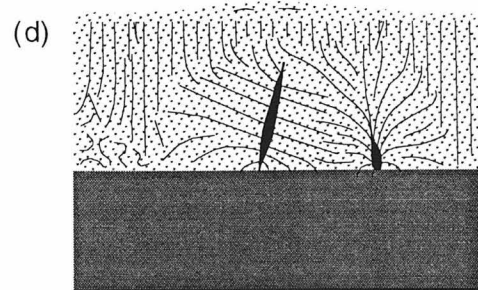
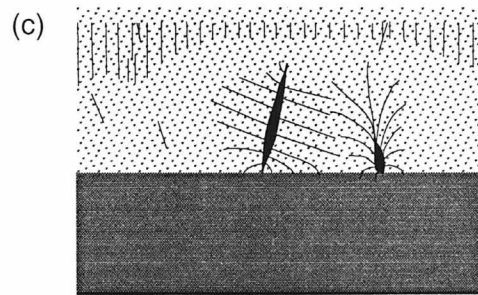
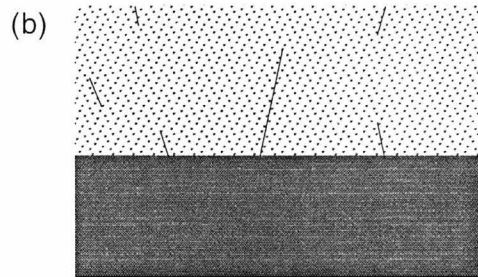
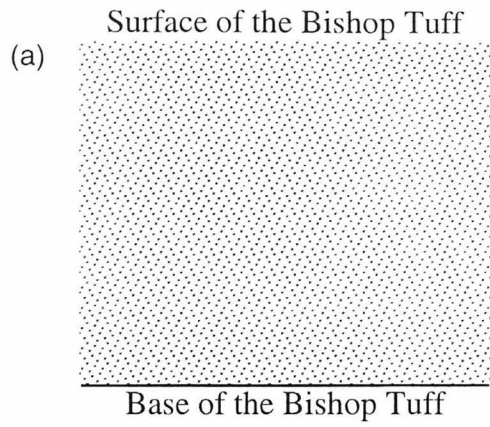
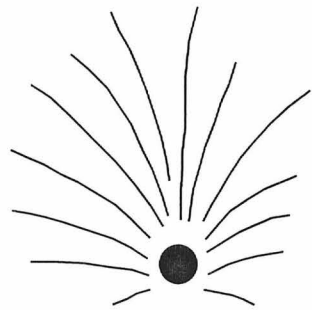
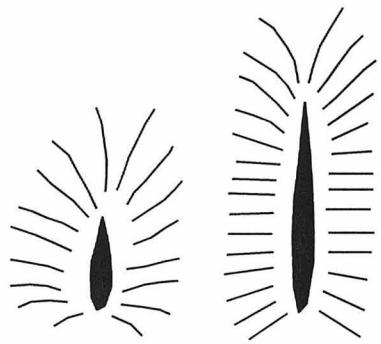


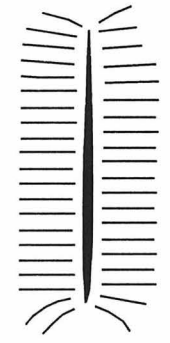
Fig.3.8



Tubular  
Conduit



Intermediate  
Structures



Steep  
Fissure

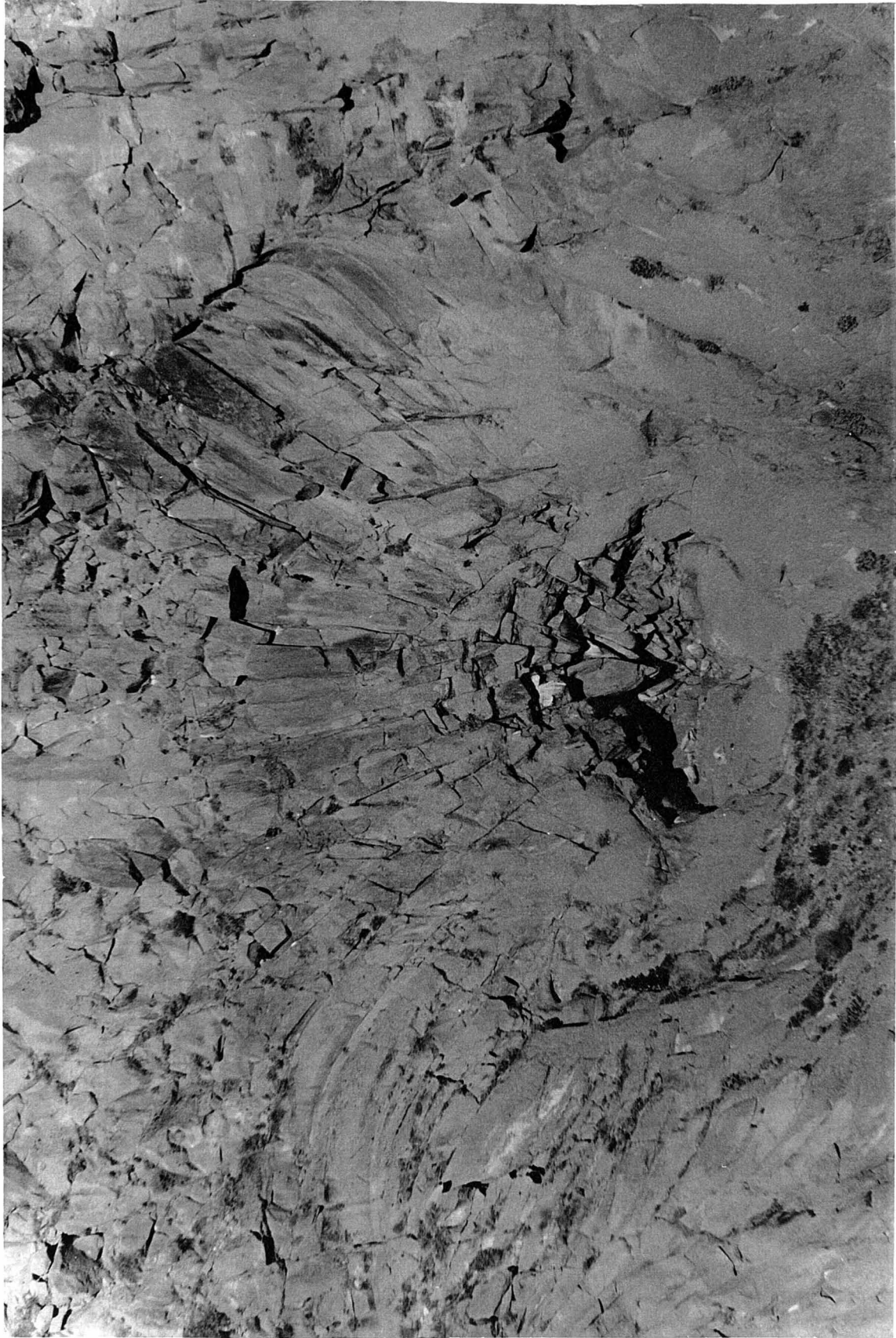


Fig. 3.10





Fig. 3.11

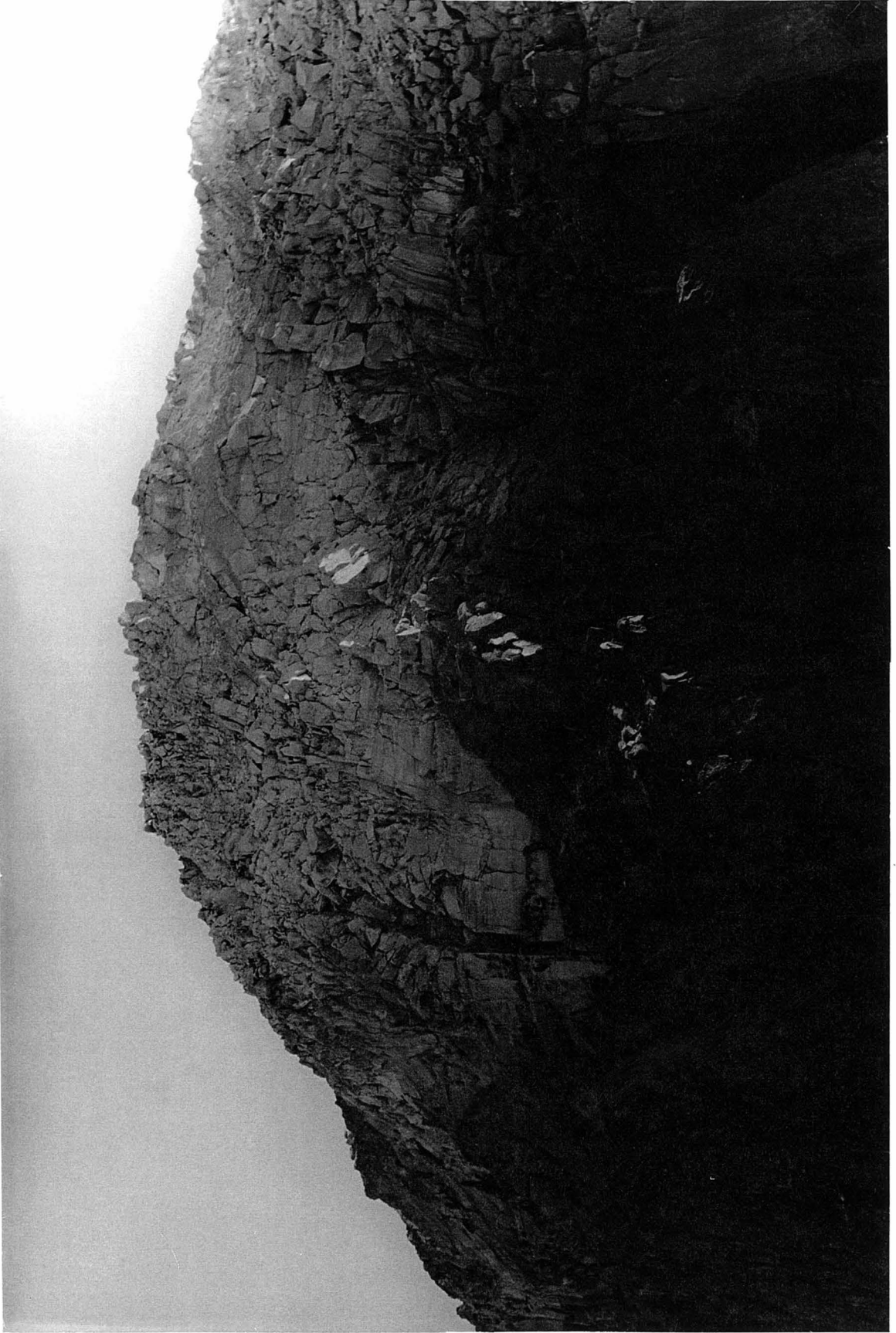


Fig. 3.12



Fig. 3.13

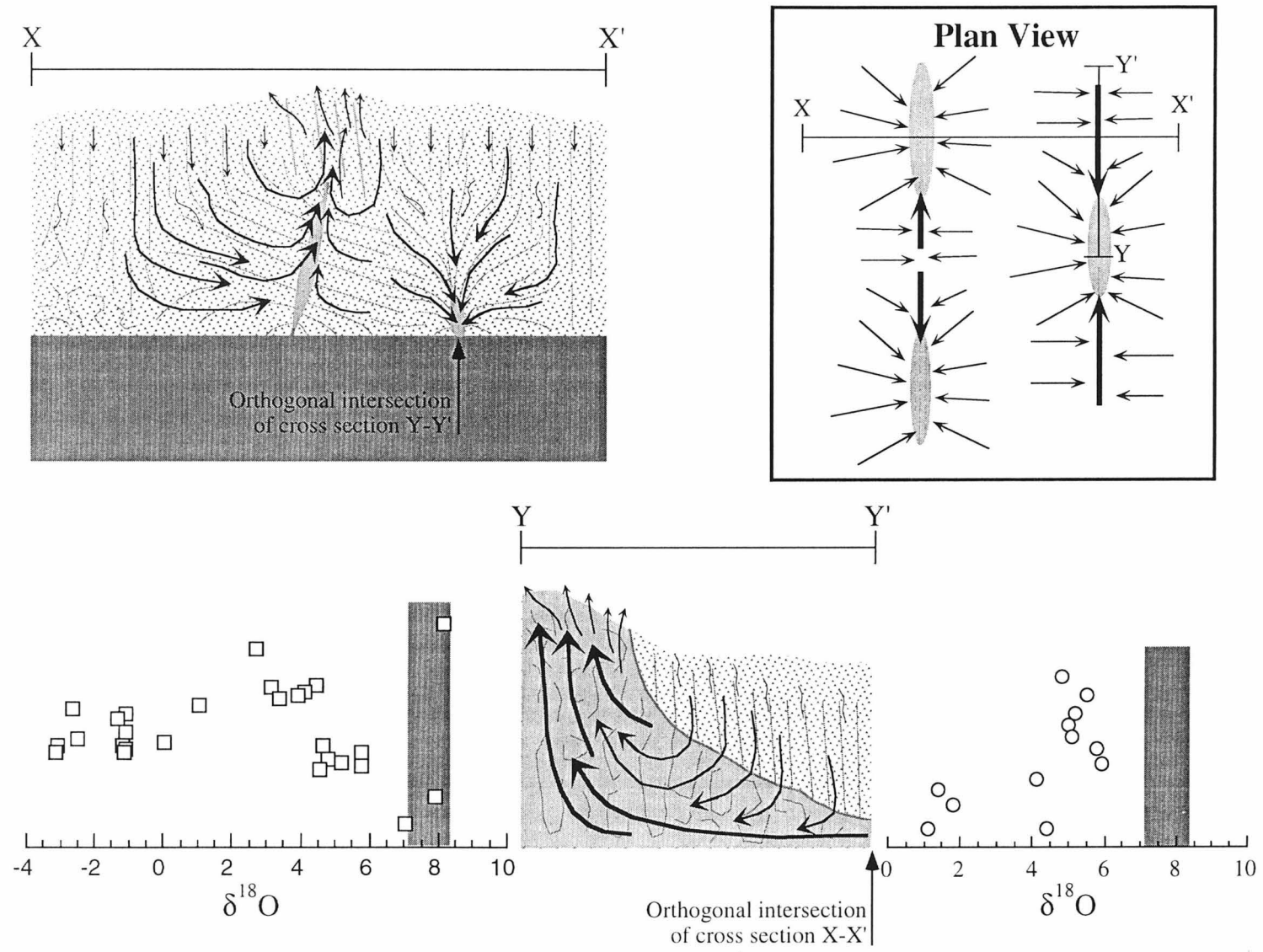


Fig. 3.14

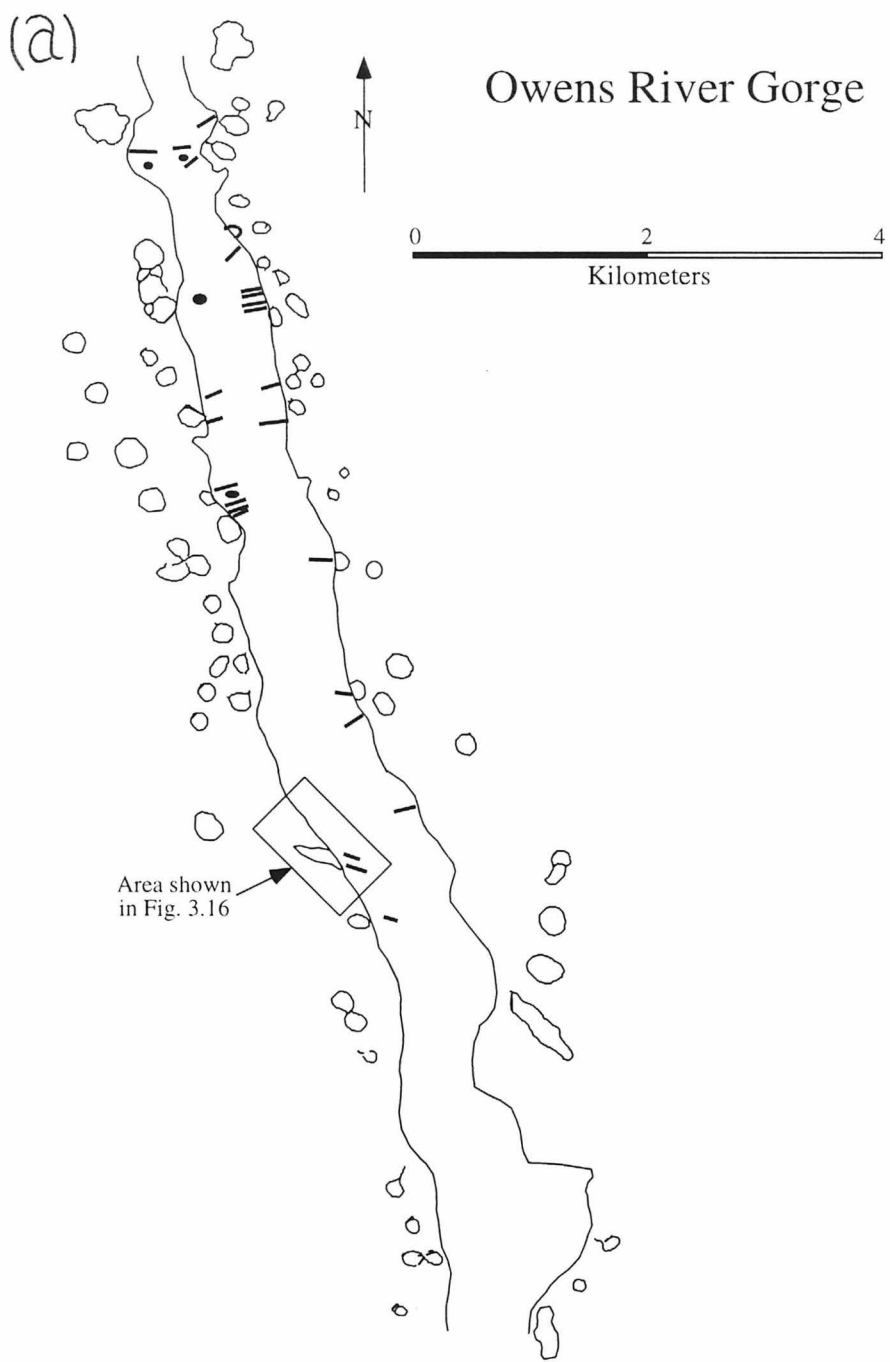


Fig. 3.15a

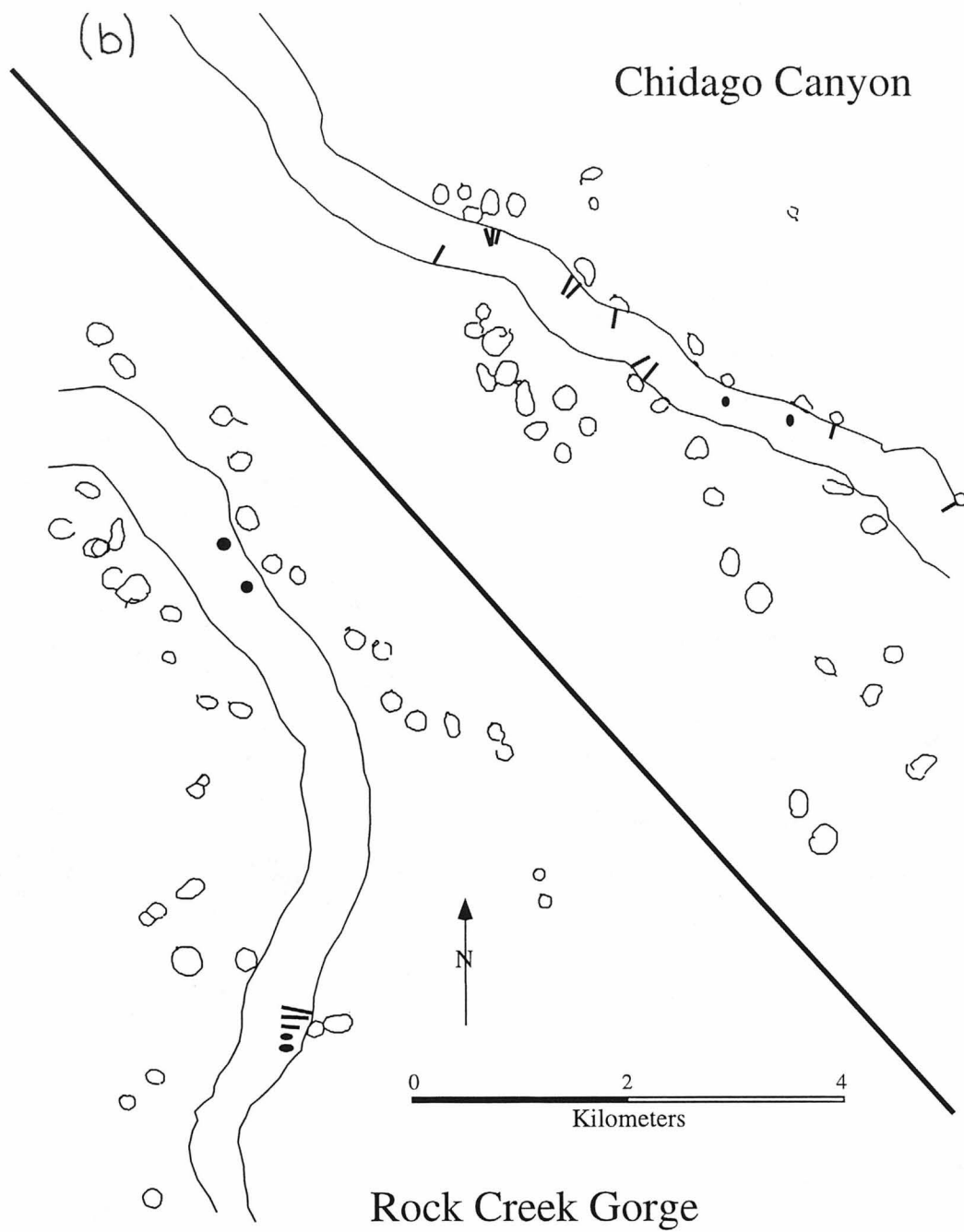


Fig. 3.15b

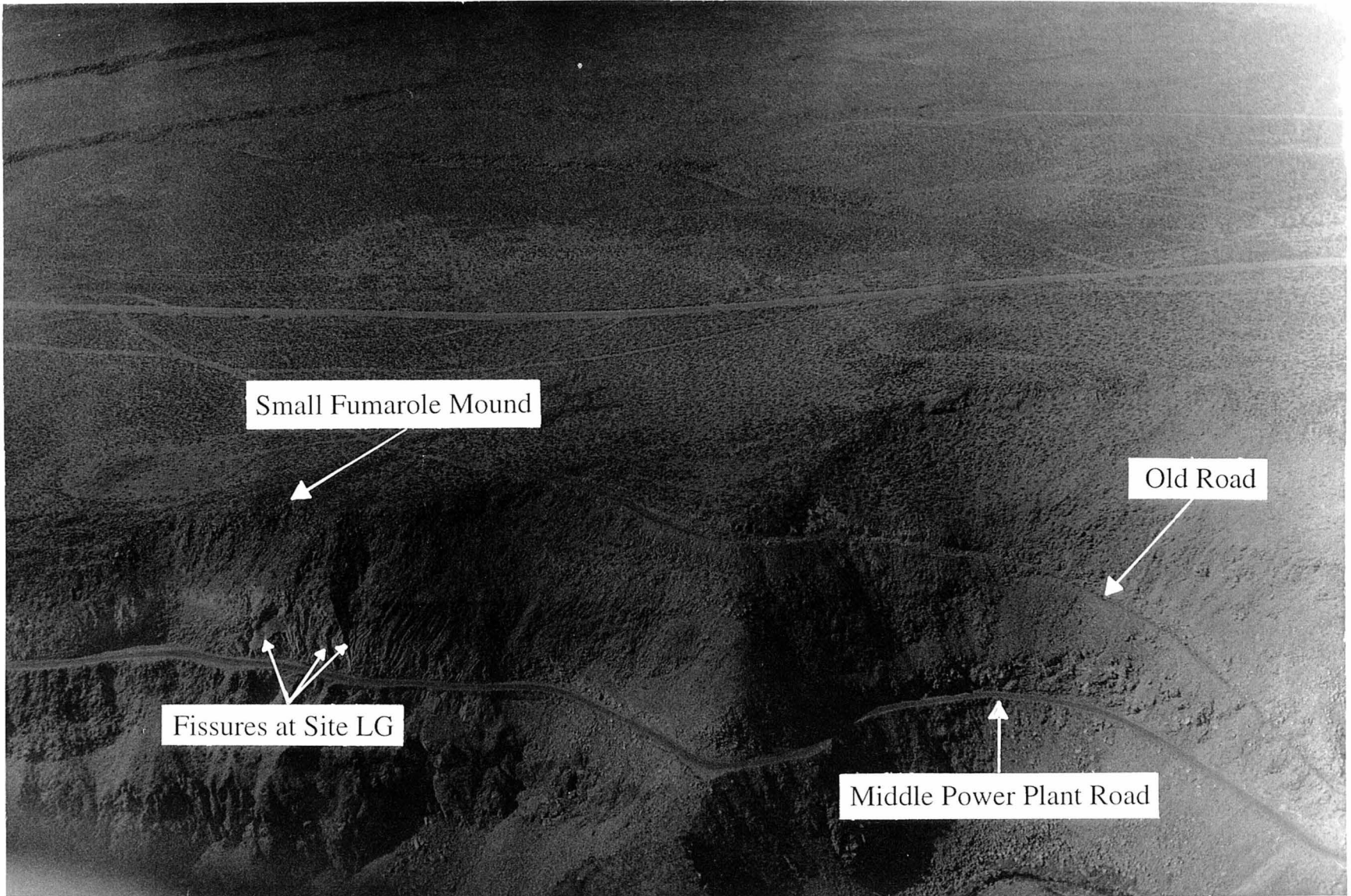


Fig. 3.16

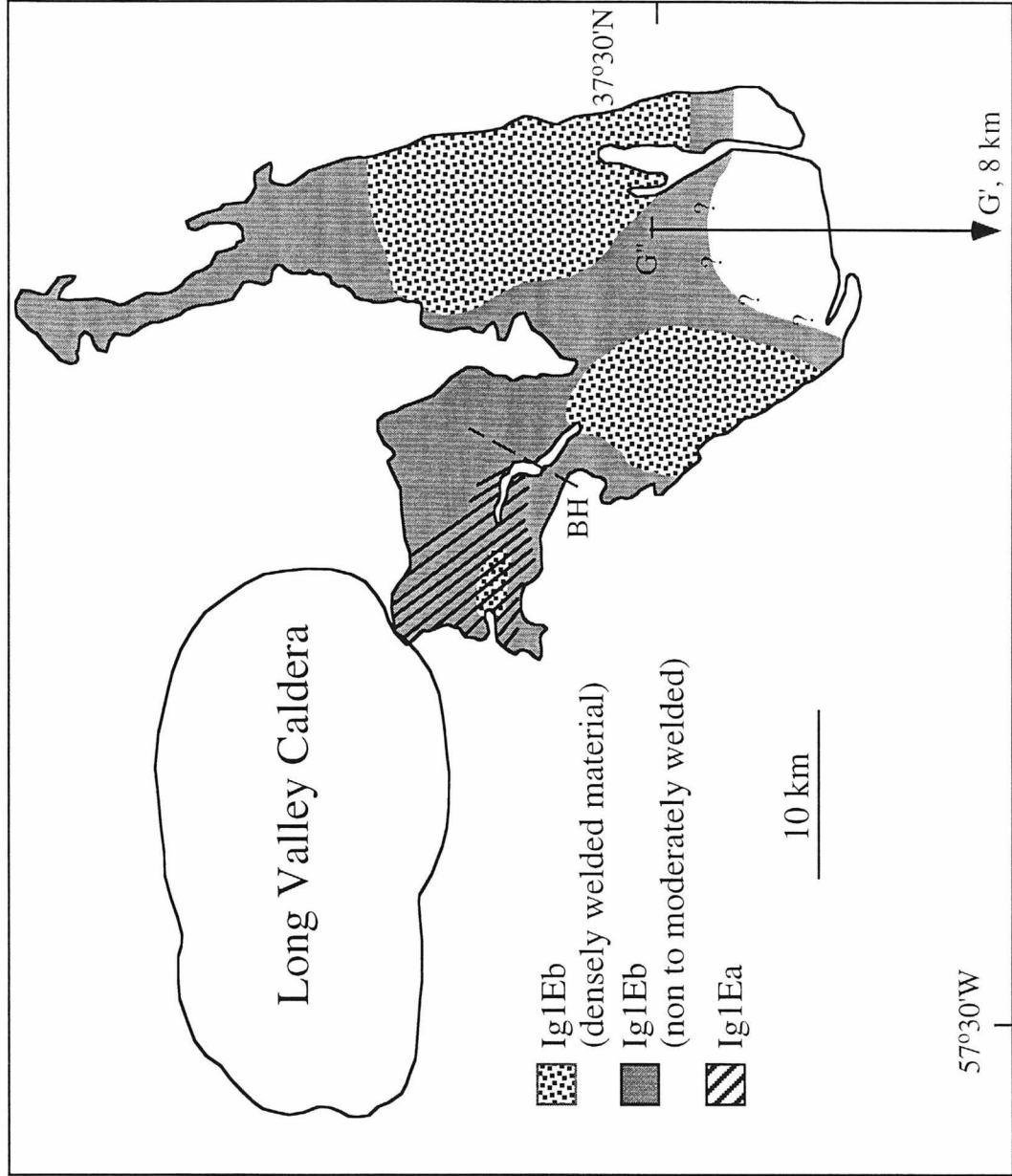
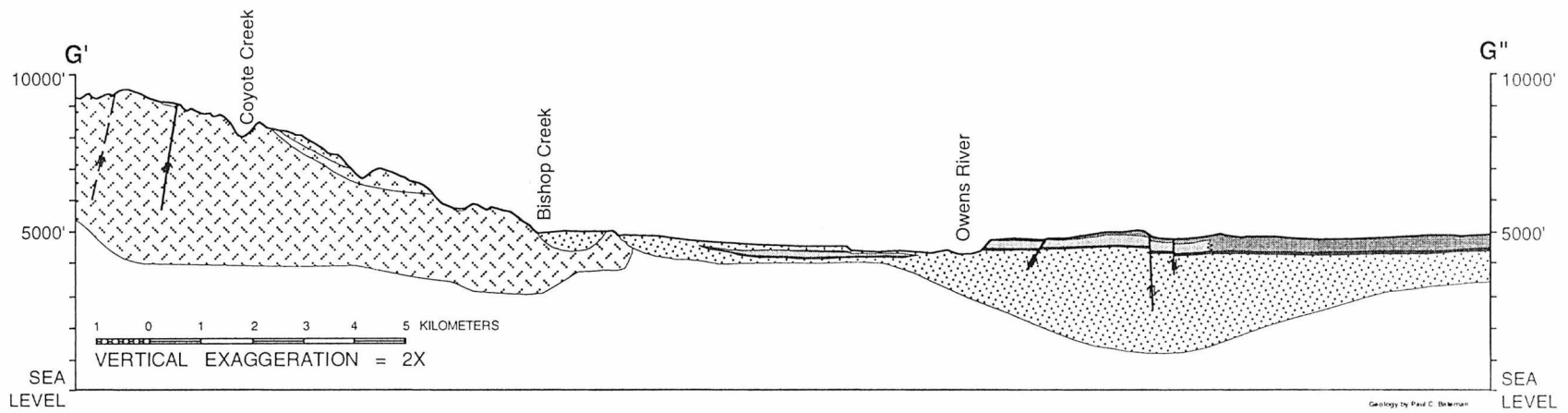





Fig. 3.17a





-  Pleistocene to Recent undifferentiated alluvium
-  Bishop Tuff, hard agglutinated tuff
-  Bishop Tuff, soft tuff with rounded pumice fragments



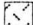
-  Bishop Tuff, basal layer of white angular pumice
-  Quaternary basalt
-  Cretaceous plutonic rocks

Fig. 3.17b

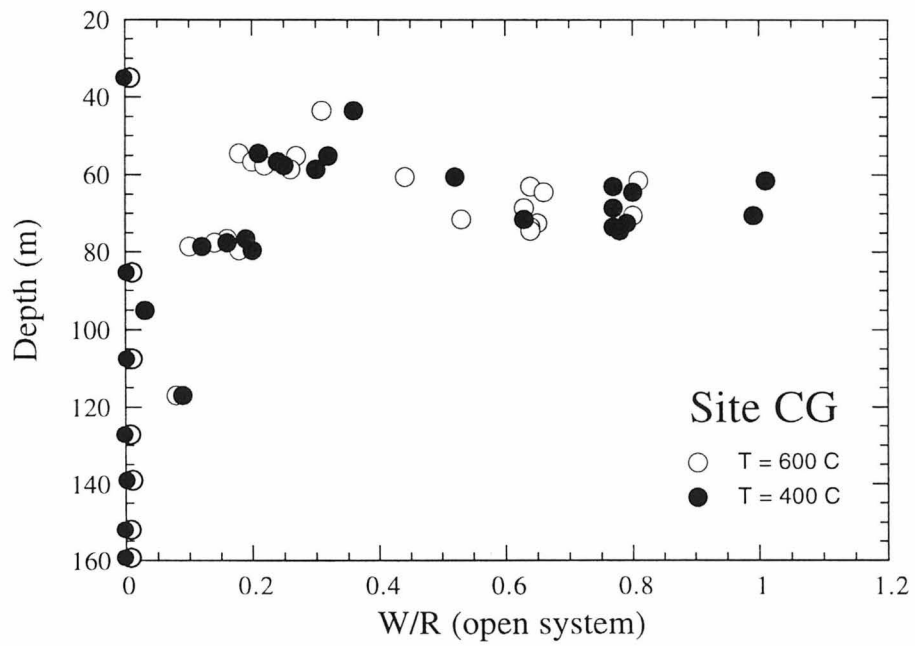
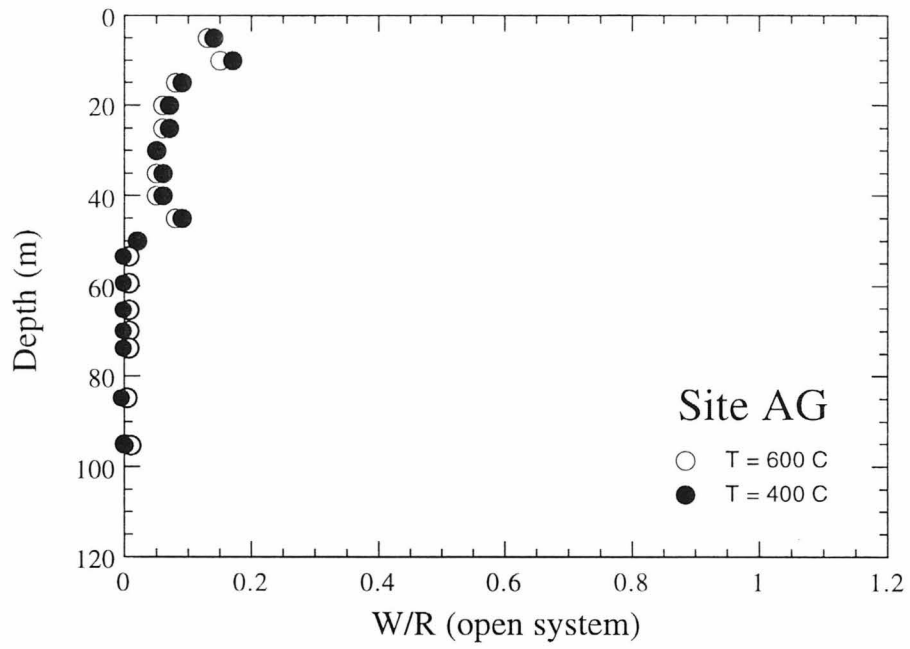


Fig.3.18

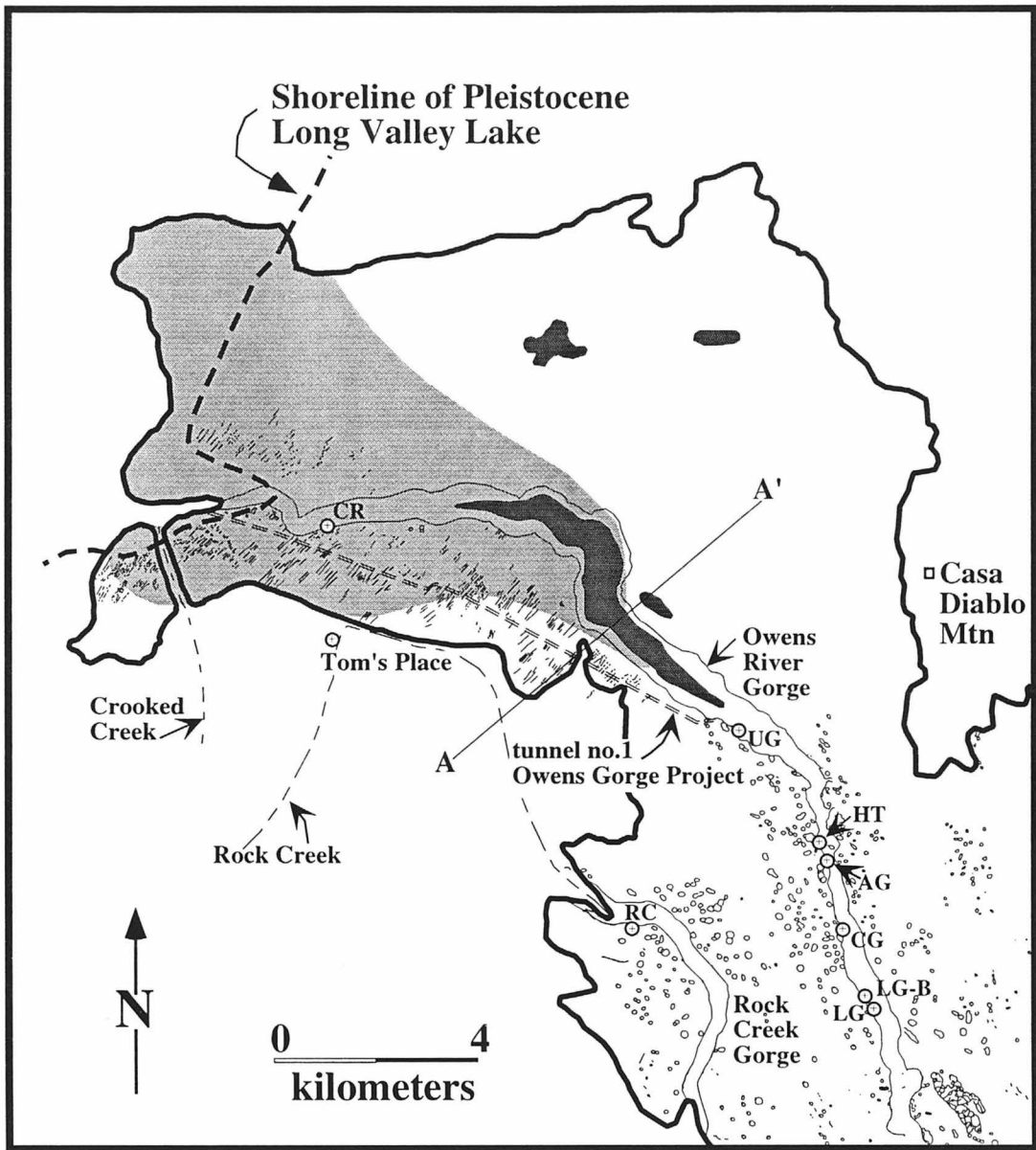
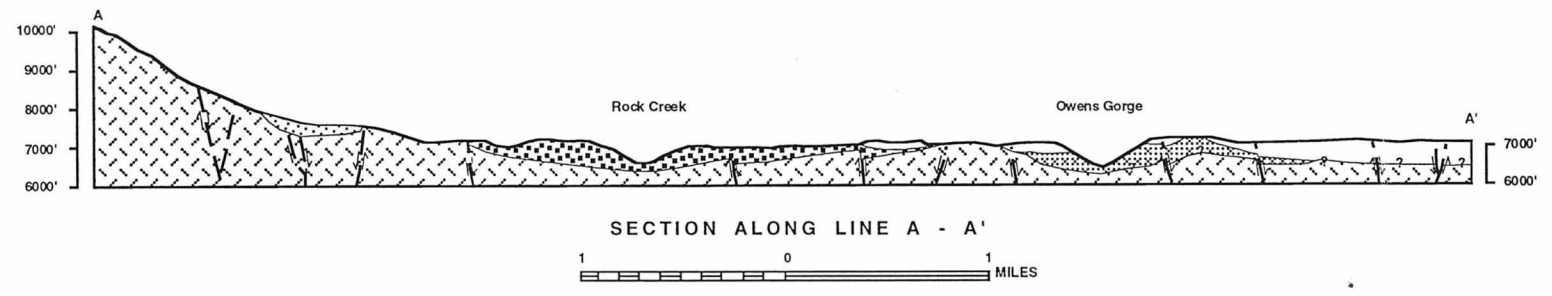
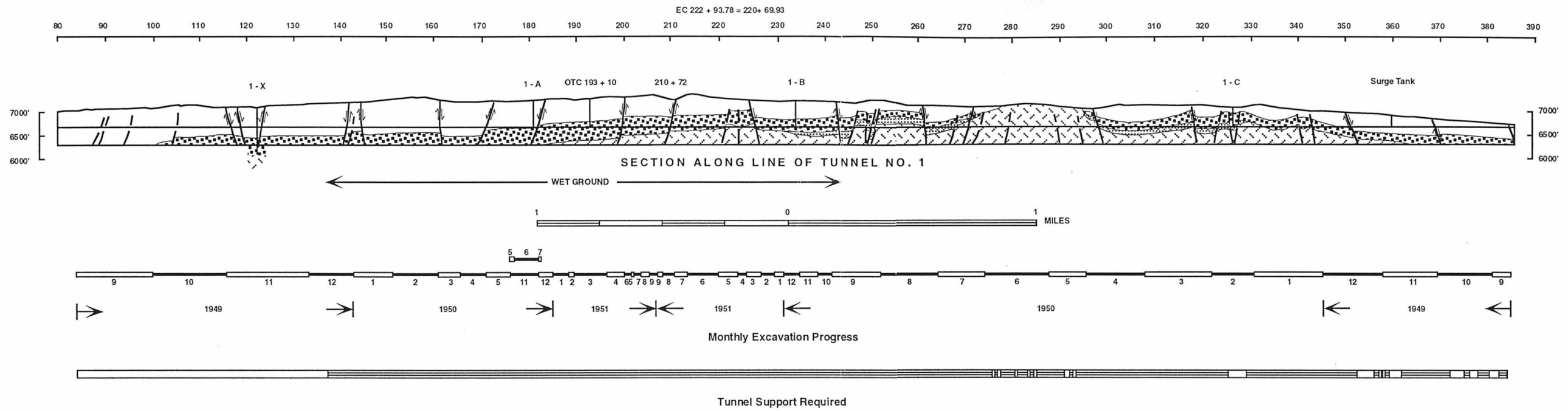


Fig. 3.19



EXPLANATION

320 Tunnel Station		Alluvium
		Bishop Tuff
		Sherwin Till
		Basalt
		Ganitic Rocks

GEOLOGIC CROSS-SECTIONS OF ROCK CREEK AND OWENS RIVER GORGES AND OF TUNNEL NO. 1, OWENS GORGE PROJECT, MONO COUNTY, CALIFORNIA

**CHAPTER 4:  $^{18}\text{O}/^{16}\text{O}$  SYSTEMATICS IN TWO FOSSIL FISSURE  
FUMARoles FROM THE 1912 ASH-FLOW SHEET AT THE VALLEY  
OF TEN THOUSAND SMOKES, ALASKA**

**4.1. Description of Sampling Sites at the Valley of Ten Thousand Smokes**

On a field trip to the Valley of Ten Thousand Smokes (VTTS) in the summer of 1998, several samples were collected from the upper part of the 1912 ash-flow sheet at three different locations (Figs. 4.1 and 4.2). Site RL is located in unwelded rhyolite exposed near the edge of the ash-flow sheet where it is dissected by the River Lethe at the base of the Buttress Range. Samples from Sites ML and KC were collected upvalley in the more mafic, dacite-rich part of the ash-flow sheet. Site ML is located in the main valley, which is drained by the River Lethe; Site KC is located in the Knife Creek drainage between Mt. Griggs and Broken Mountain. An oblique aerial photograph of the region is shown in Fig. 4.2.

Both geophysical evidence (Kienle, 1991) and the observation that blocks of welded tuff are present around phreatic craters east of Knife Creek (Curtis, 1968) indicate that there is a significant densely welded zone at depth in the tuff in the central part of the valley as well as in the upper arms of the River Lethe and Knife Creek. However, the level of erosion in these drainages is at present not yet deep enough to expose this welded material; at most, only about 50 m of largely unwelded tuff is exposed in the deeper, lower parts of Knife Creek and the River Lethe (Curtis, 1968), and this is reduced to less than 20 m in the upper parts of these drainages (Keith, 1991). It is important to point out that because of this lack of access to the deeper levels of the thicker parts of the ash-flow sheet, none of the samples of ash-flow tuff collected in this study show any significant degree of welding.

At Site RL, the River Lethe exposes about 30 m of the 1912 volcanic deposit, which in this location is unwelded rhyolite (Fig. 4.3). The base of the tuff is composed of a 50-cm-thick section of cross-bedded ash. The massive, poorly sorted, main part of the ash-flow

sheet lies atop the cross-bedded ash and the entire pile is capped by poorly bedded pumice. At Site RL, the level of the River Lethe lies close to the contact between the tuff and the Naknek formation bedrock; up to about 1.5 m above the level of the river, the base of the outcrop is grey in color and filled with pervasive disorganized fractures that give the rock a crumbly appearance. Above this horizon, the groundmass is orange-colored and broken by poorly developed columnar joints spaced about 1 m apart (Fig. 4.3). Sample RL-1 was collected from the lower, grey-colored tuff, while sample RL-2 was collected  $\approx$ 5 m above sample RL-1 from the orange-colored, columnar-jointed tuff.

Very fast-flowing springs issue from the base of some of these fractures in the walls of the gorge cut by the River Lethe downstream of Site RL; Keith (1991) estimates the flow rates of some of these springs to be about 60 liters per minute (Fig. 4.4). Such observations are indicative of the enormous fracture permeability in the ash-flow sheet, even today, 87 years after its deposition.

Site ML is located at the base of Mt. Mageik in a part of the ash-flow sheet that has been dissected by faulting. At this location, the upper 3-15 m of the tuff is exposed in 5-15 m wide extensional grabens that appear to have formed as a result of subsidence centered near the middle of a nearby lake (Fig. 4.1). Columnar joints 4-10 cm in diameter are exposed in sintered, unwelded dacite-rich tuff. The groundmass of the tuff is a dark grey-brown in color, except directly adjacent to fumarolic conduits where it is a bleached, blue-white in color. Pumice fragments at Site ML are punky as well as darker and more purplish in color compared to the adjacent groundmass. At least one discontinuous pumice-rich zone is present in the upper 5 m of the tuff at Site ML. At the time of year in which samples were collected (mid-June), the deepest grabens were filled with ice, and therefore all of the samples from Site ML are from just the upper 3 m of the ash-flow sheet.

Fumarolic conduits exposed at Site ML consist of steep fissures up to a few centimeters wide that have a bleached, blue-white zone of groundmass about 0.5-2 cm wide on either side. Columnar joints are shallowly dipping for a distance of anywhere between 10 cm to

3-4 m on either side of the fumarolic conduits (Fig. 4.5). Although the fumarolic conduits are steeply dipping, they are not necessarily planar features; some of them have curvilinear surfaces that appear sinuous when observed in cross section. The positions of some of these conduits are marked on the surface of the ash-flow sheet by the presence of small mounds of varicolored, fumarolically altered ash (Fig. 4.6). However, the iron oxide and hydroxide precipitates that coat the surface of the ash are not present coating the fumarolic conduits or any part of the tuff exposed below the surface at Site ML. The ash-flow tuff a few centimeters outside of the bleached zone along the conduit does not show any evidence for low-temperature (<300°C) mineralogical alteration. The sizes and types of fumarolic conduits at Site ML are analogous to those observed at fossil fumarole 212 (see Fig. 1.5), the geochemistry of which was investigated in detail by Spilde et al. (1993), Papike et al. (1991), and Keith (1991).

Samples from Site KC were collected in unwelded dacite-rich tuff directly beneath a large (>10 m diameter) fumarole mound dissected by Knife Creek (Fig. 4.7). The ash-flow tuff in this location is cut by a fan-like arrangement of steep fissures, most of which are less than 1 cm wide. However, the central fissure is 70 cm wide near the top and thins to ≈30 cm thick at the base of the ≈ 6-m-high exposure where the steep fissures have begun to converge. The wide central fissure is filled with pumice that has fallen in from the surface of the deposit. Shallow-dipping columnar joints 3-10 cm in width are abundant.

Not only is the fumarole mound larger and the concentration of steep fissures greater at Site KC than at Site ML, but there is also a greater abundance of amorphous silica and varicolored Fe-oxide and Fe-hydroxide precipitates, as well as more intense mineralogical alteration of glass and phenocryst phases in the upper part of the tuff. Much of the groundmass of the tuff beneath the fumarolic mound at Site KC has been bleached white compared to the grey-colored groundmass of the tuff immediately on either side of and at the base of the outcrop. At Site KC, hematite and amorphous silica cement the pumice and ash on the surface of the tuff, as well as the pumice that fills the widest fissure. Hematite

also coats much of the tuff along columnar joints and steep fissures. Rather than occurring only within a few centimeters of the fissures, as was the case at Site ML and at fumarole 212 described by Spilde et al. (1993), the mineralogical alteration of groundmass and phenocryst phases at Site KC occurs at numerous intervals throughout a large portion of the bleached, upper part of the tuff beneath the fumarolic mound. This mineralogical evidence suggests that there was a much greater degree of low-temperature (<200°C) hydrothermal activity at Site KC than at Site ML.

#### **4.2. Previous $^{18}\text{O}/^{16}\text{O}$ studies of samples from the VTTS**

$^{18}\text{O}/^{16}\text{O}$  studies of quartz, plagioclase, orthopyroxene, and titanomagnetite phenocrysts from the VTTS were analyzed by Hildreth (1987), as shown in Fig. 4.8. In addition to phenocryst separates from the rhyolite (n=4), dacite (n=3), and andesite (n=2) portions of the 1912 ash-flow sheet, Hildreth (1987) also analyzed phenocryst phases from ash-fall units A, C, D, and G, as well as from Novarupta rhyolite dome. Also included in Hildreth's (1987)  $^{18}\text{O}$  data set, and shown on Fig. 4.8, are two whole-rock samples of crystalline dacite from Falling Mountain and Cerberus, which are two Holocene domes near the southern margin of the VTTS (Fig. 4.1). As discussed by Hildreth (1987), the  $\delta^{18}\text{O}$  values of phenocryst separates are in general very uniform, with characteristic magmatic values ( $\delta^{18}\text{O}_{\text{quartz}} = +7.1$  to  $+7.6$  and  $\delta^{18}\text{O}_{\text{feldspar}} = +5.6$  to  $+6.4$ ); this uniformity implies that the phenocrysts exhibit no recognizable indications of any type of exchange with meteoric waters at either high or low temperatures. Also, the plagioclase phenocrysts exhibit slightly heavier  $\delta^{18}\text{O}$  values in the high- $\text{SiO}_2$  rhyolite than in the coeruptive andesite and dacite, exactly as is predicted for closed system fractionation at magmatic temperatures (Taylor and Sheppard, 1986). Also as pointed out by Hildreth (1987), the  $^{18}\text{O}/^{16}\text{O}$  fractionations for the various coexisting phenocryst mineral pairs is consistent with the Fe-Ti oxide temperatures of 805°-990°C previously reported for the 1912 ash-flow sheet (Hildreth, 1983).



Even though this study focused on hydrothermally altered samples, while Hildreth's (1987) study was on the freshest available samples, the feldspar  $^{18}\text{O}/^{16}\text{O}$  data in both studies are very similar (with one notable exception, see below). Thus, the oxygen isotope analyses of feldspar separates from the 1912 ash-flow sheet reported in this study (Table 4.1) basically confirm the findings of Hildreth (1987) that there is no significant evidence for any high-temperature ( $>100^\circ\text{C}$ )  $^{18}\text{O}$ -exchange or mineralogical alteration of the feldspar phenocrysts in the 1912 ash-flow sheet. With the exception of a slightly  $^{18}\text{O}$ -enriched feldspar separate from one sample that has an extremely  $^{18}\text{O}$ -enriched whole rock  $\delta^{18}\text{O}$  value of +12.6 (KC-2), all other analyzed feldspar separates fall within the  $\delta^{18}\text{O}$  range expected for feldspars that crystallized in equilibrium from the VTTS parent magma (Hildreth, 1987). Both of the feldspar separates analyzed from Site ML have identical  $\delta^{18}\text{O}$  values of +6.28 (Table 4.1), which is slightly high compared to Hildreth's (1987) range for the dacite ( $\delta^{18}\text{O} = +5.6$  to  $+5.9$ ), but is well within the range expected for the rhyolite ( $\delta^{18}\text{O} = +5.9$  to  $+6.5$ ). Also note that VTTS sample MLA-3 (Fig. 4.10; Table 4.1) has a whole-rock  $\delta^{18}\text{O}$  value that is shifted down by 6 ‰ (to  $\delta^{18}\text{O} = -0.1$ ), but it contains feldspar phenocrysts which are not at all  $^{18}\text{O}$ -depleted ( $\delta^{18}\text{O}_{\text{feldspar}} = +6.28$ ; Table 4.1).

Therefore, just as is the case for samples from the upper parts of the intracaldera Chegem Tuff (Chapter 1) and the Bishop Tuff outflow sheet (Chapter 2), the  $^{18}\text{O}$  evidence from the VTTS also shows that the groundmass of the tuff locally became strongly  $^{18}\text{O}$ -depleted while the coexisting, mm-sized feldspar phenocrysts did not undergo any significant  $^{18}\text{O}$  exchange. Thus, as at Chegem and in the Bishop Tuff, the  $^{18}\text{O}/^{16}\text{O}$  data prove that any high-temperature, meteoric-hydrothermal activity at the VTTS must have been very short-lived, which is very fortunate, because at the VTTS, we know from direct observations that the fumarolic activity there lasted only a little over 15 to 20 years (Keith, 1991; Allen and Zies, 1923). Without an historical record of fumarolic activity for the Chegem Tuff and the Bishop Tuff, Gazis et al. (1996) and Holt and Taylor (1998) had to

infer a very short-lived interval of high-temperature fumarolic activity from just the phenocryst-groundmass  $^{18}\text{O}/^{16}\text{O}$  systematics. The  $^{18}\text{O}$  data from the VTTS (Table 4.1 and Fig. 4.8) now provide clear-cut evidence that very similar phenocryst-groundmass  $^{18}\text{O}/^{16}\text{O}$  signatures were actually produced in the VTTS over a 10-25 year interval after the 1912 Katmai eruption.

### 4.3. $^{18}\text{O}/^{16}\text{O}$ systematics of samples from the VTTS

#### 4.3.1. Whole-rock $\delta^{18}\text{O}$ Values

Whole-rock  $\delta^{18}\text{O}$  values of samples collected from the ash-flow tuff in the VTTS ( $\delta^{18}\text{O} = -0.1$  to  $+12.6$ ) span an enormously wider range than the likely  $\delta^{18}\text{O}$  values of any parent magmas involved in the 1912 eruption (Fig. 4.9; Table 4.1). From the phenocryst data, it can be estimated that these magmas probably had  $\delta^{18}\text{O} \approx +5.6$  to  $+6.5$  (Hildreth, 1987), and one can absolutely rule out any magmas with  $\delta^{18}\text{O}$  lower than  $+5.0$  or higher than  $+7.5$ . A comparison of Fig. 4.9 with Table 4.1 shows that there are four samples with  $\delta^{18}\text{O}$  values lower than the lowest plausible primary  $\delta^{18}\text{O}$  value of the VTTS Tuff ( $<+5.0$ ), three of these are from Site ML (MLA-1, MLA-2, and MLA-3) and one is from Site KC (KC-13 GM, white). The one sample that is significantly elevated in  $^{18}\text{O}$  ( $>+7.5$ ) is KC-2, although two other samples, from Site KC (KC-4 and KC-5) are very slightly  $^{18}\text{O}$ -enriched. Because the equilibrium  $^{18}\text{O}/^{16}\text{O}$  fractionation factor between water and rock decreases sharply with increasing temperature (see Figs. 2.10 and 2.11), it is clear that the four  $^{18}\text{O}$ -depleted samples exchanged with a low- $^{18}\text{O}$  fluid at high-temperature, whereas the three  $^{18}\text{O}$ -enriched samples could have acquired their heavy oxygen isotope signature during exchange with a similar type of fluid at much lower temperatures. At temperatures of  $\approx 100^\circ\text{C}$  or lower, this fractionation factor is large enough to compensate for the fact that local meteoric  $\text{H}_2\text{O}$  in the VTTS area has a relatively low  $\delta^{18}\text{O}$  value of  $-14$  to  $-16$ , which is 20-22 ‰ lower than the  $\delta^{18}\text{O}$  value of the unexchanged groundmass in the tuff (Keith

et al., 1992). Therefore, at such low temperatures, meteoric-hydrothermal exchange results in a net  $^{18}\text{O}$  increase in the tuff.

Note that the two samples from Site RL, which is unwelded and also does not exhibit any evidence for fumarolic hydrothermal circulation, both have identical whole-rock  $\delta^{18}\text{O}$  values of +5.9. These are very close to the values expected for the unexchanged tuff from the VTTS, based on the phenocryst  $^{18}\text{O}/^{16}\text{O}$  data referred to above. Thus, it appears that, at least near Site RL, the unwelded marginal portion of the 1912 ash-flow sheet may not have been affected by significant fumarolic  $^{18}\text{O}$ -exchange.

The low  $\delta^{18}\text{O}$  values of groundmass in the four samples of the 1912 ash-flow sheet indicate that the exchanging fumarolic fluid must have contained a significant component of meteoric  $\text{H}_2\text{O}$ . Any low- $^{18}\text{O}$  signature in the groundmass of the tuff can be readily inferred to be the result of high-temperature fumarolic oxygen isotope exchange, because (1) the volcanic deposit at the VTTS is only 87 years old, and (2) the only significant hydrothermal activity on the ash-flow sheet was the vigorous fumarolic activity that occurred for 15-20 years following the eruption. The above result is probably no surprise. Based on the studies of the intracaldera Chegem Tuff and the Bishop Tuff outflow sheet, respectively, Gazis et al. (1996) and Holt and Taylor (1998) showed that fumarolic activity in ash-flow tuffs must involve a significant component of meteoric  $\text{H}_2\text{O}$ . Also, Allen and Zies (1923) concluded that meteoric  $\text{H}_2\text{O}$  was the dominant component of fumarolic gases they collected from active fumaroles on the surface of the 1912 ash-flow sheet in the VTTS. Allen and Zies (1923) postulated that fumaroles in the 1912 ash-flow sheet were largely supplied from streams that they observed to flow out onto the surface of the tuff. They made a rough calculation to determine that no more than 11% of the river water that entered the upper reaches of the VTTS issued forth from it downstream in the lower part of the valley; they postulated that the remainder was recycled back into the atmosphere as fumarolic vapor.

#### *4.3.2. Minor Effects of Mineralogical Alteration and $^{18}\text{O}$ -Exchange in the Feldspar Phenocrysts*

Using electron microprobe and transmission electron microscopy, Spilde et al. (1993) have shown that the calcium-rich portions of feldspar phenocrysts adjacent to fumarolic conduits in the 1912 ash-flow sheet are replaced by amorphous silica. Such mineralogical alteration is hypothesized to have occurred at temperatures below  $\approx 200^\circ\text{C}$  during the waning stages of fumarolic activity. Spilde et al. (1993) and Keith (1991) both report that mineralogical alteration of the feldspars increases with proximity to fumarolic conduits; feldspars at a distance of 35 cm from a particular fumarolic conduit were found to be unaltered, whereas those progressively closer to the vent were systematically replaced by greater amounts of amorphous silica.

Only one VTTS feldspar phenocryst separate was found to be even slightly  $^{18}\text{O}$ -enriched ( $\delta^{18}\text{O} = +8.46$ ), and this is one from the most  $^{18}\text{O}$ -enriched sample that was analyzed (KC-2; whole rock  $\delta^{18}\text{O} = +12.6$ ). Low-temperature mineralogical alteration of feldspar phenocrysts as described by Spilde et al. (1993) would almost certainly be accompanied by  $^{18}\text{O}$  enrichment of the feldspars, and the feldspars from sample KC-2 are cloudy, indicating that they have undergone at least minor mineralogical alteration. Also, sample KC-2 was collected directly adjacent to a fissure beneath a fumarolic mound (Fig. 4.7), which is an analogous location to that in which Spilde et al. (1993) observed the replacement of feldspars by amorphous silica to be most extensive. In view of the fact that the groundmass in sample KC-2 is strongly enriched in  $^{18}\text{O}$ , it is reasonable to infer that the slight elevation in the  $\delta^{18}\text{O}$  value of the coexisting feldspar phenocrysts is also a result of minor mineralogical alteration analogous to that observed in other cloudy feldspars from the VTTS fissure fumaroles (Spilde et al., 1993).

Feldspars from the upper, more mafic part of the 1912 ash-flow sheet are more calcium-rich than feldspars analyzed for  $\delta^{18}\text{O}$  from the Bishop and Chegem Tuffs, and such calcium-rich feldspars are known to be particularly susceptible to low-temperature

hydrothermal alteration. Thus, the low-temperature effects observed in feldspars from the VTTS might in general be less common in the Bishop and Chegem Tuffs, because the sanidines in those tuffs would have been inherently more stable than plagioclase phenocrysts under hydrothermal conditions. Nevertheless, recall from Chapter 2 that some samples collected within 2 m of the surface of a large fumarolic mound on the surface of the Bishop Tuff outflow sheet had even higher whole-rock  $\delta^{18}\text{O}$  values (+13.6 and +16.7; Table 2.2) than KC-2, and they were also observed to contain cloudy feldspar phenocrysts. These particular feldspar phenocrysts were not analyzed in this study, but it would be no surprise to find that they do have elevated  $\delta^{18}\text{O}$  values, analogous to the high- $^{18}\text{O}$  feldspar separate analyzed from Site KC.

The observed longevity of high-temperature fumarolic activity in the VTTS correlates very well with data on the extent of mineralogical alteration and  $^{18}\text{O}$ -exchange of feldspar phenocrysts. The high-temperature fumarolic activity at the VTTS is known to have been extremely short-lived; after about 11 years, fumaroles were mostly below  $100^{\circ}\text{C}$ , and though a temperature as high as  $645^{\circ}\text{C}$  was measured at one fumarole in 1919, by that time Allen and Zies (1923) had already pointed out that the fumarolic activity had waned considerably over all parts of the ash-flow sheet, only 7 years after eruption. Nevertheless, circulation of low-temperature fluids through the tuff continued for many years, and warm springs ( $\approx 20^{\circ}\text{--}30^{\circ}\text{C}$ ; Keith, 1992) still issue from fractures in the tuff today, 87 years after the tuff was emplaced. Thus high-temperature ( $>400^{\circ}\text{C}$ ) meteoric-hydrothermal activity in the VTTS was in general apparently too short-lived to allow for any significant mineralogical alteration and/or  $^{18}\text{O}$ -exchange of even these Ca-rich feldspar phenocrysts. However, at least locally, directly adjacent to the largest fumarolic conduits, meteoric-hydrothermal circulation evidently continued for a long enough time and at sufficiently high temperature ( $\approx 100^{\circ}\text{C}$ ) to produce some mineralogical alteration and  $^{18}\text{O}$  exchange of the feldspar phenocrysts.

Even though the evidence is scanty, it is reasonable to infer that low-temperature mineralogical alteration and associated  $^{18}\text{O}$  enrichment of feldspars in the VTTS is confined to certain high-permeability pathways (i.e., fumarolic conduits) in the uppermost part of the 1912 ash-flow sheet. The late-stage low-temperature ( $<200^{\circ}\text{C}$ ) meteoric-hydrothermal circulation was obviously *much* less vigorous than the earlier high-temperature ( $>400^{\circ}\text{C}$ ) fumarolic circulation, first of all because there was then much less heat to drive low-temperature hydrothermal circulation, but also because the transport properties of  $\text{H}_2\text{O}$  change in such a way as to reduce its ability to permeate the matrix of the rock (Norton and Knight, 1977; Criss and Taylor, 1986). Also, more of the fractures may tend to become sealed by mineral deposition. Hence upward-flowing, lower-temperature fluids associated with the less vigorous, waning stages of fumarolic activity are more likely to be focused into specific conduits rather than permeating out into the matrix of the tuff, which is compatible with the observation that mineralogical and  $^{18}\text{O}/^{16}\text{O}$  effects attributable to high water/rock ratios during the waning stages of fumarolic activity appear to be most common adjacent to fumarolic conduits.

#### **4.4. Geometry of fumarolic meteoric-hydrothermal circulation**

##### *4.4.1. General Statement*

At both of the fossil fumarole sites sampled in this study (Sites ML and KC), the presence of low- $^{18}\text{O}$  groundmass provides clear-cut evidence for high-temperature fumarolic meteoric-hydrothermal activity associated with steep fissures. The flow of fumarolic fluids through the steep fissures at both sites has markedly influenced the growth direction of nearby columnar joints during cooling of the tuff (e.g., Fig. 4.5). Also, as was *a priori* expected from analyses of the upper parts of fossil fumaroles in the Bishop Tuff outflow sheet (see Chapter 2), these high-temperature, low- $^{18}\text{O}$  signatures at the VTTS have been locally overprinted by  $^{18}\text{O}$  enrichments during shallow, low-temperature hot-spring activity. This effect is clearly discernible at Site ML, because of the nature of

the fumarolic conduits at this location (i.e., single fissures well separated by several meters of unaltered tuff). This allows one to isolate the  $^{18}\text{O}$  effects around fairly simple conduit structures and to relate these effects to a specific fracture zone. For example, the fact that samples closest to the major fissures do not necessarily have the lowest  $\delta^{18}\text{O}$  values at any particular outcrop suggests that the zones adjacent to some of these conduits were overprinted by late-stage, lower temperature fluids.

#### 4.4.2. *Small, Isolated Fissures (Site ML)*

The overlapping  $^{18}\text{O}$  effects caused by high- and low-temperature  $^{18}\text{O}$  exchange in the vicinity of a fumarolic conduit are shown by whole-rock  $\delta^{18}\text{O}$  values from two of the outcrops sampled at Site ML. Samples MLA-1, MLA-2, and MLA-3 were collected from shallow-dipping columnar joints at progressively greater distances from a steep fissure (Fig. 4.11). Samples MLB-1 through MLB-4 were collected from shallowly dipping and steeply dipping columnar joints adjacent to another of these steep fissures (Fig. 4.5). In both cases, the samples with the lowest  $\delta^{18}\text{O}$  values are not located directly adjacent to the steep fissures. Samples MLA-1 through MLA-3 are strongly  $^{18}\text{O}$ -depleted relative to the the original VTTS magma, and whereas the  $\delta^{18}\text{O}$  values of samples MLB-1, MLB-1.5, and MLB-2 are not that low, they are slightly  $^{18}\text{O}$ -depleted ( $\delta^{18}\text{O} = +6.2, +5.6, \text{ and } +6.4$ ; Fig. 4.5 and Table 4.1) compared to the more steeply dipping columnar joints located 2 m away from the steep fissure ( $\delta^{18}\text{O} = +7.1 \text{ and } +6.6$ ; Fig. 4.5 and Table 4.1).

The remaining two samples from Site ML (MLC-1 and MLC-2) were collected within 50 cm of each other from shallow-dipping columnar joints at a third outcrop. Because samples were not collected from the steeply dipping columnar joints adjacent to the site where samples MLC-1 and MLC-2 were collected, it is impossible to determine if these samples are also more  $^{18}\text{O}$  depleted than surrounding tuff. In light of the above discussion regarding the low-temperature  $^{18}\text{O}$ -effects associated with mineralogical alteration of feldspars, these data may be interpreted to mean that while the volume of rock marked by

the shallow-dipping columnar joints around such fumarolic conduits probably underwent high-temperature  $^{18}\text{O}$ -exchange in the first few years after eruption, a late-stage low-temperature ( $<200^\circ\text{C}$ ) meteoric-hydrothermal overprint is also recorded. The latter effects become progressively more important closer to the fumarolic conduits, and in the case of samples MLB-1 through MLB-4 this latter effect appears to have almost completely obscured the earlier high-temperature  $^{18}\text{O}$ -effects.

The geometry of a late-stage low-temperature overprint at Site ML can be observed at both of the outcrops mentioned above. At the first outcrop (Fig. 4.11), while samples located directly adjacent to and 50 cm away from the fissure (MLA-1 and MLA-2, respectively) are both  $^{18}\text{O}$ -depleted, the sample with the lowest  $\delta^{18}\text{O}$  value (MLA-3) is located the furthest away from the fumarolic conduit ( $\approx 1.7$  m). At the second outcrop (Fig. 4.5), none of these samples (MLB-1 through MLB-4) are  $^{18}\text{O}$ -depleted relative to the VTTS magma, and we infer that this is because these rocks have all been overprinted by later, low-temperature hydrothermal activity along this fumarolic conduit. If sample MLB-1 is representative of the 1.5 cm wide bleached alteration zone directly adjacent to this fumarolic conduit, we can conclude that this zone is slightly higher in  $\delta^{18}\text{O}$  (+6.2) than a representative sample of the brown tuff (+5.6), located only 5 centimeters away; this brown tuff sample has the lowest  $\delta^{18}\text{O}$  value observed in the entire outcrop. The most plausible explanation of these results, particularly in view of the intense  $^{18}\text{O}$ -depletions observed very nearby at the ML-1, 2, 3 outcrop (see Fig. 4.11), is that circulation centered around the fumarolic conduits at Site ML, but that locally this evolved into a lower-temperature system, which caused a high- $^{18}\text{O}$  overprint that was progressively more important closer to the conduit.

An analogous pattern of whole-rock  $^{18}\text{O}$ -enrichment and depletion is present around fossil fumarole conduits in the Bishop Tuff outflow sheet, in which the edges of steep fissures at Site LG are less  $^{18}\text{O}$ -depleted than the surrounding rock (see Section 2.4.3). The similarities between the two deposits suggests that this basic  $^{18}\text{O}/^{16}\text{O}$  pattern is formed



by the same process in each, i.e. that high-temperature meteoric fluids permeated and exchanged oxygen with the groundmass in a broad zone around steep fissures during the early stages of fumarolic activity while columnar joints were forming, but that the tuff more directly adjacent to steep fissures was then elevated in  $^{18}\text{O}$  by interaction with late-stage, low-temperature fluids.

Fossil fumarole 212, whose location is shown on Fig. 1.5, is a fissure fumarole that is morphologically similar to fumarolic conduits at Site ML, and geochemical studies performed on this fumarolic conduit have important implications with regards to oxygen isotope data collected from Site ML. As discussed in Section 1.3.6, fumarole 212 is a vertical joint in the dacite-rich tuff along which the tuff has been leached and sintered as a result of the passage of fumarolic vapors along the 1-3 cm wide conduit (Papike et al., 1991). Geochemical studies of this fumarole (Spilde et al., 1993; Papike et al., 1991; Kodosky and Keith, 1993 and 1995) have shown that early, high-temperature, vapor-phase transport of halide or oxyhalide species of trace metals enriched the tuff adjacent to the conduit beneath the fumarole mound in a variety of trace metals. Late-stage, low-temperature Fe- and Cl-rich acidic condensates (Kodosky and Keith, 1993 and 1995) not only leached Fe, Mg, Ca and an assortment of other elements from the tuff adjacent to the conduit and deposited them in the fallout on the surface of the tuff, but it also resulted in preferential replacement of Ca-rich feldspar phenocrysts by amorphous silica out to a distance of  $\approx 10$  cm from the conduit (Spilde et al., 1993). Because the alteration assemblage contains smectite and halloysite, both of which are unstable above  $100^{\circ}$ - $150^{\circ}\text{C}$  (Hurst and Kunkle, 1985; Velde and Meunier, 1987), Spilde et al. (1993) estimate that the temperatures of late-stage mineralogical alteration were considerably lower than  $200^{\circ}\text{C}$ . This correlates very well with estimates of the temperature below which groundmass in the 1912 ash-flow sheet would have become  $^{18}\text{O}$ -enriched during hydrothermal exchange ( $50^{\circ}$ - $100^{\circ}\text{C}$ , see Section 4.3.1 and Figs. 2.10 and 2.11). Thus mineralogical and geochemical studies of a fissure fumarole having characteristics similar to the fumarolic

conduits at Site ML lead to the same conclusions drawn from the the VTTS  $^{18}\text{O}/^{16}\text{O}$  data; namely, that the tuff adjacent to many fumarolic conduits was affected by early, high-temperature meteoric fluids and also by late-stage, low-temperature ( $<200^{\circ}\text{C}$ ) fluids during the lifetime of fumarolic activity. Furthermore, the mineralogical alteration of the feldspar phenocrysts clearly corresponds with the later, low-temperature activity.

Very high  $\delta^{18}\text{O}$  values are also observed in near-surface samples from both the Bishop Tuff fossil fumaroles and the Chegem Tuff, indicating that low-temperature mineralogical alteration is probably very common in the uppermost parts of fumarole systems in ash-flow tuffs. In contrast, the lower parts of those same fumarolic meteoric-hydrothermal systems show little, if any,  $^{18}\text{O}$  and/or mineralogical evidence for alteration by late-stage, low-temperature fluids (Gazis et al., 1996; Holt and Taylor, 1998). Thus by analogy it is probable that a deeper,  $^{18}\text{O}$ -depleted part of the fumarolic system, equivalent to the DFS in the Bishop Tuff outflow sheet, also exists below the level of exposure at the Valley of Ten Thousand Smokes, Alaska. If there is a complete analogy with the Bishop Tuff and the Chegem Tuff, we would also expect that these deeper VTTS rocks involved in high-temperature  $^{18}\text{O}$ -exchange would have been also less affected by the low-temperature mineralogical alteration and  $^{18}\text{O}$ -exchange than the near-surface samples analyzed from Site ML (and also from Site KC, see below).

#### *4.4.3. A Large Fissure and a Concentration of Smaller Fumarolic Conduits (Site KC)*

Site KC is a much larger fumarolic feature, both in terms of size and evidence for the passage of high-temperature fumarolic vapors, than is Site ML (see discussion in Section 4.1), and it is interesting that Site KC also exhibits a correspondingly greater degree of mineralogical evidence for low-temperature alteration. Also any low- $^{18}\text{O}$  signature that may have formed during early high-temperature fumarolic meteoric-hydrothermal activity at Site KC appears to be almost completely overprinted by circulation of late-stage, low-temperature fluids through the upper part of the tuff surrounding this fumarolic conduit. At

Site KC (Fig. 4.7), shallow-dipping columnar joints 2-4 cm in diameter surround a group of steep fractures and one wide ( $\approx 70$  cm) fissure. These columnar joints clearly formed during advective cooling by the fumarolic fluids that flowed upward along steep fractures while the tuff was still very hot. Meteoric-hydrothermal activity at these temperatures would have resulted in  $^{18}\text{O}$ -depletion of the groundmass adjacent to fumarolic conduits. However, in contrast to what we might expect by analogy with the admittedly deeper-seated but nevertheless similar features in the Bishop Tuff (see Figs. 3.3 and 3.12), only one sample at Site KC is even slightly  $^{18}\text{O}$ -depleted (KC-13,  $\delta^{18}\text{O} = +4.8$ ). Also, three samples from Site KC exhibit measurable  $^{18}\text{O}$ -enrichments (Fig. 4.7 and Table 4.1; KC-2, KC-4, and KC-5), and the remainder of the samples are within the maximum plausible range of  $\delta^{18}\text{O}$  values predicted for the original VTTS magma (i.e.,  $\delta^{18}\text{O} = +5.2$  to  $+7.3$ ). If the tuff adjacent to the steep fissures at Site KC was ever strongly  $^{18}\text{O}$ -depleted as a result of high-temperature fumarolic meteoric-hydrothermal activity, these effects have been almost completely destroyed as a result of overprinting by  $^{18}\text{O}$ -enrichments associated with late-stage, low-temperature hydrothermal circulation along these fumarolic conduits. Favoring this argument is the fact that the samples at Site KC exhibit a greater degree of  $^{18}\text{O}$  enrichment than is observed at Site ML (e.g.,  $\delta^{18}\text{O} = +12.6$  for KC-2 compared to  $\delta^{18}\text{O} = +7.1$  for MLB-4) as well as stronger mineralogical evidence for low-temperature hydrothermal circulation.

Similar to the situation at Site KC, fossil fumaroles in the Bishop Tuff outflow sheet commonly exhibit very high  $\delta^{18}\text{O}$  values associated with mineralogical alteration in their upper parts. However, those large fumarolic mounds invariably have a large volume of significantly  $^{18}\text{O}$ -depleted rock directly below and deeper in the tuff (see Chapters Two and Three); therefore it can be inferred that the deeper rocks in the unexposed tuff below the cliff at Site KC also ought to have retained the low- $^{18}\text{O}$  signature that would have been imprinted by early high-temperature fumarolic activity. The largest fumarole mounds in the Bishop Tuff outflow sheet are commonly located above the biggest concentrations of

fumarolic conduits and the largest volumes of associated  $^{18}\text{O}$ -depleted rock (see Chapters Two and Three). Thus we might expect to find a similar situation if deep drill core samples are ever obtained at Site KC, because it is fairly representative of the larger fumarole mounds in the Valley of Ten Thousand Smokes.

It may also be that if a detailed search was made, we might find more evidence for  $^{18}\text{O}$ -depleted rocks on either side of Site KC. At the first outcrop studied at Site ML (Fig. 4.11), the sample with the lowest  $\delta^{18}\text{O}$  value was collected farthest from the fissure. At progressively greater distances on either side of the fissures exposed at Site KC, the tuff exhibits less evidence for low-temperature mineralization. Thus it is conceivable that the rocks on either side of the set of fissures at Site KC might locally have preserved a low- $^{18}\text{O}$  signature related to early, high-temperature fumarolic activity. Indeed, samples with the lowest  $\delta^{18}\text{O}$  values observed anywhere at Site KC were collected at nearly the greatest lateral distance ( $\approx 3.5$  m) from the large fissure exposed there (Fig. 4.7; KC-13 and KC-14). Unfortunately, in this study, no samples were collected any farther than 3.5 m away from the fissure, so another sampling trip would be necessary to test these ideas.

## 4.5. Discussion

### 4.5.1. Level of Exposure of Fumarolic Plumbing in the VTTS

The similarities in morphology and  $^{18}\text{O}/^{16}\text{O}$  systematics of fossil fumaroles in the 1912 ash-flow sheet with fossil fumaroles in the Bishop Tuff outflow sheet strongly suggest that fumarolic activity in these systems was also very similar. Whereas the VTTS has the advantage that fumarolic activity was directly observed and could be monitored over time, the Bishop Tuff outflow sheet has the perhaps even greater advantage of extensive exposure of the underlying fumarolic plumbing system (see Chapter 2). Without drill core samples, we will never know exactly what the  $^{18}\text{O}/^{16}\text{O}$  distribution is like with depth in the VTTS ash-flow sheet. Nonetheless, because of the morphological similarities between the fumarolic features on the surfaces of the two deposits, there is every reason to believe that plumbing

systems analogous to those associated with fumarolic mounds in the Bishop Tuff also should be found beneath the present level of exposure of the (now fossil) fumaroles of the 1912 ash-flow sheet. It should also be pointed out that as far as has presently been sampled, the  $^{18}\text{O}/^{16}\text{O}$  relationships are very similar in both ash-flow sheets. For example, both exhibit a characteristic  $^{18}\text{O}/^{16}\text{O}$  signature of low- $^{18}\text{O}$  groundmass coexisting with normal- $^{18}\text{O}$  feldspar phenocrysts, and both show a similar overall range in whole-rock  $\delta^{18}\text{O}$  ( $-0.1$  to  $+12.6$  at the VTTS vs.  $-6.5$  to  $+16.7$  in the Bishop Tuff). The similarities even extend to the  $\delta^{18}\text{O}$  values of the surface meteoric waters that supplied the fumarolic activity ( $-14$  to  $-16$  at the VTTS vs.  $-13$  to  $-18$  at Long Valley caldera; Keith et al., 1992 and White et al., 1991).

Active fissure fumaroles in the 1912 ash-flow sheet were anywhere from tens of meters to over 240 m long (Keith, 1991; Allen and Zies, 1923). Allen and Zies (1923) estimated that the largest fissures were up to 1.5 m in width and up to 3 m in depth. However, with the benefit of additional depth exposure afforded by erosion along the upper portions of Knife Creek and the River Lethe in the years since 1919, it is apparent that fissures commonly extend to depths greater than tens of meters (Keith, 1991; this study). In the Bishop Tuff outflow sheet, fissures that are present in fumarolic mounds on the surface of the tuff are commonly connected to a main underlying conduit (steep fissure or tubular conduit) by many smaller, disorganized fractures. Thus the depth of the actual orifice on the mound does not reflect the vertical extent of the high-permeability structure exposed beneath it (see Chapters 2 and 3). Figs. 3.8 and 3.9 illustrate how cracks in fumarole mounds on the surface of the Bishop Tuff are only rarely directly connected to fissures present at depth. Therefore, by analogy to the Bishop Tuff outflow sheet, fissures exposed in the upper part of the 1912 ash-flow sheet almost certainly connect to underlying conduits. Also by analogy to the Bishop Tuff, these underlying conduits are probably much larger than fissures exposed in the fumarolic vents in the near-surface portions of the ash flow sheet.

There are some direct observations of the active fumaroles in the Valley of Ten Thousand Smokes VTTS regarding their underlying fumarolic plumbing systems. Allen and Zies (1923) reported that there were vents along the bottom of 3-m-deep fissures in the tuff, clearly indicating that at least these particular fissures were connected to an underlying fumarolic circulation system. Also, temperature measurements of the gases emanating from fumarolic vents (Shipley, 1920; Allen and Zies, 1923) indicated that temperatures of gases emanating directly from vigorous vents (up to 645°C) were always much higher than temperatures of gases emitted by the tuff even a few meters away (where the temperatures were typically about 100°C). Thus the more vigorous fumarolic vents were evidently tapping a deeper, much hotter source of fumarolic vapor than the immediately neighboring ash-flow tuff. By analogy to the Bishop Tuff outflow sheet, fumarolic gases emanating from vigorous vents on the surface of the 1912 ash-flow sheet would have been tapping into a DFS-type of circulation system along high-permeability structures (steep fissures and tubular conduits) at depths of up to 80 m, whereas the neighboring ash-flow tuff would have been warmed mainly by residual heat from the cooling ash-flow sheet, and by circulation of small amounts of meteoric H<sub>2</sub>O along shallow joints in the upper 25 m of the tuff (e.g., see Figs 3.6 and 3.14).

Morphological and geochemical studies of the shallow fumarolic conduits exposed in the VTTS also suggest that these are only the upper parts of a much more extensive, unexposed fumarolic plumbing system. The widest parts of fissures on the surface of the tuff rarely extend to depths greater than 3 m, but these are connected to narrow fractures that appear to extend well below the current level of erosion. For example, at Site KC, the fissure is about 70 cm wide near the top, and it thins to a width of only about 30 cm at the base of the exposure (6 m depth). Keith (1991) records that some steep fissures are at least several tens of meters deep. Also, Papike et al. (1991) reports the results of geochemical studies which indicate that, relative to the unaltered dacite-rich protolith, both the part of the tuff exposed adjacent to the fumarolic conduit and the fumarolic incrustations on the surface

of the tuff were enriched in certain elements during early, high-temperature fumarolic activity. Mass balance considerations led Papike et al. (1991) to suggest that the entire exposed part of the fossil fissure fumarole was only the upper part of a much larger, deeper fumarolic circulation system.

#### 4.5.2. *Lifetime of Fumarolic Activity in the Valley of Ten Thousand Smokes, Alaska*

Studies of fossil fumaroles in the Bishop Tuff outflow sheet indicate that fumarolic activity may have ended abruptly when the lower, densely welded part of the tuff cooled sufficiently to develop an interconnected fracture network, thereby releasing fumarolic fluids trapped in the upper part of the tuff to descend through the ash-flow sheet and into the underlying Sherwin Till (see Chapters 2 and 3). Calculations of the time interval over which this might be expected to occur are in good agreement with the lifetimes of the overall fumarolic system calculated using kinetic models of  $^{18}\text{O}$ -exchange exhibited by feldspar phenocrysts during fumarolic activity (10-25 years). Because the waning of fumarolic activity at the 1912 ash-flow sheet was actually documented using photography and temperature measurements of fumarolic gases and because the thickness of the 1912 ash-flow sheet is known (Kienle, 1991), this historical example of fumarolic activity in ash-flow tuffs provides an important test of the ideas put forward in Chapter 5 of this thesis regarding the mechanism by which such activity wanes and finally terminates.

Heat flow calculations regarding the length of time it would take for the densely welded part of the 1912 ash-flow sheet to cool are essentially identical to those carried out for the Bishop Tuff outflow sheet (see Chapter 2). This is because the thickness of the densely welded zone is probably about 100 m thick in the thickest part of the VTTS deposit in the upper River Lethe area, which is exactly the thickness of densely welded tuff used in the calculations for cooling of the densely welded part of the Bishop Tuff in Chapter 2. The longest-lived fumaroles on the surface of the tuff would *a priori* be expected to be found over this part of the VTTS ash-flow deposit, and this was indeed the case, as reported by

Keith (1991) and Lowell and Keith (1991). These authors report observations that a few fumaroles were active in the upper River Lethe area and near Baked Mountain until the mid-1930's, a little over 20 years after the eruption. Also, although the composition of the upper part of the 1912 ash-flow sheet is more mafic than the Bishop Tuff, the bulk of the deposit and possibly all of the densely welded tuff is composed of an analogous high-silica rhyolite (Hildreth, 1983), and therefore the heat capacity and latent heat value for the tuff that was used in the calculations is the same in both cases.

Heat flow calculations using the parameters discussed in Chapter 2 predict that the thickest part of the 1912 ash-flow sheet would have finished developing an interconnected fracture network through the densely welded part of the tuff between 10 and 25 years after eruption (see discussion in Section 5.8.2). This is in excellent agreement with the observed length of time over which fumarolic activity occurred at the Valley of Ten Thousand Smokes, Alaska, where active fumaroles in most areas were extinct by 1923, while fumaroles in the thickest part of the deposit along the upper part of the River Lethe were observed until the mid-1930's (Keith, 1991). Parts of the valley in which the tuff was thinnest would have cooled and fractured more quickly, releasing fumarolic fluids to descend through to the base of the tuff. Allen and Zies (1923) observed this phenomenon, and they recorded that fumaroles were cooling off and going extinct more quickly in the distal and marginal parts of the ash-flow sheet.

Hot spring development in the VTTS may have been a hydrologic response to throughgoing fracture development in the parts of the densely welded tuff, as this would release H<sub>2</sub>O to flow out of the valley along the base of the ash-flow sheet rather than to be entrained in fumarolic circulation in the upper part of the tuff. Researchers on the 1919 expedition to the VTTS observed the presence of 97°C hot springs near Three Forks that had not been there in the previous expedition to the valley in 1917 (Allen and Zies, 1923). The 1919 expedition also observed that fumarole temperatures had declined significantly even since the 1918 expedition and that many fumaroles were extinct in the distal and



marginal parts of the deposit (Allen and Zies, 1923); Thus, while the fumarolic activity was observed to be sharply decreasing each year, hot -spring activity was observed to become more wide-spread (Allen and Zies, 1923). At the present time, numerous warm springs are still observed to be active at various locations in the VTTS. Keith et al. (1992) and Lowell and Keith (1991) postulate that hundreds of these warm springs (15°-27°C) that discharge over a distance of 300 m into a 15-m-deep gorge through vertical joints in the ash-flow tuff have been heated by interaction with an incompletely cooled lobe of densely welded ash-flow tuff. In addition, present-day cold springs issue from fractures in the tuff along the River Lethe gorge just above the contact with the Naknek formation (Fig. 4.4; Keith et al., 1992), a testament to the very high fracture permeability that still exists in the ash-flow sheet.

#### **4.6. Summary**

Fossil fumaroles in the 1912 ash-flow sheet at Valley of Ten Thousand Smokes, Alaska, are analogous to fossil fumaroles in the Bishop Tuff outflow sheet, California, both in terms of morphology and  $^{18}\text{O}/^{16}\text{O}$  characteristics. The  $\delta^{18}\text{O}$  values of groundmass and feldspar phenocrysts from the 1912 ash-flow sheet exhibit an oxygen isotope signature that is unique to short-lived, high-temperature fumarolic activity in ash-flow tuffs (i.e., low- $^{18}\text{O}$  groundmass coexists with feldspar phenocrysts that retain magmatic  $\delta^{18}\text{O}$  values), and which has been previously observed only in the Bishop Tuff and the Chegem Tuff (Holt and Taylor, 1998; Gazis et al., 1996).

Exposures at the VTTS are unfortunately limited to just the uppermost 20-30 m of the fumarolic plumbing systems, and it is likely that high-permeability structures analogous to those studied in the Bishop Tuff outflow sheet (i.e., steep fissures and tubular conduits) exist at depth beneath the fumarole mounds in the VTTS. The actually observed and recorded lifetimes of fumarolic activity in the VTTS are in near-perfect agreement with estimates of the lifetimes of the meteoric-hydrothermal fumarolic system in the Bishop Tuff

outflow sheet, which are based on oxygen isotope exchange kinetics of feldspar phenocrysts, on heat-flow calculations, and on the idea that the cessation of fumarolic activity occurs when throughgoing fractures are able to penetrate the hot and initially impermeable lower zone of the tuff.

**Table 4.1** Oxygen isotope analyses of samples from the 1912 ash-flow sheet at the VTTS. WR=whole rock, PUM=pumice, FELD=feldspar, GM=groundmass

Sample No.	Description	$\delta^{18}\text{O}$	Sample No.	Description	$\delta^{18}\text{O}$
<i>Mageik Lakes (Site ML); 58°14.41', 155°10.07'</i>			<i>Knife Creek (Site KC); 58°18.52', 155°10.07'</i>		
MLA-1	PUM	3.2, 3.6	KC-1	WR	5.9
MLA-1	WR	0.2	KC-2	WR	12.6
MLA-2	PUM	3.3, 3.4	KC-2	PUM	9.8
MLA-2	WR	1.7	KC-2-feld	FELD	8.46
MLA-3	PUM	2.1, 3.0	KC-3	WR	6.5
MLA-3	WR	-0.1	KC-4	GM, white	7.6
MLA-3-feld	FELD	6.28	KC-4	PUM	7.1
MLB-1	GM, grey	6.2	KC-5	GM, pink	7.9
MLB-1.5	GM, brown	5.6	KC-5	PUM	7.3
MLB-2	WR	6.4	KC-6	WR	7.3
MLB-3	WR	7.1	KC-7	WR	6.6
MLB-3-feld	FELD	6.28	KC-7	GM, white	7.0
MLB-4	WR	6.6	KC-8	WR	6.8
MLC-1	WR	6.7	KC-9	WR	6.2
MLC-2	WR	6.5	KC-10	WR	6.6
<i>River Lethe (Site RL); 58°20.28', 155°17.48'</i>			KC-11	WR	6.2
RL-1	WR	5.9	KC-12	WR	6.2
RL-2	WR	5.9	KC-13	PUM, grey	5.6
			KC-13	PUM, brown	6.1
			KC-13	GM, pink	5.3
			KC-13	GM, white	4.8
			KC-14	PUM	5.6

### Figure Captions

Fig. 4.1. Map of the Valley of Ten Thousand Smokes, showing the distribution of the 1912 ash-flow sheet (dark grey shading; Hildreth and Fierstein, 1987), and the three sites that were sampled in this study: River Lethe (RL), Knife Creek (KC), and Mageik Lakes (ML). Novarupta is a rhyolite lava dome centered on the vent of the 1912 eruption, although caldera subsidence in 1912 also occurred atop Mt. Katmai to form a Crater Lake. Trident, Mt. Katmai, and Mt. Griggs are all andesite-dacite stratovolcanoes, as are Mt. Martin and Mt. Mageik (located 6 and 13 km southwest of Katmai Pass, respectively, and not shown on this map). Mt. Cerberus (C) and Falling Mountain (F) are Holocene dacite domes adjacent to the 1912 vent. Baked Mountain (B), Broken Mountain (Br), the Buttress Range, and Mts. Katolinat and Juhle consist of Jurassic sedimentary rocks. The light stippled pattern around the higher peaks indicates glaciers.

Fig. 4.2. U.S. Air Force aerial photograph of the Valley of Ten Thousand Smokes. The view is looking northwest across the valley towards the Buttress Range. Knife Creek runs north along the right-hand side of the photograph; the River Lethe runs horizontally from left to right across the top of the photograph. Windy Creek runs northeastward along the north side of the Buttress Range and intersects Knife Creek and the River Lethe at Three Forks, which is located in the upper right of the photograph. Novarupta Dome is visible in the left center of the photograph in the depression between Baked Mountain and the sheared off face of Falling Mountain. The rippled surfaces of glaciers on Mt. Katmai and Trident Peaks are visible in the foreground. Sample locations from this study are indicated by the three white dots (compare with Fig. 4.1).

Fig. 4.3. Photograph of the 1912 ash-flow sheet at Site RL along the River Lethe. Note conspicuous absence of shallow-dipping columnar joints in the sintered ash flow. The tuff

is about 35 m thick and unwelded at Site RL, which is located at the edge of the ash-flow sheet where it abuts the Buttress Range. The location from which sample RL-2 was collected is shown by the white dot at the base of the cliff in the foreground; the location from which sample RL-1 was collected is around the corner on this same cliff, about 5 m below sample RL-2 and about 1.5 m above the level of the River Lethe.

Fig. 4.4. Photograph of springs issuing from fractures in the tuff of the Valley of Ten Thousand Smokes along the east side of the River Lethe where its course runs close to the Buttress Range just northwest of Site RL.

Fig. 4.5. Photograph of Site ML showing a steep fissure and its associated shallow-dipping columnar joints. Note that the columnar joints steepen and become fan-shaped in the lower part of the outcrop (perhaps approaching a subhorizontal tubular conduit?). The tuff on either side of the fissure is bleached blue/white. Whole-rock  $\delta^{18}\text{O}$  values for samples MLB-1, MLB-1.5, MLB-2, and MLB-3 are shown in their respective sampling locations (see Table 4.1). Sample MLB-1 was collected from the grey tuff directly adjacent to the fissure. Sample MLB-1.5 was collected from brown tuff at a location 5 cm away from the bleached zone. Sample MLB-4 was collected within a set of steeply dipping columnar joints 1 m to the right of this photograph. At this location, the bottom of the rock face is at least 3-4 m below the level of the ice. Professor Ken Farley is shown for scale; he is 1.8 m tall.

Fig. 4.6. Photograph of two small fumarole mounds on the surface of the ash-flow sheet near Site ML. The dark patch marking the apex of each of the mounds is actually very brightly colored (red, orange, yellow, and black) as a result of Fe-oxide and Fe-hydroxide precipitation on the surface of the tuff during fumarolic activity. Note the goretex mitten in the right-center of the photograph for scale.

Fig. 4.7. (a) Photograph of the east side of Knife Creek Gorge at Site KC, showing a large fumarole mound dissected by Knife Creek and illustrating the abundant shallow-dipping columnar joints associated with a wide ( $\approx 70$  cm) steep fissure, just beneath the large mound. The groundmass in the upper part of the tuff is alternately bleached and stained with Fe-oxide mineralization. The mound itself is cemented with Fe-oxides and silica, accounting for its deep red to black color. Steep fissures converge and narrow with depth in the tuff at Site KC. Similarly, Fe-oxide staining decreases with depth and also with lateral distance away from the large fissure. (b) Photograph of the right-hand portion of the same cliff face shown in Fig. 4.7a. For the most part, the curvilinear fractures shown in the photograph are the mirror image of the fractures present on the west side of the gorge, which was much easier to sample. Relative to the appropriate structural features, which are roughly at right angles to the cliff face, the letters on this photograph of the east side of the gorge correspond very closely to the positions of the samples collected adjacent to these same structures on the west side of the gorge, as follows: A=KC-1, B=KC-2, C=KC-4, D=KC-5, E=KC-6, F=KC-7, G=KC-11, H=KC-12, I=KC-14, J=KC-13, K=KC-3, L=KC-8, M=KC-9, N=KC-10 (See Table 4.1).

Fig. 4.8. Values of  $\delta^{18}\text{O}$  for coexisting quartz, plagioclase, orthopyroxene, and titanomagnetite separated from Novarupta lava and from individual pumice blocks from the 1912 ash-flow deposits and fall units A, C, D, and G (from Hildreth, 1987). Andesite (a), dacite (d), rhyolite (r). The analyses for Falling Mountain (+) and Mount Cerberus (x) are on whole-rock crystalline dacite.

Fig. 4.9. Distribution of whole-rock, pumice, and groundmass  $\delta^{18}\text{O}$  values for all samples collected in the upper parts of the tuff from the Valley of the Ten Thousand Smokes, the intracaldera Chegem Tuff (Gazis et al., 1996), and the Bishop Tuff outflow

sheet (Table 2.2). The  $^{18}\text{O}/^{16}\text{O}$  data shown in the diagram are from only those samples collected in the uppermost 5-10% of the maximum stratigraphic thickness of each deposit. For the tuff from the Valley of Ten Thousand Smokes, multiple analyses of the same sample are shown, as are pumice and groundmass separates from the same whole-rock sample (compare with Table 4.1). Sampling site abbreviations for the tuff from the Valley of Ten Thousand Smokes and the Bishop Tuff outflow sheet are shown in the legend. The expected ranges for the  $\delta^{18}\text{O}$  values for the respective magmas from each eruption center are shown by the shaded boxes. The range in expected  $\delta^{18}\text{O}$  values for the Valley of Ten Thousand Smokes magma is estimated using the  $^{18}\text{O}/^{16}\text{O}$  data on phenocryst phases (Hildreth, 1987; see Fig. 4.8). This VTTS range is larger than that of either the Bishop Tuff or the Chegem Tuff because of the unusually large compositional range of the magmas that erupted there in 1912.

Fig. 4.10.  $\delta^{18}\text{O}$  values of three samples (MLA-3, MLB-3, and KC-2) of whole rock and pumice from the 1912 ash-flow sheet plotted against the  $\delta^{18}\text{O}$  values of the coexisting feldspar phenocrysts in these samples. Vertical bands show the ranges of  $\delta^{18}\text{O}$  values for feldspars analyzed by Hildreth (1987) for the rhyolite (solid dark grey;  $n=6$ ) and the dacite/andesite (light grey stipple;  $n=5$ ) parts of the ash-flow sheet. Together with the rhyolite  $^{18}\text{O}/^{16}\text{O}$  data of Hildreth (1987), the ML-3 and ML-2 samples define the same kind of steep trajectory that is characteristic of the Bishop Tuff (Chapter 2) and the Chegem Tuff (Gazis et al., 1996). However, the feldspars in sample KC-2 have clearly undergone an anomalous shift to a higher  $\delta^{18}\text{O}$  value (as a result of low-temperature alteration, see text). Diagonal lines for  $\Delta^{18}\text{O}_{\text{feldspar-wholerock}}$  at  $\Delta=1$  and  $0$  encompass the range of pristine, magmatic values, and they are shown for reference only ( $\Delta^{18}\text{O}_{\text{feldspar-wholerock}} = \delta^{18}\text{O}_{\text{feldspar}} - \delta^{18}\text{O}_{\text{wholerock}}$ ).

Fig. 4.11. Sketch of the outcrop at Site ML from which the extremely  $^{18}\text{O}$ -depleted samples MLA-1, MLA-2 and MLA-3 were collected. Whole-rock  $\delta^{18}\text{O}$  values are indicated at each sample location. For  $\delta^{18}\text{O}$  values of pumice and feldspar separates from these same samples, see Table 4.1. The escarpment from which these samples were collected is about 3 m high. Shallow-dipping columnar joints are shown by the thin black lines. The tuff 1-2 cm on either side of the steep fissure is lighter colored and is shown by the stippled pattern. Ash-flow tuff with grey-brown colored groundmass, which is typical of the dacite-rich ash-flow sheet away from the fissures at Site ML, is indicated by the grey shading.



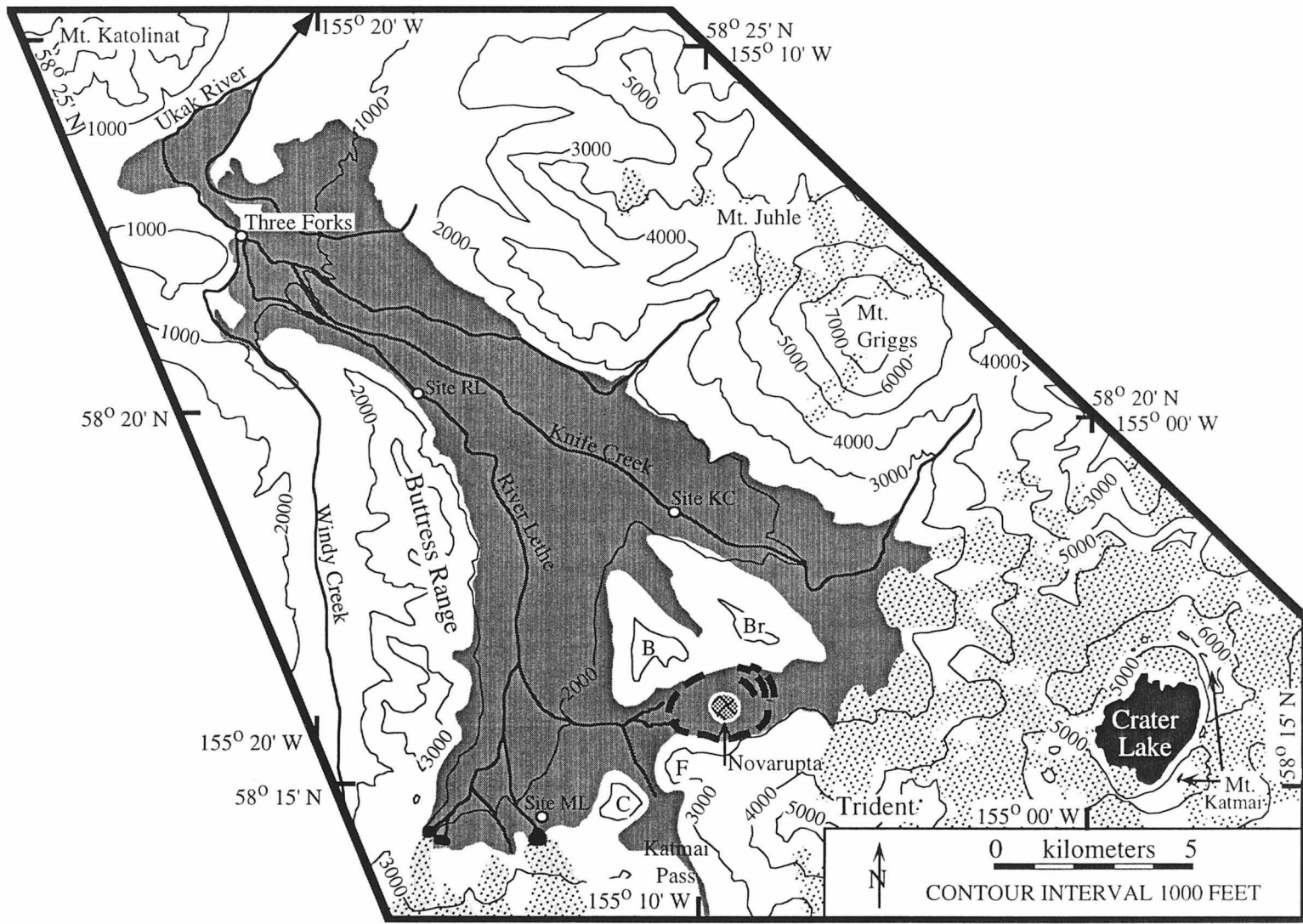


Fig.4.1



Fig. 4.2

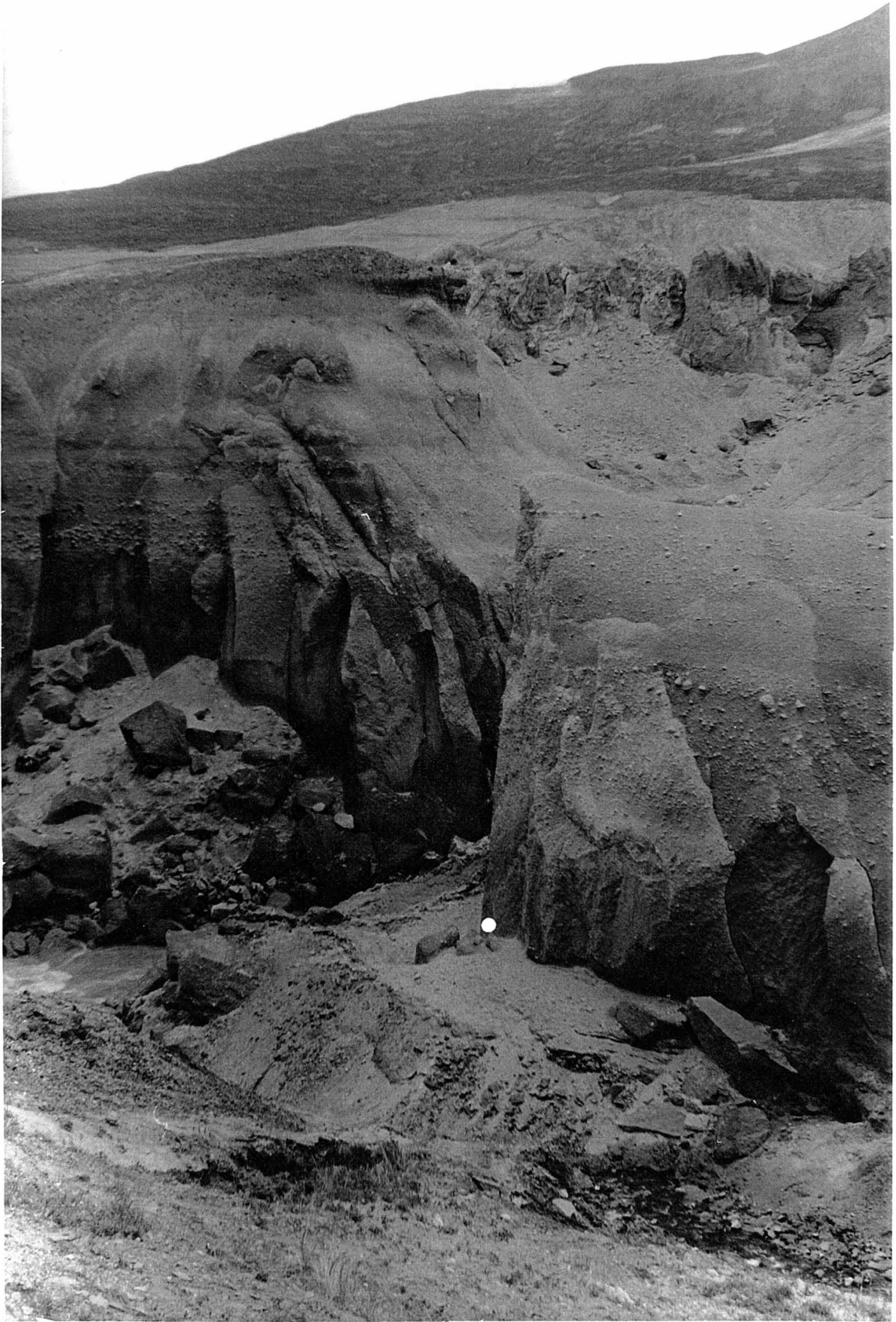


Fig. 4.3

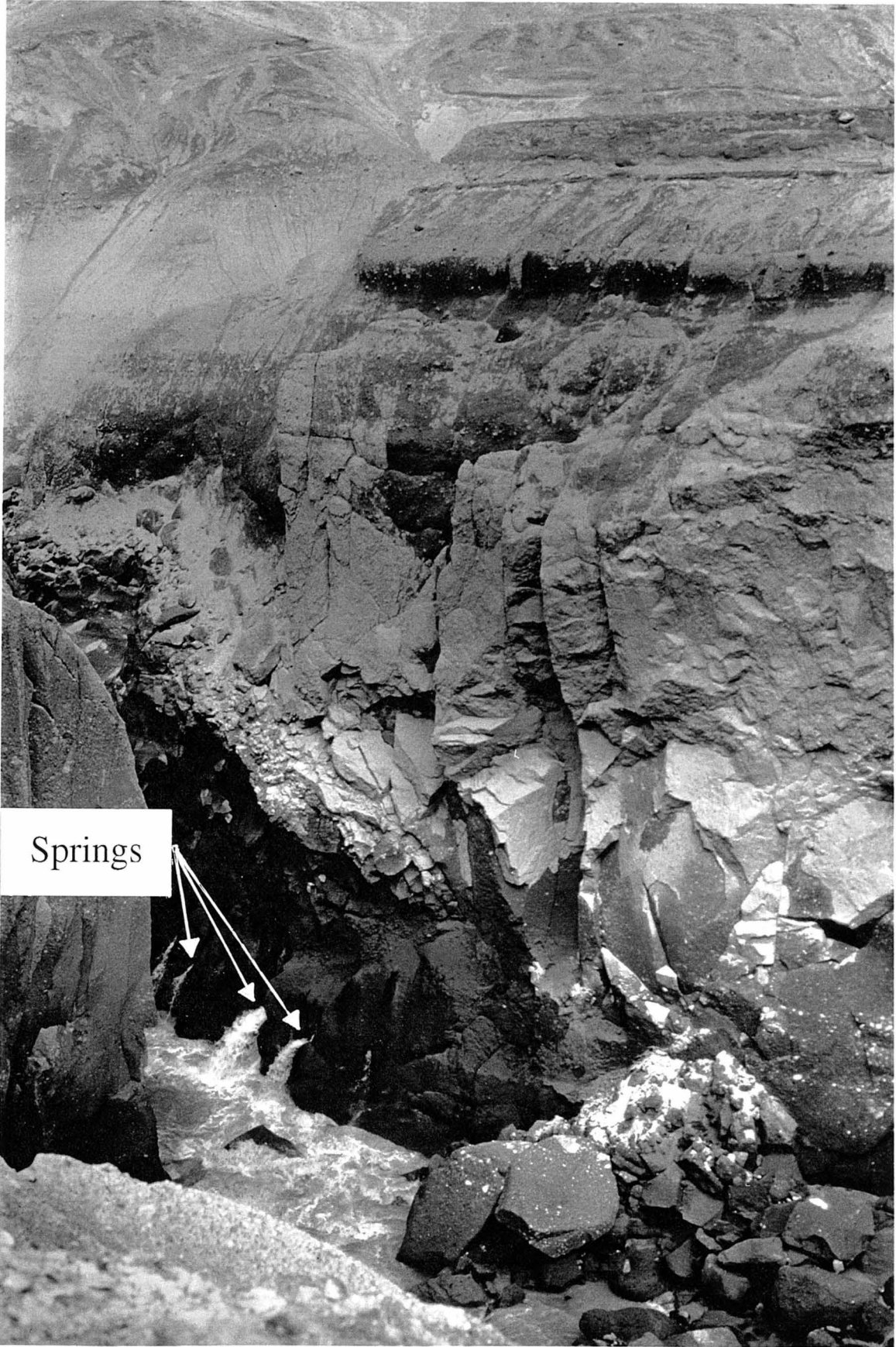
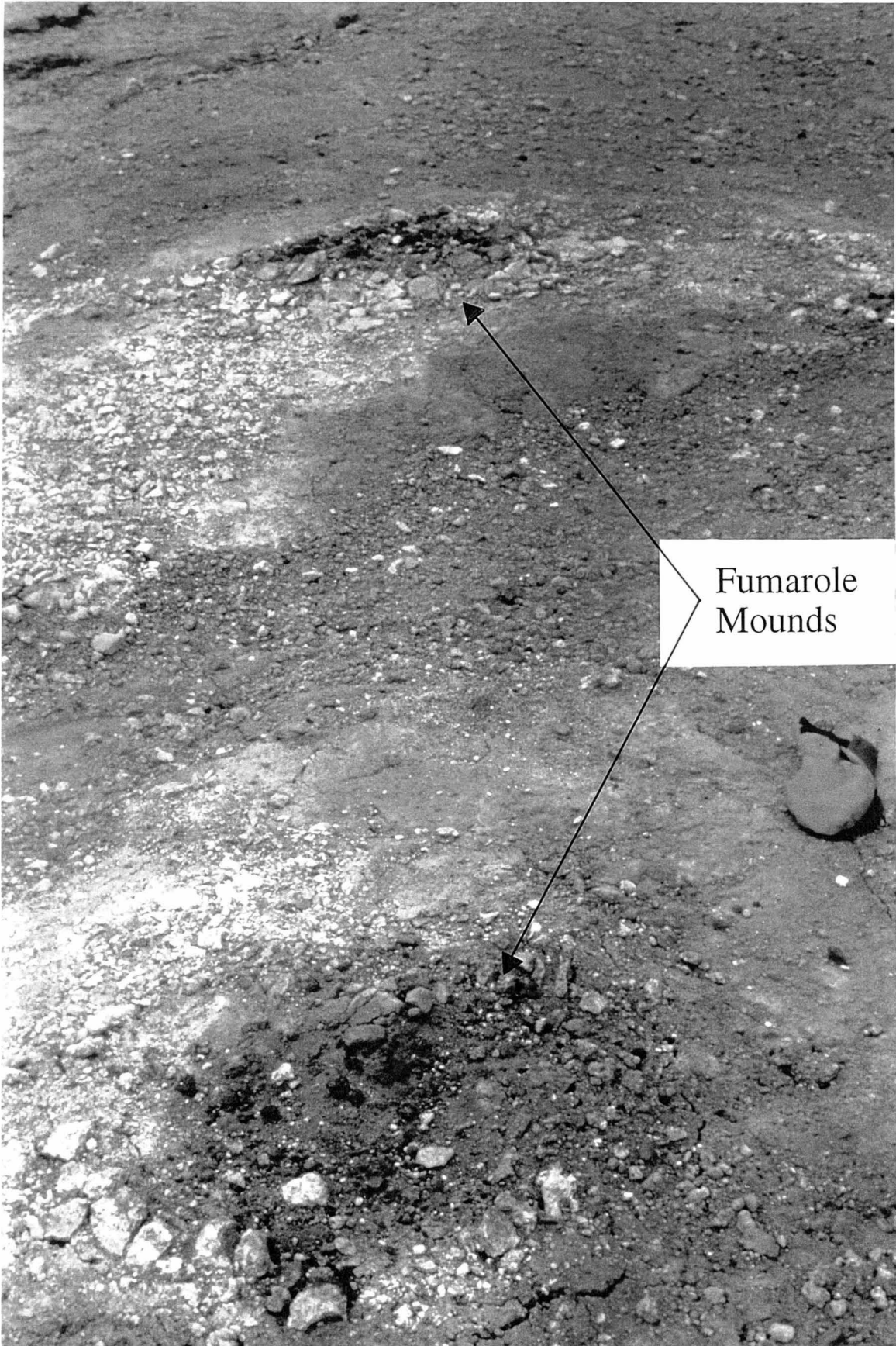


Fig 4.4



Fig. 4.5



Fumarole  
Mounds

Fig.4.6



Fig.4.7a

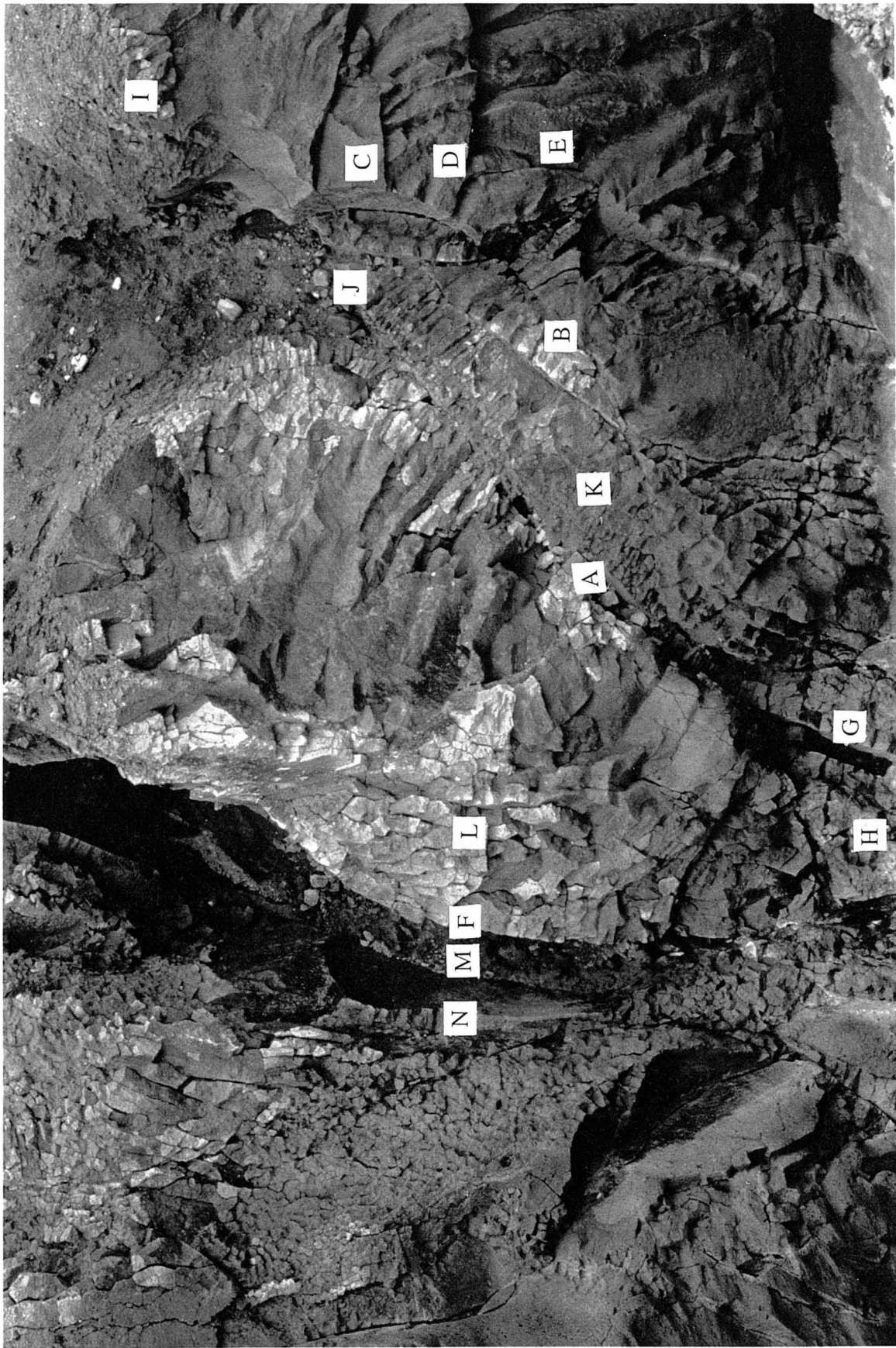


Fig. 4. 7b



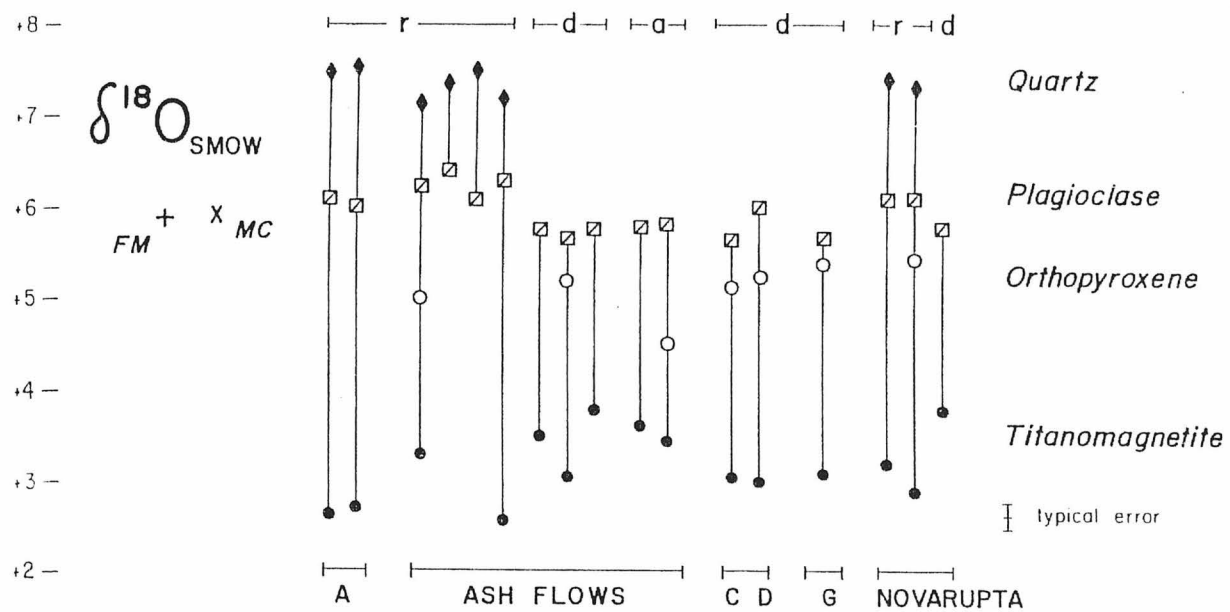


Fig. 4.8

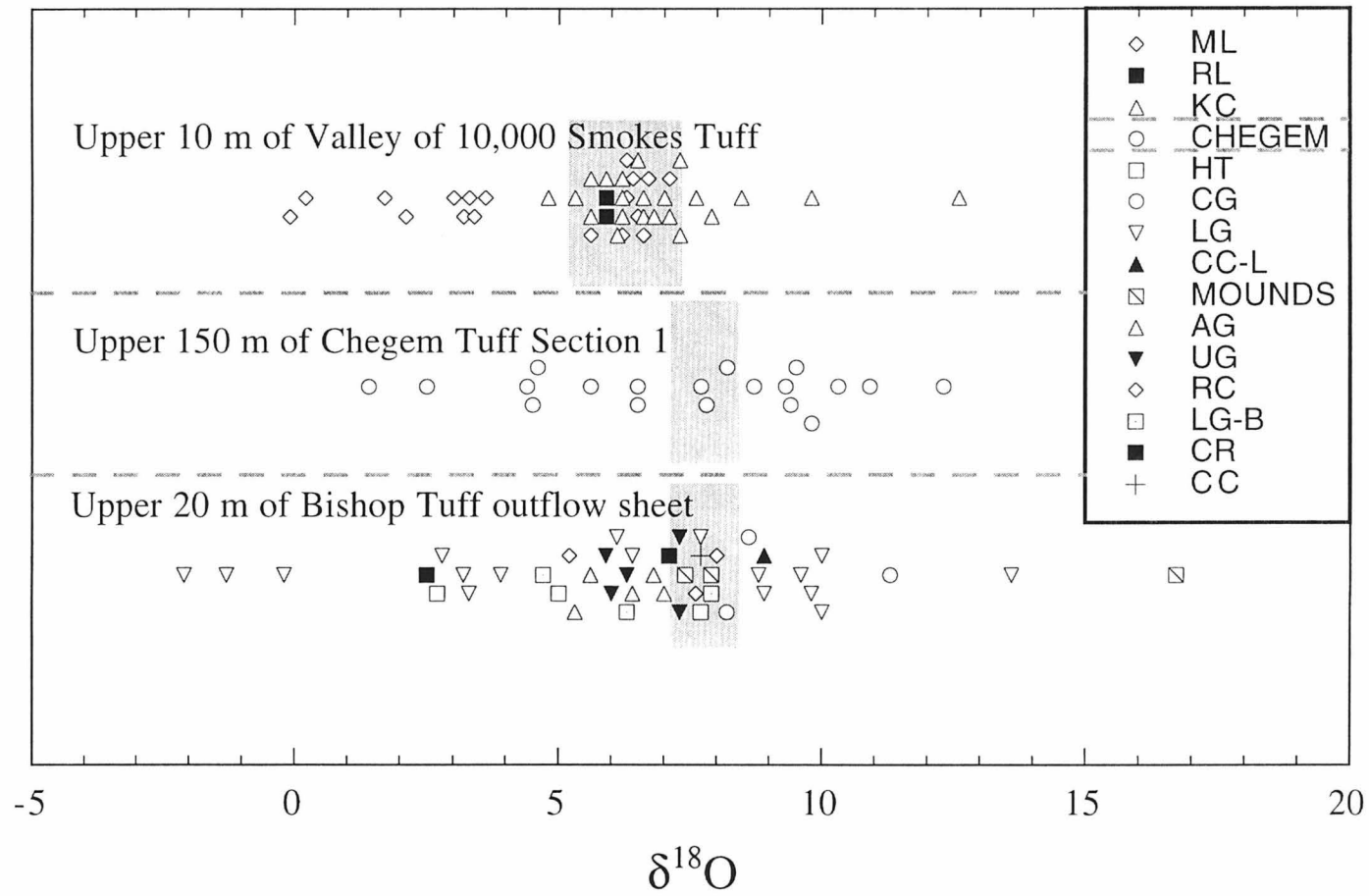


Fig.4.9

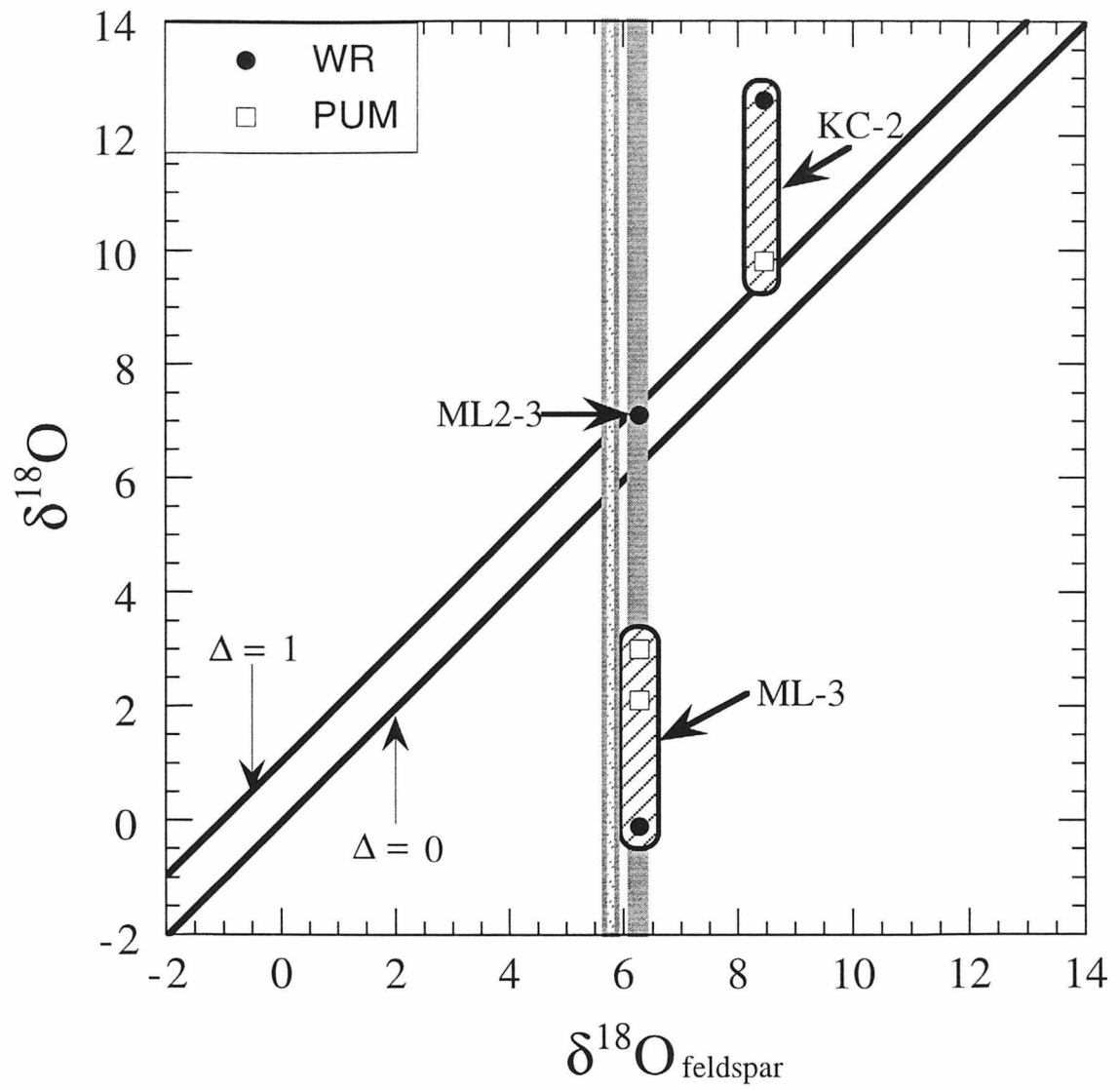


Fig. 4.10

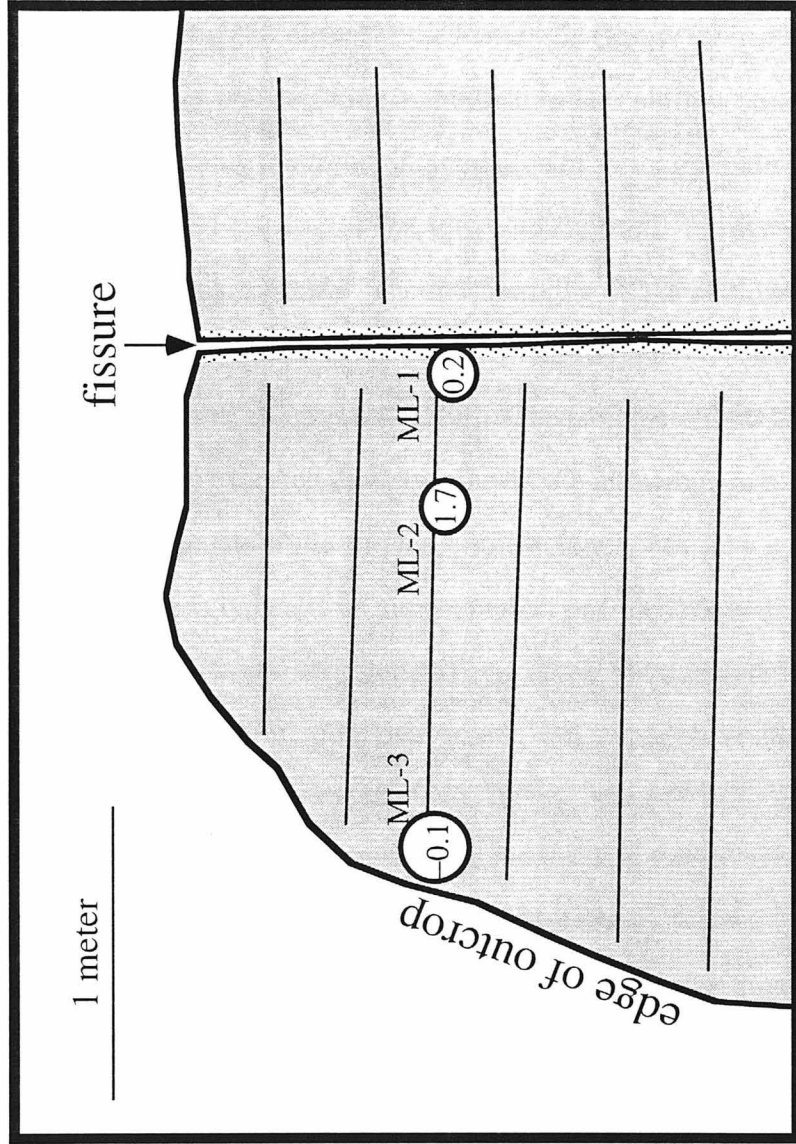


Fig. 4.11

## CHAPTER 5: CONCLUSIONS AND RELATIONSHIP OF THIS WORK TO OTHER STUDIES

### 5.1. General conclusions about fumarolic activity in the upper parts of ash-flow sheets

#### 5.1.1. Circulation Geometries and Origin of the Fumarolic Gases

The patterns of whole-rock  $^{18}\text{O}$  depletion in the Bishop Tuff outflow sheet demonstrate that fumarolic activity was mainly the result of circulation of meteoric-hydrothermal fluids in the upper, partially welded portion of the tuff, and that this involved two broadly different kinds of hydrodynamic systems. The most striking  $^{18}\text{O}$  depletions (with whole-rock  $\delta^{18}\text{O}$  as low as  $-6.5$ ) are directly associated with mapped fumarolic structures in what we have termed the Deep Fumarolic System (DFS). The isotopic effects in the DFS are confined to the volume of rock located directly beneath the numerous fumarolic mounds and ridges scattered across much of the surface of the southeastern lobe of the ash-flow sheet. Within the DFS there is typically an almost perfect one-to-one correlation between the low whole-rock  $\delta^{18}\text{O}$  values and the geometry and distribution of fumarolic conduits (e.g., steep fissures, shallow-dipping columnar joints, and tubular conduits, etc.). The DFS commonly extends downward about 60 to 100 m into the tuff, with its lower boundary being defined by a very sharp transition to the much higher  $\delta^{18}\text{O}$  values that are everywhere characteristic of the black tuff in the underlying Densely Welded Zone (DWZ).

Higher up in the section, and typically extending no deeper than about 40 to 50 m beneath the surface of the ash-flow sheet, there is another zone of  $^{18}\text{O}$ -depletion in which the whole-rock  $\delta^{18}\text{O}$  values are typically about  $+2.5$  to  $+6.5$ ; these rocks are definitely  $^{18}\text{O}$ -depleted relative to the original Bishop Tuff magma ( $\delta^{18}\text{O} = +7.6$ ), but much less so than the rocks underlying the fumarolic mounds. We have termed this broadly based, stratigraphically bound, 20- to 40-m-thick part of the section the Upper Low- $^{18}\text{O}$  Zone (ULZ). This zone in the upper part of the tuff appears to be continuous over a broad area,

including the regions where there is morphological evidence for fumarolic activity, and also locally outside those areas.

The whole-rock  $^{18}\text{O}/^{16}\text{O}$  data indicate that fumarolic activity in the Bishop Tuff involved high-temperature ( $\approx 400^{\circ}\text{--}650^{\circ}\text{C}$ ) circulation of low- $^{18}\text{O}$  meteoric  $\text{H}_2\text{O}$  through the upper 20 to 80 m of the Bishop Tuff outflow sheet. The region-wide, weaker, and shallower meteoric-hydrothermal fumarolic system (the ULZ) locally coalesced with the much more vigorous, deeper system in the vicinity of the numerous, fumarolic mounds (the DFS). In neither of these systems were the fumarolic fluids dominantly composed of magmatic volatiles, as proposed by Sheridan (1970). The Densely Welded Zone (DWZ), which forms the lower 1/2 to 2/3 of the ash-flow sheet, is pristine and not measurably  $^{18}\text{O}$ -depleted, implying that during the fumarolic activity, this hot, ductile, welded tuff was largely impermeable to the low- $^{18}\text{O}$  meteoric fluids.

#### 5.1.2. *Contrasting Fumarolic $^{18}\text{O}/^{16}\text{O}$ Signatures in Phenocrysts and Groundmass*

Fumarolic activity in ash-flow sheets results in a unique  $^{18}\text{O}$  signature, i.e., that of strongly  $^{18}\text{O}$ -depleted groundmass and fiamme in coexistence with quartz and feldspar phenocrysts that have closely preserved their original magmatic  $\delta^{18}\text{O}$  values. Such phenocrysts were analyzed in samples of tuff from fossil fumaroles in the 1912 ash-flow sheet in the Valley of Ten Thousand Smokes, Alaska (VTTS) and in the Bishop Tuff outflow sheet, and in both areas we observed a very wide range of whole-rock  $\delta^{18}\text{O}$  values (0.0 to +12.0) coexisting with extremely uniform quartz and feldspar  $\delta^{18}\text{O}$  values. In contrast, in the "classic",  $300^{\circ}\text{--}350^{\circ}\text{C}$  types of meteoric-hydrothermal systems associated with igneous plutons, coexisting feldspar phenocrysts are typically strongly depleted in  $^{18}\text{O}$  along with the groundmass. Therefore, this study confirms the hypothesis of Gazis et al. (1996) that this type of previously unrecognized  $^{18}\text{O}/^{16}\text{O}$  signature that they discovered in the upper part of the Chegem Tuff in Russia is the result of a very high temperature

fumarolic meteoric-hydrothermal system that began immediately after eruption and which was very short-lived (10-25 years).

### *5.1.3. Temperature Range of Fumarolic Activity*

Mineralogical and  $^{18}\text{O}/^{16}\text{O}$  data from the Bishop Tuff outflow sheet, from the 1912 ash-flow sheet in the Valley of Ten Thousand Smokes (VTTS), and from the Chegem Tuff (Gazis et al., 1996) are all very consistent and indicate that the early, most vigorous stage of fumarolic meteoric-hydrothermal activity was at high-temperatures ( $\approx 400^{\circ}\text{--}650^{\circ}\text{C}$ ). Additionally, in all three of these locations there is also  $^{18}\text{O}/^{16}\text{O}$  and mineralogical evidence for late-stage, "low"-temperature ( $<150^{\circ}\text{C}$ ), hot-spring activity in the shallowest parts of these ash-flow sheets. Mineralogical evidence for moderate- to low-temperature ( $\approx 200^{\circ}\text{--}300^{\circ}\text{C}$ ) hydrothermal alteration in the deeper parts of the fumarolic systems in the Bishop Tuff outflow sheet (and in the Chegem Tuff) is strikingly absent. Although a similar statement cannot yet be made regarding the interior parts of the 1912 ash-flow sheet in the VTTS, because these rocks are not yet exposed by erosion, we predict that a similar situation will be found in the interior part of the 1912 ash-flow sheet, if and when sufficiently deep drill core samples of that tuff are obtained.

## **5.2. Fumarolic plumbing and patterns of $^{18}\text{O}$ -depletion in the Gorges Area of the Bishop Tuff outflow sheet: the Deep Fumarolic System (DFS) and the Upper Low- $^{18}\text{O}$ Zone (ULZ)**

### *5.2.1. Fumarolic Mounds and the DFS*

The lowest whole-rock  $\delta^{18}\text{O}$  values, and hence the highest implied water/rock ratios in the Bishop Tuff fumarolic systems, are spatially associated with well-defined fumarolic conduits (e.g., steep fissures and tubular conduits) in the partially welded upper part of the outflow sheet. Mapping along Rock Creek Gorge, Owens River Gorge, and along Chidago Canyon indicates that in the Gorges and Chidago areas, the fumarolic conduits

and associated  $^{18}\text{O}$ -depleted rocks that are exposed in the upper part of the ash-flow sheet are invariably located beneath fumarolic mounds and ridges on the surface of the tuff, and vice versa. As postulated by Sheridan (1970) and Putnam (1960), fumarolic mounds on the surface of the tuff are mainly erosional remnants that are a result of preferential induration of the tuff by the passage of fumarolic vapors during fumarolic activity. The exact spatial correlation between the fumarolic mounds and ridges and the fumarolic conduits in the underlying DFS suggests that enormous amounts of meteoric-hydrothermal fumarolic fluids passed upward through these mounds, judging by the very high water/rock ratios calculated for the DFS from the  $^{18}\text{O}/^{16}\text{O}$  data.

#### *5.2.2. Patterns of $^{18}\text{O}$ -depletion in the ULZ and the DFS*

All of the depth profiles sampled in and around the Gorges Area of the Bishop Tuff outflow sheet, regardless of the presence or absence of fumarolic conduits or columnar jointing in the tuff, exhibit  $^{18}\text{O}/^{16}\text{O}$  evidence for a shallow, 20- to 40-m-thick stratigraphic zone of moderate whole-rock  $^{18}\text{O}$  depletions, referred to as the Upper Low- $^{18}\text{O}$  Zone (ULZ). Whole-rock  $\delta^{18}\text{O}$  values in this zone range from +2.5 to +6.5, but are more typically about +5.5 to +6.5. The maximum whole-rock  $^{18}\text{O}$ -depletions associated with this zone are nearly always located near the base of the Tableland Unit. In the vicinity of fumarolic mounds,  $^{18}\text{O}$ -depletions in the ULZ are of greater magnitude than they are elsewhere, perhaps as a result of enhanced heat transport by underlying fumarolic conduits or because of overlap with the  $^{18}\text{O}$ -effects associated with meteoric-hydrothermal circulation in the underlying DFS.

Whereas meteoric-hydrothermal circulation in the DFS clearly extended downward at least to the level of the top of the densely welded black tuff, meteoric-hydrothermal circulation in the ULZ probably extended downward no deeper than about 40-50 m. A compilation of  $^{18}\text{O}/^{16}\text{O}$  data from all sampling sites in the Bishop Tuff outflow sheet indicates that whole-rock  $^{18}\text{O}$  depletions associated with the DFS extend down to the level



of the top of the densely welded black tuff. At the base of the DFS, there is an extremely sharp  $\delta^{18}\text{O}$  gradient ( $\approx 3$  per mil per meter) at the transition to densely welded black tuff. In contrast, whole-rock  $^{18}\text{O}$ -depletions in the ULZ never extend downward to a level any closer than about 20 m above the upper contact of the densely welded black tuff. Also, because the  $^{18}\text{O}$ -depletions in the ULZ are not as great as in the DFS, the  $\delta^{18}\text{O}$  gradient at the base of the ULZ ( $\approx 0.2$  per mil per meter) is nowhere near as steep as the  $\delta^{18}\text{O}$  gradient at the base of the DFS. The reason that  $^{18}\text{O}$ -depletions in the DFS extend to greater depth in the tuff is almost certainly a direct result of the fact that the mapped fumarolic conduits (steep fissures and tubular conduits) commonly extend downward to this level in the ash-flow sheet, but never below this level. Thus, whereas the lower boundary for the DFS is defined by the fracture permeability associated with the deepest penetration of fumarolic conduits into the ash-flow sheet, the lower boundary of the ULZ may be more a function of (1) a possible permeable horizon at the base of the Tableland Unit, and (2) the degree of welding and hence the matrix permeability of the tuff.

The present study demonstrates that significant interactions between the tuff and the meteoric-hydrothermal fluids need not be associated with obvious morphological evidence for fumarolic activity, because this is most often the situation in the ULZ. The type of fumarolic activity associated with the ULZ can be identified solely by means of  $^{18}\text{O}/^{16}\text{O}$  analyses, even in cases where such activity was too weak to allow *any* fumarolic morphological features to develop, or where fumarolic morphological features are not exposed or have been largely destroyed by tectonism and erosion. This is particularly useful in the cases where the only rocks available are from drill core, as is the case in many young intracaldera tuffs (see below).

#### 5.2.5. *Material-Balance Water/Rock Ratios*

Material-balance water/rock ratios calculated for the ULZ and the DFS, integrated over the lifetimes of these fumarolic systems, indicate that whereas the material-balance

water/rock ratios for the DFS (0.42 to 0.51) are overall much higher than those calculated for the ULZ (0.17 to 0.21), the minimum amount of fresh meteoric H<sub>2</sub>O necessary to account for these material-balance water/rock ratios is roughly similar in each case ( $\approx 10^{14}$  g H<sub>2</sub>O); this is because there is 5 to 7 times more rock involved in the broadly based ULZ ( $3 \times 10^9$  m<sup>3</sup> of rock for the Gorges Area) as compared to the more localized DFS ( $0.6 \times 10^9$  m<sup>3</sup> of rock for the Gorges Area).

#### 5.2.6. *Water Supply to Fumaroles*

The amount of H<sub>2</sub>O strictly necessary to supply the fumarolic activity that produced the <sup>18</sup>O depletions in the ULZ and the DFS could be delivered by rainwater on the surface of the fumarole areas; no focusing of surface waters or groundwaters into the fumarole areas from the surrounding regions is strictly necessary to account for this minimum amount of water. Using the average lifetime of the fumarolic system estimated from the  $\delta^{18}\text{O}$  values of coexisting feldspar and groundmass ( $\approx 10$ -25 years), it is possible to calculate the minimum rainfall per year required on the surface of the fumarolic area, if the fumaroles were supplied by rainwater alone. This value is  $\approx 21$  inches per year for the Gorges Area, and  $\approx 18$  inches per year for the Southeast and Chidago Areas. This is well within the range we might expect for these regions, even in a cooler, wetter climate. However this does not preclude the likely possibility that surface waters and groundwaters were indeed focused into the fumarolic area. The fact that the main fumarolic areas lie directly above the probable pre-eruption drainage patterns means that watercourses reestablished along these drainage pathways would doubtless have also contributed to the fumarolic fluids. Note that these types of material-balance water/rock ratios are *always* minimum values, because they do not take into account any H<sub>2</sub>O that may have passed through the system without exchanging significantly with the rocks.

### 5.2.7. Heat Balance

The minimum amount of heat necessary to drive the fumarolic H<sub>2</sub>O through the hydrothermal circulation systems of the DFS and the ULZ could be supplied by the internal heat of the ash-flow sheet itself. In the case of the ULZ, this heat could be supplied solely by the rock involved in <sup>18</sup>O-exchange; in the case of the DFS, an additional 67 to 107 cal/g-rock of heat is required. The extra heat required by the DFS could be delivered by a combination of continued advection of H<sub>2</sub>O through the permeable upper part of the tuff and by conduction from the underlying, densely welded tuff during the estimated lifetime of fumarolic activity (≈10-25 years). In addition, both magmatic H<sub>2</sub>O degassed from the welded tuff and small amounts of strongly <sup>18</sup>O-shifted meteoric waters circulating in fractures in the densely welded tuff could also have advected heat from the lower part of the tuff into the overlying fumarolic system.

### 5.2.8. Fumarolic Conduits and Permeability in Ash-Flow Tuffs

Using the width of the largest fractures in the ULZ and the DFS, fracture permeabilities in the ash-flow sheet are estimated to have locally reached values as high as 10<sup>-3</sup> cm<sup>2</sup> and 2 cm<sup>2</sup>, respectively. These are 5-8 orders of magnitude higher than estimates of the matrix permeability of the ash-flow tuff from Yucca Mountain with a similar degree of welding (0.01 to 1.0 mdarcy; Nelson and Anderson, 1992). Thus, at least for a short time, the fumarolic conduits formed during fumarolic activity probably greatly increased the overall permeability of the ash-flow sheet by creating wide, throughgoing conduits through the upper part of the ash-flow sheet. It is obvious that ash-flow sheets with fumarolic conduits will be much more permeable than ash-flow sheets without these structures. In addition, they are also probably more permeable than many other types of fractured volcanic rocks, including many columnar-jointed basalt and andesite flows, which can be among the most permeable rocks on Earth.

### **5.3. Fossil fumaroles in the Crowley Area: an analogue for fumarolic morphology in intracaldera tuffs?**

Fossil fumaroles in the Crowley Area have a much different morphology than the fumaroles in the Gorges, Southeast, and Chidago Areas, and the distribution of fumarolic ridges on the surface of the ash-flow sheet indicates that they may have been supplied by groundwater flow from the directly adjacent, ancestral Long Valley Lake. The dominant fumarole morphology in the Crowley Area is represented by abundant  $\approx 400$ - to 600-m-long, N40E-striking ridges on the surface of the ash-flow sheet; a main set of N40E-striking fractures in the partially welded tuff is also apparent on aerial photographs and in cliff exposures in the canyons that cut through the upper part of the tuff in the Crowley Area. Exposures in Owens River Gorge indicate that beneath these fumarolic ridges there are no fumarolic conduits of the type observed in the Gorges and Chidago Areas. The limited  $^{18}\text{O}$  data from the Crowley Area suggest that there is a low- $^{18}\text{O}$  zone in the upper, partially welded part of the tuff, correlative with the ULZ in the Gorges Area. The distribution of fumarolic ridges on the surface of the Bishop Tuff in the Crowley Area roughly corresponds with the area enclosed by a pre-Bishop Tuff paleobasin that drained into the Long Valley Area. Inferences and extrapolations of the position of the water table, using shorelines of ancestral Long Valley Lake, suggest that this basin may have been filled by groundwater while the tuff was still hot. Thus fumaroles in the Crowley Area may have been supplied almost totally by groundwater from Long Valley Lake; hence the morphology of fumaroles in the Crowley Area might be more indicative of the types of fumarole morphology that one might see in intracaldera tuffs, where such materials are exposed by erosion. More studies of the Crowley Area and of appropriate examples of intracaldera tuffs will be required in the future to test this idea.

## 5.4. Fumarolic conduits in the Bishop Tuff outflow sheet

### 5.4.1. *Interconnected Fumarolic Plumbing Systems*

Tubular conduits and steep fissures represent two different endmembers of a more-or-less continuous morphology of fumarolic conduit structures; in three dimensions, many of these types of conduits are very likely interconnected. Several different varieties of fumarolic conduits were observed throughout the Bishop Tuff outflow sheet, but all of these can basically be considered to be either steep fissures, tubular conduits, or some variant between either of these two endmembers. The morphologies of these "intermediate" conduits are either vertically elongate tubes or steep fissures that close completely before they reach the top of the tuff; the dividing line between the two endmember structures is simply that tubular conduits have vertical columnar joints emanating from their tops, whereas steep fissures either "daylight" very near the surface of the tuff, or they are cut off by shallow-dipping columnar joints emanating from another nearby fumarolic structure. Steep fissures, tubular conduits, and the "intermediate" morphologies almost certainly form interconnected pathways underneath fumarolic mounds and ridges. It is likely, for example, that ingress of fumarolic H<sub>2</sub>O into the DFS was enhanced by formation of steep fissures, which would provide a fast pathway for meteoric H<sub>2</sub>O to enter into the deeper levels of these meteoric-hydrothermal systems.

### 5.4.2. *Formation and Growth of Fumarolic Conduits*

It is clear from observations at the Valley of Ten Thousand Smokes, as well as from the present work and that of Sheridan (1970), that the fumarolic conduits formed early in the cooling history of the Bishop Tuff, probably in the first year or two, and also that they very likely continued to become enlarged by the passage of meteoric H<sub>2</sub>O through them. That both the steep fissures and the tubular conduits formed fairly early is evidenced by the numerous shallow-dipping columnar joints that from their orientation must have grown outward from a series of different kinds of fumarolic conduits as the tuff cooled and

contracted. The fact that columnar joints radiate outward from these structures for up to 25 m is evidence that severe cooling and a great deal of heat transfer occurred along these structures during fumarolic activity. Indeed, the widest parts of these fumarolic conduits correlate with the positions of the longest sets of columnar joints on either side; the parts of the tuff in which the widest portions of the conduits are found are also the parts that exhibit the lowest whole-rock  $\delta^{18}\text{O}$  values and therefore the highest material-balance, meteoric-water/rock ratios. It makes sense that these structures would have widened in response to thermal contraction associated with cooling due to fumarolic flow, because the sides of these conduits would have been free surfaces from which heat was being removed from the surrounding volume of tuff. It is also possible that, locally, the tuff was thermally shattered or hydrofractured (by magmatic volatiles?) and then widened by internal erosion.

### **5.5. Relationship of the Densely Welded Zone (DWZ) to formation of fumarolic conduits**

The mapped areas of fumarolic mounds, and the conduits with which they are associated are concentrated in those regions of the Bishop Tuff that exhibit the thickest underlying zones of densely welded black tuff. By inference, as well as by direct observation, these thickest zones of welded tuff appear to overlie pre-Bishop Tuff paleobasins and paleodrainages. The distribution of mounds shown on Figs. 2.6 and 3.2 correlates extremely well with maps of the welding zonation in the Bishop Tuff outflow sheet shown by Wilson and Hildreth (1997) and Bateman (1965); this evidence is particularly compelling in the Gorges, Southeast, and Chidago Areas. Furthermore, those regions of the tuff that are underlain by a thick, densely welded zone have been shown by both Sheridan (1970) and Wilson and Hildreth (1997) to be correlated with the pre-Bishop Tuff topographic basins. Upward heat transfer from a thick, densely welded stratigraphic zone must have been crucial in the development of fumarolic activity in the overlying, partially welded portions of the tuff. Nevertheless, much of the upper part of the tuff, even

within the mapped areas of most intense fumarolic activity (Fig. 1.1), does not exhibit any strong  $^{18}\text{O}$  depletions; these are the intervening zones of tuff between fumarolic mounds (e.g., Sites AG and LG-B). Thus it is clear that *both* an underlying, thick, Densely Welded Zone (DWZ) and formation of localized fumarolic conduits in the partially welded tuff are necessary conditions to drive the meteoric-hydrothermal circulation in each DFS and its directly overlying fumarolic mound.

In addition to the larger energy source available from the thicker portions of the Densely Welded Zone of the tuff, there are two plausible reasons why fumarolic conduits might be concentrated over the pre-Bishop Tuff paleobasins. First, it may be that both surface waters and groundwaters are focused into these drainage areas, which would typically also be topographically lower after deposition of the tuff, as a result of greater differential compaction of the thickest parts of the ash-flow sheet during welding. It is tempting to speculate that there might be a kind of "feedback" effect operating wherein the flow of large amounts of  $\text{H}_2\text{O}$  through incipient fractures deep in the partially welded tuff might cause preferential widening of these features into well-defined fumarolic conduits, thereby markedly increasing the permeability and allowing even more  $\text{H}_2\text{O}$  to penetrate these portions of the tuff.

Another reason that fumarolic conduits might be concentrated over the thickest portions of the DWZ may be that the types of fractures that later widened to become full-fledged fumarolic conduits are in fact preferentially formed over paleobasins, because of the stresses that occur in the upper, brittle portion of the tuff during downwarping and compaction of the ductile lower part of the tuff. The  $^{18}\text{O}$  and morphological evidence presented in this work suggests at least two ways this might occur, neither of which is mutually exclusive: (1) Compaction of the underlying densely welded tuff over topographic lows in the basement rock may be the trigger that causes wider fractures to form in the upper layer of brittle, partially welded tuff. (2) Early explosive activity generated either by escape of magmatic gases or by phreatic explosions as ponds, marshes,

or glaciers were locally overridden by the tuff may have opened fractures in both the DWZ and the overlying partially welded tuff. Obviously, the fractures in the underlying densely welded tuff would necessarily have been transient, because that portion of the tuff continued to undergo ductile deformation during welding. It may be that all of the above processes together contributed to varying degrees to produce the observed distribution of fumarolic conduits in the Bishop Tuff outflow sheet. Further work is needed in order to sort out which of these hypotheses is most important, or if some additional explanation is required.

## **5.6. Discussion comparing the $^{18}\text{O}/^{16}\text{O}$ systematics in fossil fumaroles of the Bishop Tuff outflow sheet with those in the Long Valley and Chegem intracaldera tuffs**

### *5.6.1. $^{18}\text{O}/^{16}\text{O}$ -Depth Profiles*

Figure 5.1 compares profiles of  $\delta^{18}\text{O}$  with depth for all three situations where significant  $^{18}\text{O}/^{16}\text{O}$  studies have been carried out in youthful welded ash-flow tuffs: (a) The representative 150-m-thick section at Site CG in the fumarolic area of the welded Bishop Tuff outflow sheet from the present work; (b) A composite profile of  $^{18}\text{O}/^{16}\text{O}$  measurements on samples from 500-1000 m drill-core sections at 6 different sites on the flanks of the resurgent dome in Long Valley caldera (McConnell et al., 1997; Smith and Suemnicht, 1991; for locations see Fig. 5.2); and (c) A 1600-m-thick stratigraphic section from the upper part of the deeply eroded Chegem caldera in Russia (Gazis et al., 1996). Various geologic units overlie the intracaldera Bishop Tuff in the 6 drill hole sections, and therefore the published data from Long Valley caldera have been replotted on Fig. 5.1b by defining the top of the Bishop Tuff in each drill hole as zero meters depth. The thickness of pervasively devitrified tuff in the three deepest drill holes in Long Valley caldera (LVEW, Mammoth-1, and LV13-26) is sufficiently uniform that the base of this zone in the tuff plots at a constant depth of about 675 m on Fig. 5.1b. The intracaldera Bishop Tuff



itself has a maximum thickness of about 1500 m (McConnell et al., 1997), which is at least 7 times the thickness of the Bishop Tuff outflow sheet. For clarity none of the units overlying the intracaldera tuff are shown on Fig. 5.1b; these units include the Early Rhyolites, the Moat Rhyolites, and glacial till (Bailey, 1989; Smith and Suemnicht, 1991).

The most striking features of the 3 diagrams shown in Fig. 5.1 are the similarities of the whole-rock and mineral  $\delta^{18}\text{O}$  profiles as a function of stratigraphic position, including the presence of: (1) low- $^{18}\text{O}$  whole-rock and groundmass in the less-welded and/or pervasively devitrified upper portions of the tuffs; (2) densely welded lower zones displaying essentially pristine magmatic  $^{18}\text{O}/^{16}\text{O}$ ; and (3) relatively uniform, magmatic  $\delta^{18}\text{O}$  values in quartz *and feldspar* phenocrysts throughout each of the stratigraphic sections. However, note that the  $^{18}\text{O}/^{16}\text{O}$  data from the deepest parts of the intracaldera Bishop Tuff (>920 m) display an additional complexity in that both whole-rock and feldspar samples may be strongly  $^{18}\text{O}$ -depleted (see Fig. 5.1b and the discussion below). The slightly higher  $\delta^{18}\text{O}$  values commonly observed at the very top of each section, as well as locally within the densely welded zones, presumably represent the much later superposition of very low-temperature oxygen isotope exchange during incipient weathering or during the waning (hot spring?) stages of hydrothermal activity. The similarities among all 3 profiles are immediately apparent, despite differences in thickness, age, degree of erosion, position relative to their source calderas, and probable longevity of the respective fumarolic systems.

$^{18}\text{O}/^{16}\text{O}$  analyses were obtained by Smith and Suemnicht (1991) on 5 samples from the intracaldera Bishop Tuff in Clay Pit 1 drill hole (CP on Fig. 5.2). For clarity, these CP data are not plotted on the composite profile of Fig. 5.1b, because the depth to the top of the very densely welded zone is much less in Clay Pit 1 than in the other drill holes. Nevertheless, these few whole-rock  $^{18}\text{O}/^{16}\text{O}$  data from this seventh drill hole show the same kinds of correlations with relative position and welding zonation that are seen in the other 6 drill-hole profiles: (1) a single sample from the poorly welded upper part of Clay

Pit 1 (located 31 m beneath the top of the Bishop Tuff) has a relatively low whole-rock  $\delta^{18}\text{O} = +4.6$ ; (2) two samples at 326 m and 518 m, both within the very densely welded zone (which is unusually thick at this locality, >800 m) display near-magmatic  $\delta^{18}\text{O}$  values of +6.4 and +6.0, respectively; and (3) a very deep (>1160 m) sample from just above the base of the Bishop Tuff is extremely  $^{18}\text{O}$ -depleted ( $\delta^{18}\text{O} = -2.6$ , see discussion below).

### 5.6.2. Intracaldera Bishop Tuff

Whole-rock  $\delta^{18}\text{O}$  data obtained by Smith and Suemnicht (1991) and McConnell et al. (1997) from drill holes in Long Valley caldera (Fig. 5.1b) are all consistent with the proposal that the *upper part* of the intracaldera Bishop Tuff hosted a high-temperature meteoric-hydrothermal fumarolic system like the ones documented for the Bishop Tuff outflow sheet (this study) and Chegem caldera (Gazis et al., 1996). However, it is the *feldspar* phenocryst data reported by McConnell et al. (1997) from 3 of these drill holes (LVEW, LV13-21, and LV130-26) that allow the effects of such fumarolic activity to be definitively identified. It is apparent in Fig. 5.1b that the upper part of the intracaldera Bishop Tuff, where the sanidine phenocrysts exhibit the *least* amount of mineralogical hydrothermal alteration and are only very slightly  $^{18}\text{O}$ -depleted, is also a region of *extreme*  $^{18}\text{O}$ -depletion of groundmass/matrix. Although McConnell et al. (1997) did not recognize these implications of their  $^{18}\text{O}/^{16}\text{O}$  data on coexisting groundmass and feldspar with respect to possible high-temperature fumarolic activity in the caldera fill, they do report a critical observation: namely that the sanidine phenocrysts are "clear" in the strongly  $^{18}\text{O}$ -depleted higher levels of the intracaldera Bishop Tuff, but that at great depth in the drill holes these phenocrysts become increasingly "cloudy and skeletal, and contain clay or calcite inclusions". In addition, McConnell et al. (1997) describe the deepest samples in the LVEW drill core (i.e. within the light shaded region at depths of 920-1200 m on Fig. 5.1b) as "silicified". Thus, mineralogical and  $^{18}\text{O}/^{16}\text{O}$  alteration of phenocrysts and

silicification of groundmass all sharply increase in the deepest parts of the caldera section (and with proximity to underlying resurgent intrusions?).

Several authors have in fact postulated that long-lived fossil meteoric-hydrothermal systems were important in the area of the Long Valley resurgent dome during the past 500,000 years (Bailey et al., 1976; Sorey, 1985; Smith and Suemnicht, 1991; McConnell et al. 1997). In the deepest parts of the intracaldera Bishop Tuff, a number of ( $\approx 300^{\circ}\text{C}$ ) hydrothermal alteration effects are observed, including silicification, obviously leached densely welded tuff, and cloudy feldspar phenocrysts with very negative  $\delta^{18}\text{O}$  values (McConnell et al., 1997). All of these features can be observed within the suite of 13 samples reported by McConnell et al. (1997) and Smith and Suemnicht (1991) from the deepest zone of Bishop Tuff, which is exposed in the LVEW, the Clay Pit-1, and the Mammoth-1 drill holes ( $> 920$  m).

The above-described features of the deepest parts of the intracaldera Bishop Tuff are completely analogous to the effects observed around the resurgent and ring intrusions emplaced into the 23 Ma intracaldera Sunshine Peak Tuff at Lake City caldera in Colorado (see Fig. 2.2). The mineralogical and  $^{18}\text{O}/^{16}\text{O}$  systematics now established for intracaldera tuff at Chegem, Long Valley, and Lake City all appear to be straightforward enough that it is probably going to be possible to determine whether low- $\delta^{18}\text{O}$  whole-rock samples from ash-flow tuffs are recording a high-temperature, short-lived fumarolic  $^{18}\text{O}/^{16}\text{O}$  signature or a moderate-temperature, long-lived, hydrothermal  $^{18}\text{O}/^{16}\text{O}$  signature, even without actually carrying out  $\delta^{18}\text{O}$  analyses of the feldspar phenocrysts themselves: (1) pristine, colorless, transparent sanidine phenocrysts embedded in a variably  $^{18}\text{O}$ -depleted groundmass would immediately suggest a short-lived fumarolic event; whereas (2) cloudy, opaque, or mineralogically altered feldspar phenocrysts in the same kind of low- $^{18}\text{O}$  matrix probably would imply either a more typical, longer-lived meteoric-hydrothermal system, or superposition of such a system upon the former. A possible example of such superposition in the intracaldera Bishop Tuff is illustrated by a sample from drill hole LV13-26

(McConnell et al., 1997), where a "milky" sanidine ( $\delta^{18}\text{O} = +2.8$ ) coexists with a "clear" sanidine ( $\delta^{18}\text{O} = +5.8$ ), both of which are embedded in a low- $^{18}\text{O}$  matrix ( $\delta^{18}\text{O} = +1.8$ ).

In the deepest available samples of caldera fill at Long Valley, which are from the LVEW hole, the sanidines have  $\delta^{18}\text{O} = -4.5$  to  $-6.1$  and coexisting quartz has  $\delta^{18}\text{O} = +7.3$  to  $+7.4$  (Fig. 5.1); these coexist with matrix that varies widely from  $\delta^{18}\text{O} = -4.0$  to  $+0.8$ . These  $^{18}\text{O}$ -depletions are almost certainly related to the longer-lived hydrothermal systems associated with post-caldera intrusive events. The low- $^{18}\text{O}$  matrix and feldspar samples from the deepest portions of the intracaldera tuff are physically separated from the low- $^{18}\text{O}$  rocks and "normal"- $^{18}\text{O}$  feldspars of the shallow, short-lived fumarolic system by a zone of relatively "normal"  $\delta^{18}\text{O}$  values that characterizes the intervening section of very densely welded tuff (shown at depths of about 700-900 m on Fig. 5.1b).

Thus, in spite of a number of complexities associated with superposition of different hydrothermal phenomena, it is still possible in the Long Valley drill holes to perceive a physical separation between the effects of these two major types of contrasting hydrothermal systems. This could also be done at Chegem caldera, where the resurgent intrusion is relatively small, and confined to the extreme northern edge of the caldera (Gazis et al., 1996). However, it may be very difficult to distinguish these two kinds of systems in many older calderas because of the effects of erosion and weathering, and because once the densely welded tuff has cooled sufficiently to fracture, there is nothing to prevent the deep, long-lived, hydrothermal system associated with large-sized post-caldera intrusions from expanding upward and outward to overprint rocks already altered by the shallow, short-lived fumarolic system. This has in fact occurred locally in both the Chegem and Long Valley calderas, and it is probably only because these relatively youthful calderas are so well preserved that we are at all able to decipher these disparate phenomena. For example, no  $^{18}\text{O}/^{16}\text{O}$  evidence for a fumarolic system was recognized at Lake City caldera by Larson and Taylor (1986a; 1986b). However, now that we know what kinds of rocks to look at, it would be interesting to re-sample that 23 Ma caldera to try to find some

preserved evidence of such a fumarolic event in the uppermost remnants of the intracaldera Sunshine Peak Tuff.

### 5.6.3. *Material-Balance Water/Rock Ratios in Intracaldera Tuff*

Using the  $^{18}\text{O}/^{16}\text{O}$  data of McConnell et al. (1997) and Smith and Suemnicht (1991) for the intracaldera Bishop Tuff, water/rock ratios have been calculated in the same fashion as was done for the ULZ and the DFS in the Bishop Tuff outflow sheet (see Section 5.2.1). These material-balance water/rock ratios are reprinted from Holt and Taylor (1998) in Fig. 5.3 (top) along with material-balance water/rock ratios calculated by Gazis et al. (1996) for the intracaldera Chegem Tuff (Fig. 5.3, bottom). In general, the material-balance water/rock ratios are higher in the intracaldera Bishop Tuff (0.4 to 1.2, Fig. 1.3) and the intracaldera Chegem Tuff (0.5 to 1.2, Fig. 5.3) than they are in the Bishop Tuff outflow sheet, because although the water/rock ratios are locally higher in the DFS (0.42 to 0.51, Fig. 3.18), they are much lower in the areally extensive ULZ (0.17 to 0.21, Fig. 3.18). The minimum estimates of the amount of water required by these material-balance water/rock ratios for the intracaldera Bishop Tuff ( $1.4 \times 10^{17}$  to  $1.9 \times 10^{17}$  g of  $\text{H}_2\text{O}$ ) and the intracaldera Chegem Tuff ( $0.5 \times 10^{17}$  to  $1.0 \times 10^{17}$  g) are almost 100 times greater than the amount of water required for the combined ULZ and DFS ( $\approx 6.7 \times 10^{14}$  to  $8.6 \times 10^{14}$  g of  $\text{H}_2\text{O}$ ) in the Gorges Area. This partly a result of the higher average material/balance water/rock ratios in the intracaldera tuffs and partly because each of these intracaldera tuffs contain  $\approx 50$  times more hydrothermally exchanged rock than does the combined ULZ and DFS in the Gorges Area. Holt and Taylor (1998) pointed out that the minimum amount of water required by these material-balance water/rock calculations is extraordinarily high considering the lifetime of fumarolic activity in the intracaldera tuffs (10-100 years); the minimum amount of precipitation required on the surfaces of these calderas, assuming fumaroles were supplied by this meteoric  $\text{H}_2\text{O}$  alone, is on the order of 130 inches of rain per year. As discussed by Holt and Taylor (1998), it thus seems much more likely that

intracaldera fumaroles in both the Long Valley and the Chegem calderas were supplied by groundwater percolating downward from overlying caldera lakes, which would have represented an essentially inexhaustible supply of H<sub>2</sub>O.

#### *5.6.4. Relationship of Climate and Abundance of Surface Water to Fumarolic Activity*

It may be that the development of intense fumarolic activity in the upper parts of welded ash-flow sheets requires the contribution of relatively large amounts of surface water or groundwater. This certainly seems to have been a necessary factor in producing the whole-rock <sup>18</sup>O-depletions and fumarole morphology of the type and magnitude that has been observed in the three localities that have now been studied in detail. The inferred (i.e., for the Chegem Tuff and the Bishop Tuff) or observed (for the 1912 ash-flow sheet at the VTTS) climatic environments of each of these fumarolic areas are characterized by a truly enormous availability of surface H<sub>2</sub>O at the time fumaroles were active. The VTTS is surrounded by glaciers, and two medium-sized rivers and numerous smaller streams empty directly onto the ash-flow sheet. The Bishop Tuff was deposited during a cooler period at relatively high altitudes on the eastern slopes of the Sierra Nevada range, and glaciers are known to have been locally present along the western boundary of this ash-flow sheet (Bailey et al., 1976). The intracaldera Bishop Tuff and the intracaldera Chegem Tuff were both covered by caldera lakes at some point after eruption (Bailey et al., 1976; Gazis et al., 1996), thereby insuring a virtually unlimited supply of H<sub>2</sub>O.

In the course of conducting this thesis research, it has become apparent that whereas calderas and ash-flow tuffs are numerous in the western United States, there are a few occurrences of fumarolic systems of the type and magnitude of those identified in the Bishop Tuff outflow sheet. For example, preliminary <sup>18</sup>O/<sup>16</sup>O and field evidence from the 400 km<sup>3</sup> Bandelier Tuff, a thick, rhyolitic, ash-flow sheet composed of two members (Otowi, 1.61 Ma; Tshirege, 1.22 Ma) surrounding Valles caldera, New Mexico, indicate that there are no prominent exposures of any large volumes of <sup>18</sup>O-depleted rock, or of

shallow-dipping columnar joints or fumarolic conduits in the numerous cliffs that are cut through the 150-m-thick ash-flow sheet on the Pajarito Plateau, located to the west of the Valles caldera. Nor are there any of these types of exposures along San Diego Canyon and other exposed  $\approx 300$ -m-thick sections of the Bandelier tuff to the east of the caldera.

Exposures of thin zones of tuff ( $\approx 15$ -m-thick) containing the type of shallow-dipping columnar jointing observed in the Bishop Tuff fossil fumaroles are found only locally in canyons in the Pajarito Plateau along the trace of the ancestral drainage of the Rio Grande (Broxton and Reneau, 1996; Reneau and Dethier, 1996). In these areas, steep fissures ( $\approx 10$  cm wide) are found in the cliff faces of the exposed tuff, and on the top of the tuff above these features are 50-cm-high fumarolic ridges that extend for up to 30 m, as well as small, 3-m-diameter fumarolic mounds with arcuate roof joints. Preliminary  $^{18}\text{O}/^{16}\text{O}$  evidence from samples collected at these localities shows that these fumarolic zones do indeed exhibit a slight  $^{18}\text{O}$ -depletion (about 0.7 to 1.7 per mil) in the groundmass relative to the original  $\delta^{18}\text{O}$  value of the Bandelier Tuff magma ( $\approx +7.6$ ). Also, the coexisting feldspar phenocrysts in these same samples have preserved their magmatic  $\delta^{18}\text{O}$  values (+6.9 to +7.3). However, these occurrences along the ancestral drainage of the Rio Grande River represent the only examples that we have found for even a small systematic  $^{18}\text{O}$  depletion associated with fumarolic structures in the Bandelier Tuff. This suggests that fumaroles were rare or non-existent in much of the Bandelier Tuff, but that they were localized in this area because this is where groundwaters and/or surface waters were available to supply the fumarolic activity.

Our preliminary conclusion is that, overall, the severe  $^{18}\text{O}$  depletions associated with fumarolic activity of the type seen in the DFS of the Bishop Tuff outflow sheet are much less significant in the Bandelier Tuff. Assuming that this is not simply a result of a lack of appropriate outcrop exposures, this may imply that the development of these types of fumarolic hydrothermal systems is limited by the amount of  $\text{H}_2\text{O}$  that can be delivered to the fumaroles in the short time that they are active. Perhaps this area in northern New

Mexico was semi-arid at the time the Bandelier Tuff was emplaced, as it is at present, and therefore significant amounts of surface waters and groundwater may have been confined to the ancestral Rio Grande drainage. If this is the case, we might expect that short-lived, high-temperature ( $>400^{\circ}\text{C}$ ) fumarolic meteoric-hydrothermal activity might be most common: (1) in areas of heavy rainfall; (2) in the permeable upper zones of those densely welded intracaldera tuffs that were inundated by caldera lakes immediately after eruption; or (3) in outflow sheets emplaced in glaciated valleys that were receiving abundant run-off. A corollary to this statement is that such fumarolic activity might be completely absent in thick, welded ash-flow tuffs emplaced in arid, desert regions. It would be interesting to test this prediction by doing an  $^{18}\text{O}/^{16}\text{O}$  study on a suitable occurrence somewhere in the world (e.g., in Chile?).

#### **5.7. Is this type of fumarolic activity confined to welded ash-flow tuffs, or can it also be observed in lavas?**

As a supplement to this thesis study, three localities were chosen to determine if the kinds of  $\delta^{18}\text{O}$  signatures associated with high-temperature meteoric-hydrothermal fumarolic activity in rhyolitic ash-flow tuffs can also be observed in rhyolitic or basaltic lavas that may have been penetrated by large amounts of meteoric  $\text{H}_2\text{O}$  while they were still hot. The occurrences investigated in reconnaissance fashion include: rhyolite lava from Novarupta dome in Alaska; basalts and basaltic andesites from Island Park, Idaho, near Yellowstone Park; and basalts that have, in the past, locally dammed the Colorado River in the western Grand Canyon, Arizona. These lavas were all erupted very recently ( $<1.2$  Ma) in areas where there was abundant surface  $\text{H}_2\text{O}$  available, and therefore it is known that the meteoric  $\text{H}_2\text{O}$  at all three of these locations had relatively low  $\delta^{18}\text{O}$  values at the time of eruption. This makes it easier to detect any high-temperature interactions between the groundmass of the lavas and the meteoric  $\text{H}_2\text{O}$ . Also, the fact that they are recently erupted minimizes the likelihood of any low-temperature (i.e., high- $^{18}\text{O}$ ) overprinting and



destruction of the low- $^{18}\text{O}$  signatures that the lavas may have acquired during fumarolic exchange with meteoric  $\text{H}_2\text{O}$  at high temperatures. In addition, many of the basalt flows were sampled specifically because they display shallow-dipping columnar joints and other structures analogous to those observed in the Bishop Tuff fossil fumaroles and in the fossil fumaroles in the VTTS (and locally in the Bandelier Tuff). Other researchers (e.g., Hamblin, 1994; Long and Wood, 1986; Swanson, 1987; DeGraff et al., 1989) have attributed these structures to the influx of large amounts of cold meteoric  $\text{H}_2\text{O}$  into the basalts while they were still hot.

Rhyolite from Novarupta dome was chosen for sampling because of its association with the Valley of Ten Thousand Smokes, and also because the groundmass in the upper part of this lava dome exhibits mineralogical evidence of interaction with meteoric  $\text{H}_2\text{O}$  during cooling (Weisneth and Eichelberger, 1996). Wiesneth and Eichelberger (1996) interpret the sharp transition from glassy carapace to crystalline lava near the eruptive conduit at Novarupta to be the result of a lava-lake like temperature gradient of  $\approx 1000$   $^\circ\text{C}/\text{m}$  maintained by the rhyolite lava in response to the impingement of downward circulating meteoric water on upward-streaming magmatic gases from the eruptive conduit. In order to investigate any possible  $^{18}\text{O}$  effects due to this hypothetical interaction with meteoric  $\text{H}_2\text{O}$ , samples were collected across the glassy to crystalline transition zone at two locations in the vicinity of the eruptive conduit at Novarupta Dome.

The basalts of the western Grand Canyon were chosen for sampling mainly because they exhibit spectacular columnar jointing structures that are strikingly similar to those observed in the vicinity of fossil fumaroles in the Bishop Tuff outflow sheet (Hamblin, 1994). Also, Hamblin (1994) has shown that these basalt flows formed dams across the Colorado River in the bottom of the Grand Canyon. The giant lakes behind these basalt dams would provide an abundant source of meteoric water that could have interacted with the basalt flows as they cooled, with the numerous cooling fractures and columnar joints

allowing access for Colorado River water to penetrate and possibly exchange with the hot basalt.

Basalts and basaltic andesites from the Island Park area in Idaho were sampled in order to investigate whether the groundmass of these lavas might be analogous to the low- $^{18}\text{O}$  groundmass of the rhyolite ash-flow tuffs at Chegem. It was already known, through the work of Hildreth et al. (1984), that many of the basalt samples from this area had  $\delta^{18}\text{O}$  values lower than normal basalts. Hildreth et al. (1984) interpreted these results as indicating that these flows were erupted as low- $^{18}\text{O}$  magmas, which is a very plausible hypothesis considering that the Island Park basalts and basaltic andesites are part of the Yellowstone magmatic province, one of only two caldera complexes in North America that are known to have erupted large volumes of low- $^{18}\text{O}$  rhyolite magma (Larson and Taylor, 1986c; Hildreth et al., 1984). However, although they are abundant in the eastern rift zone of Iceland, low- $^{18}\text{O}$  basaltic magmas are in general very rare, so it was important to test the Hildreth et al. (1984) hypothesis. The origin of low- $^{18}\text{O}$  magmas has been a subject of heated debate, although there is a growing consensus that they generally form as a result of assimilation and/or exchange with hydrothermally altered roof rocks (e.g., Taylor, 1987).

An alternative to the hypothesis that the Island Park basalts formed from low- $^{18}\text{O}$  magmas is the possibility that, like the ash-flow tuffs at Chegem and Long Valley, these basaltic magmas were erupted with normal  $\delta^{18}\text{O}$  values, but that subsequently they interacted with meteoric  $\text{H}_2\text{O}$  while they were still hot, allowing the basaltic glass and groundmass to acquire an  $^{18}\text{O}$ -depleted signature after eruption. This alternative hypothesis could be tested by analyzing the phenocrysts from these lavas, because low- $^{18}\text{O}$  magmas always produce low- $^{18}\text{O}$  phenocryst minerals as well as a low- $^{18}\text{O}$  groundmass. Previous  $^{18}\text{O}/^{16}\text{O}$  studies of ash-flow tuffs have shown that even the fast-exchanging feldspar phenocrysts are largely unaffected by short-lived, high-temperature interactions with meteoric  $\text{H}_2\text{O}$  during cooling (Gazis et al., 1996, Holt and Taylor, 1998). Therefore,

by analyzing feldspar and olivine phenocrysts from the Island Park basalts and basaltic andesites, it ought to be possible to distinguish whether their low whole-rock  $\delta^{18}\text{O}$  values are the result of crystallization from low- $^{18}\text{O}$  magmas, or whether it is only their glassy groundmass that has been depleted in  $^{18}\text{O}$  as a result of post-eruptive exchange with meteoric  $\text{H}_2\text{O}$  at high temperatures.

In our preliminary sampling in these lavas of several occurrences of shallow-dipping columnar joints that seem to be quite analogous to those observed in the Bishop Tuff outflow sheet, the Bandelier Tuff, and the 1912 ash-flow sheet at the VTTS, we have found no instance where these lavas exhibited  $^{18}\text{O}$ -depletions in excess of 0.5‰ relative to what we infer was the  $\delta^{18}\text{O}$  value of the original magma (based on the  $\delta^{18}\text{O}$  values of coexisting phenocryst phases). Instead, even in zones of abundant, shallow-dipping columnar joints, the  $\delta^{18}\text{O}$  values for each lava sampled turned out to be very uniform, analogous to the situation in the zone of densely welded black tuff in the Bishop Tuff outflow sheet. Therefore, in contrast to the ash-flow tuffs, it is clear that large amounts of low- $^{18}\text{O}$  meteoric- $\text{H}_2\text{O}$  did not circulate through and interact with any of these lavas while they were still hot.

The  $\delta^{18}\text{O}$  values for phenocrysts and groundmass from basalts erupted in the Island Park caldera largely confirm the findings of Hildreth et al. (1984) that these basalts probably crystallized from low- $^{18}\text{O}$  magmas ( $\delta^{18}\text{O} < +6$ ); however, the only basalt flow that we studied that has low whole-rock  $\delta^{18}\text{O}$  values is one of the Warm River basalt flows ( $\delta^{18}\text{O}_{\text{olivine}} = +5.12$ ,  $\delta^{18}\text{O}_{\text{feldspar}} = +4.52$  and  $+5.30$ ,  $\delta^{18}\text{O}_{\text{whole-rock}} = +5.5$  to  $+6.3$ ). Coexisting olivine and feldspar phenocrysts in such a basalt are expected to have  $\Delta^{18}\text{O}_{\text{feldspar-olivine}} \approx 2.0$ , and therefore the phenocryst  $\delta^{18}\text{O}$  values here are out of equilibrium, in that the  $\delta^{18}\text{O}$  values of the feldspar phenocrysts are actually lower than in the olivine phenocrysts. This particular basalt flow is relatively young (0.6 to 1.2 Ma; Hildreth et al., 1984), and whereas the feldspar phenocrysts exhibit no mineralogical alteration, the olivine phenocrysts do show small evidence for low-temperature degradation

and the formation of iddingsite. Could it be that the olivine phenocrysts and the groundmass of this basaltic lava were more susceptible to low-temperature weathering processes than the feldspars and thus became slightly  $^{18}\text{O}$ -enriched?

One could speculate about many reasons why lavas containing abundant shallow-dipping columnar joints do not exhibit the kinds of  $\delta^{18}\text{O}$  systematics seen in ash-flow tuffs. Certainly it is to be expected that differences in permeability between fragmental, partially welded tuff and homogenous, crystallized lava flows may be an important factor. Also, the types of large fumarolic conduits that are observed in ash-flow tuffs have not been reported from the areas of shallow-dipping columnar joints in lava flows, even where these joints are abundant. The shallow-dipping columnar joints in the upper parts of ash-flow tuffs are always connected to some type of fumarolic conduit, and they can, for example, be traced either radially inward toward a tubular conduit, or laterally toward a steep fissure. In contrast, the columnar joints in lavas merge with adjacent, steeply dipping columnar joints, commonly without a space in between; therefore shallow-dipping columnar joints in basaltic lavas do not seem to be associated with fumarolic conduits, and there may have been little or no true fumarolic activity associated with these features. Indeed, our  $^{18}\text{O}/^{16}\text{O}$  studies suggest that this might be so. Perhaps the fumarolic conduits that form in ash-flow tuffs require the presence of a brittle zone of permeable material (the partially welded tuff) overlying a hot, ductile, deforming material (the densely welded black tuff), and such features are simply not present in lavas.

## **5.8. Discussion about the timescales of fumarolic activity and the mechanisms by which such activity is terminated**

### *5.8.1. The Oxygen Isotope Clock*

Because the diffusion of oxygen in feldspars is several orders of magnitude slower than in glass (Zhang et al., 1991), the measured slopes of the data-point arrays on Fig. 5.4 (Bishop Tuff outflow sheet:  $\approx 20$ -25; intracaldera Bishop Tuff:  $\approx 5$ -13; intracaldera

Chegem Tuff:  $\approx 7-11$ ) can be shown to be equal to  $1/f$ , where  $f$  is the fractional approach of the feldspar to  $^{18}\text{O}/^{16}\text{O}$  equilibrium with the surrounding medium (Gregory et al., 1989). Combining this information with the oxygen diffusion coefficients in alkali feldspar as a function of temperature ( $D = 2.31 \times 10^{-9} \exp[-10,700/RT]$   $\text{cm}^2/\text{s}$ , as determined by Giletti et al., 1978), and with the equation relating the kinetic rate constant to the diffusion coefficient for fluid-buffered, open-system conditions ( $\exp[-kt] = 1 - f \approx \exp[-3.5(Dt/a^2)^{1/2}]$  for  $(Dt/a^2)^{1/2} < 0.1$ , as derived by Criss et al., 1987), we can repeat the kinds of calculations done by Gazis et al. (1996) at Chegem, and thereby estimate the lifetimes of the Bishop Tuff fumarole systems (Fig. 5.5). Because we observe fairly well-defined, very steep arrays for all three fumarolic examples in Fig. 5.4, it is clear that these meteoric-hydrothermal systems were active for only a short period of time. At temperatures of about  $500^\circ\text{C}$ , these calculated lifetimes in the intracaldera tuff at Long Valley and Chegem are indistinguishable ( $\approx 10-100$  years), and both are somewhat longer than the lifetime calculated for the Bishop Tuff outflow sheet ( $\approx 1-10$  years). These differences are, however, just what one would expect for hydrothermal systems driven only by heat from the host tuff, because the thick, intracaldera volcanic pile has a much higher heat content per unit surface area than does the thin outflow sheet.

In a strict sense, the lifetimes shown in Fig. 5.5 are only *minimum* values for each fumarolic system *taken as a whole*. Those estimates actually represent the hydrothermal lifetime of each packet of rock nested within a given zone of interconnected porosity, rather than the lifetime of the entire fumarolic system. Even though such zones of interconnected porosity were probably common in the upper part of the tuff very soon after deposition, it is obvious that this permeability would be enhanced as new fractures and columnar joints formed. The extent of downward penetration of low- $^{18}\text{O}$  fluids into the densely welded tuff can be mapped by welding and devitrification textures, joint patterns, groundmass coloration, and  $^{18}\text{O}$  analyses; this distance is at most only 10-15 m in the outflow sheet, but is much more extensive in the intracaldera tuff, where the  $^{18}\text{O}$ -exchanged sections are

as much as 700 m thick in the Long Valley and Chegem calderas. The rapidity of advance of such a "cracking front" as it proceeds into the underlying densely welded tuff may be an important rate-controlling step on the lifetimes of fumarolic systems. Taking this into account, the estimated lifetimes for each complete fumarolic hydrothermal system shown on Fig. 5.5 might be too small by a factor of 2 to 3, or more. Direct observations by scientists who visited the VTTS at various times from 1916 to the 1930's indicates that, for an ash-flow thickness of  $\approx 200$  m, high-temperature fumaroles can be expected to be active on the surface of the tuff for no longer than about 10 to 25 years following eruption.

#### *5.8.2. Fracturing of the Densely Welded Tuff and the Lifetime of Fumarolic Activity*

While  $^{18}\text{O}/^{16}\text{O}$  data indicate a fairly restricted time span for fumarolic activity in the Bishop Tuff outflow sheet ( $< 25$  years), they do not suggest a physical mechanism to explain why this activity was so short-lived. There are two ways to stop a hydrothermal system: one is to remove the source of heat, the other is to cut off the supply of  $\text{H}_2\text{O}$ . Typical meteoric-hydrothermal systems die when the heat "engine", usually a shallow pluton, cools sufficiently that it can no longer drive vigorous hydrothermal circulation; while there are exceptions, these types of meteoric-hydrothermal systems are usually very long-lived (tens to hundreds of thousands of years) and because they cool so slowly, they are typically associated with large amounts of  $\approx 250^\circ\text{C}$  mineralogical alteration (i.e., formation of chlorite and sericite). The absence of these kinds of alteration minerals in the Deep Fumarolic System (the DFS) in the Bishop Tuff outflow sheet obviously does not mean that the tuff cooled through  $250^\circ\text{C}$  in the absence of  $\text{H}_2\text{O}$ , but if it did, that would of course preclude any significant mineralogical alteration of the groundmass involving OH-bearing minerals. The absence of these OH-bearing minerals in the DFS of the Bishop Tuff outflow sheet may be due to some combination of the following: First, meteoric-hydrothermal circulation at these more moderate temperatures ( $\approx 250^\circ\text{C}$ ) may have slackened off considerably from that at higher temperatures ( $400^\circ\text{C}$ - $650^\circ\text{C}$ ), because the

underlying heat source (the densely welded tuff) itself cooled off very rapidly, causing a rapid shutdown of the entire circulation system. Secondly, at these low- to moderate-temperatures (<300°C), the kinetics of formation of the OH-bearing minerals in question probably requires that the rocks remain continuously in contact with H<sub>2</sub>O for a significant time interval in order for even micron-sized crystals to grow and thereby replace any of the quartz and feldspar in the tuff. Thirdly, and perhaps most importantly, the cumulative H<sub>2</sub>O flux values calculated for these fumarolic systems (0.3 to 3 kg of H<sub>2</sub>O per cm<sup>2</sup>; see Section 3.5) are extremely low when compared with the cumulative H<sub>2</sub>O flux values determined for the long-lived (100,000 years), 250°-350°C, meteoric-hydrothermal systems driven by igneous intrusions (typically 200 to 1000 kg of H<sub>2</sub>O per cm<sup>2</sup>; Taylor, 1997; Norton and Taylor, 1979) in situations where OH-bearing minerals are known to form; therefore, during the limited time in which the tuff was cooling through 250°-350°C, it may simply have not "seen" enough H<sub>2</sub>O to drive any significant mineralogical alteration.

On the other hand, rather than solely appealing to the demise of the heat engine as a mechanism for terminating fumarolic activity, we postulate that the fumarolic system may have been terminated by cutting off the supply of H<sub>2</sub>O to the system, perhaps even before the rocks in the DFS had cooled much below 400°C. Certainly, as long as the underlying Densely Welded Zone (DWZ) remains hot, ductile, and impermeable, there would have been a source of sufficient heat to drive vigorous hydrothermal circulation in the overlying tuff. Although it is difficult to imagine a mechanism by which one could cut off the supply of water to a typical meteoric-hydrothermal system surrounding a pluton (because these kinds of systems are usually associated with ample sources of groundwater and also contain a 3-dimensional network of fractures that provide access for the water), this might indeed have been possible in the case of the Bishop Tuff. In much of the study area today, the water table is located in the Sherwin Till, which directly underlies the Bishop Tuff outflow sheet (Putnam, 1960), and therefore H<sub>2</sub>O could in theory have been removed from

the fumarolic hydrothermal system as soon as sufficiently permeable vertical fractures formed in the underlying DWZ. As long as the inner part of the ash-flow sheet remains ductile, the overlying fumarolic system is essentially a perched aquifer above the hot, impermeable, densely welded black tuff. However, once there are sufficient fractures that connect the fumarolic fluids in the upper, partially welded tuff to the base of the ash-flow sheet, the meteoric waters will descend downward into the underlying water table, perhaps effectively ending hydrothermal circulation in the upper part of the tuff. Therefore, one physical constraint on the lifetime of the fumarolic system might be the length of time that the DWZ of the ash-flow sheet takes to fracture completely.

Several types of cooling models that might be applicable to cooling of the Bishop Tuff are discussed in the literature. These models describe pure conduction and various mixtures of upper convective cooling and lower conductive cooling in both homogeneous and heterogeneous slabs (Lister, 1974; Manley, 1992; Degraff et al., 1989; Grossenbacher and McDuffie, 1995; Long and Wood, 1986). For example, the cooling of basaltic lava flows has been modeled using both pure conduction and a cooling model like that of Lister's (1974), in which the position of a "cracking front", above which the body is cooled by convective circulation of fluid, is calculated as a function of space and time as it progresses into a conductively cooling body. For pure conduction, it is predicted that the upper set of downwardly progressing fractures (the entablature) should be located at a depth that is 60% of the total thickness (Grossenbacher and McDuffie, 1995); for a model incorporating convection above a downwardly progressing conductive layer, the entablature can easily be as much as 80% of the total flow thickness (Degraff et al. 1989). The entablatures of basalt flows that have been inundated by water during cooling are in fact commonly 80% of the total flow thickness (DeGraff et al., 1989; Long and Wood, 1986).

In order to accurately estimate the amount of time it would take for the Bishop Tuff to fracture completely through, it is necessary to choose an appropriate cooling model.



Several observations indicate that none of the above cooling models are appropriate if they are applied to the entire Bishop Tuff outflow sheet. First, fracturing in the entire thickness of the outflow sheet cannot be modeled as simple cracking of a cooling slab, which cracks from the top and bottom towards the center, because it appears that the steep fissures and tubular conduits in the upper part of the Bishop Tuff formed very early; columnar joints can be shown to have nucleated at these centers, after which these joints rapidly propagated outward away from these centers. Also, beneath fumarolic mounds, the base of the low- $^{18}\text{O}$  zone is everywhere a very sharp boundary, which is always located just above the upper boundary of the densely welded black tuff. In Owens River Gorge, where the ash-flow sheet is about 200 m thick and the base is located at most a few tens of meters below the exposed cliff, this boundary is located at about 85 m depth. If the downward extent of fractures in the Bishop Tuff outflow sheet was controlled by conductive cooling or convection of fluids above a narrow conductive zone, then the kinds of calculations described above would predict that the base of the low- $^{18}\text{O}$  zone should be located much deeper in the tuff (60-80% of the total depth). It is clear that the upper part of the Bishop Tuff was inundated by fumarolic fluids during cooling, and yet the lower limit of fumarolic fluid penetration and well-developed columnar joint formation is located at a depth of only about 40% of the total depth.

By the above arguments, meteoric fluids conceivably might have had access through steep fissures and connected tubular conduits to the central part of the ash-flow sheet almost immediately after welding was complete, and at which time the tuff would locally still have been at temperatures of 650°C or higher. This explains the extremely high fumarole temperatures that were observed (645°C) at the Valley of Ten Thousand Smokes, Alaska and that are estimated for the Bishop Tuff fumaroles. Thus, cooling in the upper part of the Bishop Tuff outflow sheet would have been facilitated by meteoric-hydrothermal convection for almost the entire cooling history of the tuff.

However, cooling of the lower, densely welded part of the tuff may have been primarily by conduction. While the brittle upper part of the tuff did not cool in a simple fashion from the top down, the densely welded portion of the tuff was certainly ductile during welding, and during that time period no permeable, through-going fractures could have formed in this part of the tuff. Indeed, the  $^{18}\text{O}/^{16}\text{O}$  evidence is very clear that the densely welded lower part of the Bishop Tuff must have been relatively impermeable to influx of meteoric fluids throughout the lifetime of fumarolic activity.

Beneath Site CG in Owens River Gorge, steep cooling fractures in the upper 70 m of the densely welded tuff are spaced at intervals of approximately 3 to 4 m, while in the lower part of the densely welded tuff, cooling fractures are more widely spaced (about 10-12 m) and form crude columns. The outlines of enormous (10-12 m thick), six-sided columns in the lower part of the densely welded tuff are exposed in a deep overhang at the base of the eastern cliff about 0.5 km north of Site CG. Thus, upper cooling fractures in the densely welded tuff penetrate to a depth almost exactly 60% that of the total thickness of the DWZ, which at Site CG is probably about 115 m thick, consistent with the idea that this part of the tuff cooled conductively.

Therefore we can calculate the time it takes for the Bishop Tuff to fracture completely through by assuming that fractures are generated at a certain temperature, and that a cracking front propagates into the conductively cooling slab of densely welded tuff at a rate determined by the inward progression of the cracking temperature isotherm with time (Fig. 5.6). This model is that of conductive cooling of a homogeneous semi-infinite slab (Carslaw and Jaeger, 1959; pp. 59-62). The top of the slab of densely welded tuff (initially at  $750^{\circ}\text{C}$ ) is assumed to be thermally buffered at a temperature of  $400^{\circ}\text{C}$  by the overlying fumarolic system, and the country rock below the base is assumed to have been initially at a temperature of  $25^{\circ}\text{C}$ .

In Fig. 5.6, the effect of latent heat on the temperature vs. depth distribution is neglected. The densely welded tuff is devitrified, and therefore the assumption that no

latent heat is released during cooling is invalid. The effect of latent heat on the above cooling model can be approximated by incorporating the latent heat ( $\approx 50$  cal/g) into a change in heat capacity and allowing it to be released over a  $350^{\circ}\text{C}$  temperature range between  $400^{\circ}\text{C}$  and  $750^{\circ}\text{C}$ . This is a reasonable approximation for the Bishop Tuff, because the entire thickness of densely welded tuff is now thoroughly devitrified, and Sheridan (1970) concluded that devitrification occurred very soon after emplacement of the ash-flow sheet (he attributed it mainly to degassing of magmatic volatiles). Incorporating the effect of latent heat in this manner results in a  $30^{\circ}\text{C}$  temperature increase for the 25 year time step at a depth of 50 meters within the densely welded Bishop Tuff, making the temperature about  $745^{\circ}\text{C}$  at this horizon instead of about  $715^{\circ}\text{C}$ .

Although the exact temperature at which fractures are initiated at a cracking front is certainly a function of many different parameters, observations and theory seem to agree that, at least for cooling basaltic lavas it would be somewhere between the solidus and the glass transition temperature (Peck and Minakami, 1968; Ryan and Sammis, 1981; Grossenbacher and McDuffie, 1995; DeGraff et al., 1989). It has been shown that joint or crack formation in basaltic lava lakes follows closely behind the solidus as it moves towards the center of the molten body during cooling (Peck and Minakami, 1968). Ryan and Sammis (1981) argue that the temperature at which fractures are initiated in basalts corresponds to the glass transition temperature.

The Bishop Tuff is not a lava, was not molten, and was emplaced and welded at temperatures of about  $650^{\circ}\text{C}$  and  $750^{\circ}\text{C}$ , very close to the glass transition temperature of rhyolite (Manley, 1992; Stebbins et al., 1984; Westrich et al., 1988). Indeed, the top of the densely welded zone records the brittle/ductile transition within the tuff at the time of welding, because below this horizon, temperatures were high enough that the tuff behaved ductilely in response to the overburden pressure. Thus it is a fair approximation to assume that the tuff locally began to fracture almost immediately, as it cooled below the temperature of emplacement. In these calculations, this temperature was assumed to be  $750^{\circ}\text{C}$ .

Accounting for varying effects of latent heat, this implies that the densely welded Bishop Tuff would have fractured completely through, from the base to the top, in about 10 to 25 years. If the cracking temperature was 700°C rather than 750°C, then complete fracturing takes between 25 and 40 years. Changing the emplacement temperature to 650°C changes the thermal gradient, and complete fracturing (cracking temperature = 650°C) takes about 10 to 20 years.

These values are in excellent agreement with the lifetime of the overlying fumarolic hydrothermal system calculated in a completely independent fashion using measured  $\delta^{18}\text{O}$  values and the diffusion coefficient of feldspar (10-25 years), as well as with the actually observed lifetimes of the fumaroles at the Valley of Ten Thousand Smokes. Thus, the lifetime of the fumarolic hydrothermal system in the Bishop Tuff outflow sheet may have been in large part controlled by the rate of heat transfer from the densely welded portion of the tuff into the overlying fumarolic system; it is this parameter that determines when complete fracturing will release the perched fumarolic fluids so that they can flow downward and out along the base of the tuff.

Although the above cooling model accurately predicts the lifetime of the fumarolic system and explains many aspects of fumarole morphology and  $^{18}\text{O}$ -distribution in the tuff beneath fumarolic mounds, it is not clear from this model why we see so little evidence for the passage of significant amounts of meteoric  $\text{H}_2\text{O}$  along fractures in the upper part of the densely welded tuff. As discussed previously, all of the evidence suggests that the entire thickness of the densely welded black tuff was basically impermeable to influx of any large amounts of meteoric fluid during the lifetime of fumarolic meteoric-hydrothermal activity. This is particularly mystifying in that there were clearly large amounts of meteoric  $\text{H}_2\text{O}$  circulating in the partially welded tuff directly above. The most likely explanation, but again one that will require a good deal of further research to prove, is that magmatic gases, which would have been progressively released at lithostatic pressures during devitrification

and transient cracking of the densely welded tuff, filled these cracks and prevented meteoric fluids at hydrostatic pressures from penetrating downward into the densely welded zone.

In addition, while a certain amount of permeability would have developed in the upper part of the densely welded tuff as it fractured, it still would have been *much* less permeable than the overlying partially welded tuff, especially with regards to lateral transport of fumarolic fluids. Long, open conduits in the partially welded upper part of the Bishop Tuff outflow sheet clearly allowed for extensive lateral migration of fluids, as well as enhancing delivery of meteoric H<sub>2</sub>O to hot areas in the partially welded upper part of the tuff. These structures are not present in the lower part of the tuff, and therefore delivery of fresh supplies of meteoric H<sub>2</sub>O to newly opened fractures would have been far more difficult. Perhaps more importantly, the matrix permeability of the densely welded tuff is much less than that in the overlying partially welded tuff. Therefore, interconnection of fractures is that much more difficult to achieve in the densely welded tuff relative to partially welded tuff. Once fractures opened completely through the densely welded tuff, however, throughgoing permeability would have been instantaneously increased, as H<sub>2</sub>O was flushed from the perched aquifer into the underlying water table. In the zones directly beneath fumarolic mounds, we might then expect to see <sup>18</sup>O-depletions at the junction between the upper and lower fracture sets in the densely welded tuff. Sample CG-10 is the only sample collected from such a location, and it is indeed slightly <sup>18</sup>O-depleted, suggesting that a small amount of high-temperature oxygen exchange *did* occur at this boundary. This probably would have been the hottest part of the densely welded tuff at the instant fractures penetrated through it, and it is thus possible that sample CG-10 may have recorded the almost instantaneous interaction of the hottest part of the densely welded tuff with meteoric-fluids suddenly released from the overlying perched aquifer. A more detailed study of these kinds of occurrences in the future would be necessary to prove or disprove this conjecture.

## Figure Captions

Fig. 5.1. Comparison of  $\delta^{18}\text{O}$ -depth profiles for: (a-top) Site CG in the Bishop Tuff outflow sheet (this study); (b-middle) Long Valley intracaldera fill (Smith and Suemnicht, 1991; McConnell et al., 1997); and (c-bottom) Chegem intracaldera fill (Gazis et al., 1996). The locations of drill holes in Long Valley caldera from which the data in (b) were collected are shown in Fig. 5.2. The shaded fields on the 3 diagrams enclose essentially all measured data points for whole-rock, glass, groundmass/matrix, and pumice from the 3 different areas. The  $\delta^{18}\text{O}$  values of quartz and feldspar phenocrysts are indicated by open circles and black circles, respectively, and the range of primary magmatic  $\delta^{18}\text{O}$  for the Bishop Tuff and Chegem Tuff is shown by the two vertical lines on each diagram. The lightly shaded zone at depths of 920-1200 m on the middle diagram encompasses the deep intracaldera samples that are inferred to have been altered more than 100,000 years later by long-lived meteoric-hydrothermal systems associated with the underlying resurgent intrusions (see text). Symbols for the middle diagram are as follows: Mammoth-1 (inverted triangles), IDFU44-16 (small filled squares), Shady Rest (triangles), LVEW (squares with crosses), LV13-26 (open squares), and LV13-21 (diamonds). Pervasively devitrified tuff refers to the relatively permeable upper zones of the tuff in which the groundmass is thoroughly devitrified and the pumice/fiamme are locally devitrified and/or vapor-phase altered. Very densely welded tuff refers to the higher-density, dark-colored (not necessarily completely glassy) regions in the lower parts of the respective ash-flow sheets, where pumice fragments are indistinguishable from groundmass in hand specimen or drill core.

Fig. 5.2. Map of Long Valley caldera and vicinity showing drill-hole locations (black circles) of intracaldera tuff samples studied by Smith and Suemnicht (1991) and McConnell et al. (1997). The outcrop area of the Bishop Tuff outflow sheet is shown by dark grey

shading (Hildreth and Mahood, 1986) and that of the Early Rhyolites in the resurgent dome of the caldera is shown by the hatchured pattern (Bailey et al., 1976). The intracaldera drill-hole locations are: Clay Pit-1 (**CP**), Mammoth-1 (**M1**), IDFU 44-16 (**16**), Shady Rest (**SR**), LVEW (**EW**), LVEW 13-21 (**21**), and LVEW 13-26 (**26**).

Fig. 5.3. Calculated open-system water/rock ratios for the Long Valley intracaldera fill (top diagram) from Fig. 10 of Holt and Taylor (1998) and for the Chegem intracaldera fill (bottom diagram) from Fig. 12 of Gazis et al. (1996). These values were calculated using the equation of Taylor (1977) for the material-balance water/rock ratio (i.e., the ratio of the amount of water oxygen to the amount of rock oxygen) for an open system, in which the fine-grained, devitrified groundmass/glass is assumed to have reached approximate  $^{18}\text{O}/^{16}\text{O}$  equilibrium with the interacting water, integrated over the lifetime of the hydrothermal system. For these calculations, an initial meteoric water  $\delta^{18}\text{O} = -16$  was used for both the Chegem and the Long Valley areas; initial  $\delta^{18}\text{O}$  values of +7.8 and +8, were used for the Bishop Tuff groundmass and the Chegem Tuff groundmass, respectively. For these calculations, groundmass  $\delta^{18}\text{O}$  values were either directly measured or estimated from whole-rock  $\delta^{18}\text{O}$  values assuming 80% groundmass and 20% phenocrysts (see text). In the top diagram, fractionations between water and groundmass at 600°C and 400°C are calculated (1) using feldspar/water  $^{18}\text{O}/^{16}\text{O}$  fractionations from O'Neil and Taylor (1967), (2) combining the latter with the quartz/feldspar fractionations from Clayton and Keiffer (1991) to calculate quartz/water fractionations, and finally, by (3) assuming that the groundmass is made up of 2/3 alkali feldspar and 1/3 quartz. In the bottom diagram, the fractionation factors between water and groundmass at 850°C and 300°C were estimated by averaging the fractionation factors for quartz and albite given in Clayton and Kieffer (1991).

Fig. 5.4. A plot of  $\delta^{18}\text{O}$  feldspar vs.  $\delta^{18}\text{O}$  groundmass/whole rock, showing the steep data-point arrays from the Bishop Tuff outflow sheet (this study), from the intracaldera Bishop Tuff (McConnell et al., 1997), and from the intracaldera Chegem Tuff (Gazis et al., 1996). The large open square pinpoints the  $\delta^{18}\text{O}$  value of primary melt and sanidine from the Bishop Tuff magma. Note that most of the data from the Chegem Tuff and the intracaldera Bishop Tuff are from groundmass separates, whereas most of the data from the Bishop Tuff outflow sheet are from whole-rock analyses. Because all of these rocks are composed primarily of groundmass, there is very little difference between these various kinds of analyses; also because the only remaining significant components are quartz and feldspar phenocrysts, which have very uniform  $\delta^{18}\text{O}$  values, one can use simple material-balance to calculate a groundmass  $\delta^{18}\text{O}$  value from the whole-rock  $\delta^{18}\text{O}$  value. For example, groundmass separates were analyzed for 3 different samples from the Bishop Tuff outflow sheet (Table 2.1), and in each case a material-balance calculation of the whole-rock  $\delta^{18}\text{O}$  value was indistinguishable from the measured  $\delta^{18}\text{O}$  value. Diagonal lines for  $\Delta^{18}\text{O}_{\text{wholerock-feld}}$  at  $\Delta = 0$  and 1.0 are shown for reference only.

Fig. 5.5. Calculated lifetimes of fumarolic meteoric-hydrothermal systems as a function of temperature, based on the time required to achieve  $^{18}\text{O}/^{16}\text{O}$  exchange equilibrium with feldspar phenocrysts, using the measured slopes from Fig. 5.4, an equation relating the kinetic rate constant for oxygen exchange in feldspar to the diffusion coefficient, and assuming fluid-buffered, open-system conditions (e.g., Crank, 1975; Criss et al., 1987; see text). The diffusion coefficient for oxygen in glass is several orders of magnitude higher than in feldspar (Zhang et al., 1991); therefore: (a) the time-scales in these systems are determined solely by the rate constants for feldspar; and (b) the slope of a steep array of data points on a  $\delta^{18}\text{O}$ - $\delta^{18}\text{O}$  plot (as shown on Fig. 5.4) is equal to  $1/f$ , where  $f$  is the fractional approach to isotopic equilibrium. The two upper envelopes are for the intracaldera Bishop Tuff (dark grey) and intracaldera Chegem Tuff (black), whereas the



lower, lightly stippled envelope is based on data from the Bishop Tuff outflow sheet; the positions of these envelopes are determined by the slopes of the data-point arrays shown on Fig. 5.4 (5 to 13, 7 to 11, and 20 to 25, respectively). The grain-size radius used in the calculation ( $a = 500 \mu\text{m}$ ) represents a spherical approximation to the average grain size of phenocrysts analyzed for  $\delta^{18}\text{O}$  from the Bishop Tuff outflow sheet (see Hildreth, 1977). The horizontally ruled vertical band delineates the probable temperature range (400-650°C) applicable to fumarolic meteoric-hydrothermal systems in the Bishop Tuff, the Chegem caldera, and the Valley of Ten Thousand Smokes (see text).

Fig. 5.6. Heat flow calculations for conductive cooling of the densely welded lower part of the Bishop Tuff, which is thermally buffered at the top by overlying fumarolic meteoric-hydrothermal circulation (400°C). The thickness of the densely welded tuff is assumed to be 100 m, which is a reasonable estimate of the average of the thickness of the densely welded zone beneath fumarolic mounds and ridges. Latent heat is neglected in this calculation (see discussion in the text), and the following parameters were used: thermal diffusivity ( $\kappa$ )=0.0042 cal/(cm s °C) (Riehle, 1995), fumarole temperature ( $T_t$ ) = 400°C, initial temperature of the interior of the Bishop Tuff ( $T_i$ ) = 750°C, initial temperature of underlying country rock ( $T_b$ ) = 25°C. The relevant equation relating temperature to depth(cm) is:

$$T=(1/2)\{2[T_t+(T_i-T_t)\text{erf}(x/2(\kappa t)^{1/2})]+[T_b-T_i][\text{erf}(x-d)/2(\kappa t)^{1/2})+\text{erf}(x+d)/2(\kappa t)^{1/2})]\}.$$

Isotherms at 750°C, 650°C, and 600°C are shown by the grey dashed lines. Assuming that fracture propagation occurs at a specific temperature (see text), fractures penetrate completely through the densely welded tuff at approximately 10 years, 25 years, and 40 years, respectively, for each of the above temperatures. For each of these fracture propagation temperatures, the approximate depths at which fractures would be expected to meet are shown by the horizontal dashed line.

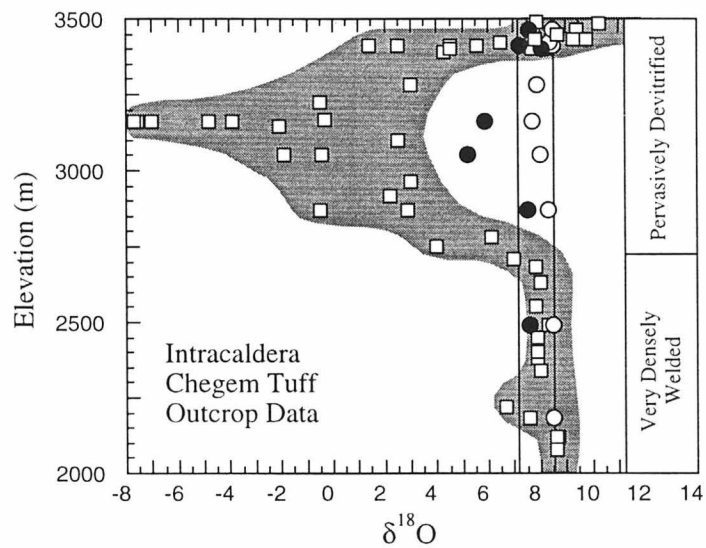
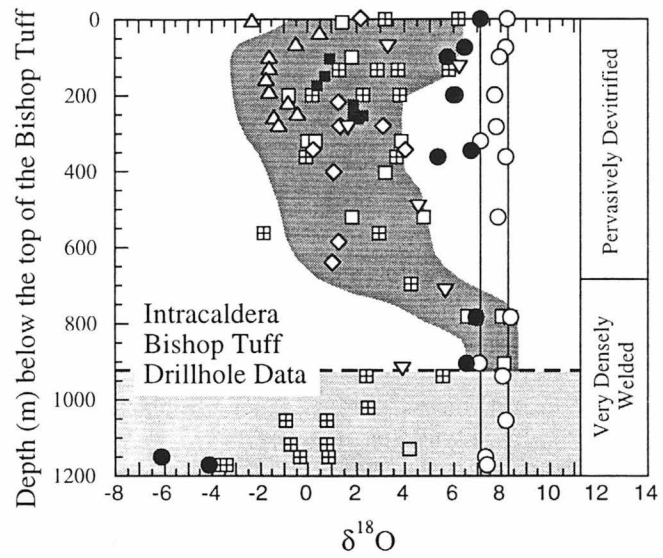
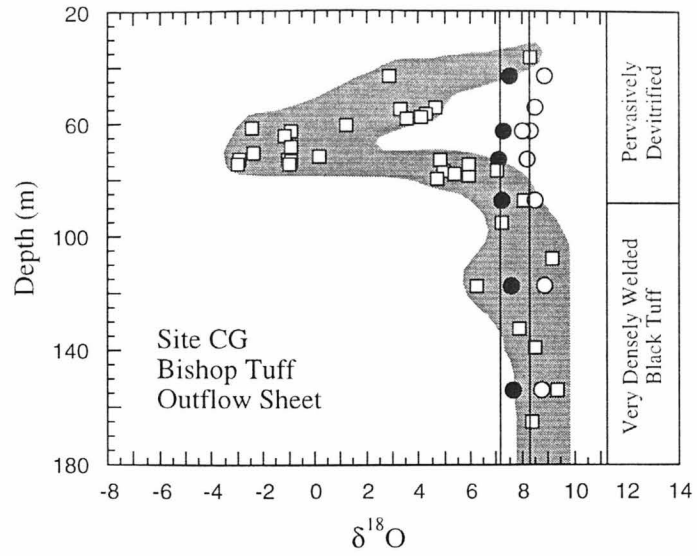


Fig. 5.1

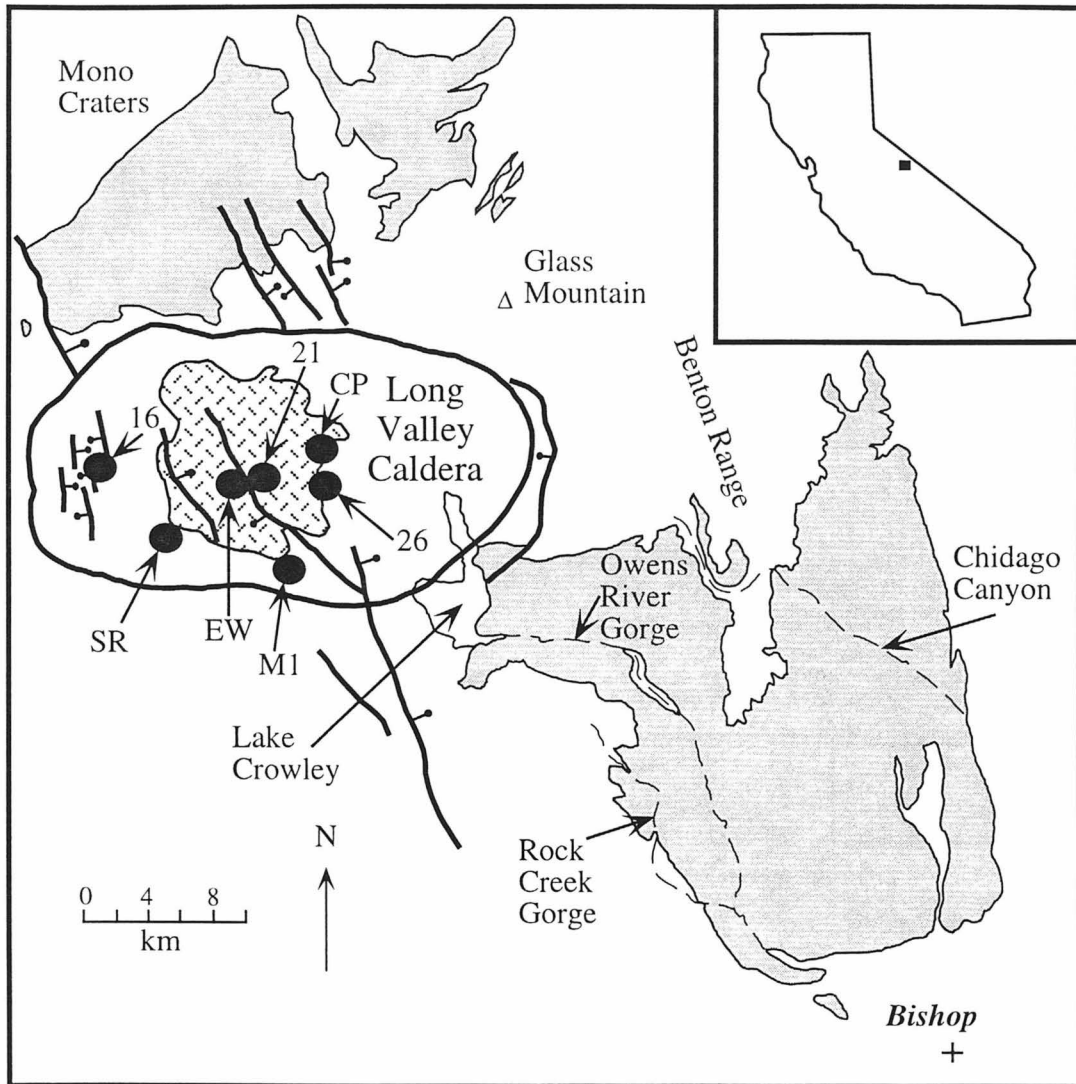


Fig.5.2

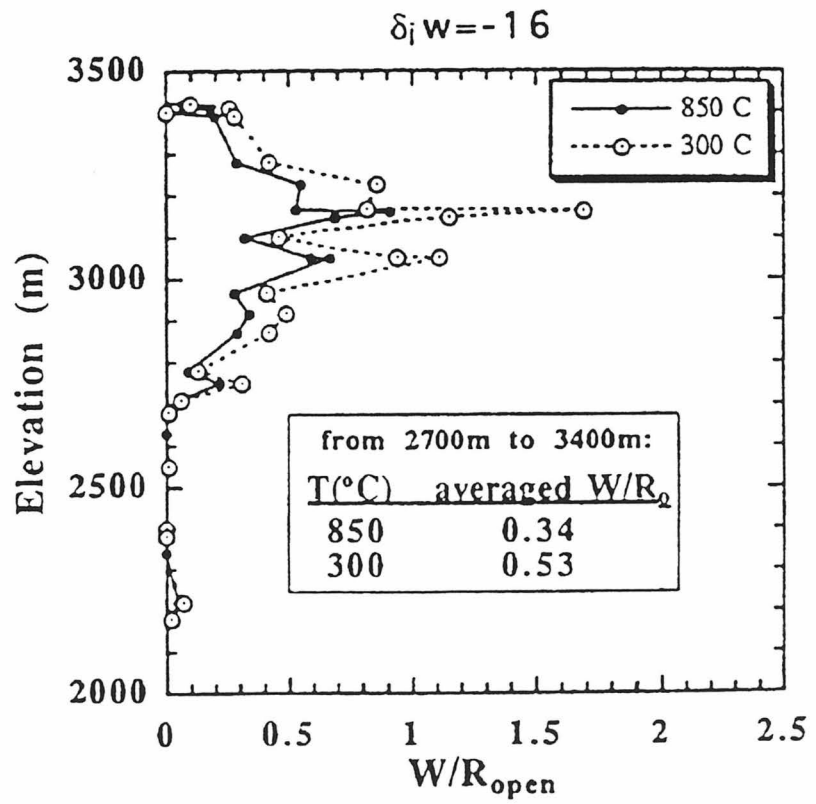
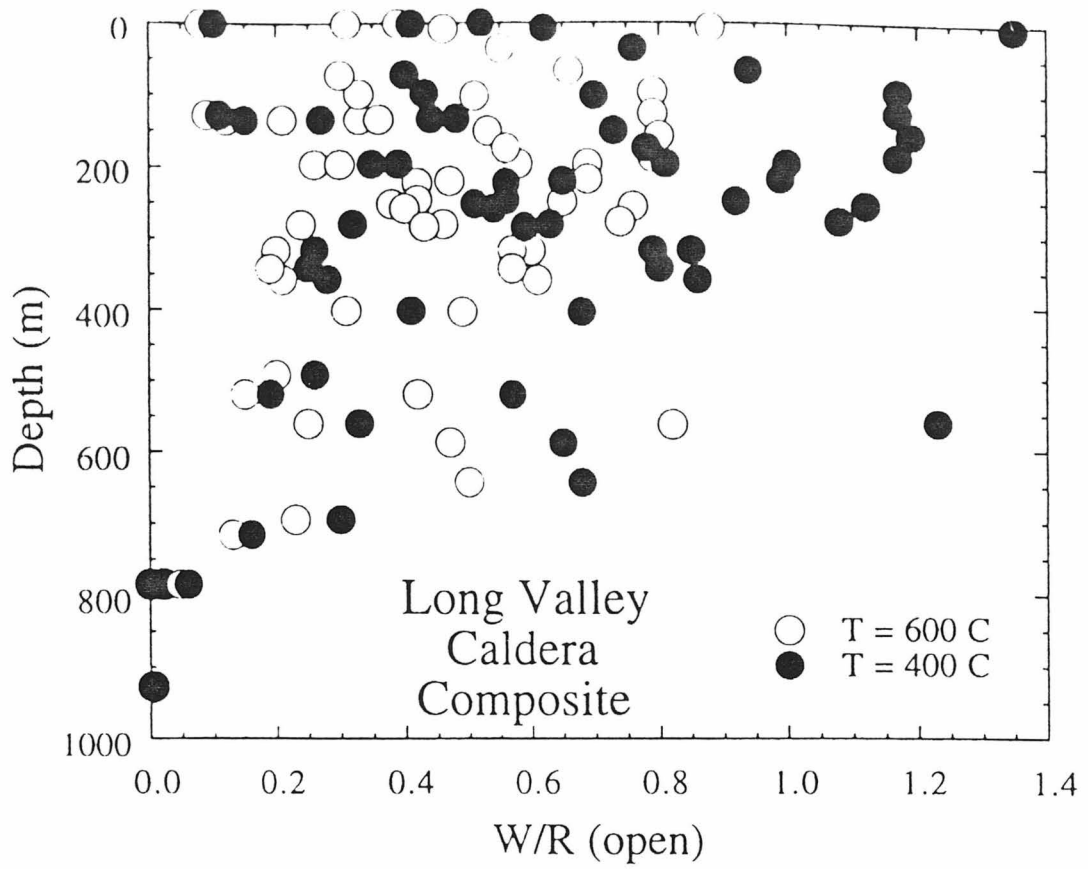


Fig.5.3

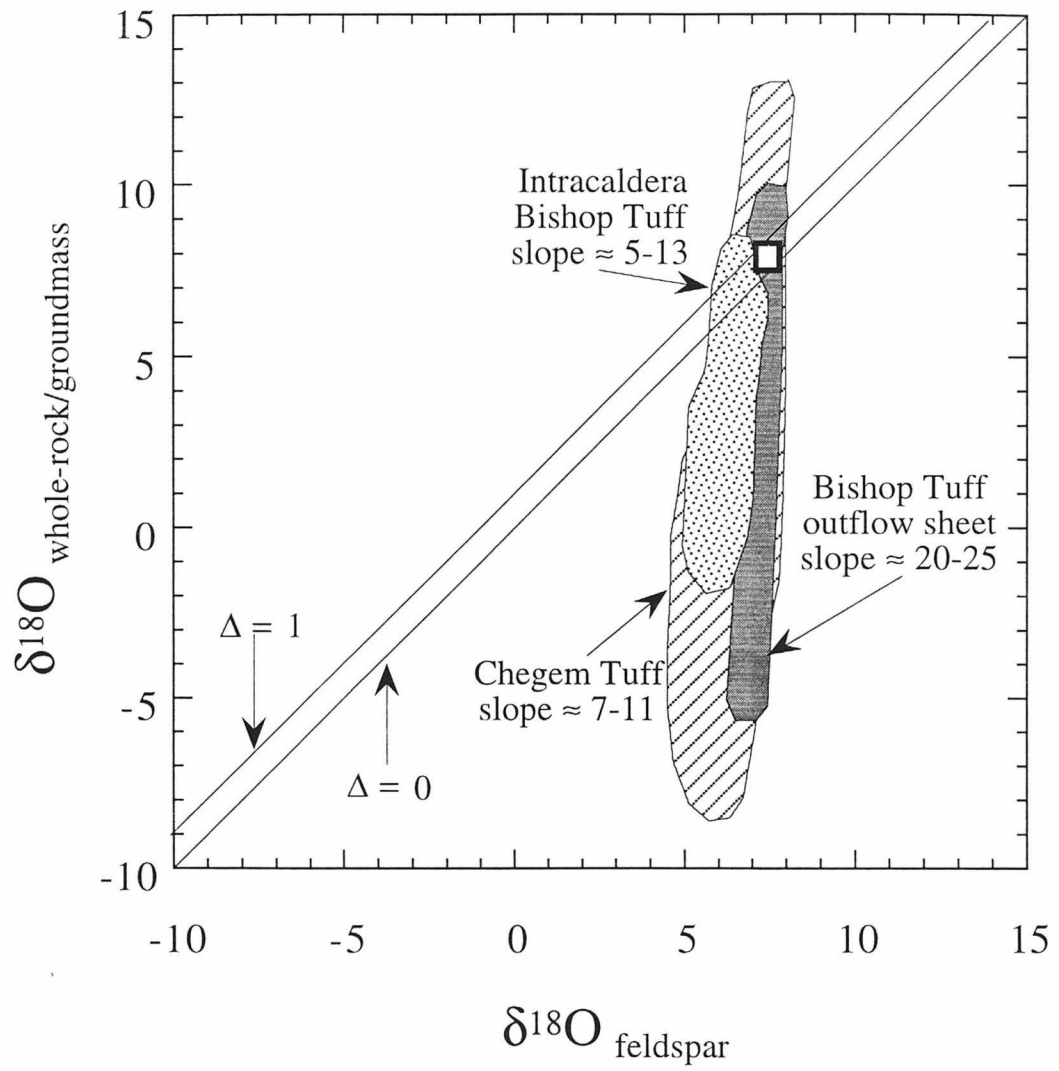


Fig.5.4

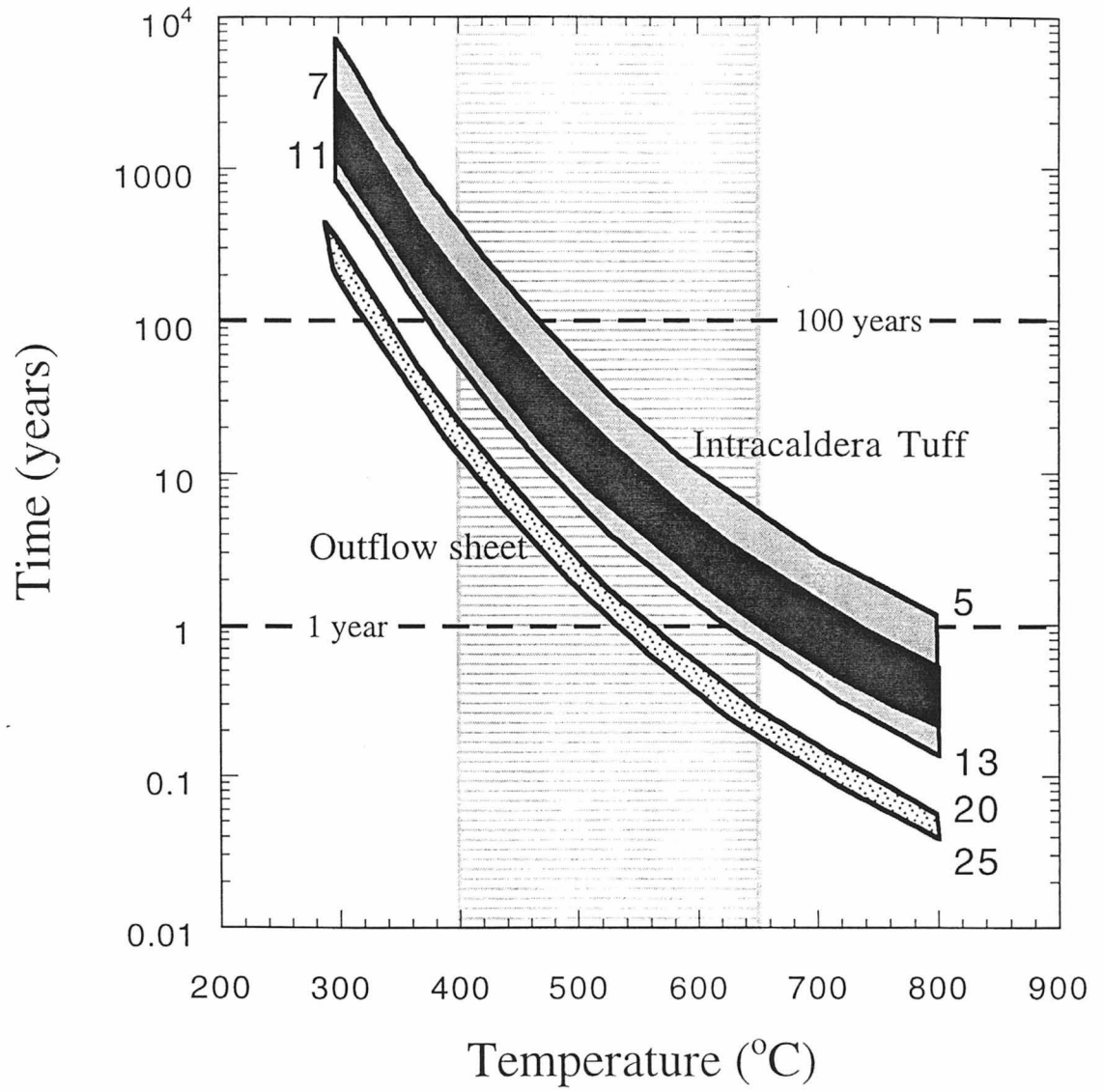


Fig. 5.5

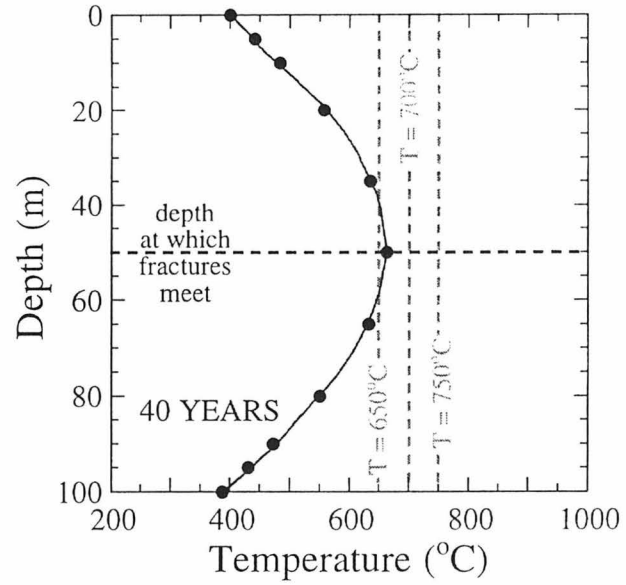
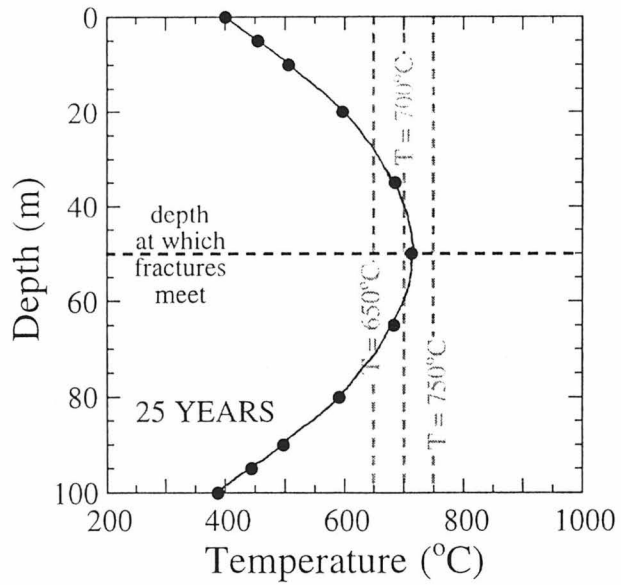
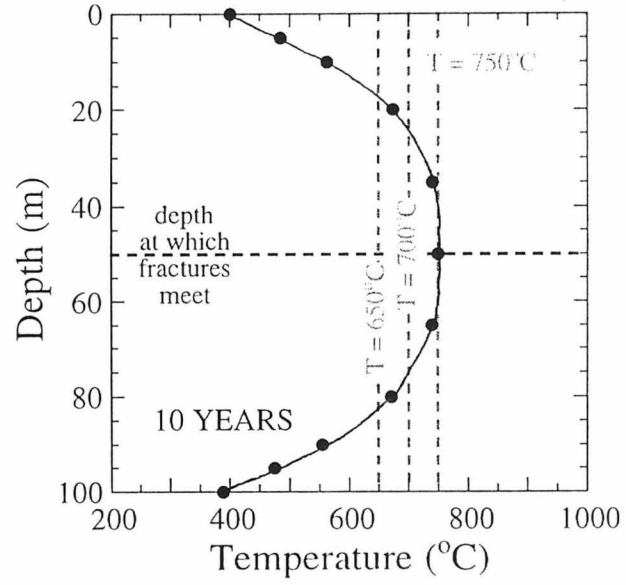
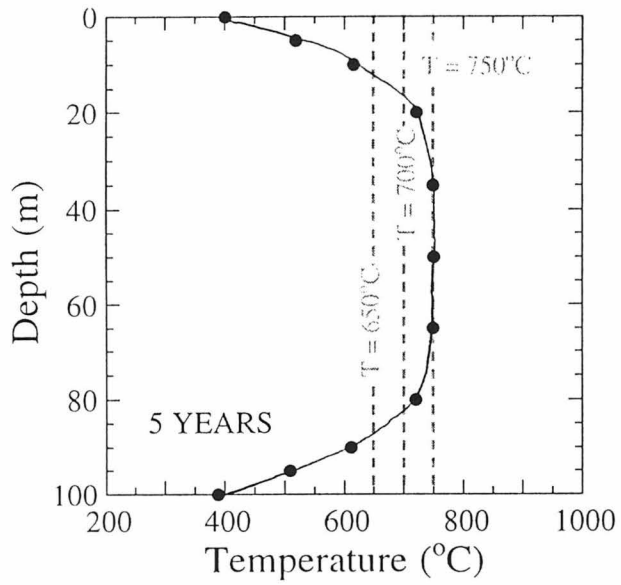


Fig. 5.6

## Appendix A: Analytical Techniques

Except for a few mineral separates, oxygen extractions from all silicate samples were carried out on 15-30 mg samples in nickel reaction vessels, using conventional fluorination techniques (Taylor and Epstein, 1962; Gazis, 1995). Laser fluorination was used to liberate oxygen from certain mineral separates (1-2 mg samples; see Table 1), using a technique similar to that described by Sharp (1990), except that samples were reacted with pure  $F_2$  instead of  $BrF_5$ . After sample loading and before reacting the samples to extract their oxygen, it has been standard practice to pretreat the laser reaction chamber with the fluorinating reagent for several hours at room temperature, in order to remove any  $H_2O$  adsorbed on the walls of the chamber (Sharp, 1990); we have followed a similar procedure using 100 torr of fluorine for 12-15 hours. The extracted oxygen was converted to  $CO_2$  using a heated carbon rod, and this  $CO_2$  was analyzed on a Finnegan MAT 252 mass spectrometer. Precision is better than 0.15 ‰ (1  $\sigma$ ) for samples analyzed using conventional oxygen extraction and 0.20 ‰ (1  $\sigma$ ) for samples analyzed using laser oxygen extraction.

Sanidine phenocrysts in all of our samples from the Bishop Tuff are pristine, colorless, and transparent. Analysis of these sanidines using the laser fluorination technique gave excellent oxygen yields (97% to 103%) and identical  $\delta^{18}O$  values (within analytical precision) to Bishop Tuff sanidines analyzed using the conventional technique. This strongly suggests that, in contrast to feldspars run using  $BrF_5$  as a fluorinating reagent (Elsenhimer and Valley, 1992; Sharp and Moecher, 1994), sanidines from the Bishop Tuff did not partially react with fluorine during our pre-treatment. However, in order to further investigate the possibility that Bishop Tuff sanidines might partially react with fluorine, multiple experiments were run in which two aliquots of 3 different kinds of feldspar were loaded into the laser fluorination reaction chamber and pre-fluorinated at room temperature. One aliquot from each sample pair was extracted after 14 hours of pre-treatment, whereas the other aliquot was left in the chamber for more than a week under



100 torr fluorine and then extracted. No change in  $\delta^{18}\text{O}$  value or yield was noted upon analysis of any of these feldspar samples (which included Bishop Tuff sanidines).

The above experiments confirm that our analyses of Bishop Tuff sanidines were not compromised by the pre-treatment. On the other hand, cloudy, hydrothermally altered feldspars, as well as whole-rock samples of fine-grained tuff, *do* react with ambient fluorine during such pre-treatment, as evidenced by drastically lower yields for liberated oxygen (<90%) for such samples. Thus, as a further precaution, blanks were run at the beginning of each day when feldspars were in the reaction chamber; these blanks were invariably negative. Also, all of our whole-rock analyses of Bishop Tuff were done by the conventional fluorination procedure, where such pre-treatment problems do not exist. Our  $\delta^{18}\text{O}$  values for Bishop Tuff sanidines and quartz samples obtained using laser fluorination ( $+7.2\pm 0.3\text{‰}$  and  $+8.4\pm 0.3\text{‰}$ , respectively) correspond very well to values obtained using conventional extraction techniques, both in our own laboratory (Table 1), and by Halliday et al. (1984, sanidine  $\delta^{18}\text{O} = +7.3\pm 0.6\text{‰}$ ).

## Appendix B: Standardization

Isotopic data are reported using the standard  $\delta$  notation in per mil (‰), and raw  $\delta^{18}\text{O}$  values are corrected to the SMOW scale using the Caltech Rose Quartz (V) standard ( $\delta^{18}\text{O} = +8.14$ ), aliquots of which were run with each sample set; NBS-28 has  $\delta^{18}\text{O} = +9.60$  on this scale, and Rose Quartz (I) standard has a value of  $\delta^{18}\text{O} = +8.45$  on this scale. At the time that Holt and Taylor (1998) was published, it was not known that Rose Quartz (V) standard had a different  $\delta^{18}\text{O}$  value than that of Rose Quartz (I) standard, and therefore raw  $\delta^{18}\text{O}$  values were miscorrected. In 1998, this problem was identified, and all raw  $\delta^{18}\text{O}$  values reported in this thesis have been corrected to reflect the lab standard Caltech Rose Quartz (V) with  $\delta^{18}\text{O} = 8.14$ .

The following tables are the  $^{18}\text{O}$ -data for standards run in the course of this thesis research. Table B.1 is for standards run using conventional oxygen extraction techniques on the North Mudd Penthouse West Line. Table B.2 is for standards run using laser oxygen extraction techniques in the basement of North Mudd building. Table B.3 is a comparison of Rose Quartz (V) standard with Rose Quartz (I) standard and with NBS-28.

On Table B.1, standards with prefix "RQS-EH-" are all Caltech Rose Quartz (V) standards. For most of the period of lab work, two manifolds (Y and Z) were used for conventional oxygen extraction. However, for a brief period, standards were also run on two other manifolds (X and W) before this attempt to get a third manifold running was abandoned. For both conventional and laser oxygen extraction lines, samples were only run when standards were running with good precision (see Appendix A).

Standards run on the laser line and shown on Table B.2 include Caltech Rose Quartz standard (**RQS**) fractions I and V, Hualali Olivine (**HOS**; Holk, 1997), a Gore Mountain Garnet (**GMG**; not the same Gore Mountain Garnet standard of Valley), a feldspar sample from the Omineca extended belt (bs24), quartz and sanidine separates from the Bishop Tuff (BT-qtz and BT-san, respectively), and quartz standards NBS-28 and MM-1. On Table B.2., it is unknown whether the first six Rose Quartz standards run on the laser extraction

line were from fraction (I) or fraction (V), and therefore these are marked by a (?). The remaining Rose Quartz standards run on the laser extraction line are from fraction (V), and they are so noted in the table. Cumulative averages for 1996 include only Rose Quartz from fraction (V). In 1996, Table B.2. indicates the % of the expected yield obtained for each standard run. In this first few months of running the laser extraction line, the analyst (Liz Holt) was inexperienced in laser fluorination, and therefore the expected yield was not always within reasonable limits (95%-105%). In later years (1997 and 1998), all but one of the standard runs gave expected yields within the above range, and therefore yields are not shown on Table B.2 for these years. The one anomalous run, which had a low yield, is shaded on Table B.2. Also, on Table B.2,  $\Delta$  (or Big Delta on Table B.2) values are shown for  $\Delta_{\text{RQS-HOS}}$  (or **R-H** on Table B.2),  $\Delta_{\text{GMG-HOS}}$  (or **G-H** on Table B.2), and  $\Delta_{\text{RQS-GMG}}$  (or **R-G** on Table B.2).

The Caltech Gore Mountain Garnet, which was given a cursory test as a back-up standard, is from a 3.5 cm wide porphyroblast of garnet from Gore Mountain. This standard lases very smoothly and gives reasonable precision (0.10 ‰; 1  $\sigma$ ). Nineteen analyses of Caltech Gore Mountain Garnet give  $\delta^{18}\text{O} = +6.7$  and an yield of 13.3  $\mu\text{mol/mg O}_2$ .

Table B.1. Raw  $^{18}\text{O}$  data for Caltech Rose Quartz (V) Standard  
expressed in per mil relative to SMOW

Standard	Number	Manifold Z	Manifold Y	Reruns	Comments
RQS-EH-	46	8.622			
RQS-EH-	47	8.620			
RQS-EH-	48	8.516			
RQS-EH-	49	8.933			
RQS-EH-	50	8.530			
RQS-EH-	51	8.604		8.631	
RQS-EH-	53		8.906		
RQS-EH-	54		8.853		
RQS-EH-	55		8.511		
RQS-EH-	56		8.480		
RQS-EH-	57		8.337		
Mass Spec vented during power outage					
RQS-EH-	58	8.292		8.337	
RQS-EH-	59	8.440		8.445	
RQS-EH-	60	8.325		8.371	
RQS-EH-	61	8.495		13.517	
RQS-EH-	62	8.337			
RQS-EH-	63	8.481		8.567	
RQS-EH-	64		8.710	8.831	
RQS-EH-	65		8.534		
RQS-EH-	66		8.549		
RQS-EH-	67		8.330		
RQS-EH-	68		8.254		
RQS-EH-	69		8.572		
RQS-EH-	70	8.284			
RQS-EH-	71	8.472			
RQS-EH-	72	8.320			
RQS-EH-	73	8.042			
RQS-EH-	74	8.305			
RQS-EH-	75	8.395			
RQS-EH-	76		8.537		
RQS-EH-	77		8.554		
RQS-EH-	78		8.274		
RQS-EH-	79	8.360			
RQS-EH-	80	8.450			
RQS-EH-	81	8.460			
RQS-EH-	82		8.270		Leaky
RQS-EH-	83		6.380		Reaction
RQS-EH-	84		8.020		Vessels
RQS-EH-	85	8.500			
RQS-EH-	86	8.460			
RQS-EH-	87	8.350			

**Table B.1. (cont.)**

Standard	Number	Manifold Z	Manifold Y	Reruns	Comments
RQS-EH-	88		8.880		
RQS-EH-	89		8.599		
RQS-EH-	90		8.586		
RQS-EH-	91	8.420			
RQS-EH-	92	8.490			
RQS-EH-	93	8.480			
<b>line rested for 2 months and new standard on mass spec</b>					
RQS-EH-	94		7.982		
RQS-EH-	95		8.007		
RQS-EH-	96		7.956		
RQS-EH-	97		8.086		
RQS-EH-	98		7.933		
RQS-EH-	99		8.030		
RQS-EH-	100	7.587			
RQS-EH-	101	7.964			
RQS-EH-	102	8.100			
RQS-EH-	103	7.753			
RQS-EH-	104	7.816			
RQS-EH-	105	7.777			
RQS-EH-	106	7.859			
RQS-EH-	107	7.993			
RQS-EH-	108	8.028			
RQS-EH-	109	7.921			
RQS-EH-	110	7.935			
RQS-EH-	111	7.935			
RQS-EH-	112		8.083		
RQS-EH-	113		8.005		
RQS-EH-	114	7.764			
RQS-EH-	115	7.981			
RQS-EH-	116		8.088		
RQS-EH-	117		8.010		
RQS-EH-	118	7.923			
RQS-EH-	119	8.743			
RQS-EH-	120		8.135		
RQS-EH-	121		8.096		
RQS-EH-	122	7.926			
RQS-EH-	123	8.129			
RQS-EH-	124		8.096		
RQS-EH-	125		8.016		
RQS-EH-	126				samples lost
RQS-EH-	127				
<b>line rested one month</b>					

Table B.1. (cont.)

Standard	Number	Manifold Z	Manifold Y	Reruns	Comments
RQS-EH-	128		7.130		all water not pumped out of glass yet
RQS-EH-	129		7.756		
RQS-EH-	130		7.659		
RQS-EH-	131		7.684		
RQS-EH-	132		7.855		
RQS-EH-	133		9.063		
RQS-EH-	134	7.902			
RQS-EH-	135	9.085			
RQS-EH-	136	8.302			
RQS-EH-	137	8.120			
RQS-EH-	138	8.092			
RQS-EH-	139	8.041			
RQS-EH-	140		7.990		
RQS-EH-	141		8.206		
RQS-EH-	142		8.155		
RQS-EH-	143		8.097		
RQS-EH-	144		7.995		
RQS-EH-	145		8.079		
RQS-EH-	146	7.846			
RQS-EH-	147	8.054			
RQS-EH-	148	7.934			
RQS-EH-	149	8.242			
RQS-EH-	150				blank
RQS-EH-	151	8.052			
RQS-EH-	152		8.019		
RQS-EH-	153	7.927			
line rested 3 weeks					
RQS-EH-	154		8.197		
RQS-EH-	155		8.178		
RQS-EH-	156		8.198		
RQS-EH-	157		7.984		
RQS-EH-	158		7.935		
RQS-EH-	159		8.174		
RQS-EH-	160	7.920			
RQS-EH-	161	7.838			
RQS-EH-	162	8.015			
RQS-EH-	163	8.110			
RQS-EH-	164	8.006			
RQS-EH-	165	7.996			
RQS-EH-	166		7.843		
RQS-EH-	167	7.913			
RQS-EH-	168		7.386	7.328	
RQS-EH-	169	7.898			
line rested 4 weeks					

**Table B.1. (cont.)**

Standard	Number	Manifold Z	Manifold Y	Reruns	Comments
RQS-EH-	170		8.006		
RQS-EH-	171		8.365		
RQS-EH-	172		8.208		
RQS-EH-	173		8.213		
RQS-EH-	174		8.182		
RQS-EH-	175		8.298		
RQS-EH-	176	7.968			
RQS-EH-	177	8.142			
RQS-EH-	178	8.038			
RQS-EH-	179	9.440			pumped on
RQS-EH-	180	8.049			
RQS-EH-	181	8.035			
RQS-EH-	182		7.990		
RQS-EH-	183		8.109		
RQS-EH-	184		8.251		
RQS-EH-	185		8.071		
RQS-EH-	186		8.129		
RQS-EH-	187				dumped
RQS-EH-	188	7.466			
RQS-EH-	189	7.814			
RQS-EH-	190		8.082		
RQS-EH-	191		8.075		
RQS-EH-	192	7.851			
RQS-EH-	193	7.950			
RQS-EH-	194				bad sample
RQS-EH-	195				tubes
regreased sample tubes and glass part of line					
started messing with manifold X					
RQS-EH-	196	7.583			
RQS-EH-	197	8.069			
RQS-EH-	198	8.438			bad run
RQS-EH-	199	8.053			
RQS-EH-	200	7.938			
RQS-EH-	201	8.006			
RQS-EH-	202		8.373		
RQS-EH-	203		8.244		
RQS-EH-	204		8.449		
RQS-EH-	205		8.475		
RQS-EH-	206		8.208		
RQS-EH-	207		8.588		
RQS-EH-	208	7.063			
RQS-EH-	209	8.564			
RQS-EH-	210		8.131		
RQS-EH-	211		8.374		

**Table B.1. (cont.)**

Standard	Number	Manifold Z	Manifold Y	Manifold W	Comments
RQS-EH-	212		8.322		
RQS-EH-	213		8.349		
RQS-EH-	214		8.167		
RQS-EH-	215		8.435		
RQS-EH-	216				pumped away
RQS-EH-	217	7.425			
RQS-EH-	218	7.879			
RQS-EH-	219	7.608			
RQS-EH-	220	8.001			
RQS-EH-	221	7.896			
RQS-EH-	222				pumped away
RQS-EH-	223				all of
RQS-EH-	224				these
RQS-EH-	225				from
RQS-EH-	226				man.
RQS-EH-	227				X
RQS-EH-	228		8.274		
RQS-EH-	229		8.187		
RQS-EH-	230		8.368		pumped on
RQS-EH-	231		8.162		
RQS-EH-	232		8.141		
RQS-EH-	233		8.262		
RQS-EH-	234			7.553	
RQS-EH-	235				pumped
RQS-EH-	236				these
RQS-EH-	237				away
RQS-EH-	238			8.802	
RQS-EH-	239			8.569	
RQS-EH-	240	6.757			
RQS-EH-	241	8.309			
RQS-EH-	242	8.490			
RQS-EH-	243	8.382			
RQS-EH-	244	8.003			
RQS-EH-	245	8.085			
RQS-EH-	246		8.196		
changed C-rod					
RQS-EH-	247			7.866	
RQS-EH-	248			8.442	
RQS-EH-	249			7.301	
RQS-EH-	250			7.914	
RQS-EH-	251			8.661	
RQS-EH-	252			7.962	
RQS-EH-	253	7.089			bad p-balance
RQS-EH-	254	8.293			



**Table B.1. (cont.)**

Standard	Number	Manifold Z	Manifold Y	Manifold W	Comments
RQS-EH-	255		8.250		
RQS-EH-	256			7.987	
RQS-EH-	257			8.268	
RQS-EH-	258			9.563	
RQS-EH-	259			8.461	
RQS-EH-	260			8.897	
RQS-EH-	261			8.684	
RQS-EH-	262	7.962			
RQS-EH-	263				
line rested two months					
RQS-EH-	264		7.940		low yield
RQS-EH-	265		9.130		low yield
RQS-EH-	266		8.100		
RQS-EH-	267		8.170		
RQS-EH-	268		8.050		
RQS-EH-	269		8.340		
RQS-EH-	270			7.62	
RQS-EH-	271			9.563	
RQS-EH-	272			8.125	
RQS-EH-	273			7.751	
RQS-EH-	274			8.562	
RQS-EH-	275			6.37	
RQS-EH-	276	7.760			
RQS-EH-	277	7.996			
RQS-EH-	278	7.985			
RQS-EH-	279	8.192			
RQS-EH-	280	7.967			
RQS-EH-	281	7.974			
RQS-EH-	282		8.098		
RQS-EH-	283		8.052		
RQS-EH-	284		8.176		
RQS-EH-	285			7.929	
RQS-EH-	286			7.939	
RQS-EH-	287			8.958	low yield
RQS-EH-	288			8.198	
RQS-EH-	289			8.778	
RQS-EH-	290			8.434	
RQS-EH-	291	7.658			
RQS-EH-	292	8.109			
RQS-EH-	293		6.943		low yield
RQS-EH-	294				
RQS-EH-	295				
RQS-EH-	296				
RQS-EH-	297				

**Table B.1. (cont.)**

Standard	Number	Manifold Z	Manifold Y	Manifold W	Comments
RQS-EH-	298				
RQS-EH-	299				
RQS-EH-	300	7.879			
RQS-EH-	301	8.200			
RQS-EH-	302		8.091		
RQS-EH-	303			7.827	
RQS-EH-	304			8.519	
RQS-EH-	305			8.826	low yield
RQS-EH-	306			7.983	
RQS-EH-	307			8.432	low yield
RQS-EH-	308				
RQS-EH-	309	7.900			
RQS-EH-	310	8.078			
RQS-EH-	311		7.821		
RQS-EH-	312				
RQS-EH-	313				
RQS-EH-	314				
RQS-EH-	315				
RQS-EH-	316				
RQS-EH-	317				
RQS-EH-	318	8.101			
line rested five months					
RQS-EH-	319		8.149		
RQS-EH-	320		8.018		
RQS-EH-	321		8.009		
RQS-EH-	322		7.986		
RQS-EH-	323		7.968		
RQS-EH-	324		7.948		
RQS-EH-	325		8.104		
RQS-EH-	326	7.606			
RQS-EH-	327	8.131			
RQS-EH-	328	7.998			
RQS-EH-	329	7.946			
RQS-EH-	330	7.820			
RQS-EH-	331	7.779			
RQS-EH-	332		7.974		
RQS-EH-	333	7.904			
RQS-EH-	334	8.204			
RQS-EH-	335	8.517			
LINE RESTED 3 MONTHS					
RQS-EH-	336	7.508			
RQS-EH-	337	7.590			
RQS-EH-	338	7.699			
RQS-EH-	339	7.801			

Table B.1. (cont.)

Standard	Number	Manifold Z	Manifold Y	Manifold W	Comments
RQS-EH-	340	8.153			
RQS-EH-	341	7.546			
RQS-EH-	342		SAMPLES		
RQS-EH-	343		LOST		
RQS-EH-	344		DUE		
RQS-EH-	345		TO		
RQS-EH-	346		FLUORINE		
RQS-EH-	347		PROBLEM		
RQS-EH-	348			STILL	
RQS-EH-	349			HAVE	
RQS-EH-	350			FLUORINE	
RQS-EH-	351			PROBLEM	
RQS-EH-	352			WITH	
RQS-EH-	353			LINE	
RQS-EH-	354	8.122			
RQS-EH-	355	7.924			
RQS-EH-	356	8.114			
RQS-EH-	357	8.036			
RQS-EH-	358	8.154			
RQS-EH-	359	7.953			
RQS-EH-	360		MORE		
RQS-EH-	361		PROBLEMS		
RQS-EH-	362		WITH		
RQS-EH-	363		FLUORINE		
RQS-EH-	364		DELIVERY		
RQS-EH-	365		SYSTEM		
RQS-EH-	366	8.070			
RQS-EH-	367		8.156		
RQS-EH-	368		8.178		
RQS-EH-	369		8.058		
RQS-EH-	370		8.065		
RQS-EH-	371		8.078		
RQS-EH-	372		8.325		
RQS-EH-	373	6.966			
RQS-EH-	374		8.123		
RQS-EH-	375	6.950			
RQS-EH-	376		7.675		
RQS-EH-	377	7.790			
RQS-EH-	378	7.710			
RQS-EH-	379	7.488			
RQS-EH-	380	7.732			
RQS-EH-	381	7.994			
RQS-EH-	382	7.798			
RQS-EH-	383		8.196		

dry-box  
not getting  
dry

Table B.1. (cont.)

Standard	Number	Manifold Z	Manifold Y	Reruns	Comments
RQS-EH-	384		8.094		
RQS-EH-	385		8.052		
RQS-EH-	386		8.115		
RQS-EH-	387		8.131		
RQS-EH-	388		8.335		
RQS-EH-	389	7.680			
RQS-EH-	390	7.888			
RQS-EH-	391	7.927			
RQS-EH-	392	8.227			
RQS-EH-	393	8.255			
RQS-EH-	394	8.374			
RQS-EH-	395		7.181		
RQS-EH-	396	7.686			
RQS-EH-	397	7.797			
RQS-EH-	398				
RQS-EH-	399		8.362		
RQS-EH-	400		8.224		
RQS-EH-	401		8.371		
RQS-EH-	402		8.309		
RQS-EH-	403		8.102		
RQS-EH-	404		8.498		
RQS-EH-	405	7.833			
RQS-EH-	406	8.431			
RQS-EH-	407	8.007			
RQS-EH-	408	8.242			
RQS-EH-	409	8.379			
RQS-EH-	410	8.342			
RQS-EH-	411		8.359		
RQS-EH-	412	8.188			
RQS-EH-	413		8.267		
RQS-EH-	414				
RQS-EH-	415		8.183		
line rested two months					
RQS-EH-	416	7.880			
RQS-EH-	417	8.215			
RQS-EH-	418	8.274			
RQS-EH-	419	8.397			
RQS-EH-	420	8.099			
RQS-EH-	421	8.240			
RQS-EH-	422		8.053		
RQS-EH-	423		8.106		
RQS-EH-	424		8.261		
RQS-EH-	425		7.951		
RQS-EH-	426		8.227		

**Table B.1. (cont.)**

Standard	Number	Manifold Z	Manifold Y	Reruns	Comments
RQS-EH-	427		8.036		
RQS-EH-	427	7.991			
RQS-EH-	428	8.058			
RQS-EH-	429		8.373		
RQS-EH-	430		8.266		
RQS-EH-	431	7.862			
RQS-EH-	432	8.105			
RQS-EH-	433				pumped away
RQS-EH-	434	8.024			
RQS-EH-	435	8.357			
RQS-EH-	436	8.201			
new converter wire					
RQS-EH-	437		8.264		
RQS-EH-	438		8.099		
RQS-EH-	439		8.310		
RQS-EH-	440		8.290		
RQS-EH-	441		8.180		
RQS-EH-	442		8.259		
RQS-EH-	443	7.934			
RQS-EH-	444	8.149			
RQS-EH-	445	8.229			
RQS-EH-	446		8.338		
RQS-EH-	447		8.360		
RQS-EH-	448	8.026			
RQS-EH-	449	8.105			
RQS-EH-	450		8.500		
RQS-EH-	451		8.109		
RQS-EH-	452	8.139			
RQS-EH-	453	8.131			
RQS-EH-	454				
RQS-EH-	455				
RQS-EH-	456				
RQS-EH-	457				
RQS-EH-	458				
RQS-EH-	459				
RQS-EH-	460				
RQS-EH-	461				
RQS-EH-	462				
RQS-EH-	463				
RQS-EH-	464				
RQS-EH-	465				
RQS-EH-	466		8.279		
RQS-EH-	467		8.111		
RQS-EH-	468		8.237		

**Table B.1. (cont.)**

Standard	Number	Manifold Z	Manifold Y	Reruns	Comments
RQS-EH-	469		7.915		
RQS-EH-	470		7.941		
RQS-EH-	471		8.080		
RQS-EH-	472	7.940			bad rxn vsI
RQS-EH-	473	8.209			
RQS-EH-	474	8.202			
RQS-EH-	475	8.215			
RQS-EH-	476	8.008			
RQS-EH-	477	8.127			
RQS-EH-	478		8.591		
RQS-EH-	479		7.990		
RQS-EH-	480		8.024		
RQS-EH-	481	7.667			bad rxn vsI
RQS-EH-	482	7.954			
RQS-EH-	483		7.963		
RQS-EH-	484		7.881		
RQS-EH-	485		8.158		
RQS-EH-	486		8.171		
RQS-EH-	487		7.839		
RQS-EH-	488	7.679			bad rxn vsI
RQS-EH-	489	7.975			
RQS-EH-	490	7.685			rxn vsI looks good
RQS-EH-	491	7.897			
RQS-EH-	492		8.382		
RQS-EH-	493	7.948			
RQS-EH-	494	8.016			
RQS-EH-	495		7.979		
RQS-EH-	496	7.781			
RQS-EH-	497	8.023			
RQS-EH-	498		8.045		
RQS-EH-	499	7.909			
RQS-EH-	500	7.728			
RQS-EH-	501		7.947		
RQS-EH-	502	8.296			
RQS-EH-	503		8.089		
RQS-EH-	504	7.991			
RQS-EH-	505		8.094		
RQS-EH-	506	8.257			
RQS-EH-	507		8.223		

**Table B.2: Raw <sup>18</sup>O data expressed in per mil relative to SMOW for standards obtained using laser oxygen extraction techniques.**

Cumulative Statistics for three major standards in 1996						
	<b>RQS(V)</b>	<b>HOS</b>	<b>GMG</b>	Big Delta Values		
average	8.19	5.62	6.98	<b>R-H</b>	<b>G-H</b>	<b>R-G</b>
stdev	0.27	0.21		2.57	1.36	1.21

Run Date	<b>RQS(?)</b>	<b>HOS</b>	bs24	nbs-28	<b>GMG</b>	mm1	% yield
11/15/95	8.708						111
11/16/95	8.469						97
New filament and new mass spec standard							
1/31/96		5.667					106
1/31/96			12.822				93
1/31/96	8.692						89
1/31/96	8.481						99
2/1/96		5.622					102
2/1/96	8.500						99
2/2/96	8.441						98
Run Date	<b>RQS(V)</b>	<b>HOS</b>	bs24	nbs-28	<b>GMG</b>	mm1	% yield
2/7/96		5.672					99
2/7/96	8.074						103
2/8/96	8.707						96
2/9/96		5.328					103
2/9/96			13.091				76
2/9/96	8.167						100
2/13/96	8.094						97
2/13/96				9.554			100
2/13/96		5.615					103
2/14/96						13.272	100
2/14/96		5.698					103
2/19/96	8.001						104
2/19/96	8.072						101
2/19/96		5.497					104
2/19/96	8.062						97
2/19/96			11.783				98
2/19/96	7.810						111
2/19/96		5.656					141
2/20/96	8.062						103
2/20/96							119
2/21/96							103
2/21/96							109
2/21/96							97
2/21/96	8.226						104
2/22/96			12.272				94

Table B.2. (cont.)

Run Date	RQS(V)	HOS	bs24	nbs-28	GMG	mm1	% yield
2/22/96	8.342						101
2/22/96	8.056						97
2/23/96					6.977		
2/23/96	8.055						103
2/23/96							103
2/23/96							114
2/23/96							110
2/23/96	8.097						96
2/23/96							103
2/24/96	8.257						116
2/24/96		5.175					103
2/26/96			12.138				98
2/26/96	7.989						98
2/26/96							111
2/26/96							92
2/26/96	8.323						99
2/27/96	8.331						114
2/27/96		5.571					98
2/27/96		6.067					100
2/27/96	8.071						130
2/28/96		5.801					102
2/28/96		5.651					108
2/28/96		5.457					102
2/28/96		5.905					98
2/28/96	8.237						123
2/28/96	8.154						130
2/29/96	9.152						123
2/29/96	8.013						120
2/29/96		5.523					98

## Cumulative Statistics for standards run in 1997

	RQS(V)	HOS	GMG	Big Delta Values		
average	8.35	5.79	6.88	R-H	G-H	R-G
stdev	0.10	0.10	0.09	2.56	1.09	1.47

Run Date	RQS(V)	HOS	GMG
1/31/97	8.141	5.993	7.024
2/1/97	8.415	5.883	6.839
2/1/97	8.187		6.818
2/2/97	8.244	5.639	6.990
2/16/97	8.436		6.757
2/17/97	8.482		
2/20/97	8.302	5.719	



**Table B.2. (cont.)**

Run Date	RQS(V)	HOS	GMG
2/27/97	8.356	5.835	6.98
2/27/97	8.455	5.908	
3/2/97	8.285	5.738	6.89
3/2/97	8.351		

## Cumulative Statistics for standards run in 1998

	RQS(V)	HOS	Big Delta Values
average	8.30	5.63	<b>R-H</b>
stdev	0.07	0.09	2.67

Run Date	RQS(V)	HOS
1/25/98	8.314	5.639
1/26/98	8.255	5.725
5/7/98	8.195	
5/8/98	8.303	
5/8/98	8.325	
11/16/98	8.285	5.507
11/17/98	8.419	5.663

**Table B.3. Comparison of  $\delta^{18}\text{O}$  values for RQS(V) with those of RQS(I) and NBS-28**

Standard	Run Nc	Manifold Y	Manifold Z	Comment
RQSV	1		7.772	bad rxn vsI
RQSV	2		7.998	
NBS-28	1		9.367	
NBS-28	2		9.513	
RQSI	1		8.545	
RQSI	2		8.251	
RQSV	3		7.859	bad rxn vsI
RQSV	4			converter died
RQSI	3		8.486	
RQSI	4		8.367	
NBS-28	3		9.388	
NBS-28	4		9.673	
RQSV	5	7.916		low yield
RQSV	6	7.780		
RQSV	7	7.771		
RQSI	5	7.853		
RQSI	6	7.869		
RQSI	7	7.953		
NBS-28	5		9.698	
RQSV	8	8.177		glass broke
NBS-28	6	9.873		
RQSV	9		8.144	
NBS-28	7		9.655	
RQSV	10	8.223		
NBS-28	8	9.540		
RQSV	11		8.132	
NBS-28	9		9.558	
RQSV	12	8.173		
RQSV	13		8.177	
NBS-28	10		9.709	
RQSV	14	8.209		
NBS-28	11	9.546		
RQSV	15		8.205	
NBS-28	12		9.565	
NBS-28	13	10.085		high yield

**Appendix C: References**

- Allen, E.T. and Zies, E.G., 1923. A chemical study of fumaroles of the Katmai region. National Geographic Society, Contributed Technical Papers, Katmai Series, 2: 75-155.
- Bailey, R.A., 1989. Geologic map of Long Valley Caldera, Mono-Inyo Craters volcanic chain, and vicinity, eastern California. U.S. Geol. Surv. I-1933.
- Bailey, R.A., Dalrymple, G.B., and Lanphere, M.A., 1976. Volcanism, structure, and geochronology of Long Valley caldera, Mono County, California. *Jour. of Geophys. Res.*, 81: 725-744.
- Bateman, P.C., 1965. Geology and tungsten mineralization of the Bishop district, California. U. S. Geol. Survey Prof. Paper, 470: 208 p.
- Bogaaard, P.V.D. and Schirnick, C., 1995.  $^{40}\text{Ar}/^{39}\text{Ar}$  laser probe ages of Bishop Tuff quartz phenocrysts substantiate long-lived silicic magma chamber at Long Valley, United States. *Geology*, 23: 759-762.
- Broxton, D.E. and Reneau, S.L., 1996. Buried Pleistocene landscapes beneath the Pajarito Plateau, Northern New Mexico. New Mexico Geological Society Guidebook, 47th Field Conference, Jemez Mountains Region, pp 325 - 334.
- Byers, F.M., Jr., 1961. Petrology of three volcanic suites, Umnak and Bogoslof Islands, Aleutian Islands, Alaska. *Geol. Soc. Am. Bull.*, 72: 93-128.
- Carslaw, H.S. and Jaeger, J.C., 1959. *Conduction of Heat in Solids*. Clarendon Press, Oxford, 510 pp.
- Clayton, R.N. and Kieffer, S.W., 1991. Oxygen isotopic thermometer calibrations. In: Taylor, H.P., Jr., O'Neil, J.R., and Kaplan, I.R. (Editors), *Stable Isotope Geochemistry: A Tribute to Samuel Epstein*. *Geochem. Soc. Spec. Publ.*, 3: 3-10.
- Crank, J., 1975. *The Mathematics of Diffusion*. Clarendon Press, Oxford, 414 pp.

- Criss, R.E., Gregory, R.T., and Taylor, H.P., Jr., 1987. Kinetic theory of oxygen isotope exchange between minerals and water. *Geochim. et Cosmochim. Acta*, 51: 1099-1108.
- Criss, R.E. and Taylor, H.P., Jr., 1986. Meteoric-hydrothermal systems. In: Valley, J.W., Taylor, H.P., Jr., and O'Neil, J.R. (Editors), *Stable Isotopes in High Temperature Geological Processes*. *Reviews in Mineralogy*, 16: 373-424.
- Curtis, G.H., 1968. The stratigraphy of the ejecta from the 1912 eruption of Mount Katmai and Novarupta, Alaska. In: R.R. Coats, R.L. Hay, and C.A. Anderson (Editors), *Studies in Volcanology*. *Geol. Soc. Am. Mem.*, 116: 153-210.
- DeGraff, J.M., Long, P.E., and Aydin, A., 1989. Use of joint-growth directions and rock textures to infer thermal regimes during solidification of basaltic lava flows. *Jour. Volcanol. Geotherm. Res.*, 38: 309-324.
- Elsenhimer, D. and Valley, J.W., 1992. In situ oxygen isotope analysis of feldspar and quartz by Nd: YAG laser microprobe. *Chemical Geology*, 101: 21-42.
- Farrar, C.D., Howle, J.F., Neil, J.M., Sorey, M.L., and Evans, W.C., 1998. Volcanogenic CO<sub>2</sub> emissions at Mammoth Mountain, California, USA. *EOS Trans. AGU* 79(45): F941.
- Gazis, C., Taylor, H.P., Jr., Hon, K., and Tsvetkov, A., 1996. Oxygen isotopic and geochemical evidence for a short-lived, high-temperature hydrothermal event in the Chegem caldera, Caucasus Mountains, Russia. *Jour. of Volcanol. Geothermal Res.*, 73: 213-244.
- Giletti, B.J., Semet, M.P., and Yund, R.A., 1978. Studies in diffusion III. Oxygen in feldspars: an ion microprobe determination. *Geochim. Cosmochim. Acta*, 42: 45-57.
- Gregory, R.T., Criss, R.E., and Taylor Jr., H.P., 1989. Oxygen isotope exchange kinetics of mineral pairs in closed and open systems: Applications to problems of

- hydrothermal alteration of igneous rocks and Precambrian iron formations. *Chemical Geology*, 75: 1-42.
- Griggs, R.F., 1922. *The Valley of Ten Thousand Smokes*. National Geographic Society, Washington, D.C., 340 pp.
- Grossenbacher, K.A. and McDuffie, S.M., 1995. Conductive cooling of lava: columnar joint diameter and stria width as functions of cooling rate and thermal gradient. *Jour. Volcanol. Geotherm. Res.*, 69: 95-103.
- Halliday, A.N., Fallick, A.E., Hutchinson, J., and Hildreth, W., 1984. A Nd, Sr and O isotopic investigation into the causes of chemical and isotopic variation in the Bishop Tuff, California. *Earth Planet. Sci. Lett.*, 68: 379-391.
- Hamblin, W.K., 1994. Late Cenozoic lava dams in the western Grand Canyon. *Geol. Soc. Am. Mem.*, 183: 139 pp.
- Hildreth, W., 1991. The timing of caldera collapse at Mount Katmai in response to magma withdrawal toward Novarupta. *Geophys. Res. Lett.*, 18(8): 1541-1544.
- Hildreth, W., 1987. New perspectives on the eruption of 1912 in the Valley of Ten Thousand Smokes, Katmai National Park, Alaska. *Bull. Volcanol.*, 49: 680-693.
- Hildreth, W. and Fierstein, J., 1987. Valley of Ten Thousand Smokes, Katmai National Park, Alaska. *Geol. Soc. Am. Centennial Field Guide - Cordilleran Section*, pp. 425-432.
- Hildreth, W. and Mahood, G., 1986. Ring-fracture eruption of the Bishop Tuff. *Geol. Soc. America Bull.*, 97: 396-403.
- Hildreth, W., Christiansen, R.L., and O'Neil, J.R., 1984. Catastrophic isotopic modification of rhyolitic magma at times of caldera subsidence, Yellowstone Plateau Volcanic Field. *Jour. Geophys. Res.*, 89: 8339-8369.
- Hildreth, W., 1983. The compositionally zoned eruption of 1912 in the Valley of Ten Thousand Smokes, Katmai National Park, Alaska. *Journal of Volcanology and Geothermal Research*, 18: 1-56.

- Hildreth, W., 1983. The compositionally zoned eruption of 1912 in the Valley of Ten Thousand Smokes, Katmai National Park, Alaska. *Jour. Volcanol. Geotherm. Res.*, 18: 1-56.
- Hildreth, W., 1979. The Bishop Tuff: Evidence for the origin of compositional zonation in silicic magma chambers. *Geol. Soc. America Spec. Paper*, 180: 43-75.
- Hildreth, W., 1977. The magma chamber of the Bishop Tuff: Gradients in temperature, pressure, and composition. Ph.D. Thesis, University of California, Berkeley, 328 pp.
- Holt, E.W. and Taylor, H.P., Jr., 1998.  $^{18}\text{O}/^{16}\text{O}$  mapping and hydrogeology of a short-lived ( $\approx 10$  years) fumarolic ( $>500^\circ\text{C}$ ) meteoric-hydrothermal event in the upper part of the Bishop Tuff outflow sheet, California. *Jour. Volcanol. Geotherm. Res.*, 83: 115-139.
- Holt, E.W. and Taylor, H.P., Jr., 1996. Low- $^{18}\text{O}$  meteoric hydrothermal signatures in groundmass and fiamme of the 0.76 Ma Bishop Tuff, California. *EOS Trans. AGU*, 77(46): A106.
- Hurst, V.J. and Kunkle, A.C., 1985. Dehydroxylation, rehydration, and stability of kaolinite. *Clays and Clay Minerals*, 33:1-14.
- Izett, G.A., and Obradovich, J.D., 1991. Dating of the Matuyama-Brunhes Boundary based on  $^{40}\text{Ar}/^{39}\text{Ar}$  ages of the Bishop Tuff and Cerro San Luis Rhyolite. *Geol. Soc. Am. Abstr.*, 23: A106.
- Keating, G.N., Zylvovski, G.A., and Valentine, G.A., 1998, Multiphase thermal modeling of cooling ignimbrites. *EOS Trans. AGU*, 79(45): F281.
- Kienle, J., 1991. Depth of the ash flow deposit in the Valley of Ten Thousand Smokes, Katmai National Park, Alaska. *Geophys. Res. Lett.*, 18(8): 1533-1536.
- Keith, T.E.C., Thompson, J.M., Hutchinson, R.A., and White, L.D., 1992. Geochemistry of waters in the Valley of Ten Thousand Smokes region, Alaska. *Jour. Volcanol. Geotherm. Res.*, 49: 209-231.

- Keith, T.E.C., 1991. Fossil and active fumaroles in the 1912 eruptive deposits, Valley of Ten Thousand Smokes, Alaska. *Jour. Volcanol. Geotherm. Res.*, 45: 227-254.
- Kodosky, L.G. and Keith, T.E.C., 1995. Further insights into the geochemical evolution of fumarolic alteration, Valley of Ten Thousand Smokes, Alaska. *Jour. Volcanol. Geotherm. Res.*, 65: 181-190.
- Kodosky, L.G. and Keith, T.E.C., 1993. Factors controlling the geochemical evolution of fumarolic encrustations, Valley of Ten Thousand Smokes, Alaska. *Jour. Volcanol. Geotherm. Res.*, 55: 185-200.
- Larson, P.B. and Taylor, H.P., Jr., 1986a. An oxygen isotope study of hydrothermal alteration in the Lake City caldera, San Juan Mountains, Colorado. *Jour. Volcanol. Geotherm. Res.*, 30: 47-82.
- Larson, P.B. and Taylor, H.P., Jr., 1986b. An oxygen-isotope study of water-rock interaction in the granite of Cataract Gulch, western San Juan Mountains, Colorado. *Geol. Soc. America Bull.*, 97: 505-515.
- Lister, C.R.B., 1974. On the penetration of water into hot rock. *Geophys. Soc. Edinburgh Res. Lett.*, 39: 465-509.
- Long, P.E. and Wood, B.J., 1986. Structures, textures, and cooling histories of Columbia River Basalt flows., *Geol. Soc., Am. Bull.*, 97: 1144-1155.
- Lowell, R.P. and Keith, T.E.C., 1991. Chemical and thermal constraints on models of thermal springs Valley of Ten Thousand Smokes, Alaska. *Geophys. Res. Lett.*, 18(8): 1553-1556.
- Manley, C.R., 1992. Extended cooling and viscous flow of large, hot rhyolite lavas: implications of numerical modeling results. *Jour. Volcanol. Geotherm. Res.*, 53: 27-46.
- Martin, G.C., 1913. The recent eruption of Katmai volcano in Alaska. *National Geographic Magazine*, 24: 131-181.

- Miller, T.P. and Smith, R.L., 1977. Spectacular mobility of ash flows around Aniakchak and Fisher calderas, Alaska. *Geology*, 5: 173-176.
- Matsuhisa, Y., Imaoka, T., and Murakami, N., 1980. Hydrothermal activity indicated by oxygen and hydrogen isotopes of rocks and minerals from a Paleogene cauldron, southwest Japan. In: Ishihara, S., and Takenouchi, S. (Editors), *Granitic magmatism and related mineralization*. Soc. Min. Geol. Japan, Min. Geol. Spec. Iss., 8: 49-65.
- Mayo, E.B., 1934. The Pleistocene Long Valley Lake in eastern California. *Science*, 80: 95-96.
- McConnell, V.S., Valley, J.W., and Eichelberger, J.C., 1997. Oxygen isotope compositions of intracaldera rocks: hydrothermal history of the Long Valley Caldera, California. *Jour. Volcanol. Geotherm. Res.*, 76: 83-109.
- Nelson, P.H. and Anderson, L.A., 1992. Physical properties of ash flow tuff from Yucca Mountain, Nevada. *J. Geophys. Res.*, 97: 6823-6841.
- Norton, D. and Taylor, H.P., Jr., 1979. Quantitative simulation of the hydrothermal systems of crystallizing magmas on the basis of transport theory and oxygen isotope data: An analysis of the Skaergaard intrusion. *J. Petrol.*, 20: 421-486.
- O'Neil, J.R. and Taylor, H.P., Jr., 1967. The oxygen isotope and cation exchange chemistry of feldspars. *Amer. Mineral.*, 52: 1414-1437.
- Papike, J.J., Keith, T.E.C., Spilde, M.N., Galbreath, K.C., Shearer, C.K., and Laul, J.C., 1991. Geochemistry and mineralogy of fumarolic deposits, Valley of Ten Thousand Smokes, Alaska: Bulk chemical and mineralogical evolution of dacite-rich protolith. *Amer. Mineral.*, 76: 1662-1673.
- Peck, D.L. and Minakami, T., 1968. The formation of columnar joints in the upper part of Kilauean lava lakes, Hawaii. *Geol. Soc. Amer. Bull.*, 79: 1151-1166.
- Putnam, W.C., 1960. Origin of Rock Creek and Owens River Gorges, Mono County, California. *Univ. Calif. Pub. Geol. Sci.*, 34: 221-279.



- Ragan, D.M. and Sheridan, M.F., 1972. Compaction of the Bishop Tuff, California. *Geol. Soc. Amer. Bull.*, 83: 95-106.
- Reneau, S.L. and Dethier, D.P., 1996. Pliocene and Quaternary History of the Rio Grande, White Rock Canyon and vicinity, New Mexico. *New Mexico Geological Society Guidebook, 47th Field Conference, Jemez Mountains Region.* pp. 317-323.
- Riehle, J.R., Miller, T.F., and Bailey, R.A., 1995. Cooling degassing and compaction of rhyolitic ash flow tuffs: a computational model. *Bull. Volcanol.*, 57: 319-336.
- Ryan, M.P. and Sammis, C.G., 1981. The glass transition in basalt. *J. Geophys. Res.*, 86(B10): 9519-9535.
- Sharp, Z.D. and Moecher, D.P., 1994. O-isotope variations in a porphyroclastic meta-anorthosite: Diffusion effects and false isotherms. *Amer. Mineral.*, 79: 951-959.
- Sharp, Z.D., 1990. A laser-based microanalytical method for the in situ determination of oxygen isotope ratios of silicates and oxides. *Geochim. Cosmochim. Acta*, 54: 1353-1357.
- Sheridan, M.F., 1970. Fumarolic mounds and ridges of the Bishop tuff, California. *Geol. Soc. America Bull.*, 81: 851-868.
- Shevenell, L. and Goff, F., 1995. Evolution of hydrothermal waters at Mount St. Helens, Washington, USA. *Jour. Volcanol. Geotherm. Res.*, 69: 73-94.
- Shipley, J.W., 1920. Some chemical observations on the volcanic emanations and incrustations in the Valley of 10,000 Smokes, Katmai, Alaska. *American Journal of Science*, 50: 141-153.
- Smith, B.M. and Suemnicht, G.A., 1991. Oxygen isotope evidence for past and present hydrothermal regimes of Long Valley caldera, California. *Journal of Volcanology and Geothermal Research*, 48: 319-339.
- Smith, R.L. and Bailey, R.A., 1966. The Bandelier Tuff: a study of ash-flow eruption cycles from zoned magma chambers. *Bull. of Volcanol.* 29: 83 - 104.

- Smith, R.L., Friedman, I., and Long, W.D., 1958. Welded tuffs, Expt I. American Geophysical Union Transactions, 39: 532-533.
- Snow, E. and Yund, R.A., 1988. Origin of cryptoperthites in the Bishop Tuff and their bearing in its thermal history. Jour. Geophys. Res., 93: 8975-8984.
- Sorey, M.L., 1985. Evolution and present state of the hydrothermal system in Long Valley caldera. Jour. Geophys. Res., 90: 11219-11228.
- Spilde, M.N., Brearley, A.J., Papike, J.J., 1993. Alteration of plagioclase and pyroxene phenocrysts in a fissure fumarole, Valley of Ten Thousand Smokes, Alaska. American Mineralogist, 78: 1066-1081.
- Stebbins, J.F., Carmichael, I.S.E., and Moret, L.K., 1984. Heat capacities and entropies of silicate liquids and glasses. Contrib. Mineral. Petrol., 86: 131-128.
- Swanson, D.A., 1987. Regional variation of jointing style in Grande Ronde Basalt related to Miocene geography, Columbia Plateau. Geol. Soc. Am. Abst. Prog. 19: 455-456.
- Symonds, R.B., Rose, W.I., Reed, M.H., Lichte, F.E., and Finnegan, D.L., 1987. Volatilization, transport and sublimation of metallic and non-metallic elements in high temperature gases at Merapi Volcano, Indonesia. Geochim. Cosmochim. Acta, 51: 2083-2101.
- Taylor, H.P., Jr., 1997. Oxygen and hydrogen isotope relationships in hydrothermal mineral deposits. In: Barnes, H.L. (Editor) Geochemistry of Hydrothermal Ore Deposits (3rd Ed.). John Wiley and Sons, Inc., New York. pp. 229-288.
- Taylor, H.P., Jr., 1977. Water/rock interactions and the origin of H<sub>2</sub>O in granitic batholiths. Jour. Geol Soc. London, 133: 509-558.
- Taylor, H.P., Jr., 1974. The application of oxygen and hydrogen isotope studies to problems of hydrothermal alteration and ore deposition. Econ. Geol., 69: 843-883.
- Taylor, H.P., Jr., 1968. The oxygen isotope geochemistry of igneous rocks. Contrib. Mineral. Petrol., 19: 1-71.

- Taylor, H.P., Jr., and Epstein, S., 1962. Relationships between  $^{18}\text{O}/^{16}\text{O}$  ratios in coexisting minerals of igneous and metamorphic rocks. *Geol. Soc. America Bull.*, 73: 461-480.
- Taylor, H.P., Jr., and Sheppard, S.M.F., 1986. Igneous Rocks: I. Processes of isotopic fractionation and isotope systematics. In: Valley J.W., Taylor, H.P., Jr., and O'Neil, J.R. (eds.) *Stable Isotopes in high-temperature geological processes*. *Min Soc. Am. Rev. Mineral.*, 16: 227-271.
- Velde, D., and Meunier, A., 1987. Petrologic phase equilibria in natural clay systems. In: A.C.D. Newman (Editor), *Chemistry of clays and clay minerals*, *Mineral. Soc. Mono.*, 6: 423-258.
- Wallace, P.J., Anderson, A.T., and Davis, A.M., 1995. Quantification of pre-eruptive exsolved gas contents in silicic magmas. *Nature*, 377: 612-616.
- Weisneth D.W., and Eichelberger, J.C., 1996, Vapor phase crystallization in rhyolite lava from Novarupta Dome, Katmai National Park, Alaska. *EOS Trans.*, 77(46): F770.
- Westrich, H.R., Stockman, H.W., and Eichelberger, J.C., 1988. Degassing of rhyolitic magma during ascent and emplacement. *J. Geophys. Res.*, 93: 6503-6511.
- Wilson, C.J.N., and Hildreth, W., 1997. The Bishop Tuff: New insights from eruptive stratigraphy. *Jour. Geol.*, 105: 407-439.
- Zhang, Y., Stolper, E.M., and Wasserburg, G.J., 1991. Diffusion of water in rhyolitic glasses. *Geochim. Cosmochim. Acta*, 55: 441-456.
- Zies, E.G., 1929. The Valley of Ten Thousand Smokes: I. The fumarolic incrustations and their bearing on ore deposition. II. The acid gases contributed to the sea during volcanic activity. National Geographic Society, *Contributed Technical Papers*, Katmai Series, 4: 1-79.
- Zies, E.G., 1924. Hot Springs of the Valley of Ten Thousand Smokes. *Jour. Geol.*, 32: 303-310.